

UNIVERSITÀ DEGLI STUDI DI GENOVA

Dipartimento di Scienze della Terra
dell'Ambiente e della Vita

Scuola di Dottorato in Scienze e Tecnologie
per l'Ambiente e il Territorio

Curriculum *Scienze della Terra*

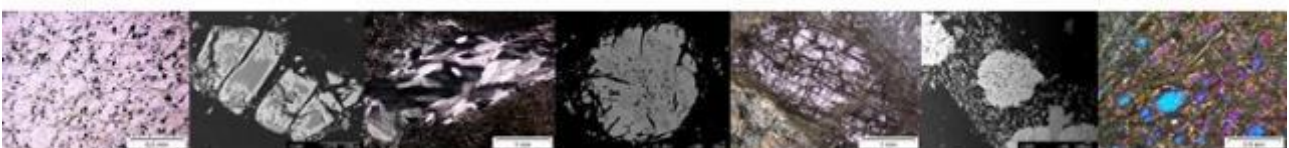
XXXI ciclo

POTENTIALLY TOXIC ELEMENTS IN ULTRAMAFIC ROCKS AND SOILS: A case study from the Voltri Massif (NW Italy)

Silvia Fornasaro



Anni accademici 2016-2018



UNIVERSITÀ DEGLI STUDI DI GENOVA

Scuola di Scienze MM.FF.NN.

Dipartimento di Scienze della Terra, Ambiente e Vita

Scuola di Dottorato in Scienze e Tecnologie per l'Ambiente e il Territorio

Curriculum: Scienze della terra

XXXI ciclo



POTENTIALLY TOXIC ELEMENTS IN ULTRAMAFIC ROCKS AND SOILS: A case study from the Voltri Massif (NW Italy)

Dott.ssa Silvia Fornasaro

Tutor: Prof. Pietro **Marescotti** (Università di Genova)

Co-tutor: Prof.ssa Laura **Crispini** (Università di Genova)

Prof.ssa Paola **Comodi** (Università di Perugia)

Settore scientifico-disciplinare: **GEO/09**

A.A. 2016-2018

INDEX

Preface	6
<u>SECTION ONE: Introduction and state of art</u>	9
<u>CHAPTER I INTRODUCTION.....</u>	10
1.1. ULTRAMAFIC ROCKS AND SOILS	10
1.1.1. Nature of ultramafic rocks	
1.1.2. Serpentine soil or ultramafic soil? An ambiguous definition	
1.1.3. Geochemistry of ultramafic rocks and soils	
1.2. AIMS OF PhD THESIS	24
References	25
<u>CHAPTER II STUDY AREA</u>	32
2.1. THE VOLTRI MASSIF	32
2.1.1. Geography and Geomorphology	
2.1.2. Climate and Pedology	
2.1.3. Geology	
2.1.4. Study sites	
References	42
<u>CHAPTER III MATERIAL AND METHODS</u>	45
3.1. FIELD WORK AND SAMPLING	45
3.1.1. Field survey and geo-structural analyses	
3.1.2. Sampling strategy	
3.2. ANALYTICAL TECHNIQUES.....	46
3.2.1. Soil physical analyses	
3.2.2. Mineralogical, petrographic and microstructural analyses	
3.2.3. Mineralogical, mineral chemical, and crystallographic analyses	
3.2.4. Trace and ultra-trace minero-chemical analyses	
3.2.5. Bulk chemistry (major, minor, and trace elements)	
References	52
<u>SECTION TWO: Investigation on the ultramafic rocks</u>	54

<u>CHAPTER IV</u> Potentially toxic elements distribution in the serpentinized and deformed ultramafic rocks from the Voltri Massif (NW, Italy)	55
4.1. INTRODUCTION.....	55
4.2. MATERIAL AND METHODS	58
4.3. RESULTS	60
4.3.1. Petrographic, mineralogical, and microstructural features of the studied rocks	
4.3.2. Mineral chemistry of the PTEs-bearing minerals	
4.3.3. Bulk chemistry	
4.4. DISCUSSION.....	82
4.5. CONCLUSIONS.....	85
References	86

<u>CHAPTER V</u> Potentially toxic elements compositional variation in spinel-group minerals of serpentinized and deformed ultramafic rocks from the Voltri Massif (NW Italy)	94
5.1. INTRODUCTION.....	95
5.2. ANALYTICAL METHODS	96
5.3. RESULTS	97
5.3.1. Spinel-group minerals in the studied rocks: a crystallographic classification	
5.3.2. Microstructures and textures of spinel-group minerals	
5.3.3. Trace and ultra-trace element variation in spinel-group minerals	
5.4. DISCUSSION.....	108
5.4.1. Textural and microstructural evolution	
5.4.2. Trace element variation in spinel-group minerals	
5.5. CONCLUSIONS.....	113
References	113

SECTION THREE: Investigation on the ultramafic soil profiles

<u>CHAPTER VI</u> Source and distribution of potentially toxic elements in ultramafic soil profiles from the Voltri Massif (NW Italy)	120
6.1. INTRODUCTION.....	120
6.1.1. Authigenic phases in the ultramafic soils	
6.1.2. Aims of study	

6.2. MATERIALS AND METHODS.....	125
6.2.1. Sampling strategy	
6.2.2. Analytical techniques	
6.3. RESULTS	127
6.3.1. The early stage of weathering in ultramafic bedrocks	
6.3.2. Soil profile characteristics	
6.3.3. Soil micromorphology	
6.3.4. Soil mineralogy	
6.3.5. Mineral chemistry	
6.3.6. Bulk chemistry	
6.4. DISCUSSION.....	152
6.4.1. Major element variation and authigenic phases formation	
6.4.2. PTEs behavior along soil profiles	
6.4.3. Environmental concerns	
6.5. CONCLUSIONS.....	160
References	161
<u>GENERAL REMARKS.....</u>	168
<u>APPENDIX.....</u>	172
A. SITE DESCRIPTION	172
B. SUPPLEMENTARY DATA.....	214

Preface

High concentrations of *potentially toxic elements* (PTEs) in surface and near-surface environment may be attributed to both anthropogenic sources, including industrial and agricultural activity, and geogenic source, mainly due to natural weathering of rocks.

Considering the geogenic sources, ultramafic rocks (e.g., dunite, peridotite, pyroxenite, and serpentinites) are among the most critical from the environmental point of view; in fact, besides the common occurrence of asbestos minerals (Schreier et al., 1987; Cheshire and Guven, 2005; Alexander et al., 2007; Hseu et al., 2007; Kumarathilaka et al., 2014; Tashakor et al., 2014), they are characterized by high contents of Cr (up to 16000 ppm; Stueber and Goles, 1967), Ni (up to 7733 ppm; Savov et al., 2007), Co (up to 950 ppm; Garnier et al., 2009), and other PTEs which can have potential harmful impact on ecosystems and human health if released into soils and waters during weathering and pedogenic processes (Brooks, 1987). As a matter of the fact, weathering of ultramafic rock produces ultramafic soil containing high concentration of PTEs, including Cr, Ni, and Co (Oze et al. 2004; Alexander et al., 2007) compared to soils derived from non-ultramafic bedrock.

Although ultramafic rocks and relative soils cover approximately 1% of the Earth's surface, they are distributed worldwide and are commonly associated with ophiolite complexes (Fig. 1; Coleman, 1977; Coleman and Jove 1992; Vaughan and Scarrow 2003; Dilek and Furnes 2009; Saccani, 2015); for this reason, they play an important role in environmental management (Kumarathilaka et al., 2014; Tashakor et al., 2014).

The three sections, that constitute this PhD thesis, describe the investigations related to the chemistry and mineralogy of ultramafic soils profiles from the meta-ophiolitic Voltri Massif (Ligurian Alps, NW Italy). In this study, the studied rock and soils samples have been analyzed using a multiscale and multi-analytical approach, combining field, analytical, and laboratory studies.

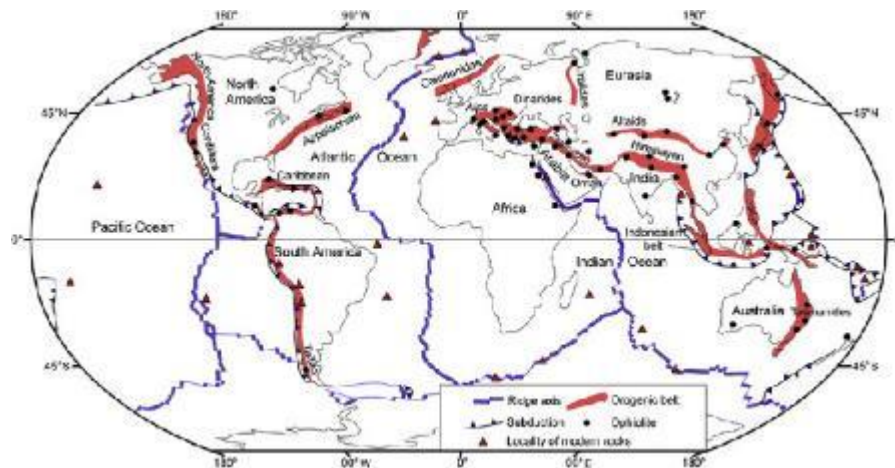


Fig. 1 Global distribution of major Proterozoic and Phanerozoic ophiolitic belts, as well as location of ophiolites and modern rocks (from Saccani, 2015).

A brief description of the three section and relative chapters is presented in the following paragraphs:

SECTION ONE: Introduction and state of art

- In *Chapter I* the main objectives of this dissertation are present. The source, fate, and environmental implication of PTEs, as well as the general characteristics of ultramafic rocks and soils are discussed and reviewed.
- In *Chapter II* the main geological characteristics of the Voltri Massif are summarized, and a detail description of studied sites are also provided.
- In *Chapter III* the materials and methods used during the main stages of this work are listed and described.

SECTION TWO: Investigation on ultramafic rocks

- In *Chapter IV* chemical, mineralogical, and microstructural features of ultramafic rocks are investigated, with detail focus on PTEs variation (mainly Cr, Ni, Co, Cu, Zn, and V).
- *Chapter V* is focused on the spinel-group minerals in ultramafic rocks. The relationships between their crystallochemical variations (with detail focus on PTEs variation) and their mode of occurrence with respect to the degree of serpentinization and deformation are also analyzed and discussed in detail.

SECTION THREE: Investigation on ultramafic soil profiles

- In *Chapter VI* primary and authigenic minerals in ultramafic soil profiles and their relationship with PTEs contents are investigated. The obtained results are discussed and compared to others ophiolite complex around the world, focusing on the environmental implications.
- The conclusions and the prospects for future applications of this work are summarized in the least part of the thesis.

References

- Alexander, E.B., Coleman, R.G., Harrison, S.P., and Keeler-Wolfe, T. (2007). *Serpentine geoecology of western North America: geology, soils, and vegetation*. OUP USA.
- Brooks, R.R. (1987). *Serpentine and its vegetation: a multidisciplinary approach*. Dioscorides Press.
- Cheshire, M., and Güven, N. (2005). Conversion of chrysotile to a magnesian smectite. *Clays and Clay Minerals*, 53(2), 155-161.
- Coleman, R.G. (1977). What is an Ophiolite? In *Ophiolites* (pp. 1-7). Springer, Berlin, Heidelberg.
- Coleman, R.G., and Jove, C. (1992). Geological origin of serpentinites. *The vegetation of ultramafic (serpentine) soils*, 1-17.
- Dilek, Y., and Furnes, H. (2009). Structure and geochemistry of Tethyan ophiolites and their petrogenesis in subduction rollback systems. *Lithos*, 113(1-2), 1-20.
- Garnier, J., Quantin, C., Guimarães, E., Garg, V.K., Martins, E.S., and Becquer, T. (2009). Understanding the genesis of ultramafic soils and catena dynamics in Niquelândia, Brazil. *Geoderma*, 151(3/4), 204-214.
- Hseu, Z.Y., Tsai, H., Hsi, H.C., and Chen, Y.C. (2007). Weathering sequences of clay minerals in soils along a serpentinitic toposequence. *Clays and Clay Minerals*, 55(4), 389-401.
- Kumarathilaka, P., Dissanayake, C., and Vithanage, M. (2014) *Geochemistry of serpentinite soils: a brief overview*.
- Oze, C., Fendorf, S., Bird, D.K., and Coleman, R.G. (2004). Chromium geochemistry in serpentinitized ultramafic rocks and serpentine soils from the Franciscan complex of California. *American Journal of Science*, 304(1), 67-101.
- Saccani, E. (2015). A new method of discriminating different types of post-Archean ophiolitic basalts and their tectonic significance using Th-Nb and Ce-Dy-Yb systematics. *Geoscience Frontiers*, 6(4), 481-501.
- Savov, I.P., Ryan, J.G., D'Antonio, M., and Fryer, P. (2007). Shallow slab fluid release across and along the Mariana arc-basin system: Insights from geochemistry of serpentinitized peridotites from the Mariana fore arc. *Journal of Geophysical Research: Solid Earth*, 112(B9).
- Schreier, H., Omuetti, J.A., and Lavkulich, L.M. (1987). *Weathering Processes of Asbestos-rich Serpentinitic Sediments 1*. *Soil Science Society of America Journal*, 51(4), 993-999.
- Stueber, A.M., and Goles, G.G. (1967). Abundances of Na, Mn, Cr, Sc and Co in ultramafic rocks. *Geochimica et Cosmochimica Acta*, 31(1), 75-93.
- Tashakor, M., Yaacob, W.Z.W., Mohamad, H., and Ghani, A.A. (2014). Geochemical characteristics of serpentinite soils from Malaysia. *Malays J Soil Sci*, 18, 35-49.
- Vaughan, A.P., and Scarrow, J.H. (2003). Ophiolite obduction pulses as a proxy indicator of superplume events? *Earth and Planetary Science Letters*, 213(3-4), 407-416.

Section One

Introduction and state of art

This *Section* reposts the main objectives of this PhD thesis. The chemistry, regulations, and toxicity of PTEs are discussed, as well as the general characteristics of ultramafic rocks and relative soils (*Chapter I*). Additionally, the geological framework of the study area is also described (*Chapter II*). In the *Chapter III*, the materials and methods used during the main stages of this PhD thesis are listed and described.

Chapter I

Introduction

In *Chapter I* the general aspects and aims of this PhD thesis are reported. The general characteristics of ultramafic rocks and relative soils, as well as, the source, fate, and environmental implication of *potentially toxic elements* (PTEs) are also summarized.

1.1. ULTRAMAFIC ROCKS AND SOILS

1.1.1. Nature of ultramafic rocks

Ultramafic rocks are defined as rocks that contain more than 90% of ferromagnesian minerals, the majority of which are olivine, clino-, and orthopyroxene. In the ultramafic rocks from the ophiolite complexes, the most common accessory minerals are spinel-group minerals: in particular, magnetite, chromite, Cr-magnetite, and ferric chromite are the most common accessory minerals (Irvine, 1967; Coleman, 1971; Dick and Bullen, 1984). They display a wide range in composition reflecting their primary magmatic or secondary origin (Colas et al., 2014).

The ultramafic rocks are classified according to the modal abundance of olivine, orthopyroxene, and clinopyroxene (Fig. 1.1; Le Bas and Streckeisen, 1991). The most common ultramafic rocks are harzburgite, dunite, and lherzolite.

Chemical composition of ultramafic rocks is characterized by silica ($\text{SiO}_2 < 45$ wt.%), magnesium ($\text{MgO} > 35$ wt.%), iron (ranging from 6–9 wt.% of FeO), minor amount of calcium and alumina (1–4 wt.% of CaO and Al_2O_3), and trace concentration of sodium and potassium (Alexander, 2004).

The interactions of water with ultramafic rocks in a wide range of P-T conditions as well as different tectonic and geological contexts (e.g., mid-ocean ridges and subduction zones; Deschamps et al., 2013 and reference therein) cause the transformation of ultramafic rocks into serpentinites. Serpentinization is a hydration and redox reaction that transforms peridotite-forming minerals (olivine and pyroxenes) into hydrous phyllosilicates (serpentine) and Fe-oxides (magnetite; Andreani et al., 2013). This process is generally accomplished with little to no change in the relative amounts of Si, Al, Mg, Cr, Mn, Fe, Co, and Ni,

which are essentially redistributed within the metamorphic minerals (Chalot-Prat et al., 2003; Iyer et al., 2008). The only component easily removed during serpentinization is calcium (Alexander et al., 2007). *More details of element mobilization in ultramafic rocks are reported in Section II.*

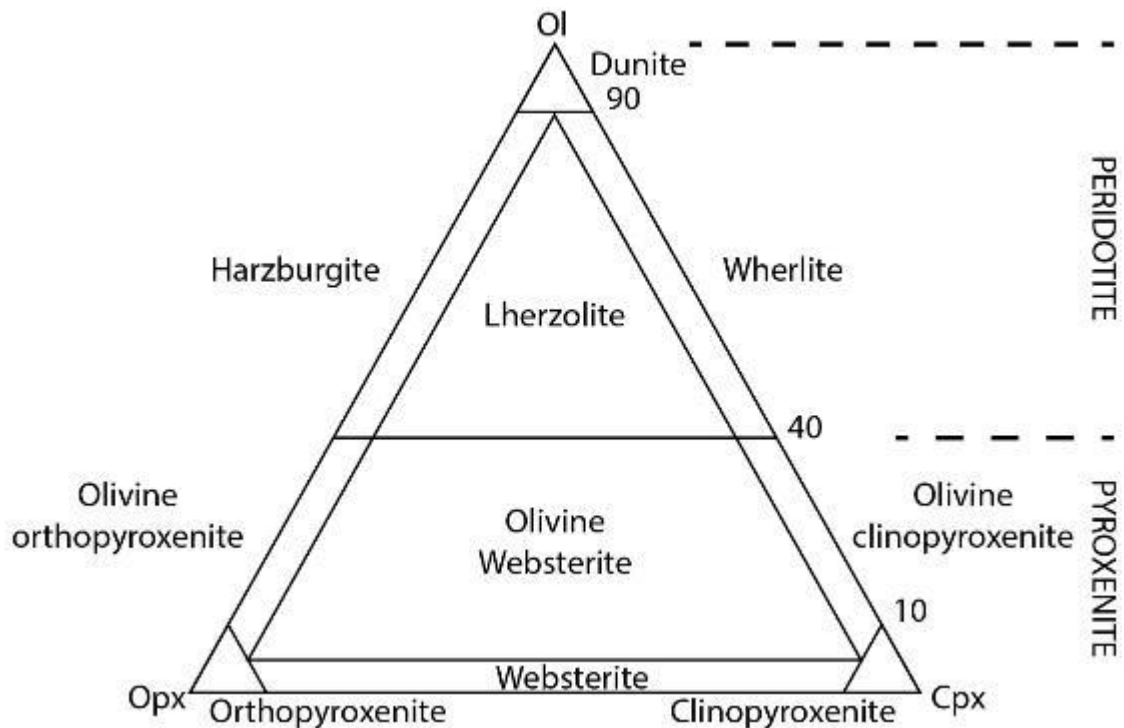


Fig. 1.1 Classification and nomenclature of the ultramafic rocks (mafic minerals >90%) based on the modal abundance of olivine (Ol), orthopyroxene (Opx) and clinopyroxene (Cpx). From Le Bas and Streckeisen (1991).

For these reasons, peridotite and serpentinite (Fig. 1.2) are chemically similar, but about 12%–15% water is added during serpentinization processes leading to important mineralogical transformation and significant variation of the physical properties.

Peridotites are mainly macrocrystalline (63 μm – 2 mm) rocks composed by olivine, clino- and orthopyroxene, plagioclase, and minor spinels, whereas serpentinites are mainly composed of macro- to microcrystalline (2 μm – 63 μm) phyllosilicate (i.e. serpentine minerals and chlorite), magnetite, accessory phases (Ti-clinohumite, brucite, Fe- and Ni-bearing sulfides, and native metal alloys), and various amounts of relic minerals (as a function of the degree of serpentinization; McCollom and Seewald, 2013).

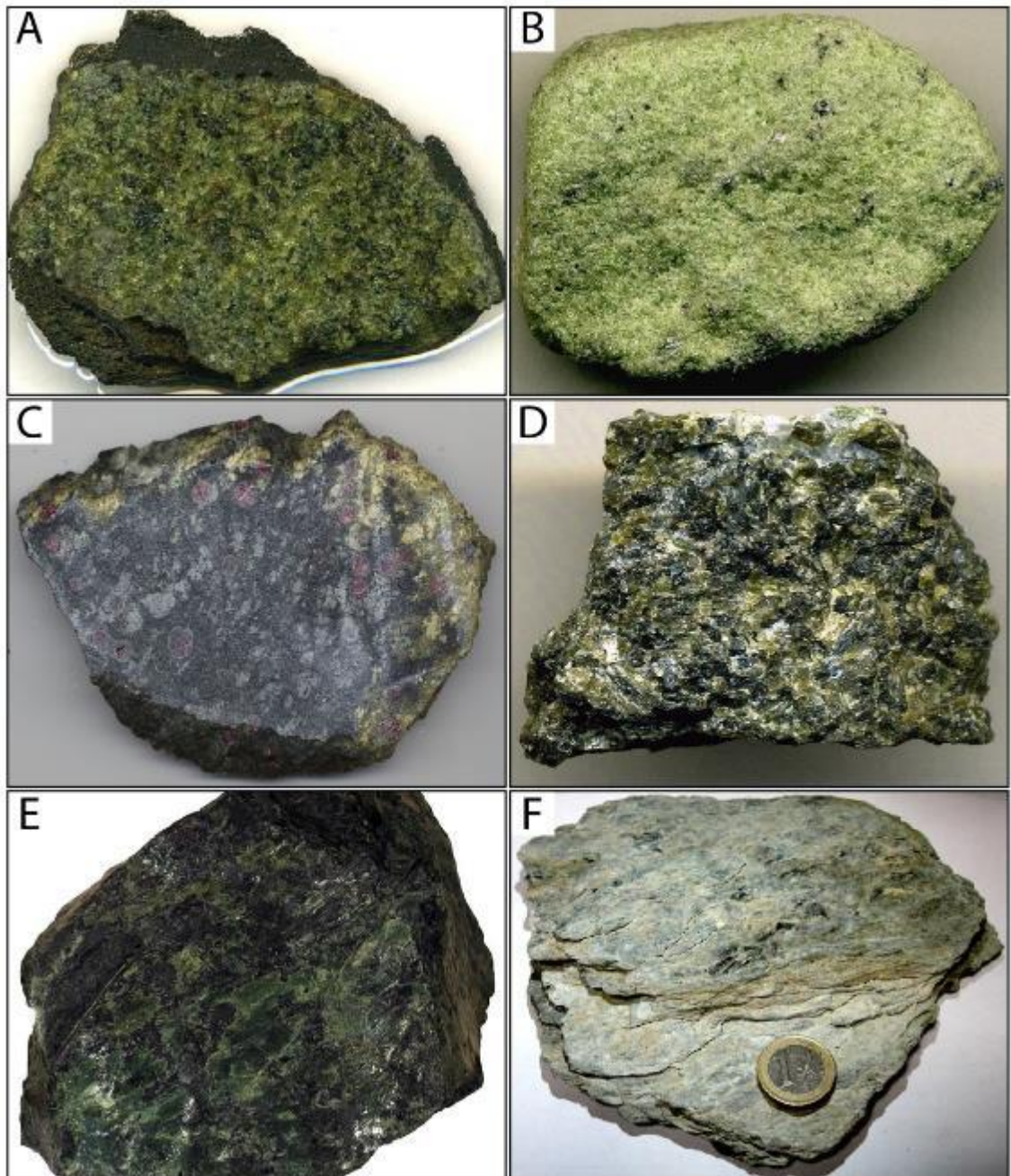


Fig. 1.2 Type of ultramafic rocks: a) spinel lherzolite; B) dunite; C) garnet lherzolite; D) harzburgite; E) serpentinites; F) serpentine schists (images from <http://www.alexstrekeisen.it/>).

Serpentinites vary in textures (Fig. 1.3) due to the different physical and chemical conditions during serpentinization (e.g., prograde vs. retrograde serpentinization) or events in an often polystage serpentinization process (e.g., deformation, weathering, dissolution, recrystallization; Viti and Mellini, 1998). Textures of serpentines can be divided into three types: i) pseudomorphic textures (formed after olivine, pyroxene, amphibole, talc, and chlorite); ii) non-pseudomorphic textures (formed either from the same primary minerals or from pseudomorphic

serpentine textures); and iii) textures formed in serpentine veins (Wicks and Whittaker, 1977).

The typical pseudomorphic textures consist of mesh and hourglasses (resulting from the hydration of olivine, according to a sub-orthogonal fracture pattern) and bastites (resulting from the hydration of pyroxene). The well-development of pseudomorphic textures varies from excellent to indistinct, and the latter grade (ribbon texture) into non-pseudomorphic textures. Non-pseudomorphic textures can be divided into interpenetrating and interlocking types. The serpentine grains in both lithotype are anhedral and mutually interfere but tend to be elongate in interpenetrating textures and equant in interlocking textures. The orientation of the elongate grains may vary from completely random, in which case a massive rock is produced, to strongly subparallel orientation, in which case a foliated rock is produced. Late veins of serpentine along fractures, shears, and joint planes can be found to a greater or lesser degree in almost every serpentinite. These set can be divided in slip-fiber vein (fibers oblique to the vein walls) or cross-fiber vein (fibers perpendicular to the vein walls; Wicks and Whittaker, 1977).

The above described mineralogical and textural differences between the ultramafic rocks can affect significantly their physical-mechanical properties; Compared with peridotites, serpentinites have a weaker rheology (e.g., decrease in density and in seismic velocities; Christensen, 1972; Reinen et al., 1994; Miller and Christensen, 1997; Escartin and Lin, 1998; Roumejon et al., 2015). Serpentinites are commonly deformed and sheared compared to the more massive peridotite (Alexander et al., 2007; Hirth and Guillot, 2013).

When exposed to the weathering process, peridotite-forming minerals (olivine and pyroxenes) are more altered than serpentinite-forming minerals (serpentine minerals, chlorite, and magnetite; Alexander, 2004; Vithanage et al., 2014), producing significant differences either in weathering features, geochemical cycles of elements, as well as in soil profiles.

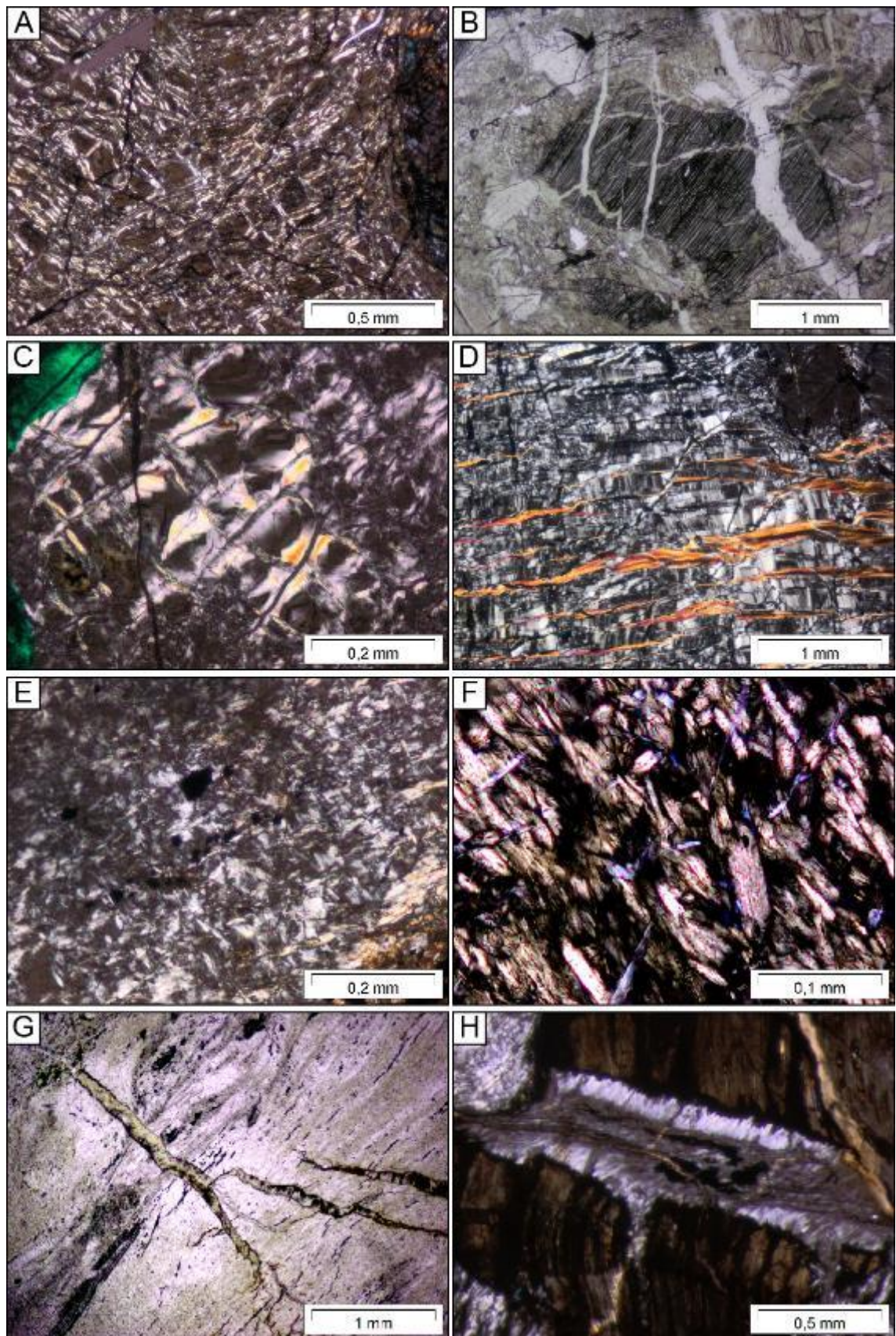


Fig. 1.3 Serpentine textures: A) mesh texture (cross-polarized light – XPL); B) bastite texture (parallel-polarized light – PPL); C) hourglass texture (XPL); D) ribbon texture, cross-cut by talc veins (XPL); E-F) non-pseudomorphic texture (XPL); G) cross-fiber vein (PPL); H) slip-fiber vein (XPL).

1.1.2. Serpentine soil or ultramafic soil? An ambiguous definition

“*Serpentine soil*” is a general term used to describe soils derived from a wide range of ultramafic rocks, including peridotitic (dunite, wehrlite, harzburgite, and lherzolite) and serpentinitic rocks (serpentinites and serpentine schists; Oze et al., 2004a). In pedological and botanic literature, these soils are commonly grouped together, without any distinction among the different ultramafic parent rocks, because they are vegetated with the same *serpentinophyte* plants (Roberts and Proctor, 1991; Alexander et al., 2007; 2009). However, chemical and physical features of *serpentine soils* can vary considerably at regional, local or even at single site scale (metric to decametric in extension; Kierczak et al., 2007, 2008, 2016; Quantin et al., 2008; Garnier et al., 2009; Morrison et al., 2009; Vithanage et al., 2014), according to the great variability in the chemical and mineralogical compositions of ultramafic bedrocks, as well as of their local structural, microstructural, and petrological features (Alexander, 2004; Caillaud et al., 2006, 2009; Burgess et al., 2009; Alexander and DuShey, 2011; Baumeister et al., 2015; Kierczak et al., 2016; van der Ent et al., 2018).

Here the generic term “*ultramafic soil*” is used whereas “*serpentine soil s.s.*” is strictly used for soil formed from serpentinites and serpentine schist and “*peridotite soil*” for those developed on peridotites or serpentinites with magmatic relics.

1.1.3. Geochemistry of ultramafic soils

Common characteristics of ultramafic soils

Ultramafic soils are commonly little-developed soils characterized by modest thickness (<30 cm) and poor horizon differentiation (*lithosols* to ranker; Cortesogno et al., 1979; Legros, 1992; Morrison et al., 2009; Kelepertzis et al., 2013); they are defined as "AC soils" because the O horizon is commonly absent or few millimeters thick and the poorly developed A horizon is directly in contact with the C horizon (Fig. 1.4; Foth, 1990; Baumeister et al., 2015). In these soils, the only pedogenic processes which have occurred are related to initial weathering of the parent material and formation of cambic horizons, or accumulation of organic matter in the soil mineral horizons with the development of umbric epipedons (Bonifacio et al., 2010).

Due to their primitive development, the bedrock is the most important factor influencing the mineralogical, geochemical, micromorphological, and pedological

properties of the soil profile (Lee et al., 2003, 2004; Chardot et al., 2007; Hseu et al., 2007; Caillaud et al., 2009; Kelepertizis et al., 2013; Baumeister et al., 2015).

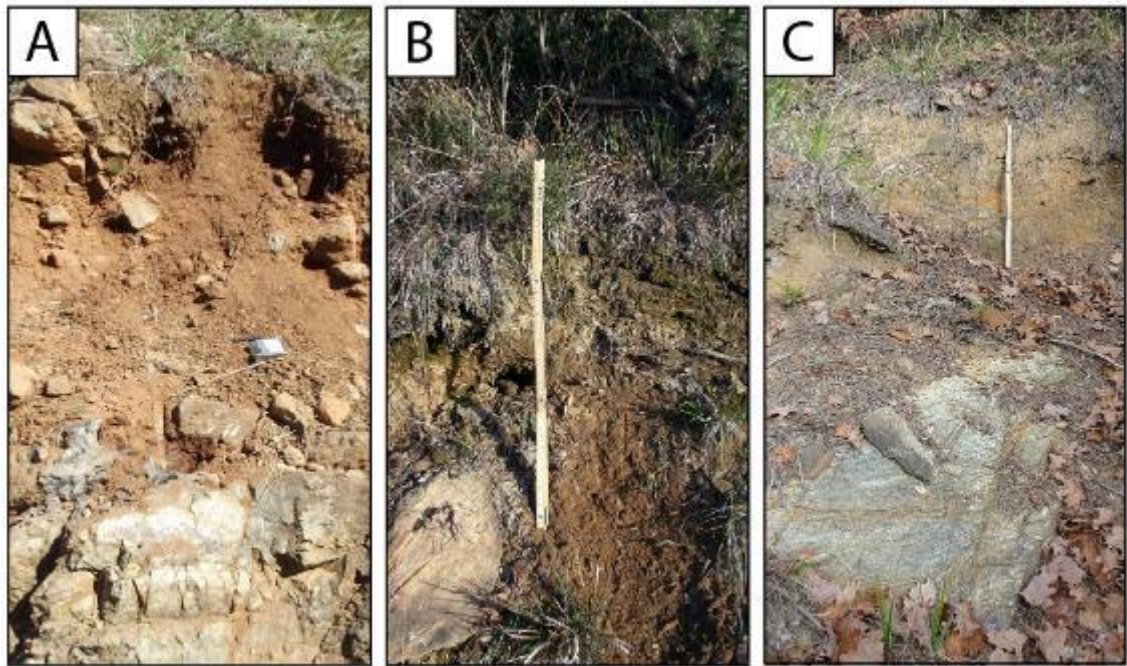


Fig. 1.4 Ultramafic soil profiles from different bedrocks from Voltri Massif: A) partially serpentinized peridotite bedrock (Rocca Grin site); B) massive serpentinite bedrock (Bric Gippone site); C) foliated serpentinite bedrock (Bric Gippone site).

In fact, the mineralogical composition of the ultramafic soils is mostly inherited from the parent rock with minor authigenic species (Fe-oxyhydroxides, clay minerals; see *chapter VI*) and very low humus and organic matter content (Oze et al., 2004a,b; Caillaud et al., 2009).

Ultramafic soils have a peculiar geochemical composition, that play a primary environmental and ecological role, such as: i) *low Ca/Mg ratio* – The abundance of Mg and the Ca deficiency in the ultramafic rocks result in the characteristically very low Ca/Mg ratio with consequent nutritional deficiencies and low fertility in the ultramafic soils (Alliani, 1997; Kumarathilaka et al., 2014). Depending on the pedological evolution of the soil the Ca/Mg ratio varies between 0.09 and 1.48 starting from the C horizon to the most superficial horizon (Bonifacio et al., 1997). ii) *low content of essential elements (P and K)* – Similarly to the Ca/Mg ratio, there is usually a strong deficiency of potassium (K) and phosphorus (P), due to their low concentrations in the parent rock-forming minerals. iii) *high content of potentially toxic elements (Cr, Ni, and Co)* - Ultramafic rocks and relative soils are enriched in some potentially toxic elements, particularly Cr, Ni, and Co, and secondly Mn, Ti, V, Zn, and Cu.

Difference between serpentine soils s.s. and peridotite soils

The pedogenetic processes on ultramafic bedrocks, and the consequent differences between serpentine s.s. and peridotite soils are strictly dependent on climate.

- *Polar climate*: Serpentine s.s. and peridotite soils are very similar in serpentinite or on peridotite in polar climate; in these conditions, the soils developed on the two different bedrocks are similar from their geochemical signature as well as for their color, depth, horizon differentiation, and weathering intensity (Kierczak et al., 2007; 2016). The weakly developed soils are mainly Regosol or Leptosol (Lessoavaia and Polekhovsky 2009). The main mineral association is inherited from ultramafic bedrocks (talc, serpentine, and chlorite) and authigenic phases are only represented by mineral of the smectite group (saponite). Under the polar environmental conditions, an important factor is represented by the acidic effect of moss and lichens, that seems to be a reason of selective decomposition of the most unstable minerals (Lessoavaia et al., 2016).
- *Temperate and Mediterranean climate*: In Temperate climate, serpentine soils s.s. are mainly Cambisols (Echevarria, 2018) and can be magnesian Cambisols (Estrade et al. 2015) in Mediterranean conditions (Cs), where weathering intensity is higher. The predominant soil type on peridotite bedrock is Cambisol with slight differences with soils on serpentine bedrock, such as the definition 'chromic' due to the accumulation of Fe oxyhydroxides (easily weatherable olivine can produce significant amounts of Fe-oxyhydroxides, up to 25 wt%; Massoura et al. 2006; Alexander 2014; Echevarria, 2018). Typically, in serpentine soils s.s., the predominant mineral phase is serpentine minerals. Clay minerals either derive from the bedrock (e.g. chlorite) or form from serpentine weathering (Caillaud et al. 2009; Chardot et al. 2007). The formation of Fe-rich smectite from serpentine is a peculiarity of temperate serpentinite soils (Bonifacio et al. 1997; Caillaud et al. 2004, 2009). The Mg-chlorite is weathered to trioctahedral vermiculite (Caillaud et al. 2009). During weathering, free Fe is released and oxyhydroxides are partly crystallized (Chardot et al. 2007). The amount of smectite in peridotite soils is less significant than in serpentine soils s.s. (Caillaud et al. 2004; Chardot et al.

2007). Fe segregation becomes a significant pedogenic process on peridotite and goethite is the predominate authigenic phase (Alexander and DuShey 2011; Alexander, 2014). Soil chroma of peridotite soils has values situated in the YR range, whereas serpentine soils s.s. are in the Y range, locally reaching YR 7.5 or redder (Chardot et al. 2007; Kierczak et al. 2016). The chroma value is associated with the accumulation of Fe oxyhydroxides: the amounts of free Fe in the soils are related to the degree of serpentinization of the parent peridotite and its weathering (Alexander, 2014). *More details of primary and authigenic minerals under temperate climate are reported in Section III.*

- *Tropical climate:* In the tropical climate, the differences between serpentine and peridotite bedrocks become more evident and the soils have two different behavior and ecosystems (Roberts and Proctor, 1991; Echevarria, 2018). In the tropical climate, serpentinite soils s.s. are mostly dominated by Cambic Leptosols or Cambisols having magnesian/hypermagnesian properties (Cheng et al. 2011; Isnard et al. 2016; van der Ent et al. 2016). Within these soils, the main pedogenic process is weathering of primary minerals (serpentine minerals and chlorite) into smectite after a significant loss of Mg (Hseu et al. 2007) and formation of a stable organo-mineral complex. In high weathered soil profiles, under the tropical condition, leaching is favorable and the loss of Si from smectite/vermiculite can lead to accumulation of kaolinite and Fe-oxides (Hseu et al. 2007). Although the presence of serpentinite reduces the speed of laterization, laterite formation on wholly serpentinized rocks is common and leads to smectite-rich saprolite owing to poor drainage of the serpentinite (Gleeson et al., 2004; Butt and Cluzel, 2013). Soil genesis occurring on peridotite in the tropical climate has been extensively documented over the last 40 years because of the economic value of Ni-laterites (Nahon et al. 1982a,b; Colin et al. 1990; Gleeson et al. 2004). In terms of soil properties, these soils are classified as Ferralsols. Some of the most developed ultramafic laterite profiles result in 60–100 m (Colin et al. 1990) of weathered material with the formation of a full lateritic horizon, i.e. goethite-dominant limonite (Colin et al. 1990; Dublet et al. 2014, 2015; Aiglsperger et al. 2016). In the lateritic horizon usually described by miners as 'limonite' or 'laterite,' the mineralogy is dominated by goethite. Hematite

is formed at the surface ('red limonite or laterite') as a consequence of extremely hot temperatures reached the soil surface where affected by sunlight. Mineralogical and geochemical changes of iron oxides occur through the distance gradient from the bedrock (Dublet et al. 2014).

Potentially toxic elements (PTEs) in the ultramafic soil

In this paragraph, the source, fate, and environmental implication of Cr, Ni, and Co are summarized.

Chromium is a transition metal of group 6 that is present in the environment as Cr^{3+} , a non-hazardous species and micronutrient, and as Cr^{6+} , a toxic and a Class A human carcinogen by inhalation, ingestion, and contact (Daugherty, 1992; Cohen et al., 1993; James et al., 1997; Alloway, 2010). Chromium is mainly found in rocks in the form of chromite (FeCr_2O_4), and also occurs in the rare mineral crocoite (PbCrO_4), as well as an accessory element in several other minerals, such as spinel, amphibole, mica, pyroxene, and garnet. The primary mineralogical residences of Cr in ultramafic rocks are chromite and Cr-rich magnetite with subordinate amounts contained in chlorite, augite, enstatite, Fe-oxide and Fe-oxyhydroxide, and clay minerals (Becquer et al., 2003; Oze et al., 2004a,b). The average concentration of Cr in rocks is 100 mg/kg, while in ultramafic complexes can be found with 1800 mg/kg in average. According to Kabata-Pendias (2011), the world average content of chromium in soils is 80 mg/kg (Table 1.1), while the Cr content can reach up to 6000 mg/kg in serpentinized ultramafic soils (Shanker et al. 2005; Adriano, 2001). Chromium concentrations of 30000 mg/kg have been reported in the lateritic deposits of New Caledonia (Amir and Pineau, 1998). Trivalent chromium is characterized by low mobility since it occurs in stable low-soluble primary minerals (e.g., spinel-group minerals) and secondary authigenic oxyhydroxides (either as substitution ion or as stable surface complexes; Schwertmann and Taylor, 1989; Trolard et al., 1995; Quantin et al., 2002); on the contrary hexavalent Cr is more mobile since it is commonly weakly adsorbed as (oxy)anion (McBride, 1994; Fendorf, 1995; Ball and Nordstrom, 1998). Acidity influences the adsorption of Cr species to clay since, at increasing pH, the adsorption of Cr^{6+} decreases and that of Cr^{3+} increases. At increasing pH, the presence of organic matter can play a reducing action on Cr^{6+} which is converted into the more stable Cr^{3+} species. Trivalent chromium co-precipitates with Fe^{3+} as insoluble $\text{Cr}(\text{OH})_3$ at high pH values (De

Vos et al., 2006 and references therein). Chromium is a non-essential element for plants, but trivalent chromium is an essential/beneficial nutrient in trace amounts for sugar and cholesterol metabolism in humans and animals, whereas its hexavalent form Cr^{6+} is a potent carcinogen and extremely toxic to animals and humans (Zayed and Terry, 2003; Hooda, 2010).

Nickel is a transition metal of group 10 that has two main oxidation states (+2 and +3). Nickel occurs in many sulfides minerals, such as millerite (NiS), pentlandite [$(\text{Fe}, \text{Ni})_9\text{S}_8$], ullmannite (NiSbS), and gersdorffite (NiAsS). Nickel is generally present as a vicariant ion in ferromagnesian minerals (olivine, orthopyroxene, and spinel), because of its intermediate size of Ni^{+2} (between Fe^{+2} and Mg^{+2}). For these reasons nickel occurs in high concentrations in ultramafic ferromagnesian silicate rocks (peridotite and serpentinite) and can be concentrated to commercially exploitable contents in highly weathered ultramafic soils (laterites). Its concentration is generally about 2000 mg/kg in ultramafic rocks, where nickel is substituted for Mg^{2+} in olivine, pyroxenes, and serpentine. Nickel released from the weathering of these primary minerals can substitute magnesium in smectites, and nickel released from the weathering of pyroxenes can substitute magnesium in garnierite (Nahon et al., 1982a,b). Garnierite is a mixture of nickeliferous serpentine and nickeliferous talc (Trescases, 1997). In addition to serpentine minerals, Ni is recognized to accumulate in magnetite. The average concentration of Ni in rocks is 75 mg/kg. Nickel, like Cr, is also found in association with mafic and ultramafic rock formations and can reach up to 7000 mg/Kg. The common background range of average soil Ni content is less than 20 mg/kg but in the presence of ultramafic bedrocks such as serpentinites, values of more than 8000 mg/kg have been cited (Oze et al., 2004a; Hseu, 2006) (Table 1.1). Nickel is mobile under acidic and oxidizing conditions and can be co-precipitated with authigenic Fe–Mn oxides and hydroxides, clay minerals and organic matter; especially in surface soil horizons, Ni could also occur in organic compounds (De Vos et al., 2006 and references therein).

Nickel is an essential nutrient for animals and a beneficial element for plants (Phipps et al., 2002; Sharma et al., 2006; Hooda, 2010). As with other trace metals, elevated Ni concentrations in soils have a potential negative impact on plants, microorganisms, and animals (Thakali et al., 2006).

Cobalt is a transition metal of group 9 that is present under the geological condition, in the oxidation states of +2 and +3 (rarely +1). This element is found in Co-bearing minerals, such as erythrite $[\text{Co}_3(\text{AsO}_4)_2 \cdot (8\text{H}_2\text{O})]$, glaucodot $[(\text{Co}_{0.50}\text{Fe}_{0.50})\text{AsS}]$ and skutterudite (CoAs_3), as well as substituting into pyrite (FeS_2). It is commonly found in association with Ni within rocks and iron-rich meteorites. Divalent cobalt substitutes magnesium and iron in olivine and pyroxenes. Cobalt, in the Earth's crust, is highly concentrated in mafic and ultramafic rocks, up to 200 mg/kg, when compared to its content in acid igneous rocks (Table 1.1; Kabata-Pendias, 2011). The worldwide mean value of Co in surface soils is calculated as 10 mg/kg. Naturally high Co contents are observed in soils over serpentine rocks (up to 520 mg/kg). The geochemical cycle of Co closely resembles that of Fe and Mn cycling and is likely to be associated with several minerals of these metals. After weathering, Co is mobile in the surface environment under acidic and reducing conditions; it co-precipitates under oxidizing, near neutral or alkaline conditions as Fe and Mn secondary oxides (Taylor, 1968). Humic and fulvic acids and inorganic colloids could reduce Co mobility in soil while some bacteria are known to mobilize Co from metal chelates (De Vos et al., 2006 and references therein). Cobalt is considered an essential nutrient in trace amounts for ruminant animals, largely due to its requirement for rumen bacteria. It is also required for atmospheric N_2 -fixation by microorganisms and for plants. Cobalt may have some beneficial effect but is not essential as such for humans (Alloway, 2010).

Matrix	Chromium	Nickel	Cobalt
Earth's crust	126 – 185 [92]	20 – 75 [47]	9 – 12 [17]
Ultramafic rock	350 – 13000 [1800]	300 – 7000 [2000]	100 – 200 [150]
Mafic rock	170 – 3400 [200]	130 – 160 [140]	35 – 200 [50]
Acid rock	10 – 50 [20]	5 – 20 [8]	1 – 15 [10]
Sedimentary rock	5 – 120 [22]	5 – 90 [11]	0.1 – 20 [12]
Soils range	1 – 1500 [80]	0.2 – 450 [20]	0.05 – 300 [10]
Ultramafic soil	1100 – 6000 [3100]	900 – 8000 [2700]	10 – 520 [150]

Table 1.1 Range and average (in square bracket) of chromium, nickel, and cobalt in rocks and soils (Hooda et al., 2010; Kabata-Pendias, 2011 and reference therein; Albanese et al., 2015). Values are in mg/kg.

Environmental concerns

The soil is a dynamic system, resulting from the weathering of the bedrocks, and is subjected to several PTEs contaminations from both natural and anthropogenic sources (Antibachi et al., 2012). The soil quality in terms of PTEs concentrations has received considerable attention by the scientific community during the last decades, mostly because of the non-degradable nature of these chemical substances and the potential hazard that may pose to the human health and ecological systems (Kelepertsiz et al., 2013). Discriminating between geogenic and anthropogenic contributions with respect to total concentrations of PTEs is fundamental in the quantitative assessment of metal contamination threats to the ecosystem and human health (Soylak and Turkoglu, 1999; Soyлак et al., 2001; Albanese et al., 2007). To assess soil contamination, the PTEs concentration is often compared with some threshold limits and guideline values, fixed by the legislation of various countries. The EU Directive 86/278/EEC establishes the reference concentrations for some PTEs (i.e. Cd, Hg, Ni, Pb, Cu, and Zn) in European agricultural soil (Directive E.C., 1986). At the national level, there is a wide variation in statutory guideline values for PTEs in natural soil, as well as a large difference in values between similar geographical areas (Reimann and Garret, 2014 and references therein). Therefore, the reference guideline intervals established by the EU Directive for agricultural soil are not always aligned with the guidelines legislated by each of the European countries. In 1999, the Italian government established intervention values for some selected toxic elements (As, Cd, Co, Cr, Cu, Hg, Ni, Pb, Sb, Se, Tl, V, and Zn) in soil and stream water (D.M. 471/1999, abrogated and now replaced by D.Lgs 152/2006).

Ultramafic soils play an important role in environmental management due to the high natural content of PTEs (such as Cr, Ni, and Co; Caillaud et al., 2009) commonly exceeds, up to one order of magnitude, the concentration limits laid down by environmental agencies and governments (Kumarathilaka et al., 2014; Tashakor et al. 2014). These extremely high PTEs (e.g., Cr, Ni, and Co) concentrations are related to the abundance of PTEs-bearing minerals inherited by bedrocks. These PTEs-bearing minerals lead to soil metal concentrations above the limits allowed by legislation, impeding, therefore, to share anthropogenic from natural contribution using threshold concentrations when these minerals are present. Hence, one of the most complex problem to be faced

for ultramafic soils is the determination of background levels and baseline values for PTEs. Several attempts have been made to separate between anthropogenic and natural contributions on PTEs contents in soils (Galan et al., 2008, 2014; Bini et al., 2011; Kelepertizis et al., 2013). These approaches range from the statistic evaluation of the outliers, as reviewed by Reimann et al. (2005), to regressions between metals and Al and Fe (e.g., Delaune et al., 2008), to several enrichment factors such as the ratio between PTEs concentration in potentially contaminated and uncontaminated areas (e.g., Massas et al., 2009) or between the concentration in the topsoil and in subsoil (e.g., Blaser et al., 2000; van Gaans et al., 2007). Nevertheless, these approaches are poorly applicable to very heterogeneous soils, such as those forming on ultramafic bedrocks which are commonly characterized by significant compositional variation at regional, local and even site-specific scale (Caillaud et al., 2009; Bonifacio et al., 2010; Antibachi et al., 2012; Kelepertizis et al., 2013; Marescotti et al., 2015). Moreover, the local lithological context can have a higher influence than the processes of soil genesis on the concentration of PTEs in the soil (Galan et al., 2009, 2013; Bern, 2009; Taghipour et al., 2011; Stone et al., 2014; dos Santos et al., 2017); thus, the geochemical data can be drastically misinterpreted when the local information is ignored (Salminen and Tarvainen, 1997; Reimann and De Caritat, 2005; Gloaguen and Passe, 2017). Therefore, the assessment of soil contamination by the environmental agencies should consider its specific geochemical and geological contexts (Bonifacio et al., 2010).

In this scenario, to better define the geochemical background and discriminate the natural input to anthropic input, it is necessary to draw up a combined approach that integrates statistical methods at the national or regional scale (Albanese et al., 2007, 2015) with site-specific studies on PTEs in rocks and relative soils (Zhao et al., 2006). These site-specific studied have to include: i) a detailed mineralogical, textural, and structural analysis of bedrocks and derived profiles; ii) identification the type and state of the weathering processes; iii) evaluation of the role of mineral species in controlling the PTEs mobility during the evolution of the soil profiles.

1.2. AIMS OF PhD THESIS

Even if numerous authors present the detailed studies of metal mobility and their relationships between mineralogy and other soil properties (e.g., Vithanage et al., 2014; Alves et al., 2011; Caillaud et al., 2009), in literature, there are still few studies (Burgess et al., 2009; Kierzack et al., 2016) about the relationships among soil evolution and lithological, textural, and structural characteristics of the bedrock even though, they have an important role in the distribution and mobility of PTEs in ultramafic soils.

The main objective of this PhD thesis is to determinate the mineralogy and the chemistry of PTEs of ultramafic rocks and soils, to evaluate how lithological, textural, and structural properties of different ultramafic bedrocks with different degree of serpentinization and deformation may affect the re-distribution and the fate of PTEs in ultramafic soils during pedogenesis, as well as to assess their environmental implications in the ecosystem.

In summary, the specific aims of the individual chapters are reported:

1) Investigations on ultramafic rocks (Chapters IV and V):

- Description and classification of the ultramafic bedrocks according to lithological and (micro)structural-textural criteria (e.g., partially serpentinized lherzolites, massive serpentinite, and foliated serpentinites) from the Voltri Massif;
- Identification and analysis of the main PTEs-bearing mineral phases focus on microstructural and textural characteristics in relation to the bedrock textures and structures;
- Investigation of the influence of serpentinization degree, deformation processes, and textural and structural setting on the distribution of PTEs-bearing minerals;
- Comparison of bulk chemistry dataset (major, minor, and trace elements) with other ultramafic rocks around the world, focus on the lithological and structural-textural variations.

2) Investigations on ultramafic soil profiles (Chapter VI):

- General characterization of soils properties and pedogenetic processes;

- Determination of the chemical and mineralogical compositions of soils derived from different ultramafic bedrocks;
- Characterization of PTEs-bearing minerals among primary minerals (e.g., serpentine minerals, spinel-group minerals, and magmatic relicts) and authigenic minerals (e.g., clay minerals and Fe- and Mn-oxides) in order to clarify the behavior of PTEs at the microscale during weathering and pedogenesis;
- Creation of an essential geochemical and mineralogical database to forecast the fate of the PTEs in the rock-soil system and their potential leaching to groundwater;
- Comparison with similar ultramafic soils developed in others climatic or geologic context (e.g., Italian Apennines, French Massif Central, Vosges Mountains, and Franciscan Complex), that can help in understanding the impact of pedoclimatic factors on the PTEs distribution at profile scale.
- Comparison of the PTEs levels of studied soil respect to the world average soil composition and the law target of different countries;
- Identification of possible factors that can explain the geochemical element variability.

References

- Adriano, D.C. (2001). *Chromium*. In *Trace elements in terrestrial environments* (pp. 219-261). Springer, New York, NY.
- Aiglsperger, T., Proenza, J. A., Lewis, J.F., Labrador, M., Svojtka, M., Rojas-Purón, A., Longo, F., and Āurišová, J. (2016). *Critical metals (REE, Sc, PGE) in Ni laterites from Cuba and the Dominican Republic*. *Ore Geology Reviews*, 73, 127-147.
- Albanese, S., De Vivo, B., Lima, A., and Cicchella, D. (2007). *Geochemical background and baseline values of toxic elements in stream sediments of Campania region (Italy)*. *Journal of Geochemical Exploration*, 93(1), 21-34.
- Albanese, S., Sadeghi, M., Lima, A., Cicchella, D., Dinelli, E., Valera, P., Falconi, M., Demetriades, A., De Vivo, B., and the GEMAS Project Team (2015). *GEMAS: cobalt, Cr, Cu and Ni distribution in agricultural and grazing land soil of Europe*. *Journal of geochemical exploration*, 154, 81-93.
- Alexander, E.B., and DuShey, J. (2011). *Topographic and soil differences from peridotite to serpentinite*. *Geomorphology*, 135(3-4), 271-276.
- Alexander, E.B. (2004). *Serpentine soil redness, differences among peridotite and serpentinite materials, Klamath Mountains, California*. *International Geology Review*, 46(8), 754-764.
- Alexander, E.B. (2009). *Soil and vegetation differences from peridotite to serpentinite*. *Northeastern Naturalist*, 16(sp5), 178-192.
- Alexander, E.B. (2014). *Arid to humid serpentine soils, mineralogy, and vegetation across the Klamath Mountains, USA*. *Catena*, 116, 114-122.
- Alexander, E.B., Coleman, R.G., Harrison, S.P., and Keeler-Wolfe, T. (2007). *Serpentine geoecology of western North America: geology, soils, and vegetation*. OUP USA.

- Alliani, N. (1997). *Alterazione biologica di una roccia serpentinitica: simulazioni in vitro e in vivo*. Tesi di dottorato di ricerca, Università di Torino, pp 95
- Alloway, B.J. (2010). *Heavy metals in soils*. Springer, Dordrecht.
- Alves, S., Trancoso, M.A., Gonçalves, M.D.L.S., and dos Santos, M.M.C. (2011). A nickel availability study in serpentinitised areas of Portugal. *Geoderma*, 164(3-4), 155-163.
- Amir, H., and Pineau, R. (2003). Release of Ni and Co by microbial activity in New Caledonian ultramafic soils. *Canadian journal of microbiology*, 49(4), 288-293.
- Andreani, M., Munoz, M., Marcaillou, C., and Delacour, A. (2013). μ XANES study of iron redox state in serpentine during oceanic serpentinization. *Lithos*, 178, 70-83.
- Antibachi, D., Kelepertzis, E., and Kelepertsis, A. (2012). Heavy metals in agricultural soils of the Mouriki-Thiva area (central Greece) and environmental impact implications. *Soil and Sediment Contamination: An International Journal*, 21(4), 434-450.
- Ball, J.W., and Nordstrom, D.K. (1998). Critical evaluation and selection of standard state thermodynamic properties for chromium metal and its aqueous ions, hydrolysis species, oxides, and hydroxides. *Journal of Chemical and Engineering Data*, 43(6), 895-918.
- Baumeister, J.L., Hausrath, E.M., Olsen, A.A., Tschauner, O., Adcock, C.T., and Metcalf, R.V. (2015). Biogeochemical weathering of serpentinites: an examination of incipient dissolution affecting serpentine soil formation. *Applied Geochemistry*, 54, 74-84.
- Becquer, T., Quantin, C., Sicot, M., and Boudot, J.P. (2003). Chromium availability in ultramafic soils from New Caledonia. *Science of the Total Environment*, 301(1-3), 251-261.
- Bern, C.R. (2009). Soil chemistry in lithologically diverse datasets: the quartz dilution effect. *Applied Geochemistry*, 24(8), 1429-1437.
- Bini, C., Sartori, G., Wahsha, M., and Fontana, S. (2011). Background levels of trace elements and soil geochemistry at regional level in NE Italy. *Journal of Geochemical Exploration*, 109(1-3), 125-133.
- Blaser, P., Zimmermann, S., Luster, J., and Shotyk, W. (2000). Critical examination of trace element enrichments and depletions in soils: As, Cr, Cu, Ni, Pb, and Zn in Swiss forest soils. *Science of the Total Environment*, 249(1-3), 257-280.
- Bonifacio, E., Falsone, G., and Piazza, S. (2010). Linking Ni and Cr concentrations to soil mineralogy: does it help to assess metal contamination when the natural background is high? *Journal of Soils and Sediments*, 10(8), 1475-1486.
- Bonifacio, E., Zanini, E., Boero, V., and Franchini-Angela, M. (1997). Pedogenesis in a soil catena on serpentinite in north-western Italy. *Geoderma*, 75(1-2), 33-51.
- Burgess, J.L., Lev, S., Swan, C.M., and Szlavecz, K. (2009). Geologic and edaphic controls on a serpentine forest community. *Northeastern Naturalist*, 366-384.
- Butt, C.R., and Cluzel, D. (2013). Nickel laterite ore deposits: weathered serpentinites. *Elements*, 9(2), 123-128.
- Caillaud, J., Proust, D., and Righi, D. (2006). Weathering sequences of rock-forming minerals in a serpentinite: influence of microsystems on clay mineralogy. *Clays and Clay Minerals*, 54(1), 87-100.
- Caillaud, J., Proust, D., Philippe, S., Fontaine, C., and Fialin, M. (2009). Trace metals distribution from a serpentinite weathering at the scales of the weathering profile and its related weathering microsystems and clay minerals. *Geoderma*, 149(3-4), 199-208.
- Caillaud, J., Proust, D., Righi, D., and Martin, F. (2004). Fe-rich clays in a weathering profile developed from serpentinite. *Clays and Clay Minerals*, 52(6), 779-791.
- Chalot-Prat, F., Ganne, J., and Lombard, A. (2003). No significant element transfer from the oceanic plate to the mantle wedge during subduction and exhumation of the Tethys lithosphere (Western Alps). *Lithos*, 69(3-4), 69-103.
- Chardot, V., Echevarria, G., Gury, M., Massoura, S., and Morel, J. L. (2007). Nickel bioavailability in an ultramafic toposequence in the Vosges Mountains (France). *Plant and Soil*, 293(1-2), 7-21.

- Cheng, C.H., Jien, S.H., Iizuka, Y., Tsai, H., Chang, Y.H., and Hseu, Z.Y. (2011). Pedogenic chromium and nickel partitioning in serpentine soils along a toposequence. *Soil Science Society of America Journal*, 75(2), 659-668.
- Christensen, N.I. (1972). The abundance of serpentinites in the oceanic crust. *The Journal of Geology*, 80(6), 709-719.
- Cohen, M.D., Kargacin, B., Klein, C.B., and Costa, M. (1993). Mechanisms of chromium carcinogenicity and toxicity. *Critical reviews in toxicology*, 23(3), 255-281.
- Colás, V., González-Jiménez, J.M., Griffin, W. L., Fanlo, I., Gervilla, F., O'Reilly, S.Y., Pearson, N.J., Kerestedjian, T., and Proenza, J.A. (2014). Fingerprints of metamorphism in chromite: New insights from minor and trace elements. *Chemical Geology*, 389, 137-152.
- Coleman, R.G. (1971). Petrologic and geophysical nature of serpentinites. *Geological Society of America Bulletin*, 82(4), 897-918.
- Colin, F., Nahon, D., Trescases, J.J., and Melfi, A.J. (1990). Lateritic weathering of pyroxenites at Niquelandia, Goiás, Brazil; the supergene behavior of nickel. *Economic Geology*, 85(5), 1010-1023.
- Cortesogno, L., Mazzucotelli, A., and Vannucci, R. (1979). Alcuni esempi di pedogenesi su rocce ultrafemiche in clima mediterraneo. *Ofioliti*, 4, 295-312.
- Daugherty, M.L. (1992). Toxicity summary for chromium. Oak Ridge National Laboratory Chemical Hazard Evaluation and Communication Group, Oak Ridge, Tenn.
- De Vos, W., Tarvainen, T., Salminen, R., Reeder, S., De Vivo, B., Demetriades, A., and O'Connor, P. J. (2006). *Geochemical atlas of Europe. Part 2. Geological Survey of Finland, Espoo 2006.*
- Decreto Legislativo 3/04/2006 n° 152 "Norme in materia ambientale". G.U. 88. 14/04/2006.
- Decreto Ministeriale 25/10/1999 n° 471 "Regolamento recante criteri, procedure e modalità per la messa in sicurezza, la bonifica e il ripristino ambientale dei siti inquinati, ai sensi dell'articolo 17 del decreto legislativo 5 febbraio 1997, n. 22", e successive modificazioni e integrazioni. G.U. 293, 15/12/1999.
- DeLaune, R.D., and Reddy, K.R. (2008). *Biogeochemistry of wetlands: science and applications.* CRC press.
- Deschamps, F., Godard, M., Guillot, S., and Hattori, K. (2013). Geochemistry of subduction zone serpentinites: A review. *Lithos*, 178, 96-127.
- Dick, H.J., and Bullen, T. (1984). Chromian spinel as a petrogenetic indicator in abyssal and alpine-type peridotites and spatially associated lavas. *Contributions to mineralogy and petrology*, 86(1), 54-76.
- Directive, E.C. 86/278/EEC of 12 June 1986. Protection of the Environment, and in particular of the soil, when sewage sludge is used in Agriculture. Available online.
- dos Santos, L.M.R., Gloaguen, T.V., de Souza Fadigas, F., Chaves, J.M., and Martins, T.M.O. (2017). Metal accumulation in soils derived from volcano-sedimentary rocks, Rio Itapicuru Greenstone Belt, northeastern Brazil. *Science of The Total Environment*, 601, 1762-1774.
- Dublet, G., Juillot, F., Morin, G., Fritsch, E., Fandeur, D., and Brown, G.E. (2015). Goethite aging explains Ni depletion in upper units of ultramafic lateritic ores from New Caledonia. *Geochimica et Cosmochimica Acta*, 160, 1-15.
- Dublet, G., Juillot, F., Morin, G., Fritsch, E., Noel, V., Brest, J., and Brown Jr, G.E. (2014). XAS evidence for Ni sequestration by siderite in a lateritic Ni-deposit from New Caledonia. *American Mineralogist*, 99(1), 225-234.
- Echevarria, G. (2018). Genesis and behaviour of ultramafic soils and consequences for nickel biogeochemistry. In *Agromining: Farming for Metals* (pp. 135-156). Springer, Cham.
- Escartin, J., and Lin, J. (1998). Tectonic modification of axial crustal structure: Evidence from spectral analyses of residual gravity and bathymetry of the Mid-Atlantic Ridge flanks. *Earth and planetary science letters*, 154(1-4), 279-293.
- Estrade, N., Cloquet, C., Echevarria, G., Sterckeman, T., Deng, T., Tang, Y., and Morel, J. L. (2015). Weathering and vegetation controls on nickel isotope fractionation in surface ultramafic environments (Albania). *Earth and Planetary Science Letters*, 423, 24-35.

- Fendorf, S.E. (1995). Surface reactions of chromium in soils and waters. *Geoderma*, 67(1-2), 55-71.
- Foth, H.D. (1991). Fundamentals of soil science. *Soil Science*, 125(4), 272.
- Galán, E., Fernández-Caliani, J.C., González, I., Aparicio, P., and Romero, A. (2008). Influence of geological setting on geochemical baselines of trace elements in soils. Application to soils of South–West Spain. *Journal of Geochemical Exploration*, 98(3), 89-106.
- Galán, E., González, I., Romero, A., and Aparicio, P. (2014). A methodological approach to estimate the geogenic contribution in soils potentially polluted by trace elements. Application to a case study. *Journal of soils and sediments*, 14(4), 810-818.
- Garnier, J., Quantin, C., Guimarães, E., Garg, V.K., Martins, E.S., and Becquer, T. (2009). Understanding the genesis of ultramafic soils and catena dynamics in Niquelândia, Brazil. *Geoderma*, 151(3/4), 204-214.
- Gleeson, S. A., Herrington, R. J., Durango, J., Velásquez, C. A., and Koll, G. (2004). The mineralogy and geochemistry of the Cerro Matoso SA Ni laterite deposit, Montelíbano, Colombia. *Economic Geology*, 99(6), 1197-1213.
- Gloaguen, T.V., and Passe, J.J. (2017). Importance of lithology in defining natural background concentrations of Cr, Cu, Ni, Pb and Zn in sedimentary soils, northeastern Brazil. *Chemosphere*, 186, 31-42.
- Hirth, G., and Guillot, S. (2013). Rheology and tectonic significance of serpentinite. *Elements*, 9(2), 107-113.
- Hooda, P. (2010). Trace elements in soils. John Wiley and Sons.
- Hseu, Z.Y. (2006). Concentration and distribution of chromium and nickel fractions along a serpentinitic toposequence. *Soil Science*, 171(4), 341-353.
- Hseu, Z.Y., Tsai, H., Hsi, H.C., and Chen, Y.C. (2007). Weathering sequences of clay minerals in soils along a serpentinitic toposequence. *Clays and Clay Minerals*, 55(4), 389-401.
- Irvine, T.N. (1967). Chromian spinel as a petrogenetic indicator: Part 2. Petrologic applications. *Canadian Journal of Earth Sciences*, 4(1), 71-103.
- Isnard, S., L'huillier, L., Rigault, F., and Jaffré, T. (2016). How did the ultramafic soils shape the flora of the New Caledonian hotspot? *Plant and soil*, 403(1-2), 53-76.
- Iyer, K., Austrheim, H., John, T., and Jamtveit, B. (2008). Serpentinization of the oceanic lithosphere and some geochemical consequences: constraints from the Leka Ophiolite Complex, Norway. *Chemical Geology*, 249(1-2), 66-90.
- James, B.R., Petura, J.C., Vitale, R.J., and Mussoline, G.R. (1997). Oxidation-reduction chemistry of chromium: Relevance to the regulation and remediation of chromate-contaminated soils. *Soil and Sediment Contamination*, 6(6), 569-580.
- Kabata-Pendias, A. (2011). Trace elements in soils and plants. CRC press.
- Kelepertzis, E., Galanos, E., and Mitsis, I. (2013). Origin, mineral speciation and geochemical baseline mapping of Ni and Cr in agricultural topsoils of Thiva valley (central Greece). *Journal of Geochemical Exploration*, 125, 56-68.
- Kierczak, J., Neel, C., Aleksander-Kwaterczak, U., Helios-Rybicka, E., Bril, H., and Puziewicz, J. (2008). Solid speciation and mobility of potentially toxic elements from natural and contaminated soils: a combined approach. *Chemosphere*, 73(5), 776-784.
- Kierczak, J., Neel, C., Bril, H., and Puziewicz, J. (2007). Effect of mineralogy and pedoclimatic variations on Ni and Cr distribution in serpentine soils under temperate climate. *Geoderma*, 142(1-2), 165-177.
- Kierczak, J., Pędziwiatr, A., Waroszewski, J., and Modelska, M. (2016). Mobility of Ni, Cr and Co in serpentine soils derived on various ultrabasic bedrocks under temperate climate. *Geoderma*, 268, 78-91.
- Kumarathilaka, P., Dissanayake, C., and Vithanage, M. (2014). Geochemistry of serpentinite soils: A brief overview. *Journal of Geological Society of Sri Lanka Vol. 16*, 53-63
- Le Bas, M.J., and Streckeisen, A.L. (1991). The IUGS systematics of igneous rocks. *Journal of the Geological Society*, 148(5), 825-833.

- Lee, B.D., Graham, R.C., Laurent, T.E., and Amrhein, C. (2004). Pedogenesis in a wetland meadow and surrounding serpentinitic landslide terrain, northern California, USA. *Geoderma*, 118(3-4), 303-320.
- Lee, B.D., Sears, S.K., Graham, R.C., Amrhein, C., and Vali, H. (2003). Secondary mineral genesis from chlorite and serpentine in an ultramafic soil toposequence. *Soil Science Society of America Journal*, 67(4), 1309-1317.
- Legros, J.P. (1992) Soils of Alpine mountains. In: Martini, I.P., Chesworth, W. (eds) *Weathering soils and paleosoils, developments in Earth surface processes*, 2nd ed. Elsevier, Amsterdam, pp 55–181.
- Lessovaia, S.N., and Polekhovsky, Y.S. (2009). Mineralogical composition of shallow soils on basic and ultrabasic rocks of East Fennoscandia and of the Ural Mountains, Russia. *Clays and Clay Minerals*, 57(4), 476-485.
- Lessovaia, S.N., Dultz, S., Plötze, M., Andreeva, N., Polekhovsky, Y., Filimonov, A., and Momotova, O. (2016). Soil development on basic and ultrabasic rocks in cold environments of Russia traced by mineralogical composition and pore space characteristics. *Catena*, 137, 596-604.
- Marescotti, P., Solimano, M., Beccaris, G., Scotti, E., Crispini, L., Poggi, E., Brancucci, M., and Fornasaro, S. (2014). La presenza naturale di metalli nei suoli: criticità operative e possibili soluzioni. *ECO*, vol. 29, p. 60-63
- Massas, I., Ehaliotis, C., Gerontidis, S., and Sarris, E. (2009). Elevated heavy metal concentrations in top soils of an Aegean island town (Greece): total and available forms, origin and distribution. *Environmental Monitoring and Assessment*, 151(1-4), 105-116.
- Massoura, S.T., Echevarria, G., Becquer, T., Ghanbaja, J., Leclerc-Cessac, E., and Morel, J.L. (2006). Control of nickel availability by nickel bearing minerals in natural and anthropogenic soils. *Geoderma*, 136(1-2), 28-37.
- McBride, M.B. (1994). *Environmental chemistry of soils*. Oxford Univ. Press, New York.
- McCollom, T.M., and Seewald, J.S. (2013). Serpentinites, hydrogen, and life. *Elements*, 9(2), 129-134.
- Miller, D.J., and Christensen, N.I. (1997). Seismic velocities of lower crustal and upper mantle rocks from the slow-spreading Mid-Atlantic Ridge, south of the Kane Transform Zone (MARK). In *PROCEEDINGS-OCEAN DRILLING PROGRAM SCIENTIFIC RESULTS* (pp. 437-456). NATIONAL SCIENCE FOUNDATION.
- Morrison, J.M., Goldhaber, M.B., Lee, L., Holloway, J.M., Wanty, R.B., Wolf, R.E., and Ranville, J.F. (2009). A regional-scale study of chromium and nickel in soils of northern California, USA. *Applied Geochemistry*, 24(8), 1500-1511.
- Nahon, D., Colin, F., and Tardy, Y. (1982a). Formation and distribution of Mg, Fe, Mn-smectites in the first stages of the lateritic weathering of forsterite and tephroite. *Clay Minerals*, 17(3), 339-348.
- Nahon, D.B., Paquet, H., and Delvigne, J. (1982b). Lateritic weathering of ultramafic rocks and the concentration of nickel in the western Ivory Coast. *Economic Geology*, 77(5), 1159-1175.
- Oze, C., Fendorf, S., Bird, D.K., and Coleman, R.G. (2004a). Chromium geochemistry in serpentinized ultramafic rocks and serpentine soils from the Franciscan complex of California. *American Journal of Science*, 304(1), 67-101.
- Oze, C., Fendorf, S., Bird, D.K., and Coleman, R.G. (2004b). Chromium geochemistry of serpentine soils. *International Geology Review*, 46(2), 97-126.
- Phipps, T., Tank, S.L., Wirtz, J., Brewer, L., Coyner, A., Ortego, L.S., and Fairbrother, A. (2002). Essentiality of nickel and homeostatic mechanisms for its regulation in terrestrial organisms. *Environmental Reviews*, 10(4), 209-261.
- Quantin, C., Becquer, T., and Berthelin, J. (2002). Mn-oxide: a major source of easily mobilisable Co and Ni under reducing conditions in New Caledonia Ferralsols. *Comptes Rendus Geoscience*, 334(4), 273-278.

- Quantin, C., Ettler, V., Garnier, J., and Šebek, O. (2008). Sources and extractibility of chromium and nickel in soil profiles developed on Czech serpentinites. *Comptes Rendus Geoscience*, 340(12), 872-882.
- Reimann, C., and de Caritat, P. (2005). Distinguishing between natural and anthropogenic sources for elements in the environment: regional geochemical surveys versus enrichment factors. *Science of the Total Environment*, 337(1-3), 91-107.
- Reimann, C., and Garrett, R.G. (2005). Geochemical background—concept and reality. *Science of the total environment*, 350(1-3), 12-27.
- Reinen, L.A., Weeks, J.D., and Tullis, T.E. (1994). The frictional behavior of lizardite and antigorite serpentinites: Experiments, constitutive models, and implications for natural faults. *Pure and Applied Geophysics*, 143(1-3), 317-358.
- Roberts, B.A., and Proctor, J. (Eds.). (1991). *The ecology of areas with serpentinized rocks: a world view* (Vol. 17). Springer Science and Business Media.
- Rouméjon, S., Cannat, M., Agrinier, P., Godard, M., and Andreani, M. (2015). Serpentinization and fluid pathways in tectonically exhumed peridotites from the Southwest Indian Ridge (62–65 E). *Journal of Petrology*, 56(4), 703-734.
- Salminen, R., and Tarvainen, T. (1997). The problem of defining geochemical baselines. A case study of selected elements and geological materials in Finland. *Journal of geochemical exploration*, 60(1), 91-98.
- Schwertmann, U.T.R.M., and Taylor, R.M. (1989). Iron oxides. *Minerals in soil environments, (mineralsinsoile)*, 379-438.
- Shanker, A.K., Cervantes, C., Loza-Tavera, H., and Avudainayagam, S. (2005). Chromium toxicity in plants. *Environment international*, 31(5), 739-753.
- Sharma, S.D., Singh, D., Saini, K.K., Kant, C., Sharma, V., Jain, S.C., and Sharma, C.P. (2006). Sol-gel-derived super-hydrophilic nickel doped TiO₂ film as active photo-catalyst. *Applied Catalysis A: General*, 314(1), 40-46.
- Soylak, M., and Türkoglu, O. (1999). Trace metal accumulation caused by traffic in an agricultural soil near a motorway in Kayseri, Turkey. *Journal of Trace and Microprobe Techniques*, 17(2), 209-217.
- Soylak, M., Elci, L., and Dogan, M. (2001). Solid phase extraction of trace metal ions with Amberlite XAD resins prior to atomic absorption spectrometric analysis. *Journal of Trace and microprobe techniques*, 19(3), 329-344.
- Stone, M., Collins, A.L., Silins, U., Emelko, M.B., and Zhang, Y.S. (2014). The use of composite fingerprints to quantify sediment sources in a wildfire impacted landscape, Alberta, Canada. *Science of the Total Environment*, 473, 642-650.
- Taghipour, M., Ayoubi, S., and Khademi, H. (2011). Contribution of lithologic and anthropogenic factors to surface soil heavy metals in western Iran using multivariate geostatistical analyses. *Soil and Sediment Contamination: An International Journal*, 20(8), 921-937.
- Tashakor, M., Yaacob, W.Z.W., Mohamad, H., and Ghani, A.A. (2014). Geochemical characteristics of serpentinite soils from Malaysia. *Malays J Soil Sci*, 18, 35-49.
- Taylor, R.M. (1968). The association of manganese and cobalt in soils—further observations. *Journal of Soil Science*, 19(1), 77-80.
- Thakali, S., Allen, H.E., Di Toro, D.M., Ponizovsky, A.A., Rooney, C.P., Zhao, F. J., and McGrath, S.P. (2006). A terrestrial biotic ligand model. 1. Development and application to Cu and Ni toxicities to barley root elongation in soils. *Environmental Science and Technology*, 40(22), 7085-7093.
- Treescases, J.J. (1997). *The lateritic nickel-ore deposits. In Soils and sediments (pp. 125-138). Springer, Berlin, Heidelberg.*
- Trolard, F., Bourrie, G., Jeanroy, E., Herbillon, A.J., and Martin, H. (1995). Trace metals in natural iron oxides from laterites: A study using selective kinetic extraction. *Geochimica et Cosmochimica Acta*, 59(7), 1285-1297.

- van der Ent, A., Cardace, D., Tibbett, M., and Echevarria, G. (2018). Ecological implications of pedogenesis and geochemistry of ultramafic soils in Kinabalu Park (Malaysia). *Catena*, 160, 154-169.
- Van Gaans, P.F. M., Spijker, J., Vriend, S.P., and De Jong, J.N. (2007). Patterns in soil quality: natural geochemical variability versus anthropogenic impact in soils of Zeeland, The Netherlands. *International Journal of Geographical Information Science*, 21(5), 569-587.
- Vithanage, M., Rajapaksha, A.U., Oze, C., Rajakaruna, N., and Dissanayake, C.B. (2014). Metal release from serpentine soils in Sri Lanka. *Environmental Monitoring and Assessment*, 186(6), 3415-3429.
- Viti, C., and Mellini, M. (1998). Mesh textures and bastites in the Elba retrograde serpentinites. *European Journal of Mineralogy*, 10(6), 1341-1359.
- Wicks, F.J., and Whittaker, E.J.W. (1977). Serpentine textures and serpentinization. *The Canadian Mineralogist*, 15(4), 459-488.
- Zayed, A.M., and Terry, N. (2003). Chromium in the environment: factors affecting biological remediation. *Plant and soil*, 249(1), 139-156.
- Zhao, F.J., McGrath, S.P., and Merrington, G. (2007). Estimates of ambient background concentrations of trace metals in soils for risk assessment. *Environmental Pollution*, 148(1), 221-229.

Chapter II

Study area

In *Chapter II* the main geographical, geomorphological, pedological and geological characteristics of Voltri Massif (VM) are summarized in the following paragraphs. A detail description of studied sites is also provided.

2.1. THE VOLTRI MASSIF

The study area is located in the highlands of western Liguria, northwest Italy, among the municipalities of Sassello (SV), Urbe (SV), Pontinvrea (SV), and Tiglieto (GE). From the geological point of view, the study area belongs entirely to the Voltri Massif (Ligurian Alps, Italy – Chiesa et al., 1975; Fig. 2.1). Even if the mineralogy, petrology, and geology of the ultramafic rocks of the Voltri Massif are deeply and well investigated (e.g., Ernst and Piccardo, 1979; Scambelluri et al., 1991; Piccardo et al., 2001; Capponi and Crispini, 2002; Rampone et al., 2005; Federico et al., 2007; Borghini et al., 2007; Padovano et al., 2015; Cannaó et al., 2016), the relationship between these rocks and the soil developed at their top, particularly in term of PTEs concentration and their mobility, has been poorly studied (Cortesogno et al., 1979; Bonifacio et al., 1997).

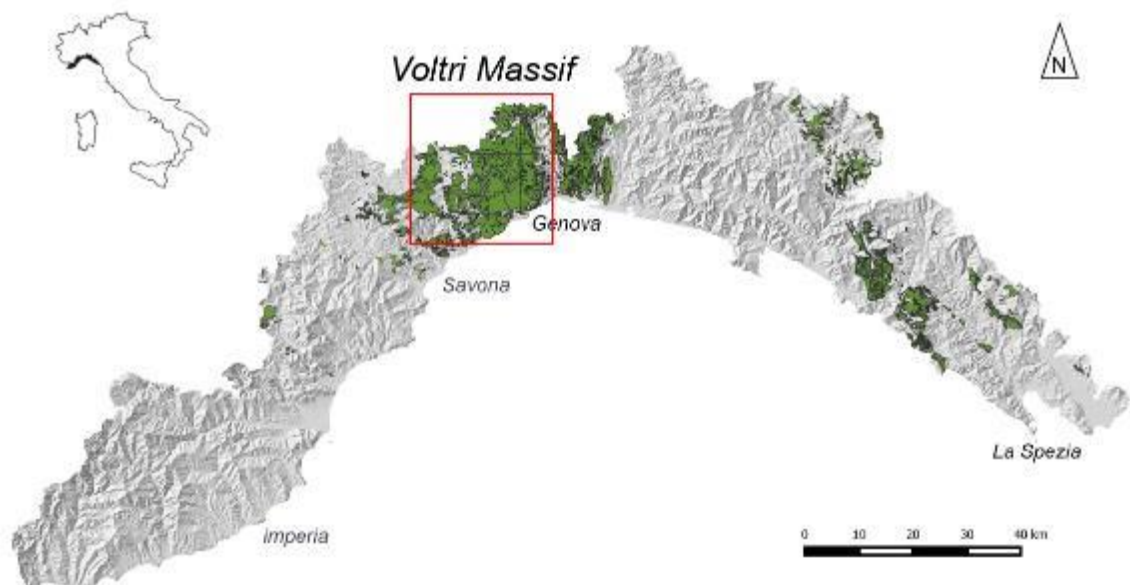


Fig. 2.1A Ophiolite complexes of Ligurian Region (Geoportale Regione Liguria, 2018). In the red box the Voltri Massif.



Fig. 2.1B Location of the studied sites (Images from Google Earth®). In red dashed line the study area.

2.1.1. Geography and Geomorphology

The Voltri Massif (VM) is located in the eastern sector of the Ligurian Alps (NW Italy), along the watershed between the Po river basin and the Tyrrhenian sea. The VM is bounded by the Erro and Orba river to the north, by the Stura and Cerusa valleys to the east, by the Ligurian sea to the south, and by the Sansobbia valley to the west (Fig. 2.2). The VM contains several summits higher than 1000 m a.s.l., with the highest at 1287 m a.s.l. (Mt. Beigua).



Fig. 2.2 Watershed (red line) maps, with the main Ligurian rivers (modified after Sacchini et al., 2012).

From a geomorphological point of view the northern slope of VM, dipping to the Po river basin, is characterized by wide valleys rich in terraces and gently tilted surfaces that are deeply influenced by running water erosion processes, increased by human activities (Firpo et al., 2006). Erosion due to running water is particularly enhanced along the steepest slopes of serpentinite rocks where the erosion exceeds the rate of soil formation, especially in areas affected by intense forest clearance. Well-developed soils one to several meters thick are preserved on protected planar landforms and slopes. The high part of the slope is characterized by the accumulation of large blocks with morphological features related to the creep and/or the gelifluction processes tentatively attributed to permafrost conditions during the Würm (blockfields and blockstreams; Firpo et al., 2006).

On the other hand, south sector, dipping to Tyrrhenian sea and with its watershed very close to the sea, is generally high and abrupt with promontories alternating with plains of limited amplitude (Firpo et al., 2006). The average slopes of the Tyrrhenian valleys range between 10 and 30 degrees. Because of high relief energy and tectonics on hydrography, the water courses are very short, with a low hierarchic organization and a very high transport capacity, especially during exceptional floods (Scopesi et al., 2017). The coastal strip is also subject to tectonic dislocations and is also characterized by the presence of relict-terraced landforms of marine origin, which are generally related to the repeated transgression/regression cycles caused by Quaternary tectonics and climatic fluctuations (Carobene and Firpo, 1994, 2002).

The hydrographic network of VM primarily follows the tectonic lineations, and the watercourses are primarily of a torrential type, consisting of valleys incised with V-shaped cross-sections (Firpo et al., 2006).

2.1.2. Climate and Pedology

The climatic features of Liguria are mainly determined by the topography, vertical relief (hilly or mountainous), and close to the sea. Liguria marks the transition between “Hot-summer Mediterranean climate” on one south side (Csa-type, sensu Köppen, 1936), and “Temperate oceanic climate” (Cfb-type, sensu Köppen, 1936) on the north side, the latter being characteristic of the southwestern part of the Po plain (Pinna, 1970; Marsili et al., 2009).

In the north slope, the data published from ARPA-Regione Liguria (weather stations of Sassello, 385 m a.s.l., Piampaludo, 865 m a.s.l., and Urbe, 810 m a.s.l.) showed mean annual precipitation ranges from 1000 to 1400 mm/y and mean annual temperatures from 9.1°C to 10.2°C (Fig. 2.3). The ombrothermic diagram (Rellini et al., 2009; 2014) shows two distinct rainy seasons with maxima in April and October and with a clear precipitation decrease between July and August. On the south slope, according to the data of the ARPA-Regione Liguria (weather station of Varazze, 22 m a.s.l.), the monthly temperatures vary from a minimum of 5 °C (in January and February) to a maximum of 28–29°C (recorded in August and July), with an average temperature of 15°C. Rainfall ranges between 1100 and 1600 mm/y and shows a unimodal distribution with a maximum in November (180 mm) and a dry season in summer (35 mm).

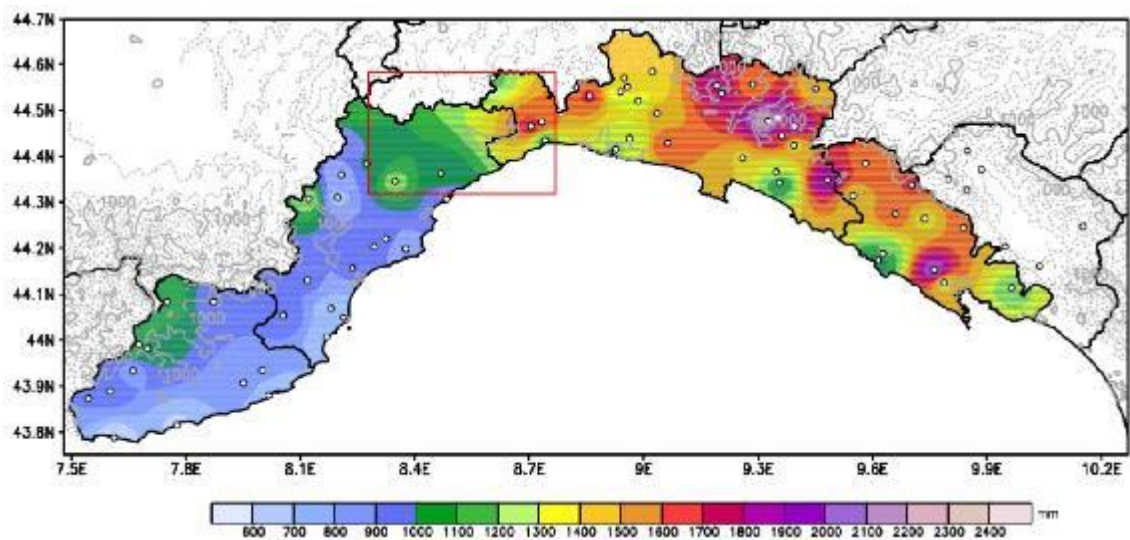


Fig. 2.3 Cumulative rainfall map over the Liguria Region (annual average 1961-2010). In red box the VM area.

The present pedoclimate (sensu USDA, 2003) is characterized by a mesic, locally cryic, soil temperature regime associated with an udic soil moisture regime (Costantini et al., 2004; Marsili et al., 2009). According to the FAO-WRB classification (IUSS, 2015), soils of this landscape are primarily of Humic, Skeletic Regosol, and Hypereutric or Dystric Cambisol (Scopesi, 2009).

From a vegetational point of view, the area can be considered transactional: in a very restricted area, it passes from the coastal environment to a mountain environment with altitudes around 1000 m a.s.l. Therefore, following this morphological structure that also influences the climatic conditions, there is the coexistence between the thermophilous plant species (e.g., *Quercus ilex* L., *Quercus pubedcens* Willd., *Pistacia terebinthus* L., *Pistacia lentiscus* L., *Myrtus*

communis L.) and species characteristic of higher altitudes (e.g., *Pinus sylvestris* L., *Sorbus aria* L.; Cortesogno et al., 1979).

2.1.3. Geology

The Voltri Massif is a wide (about 800 km²) metaophiolitic massif located at the southernmost termination of the Western Alps (Ligurian Alps, NW Italy; Fig. 2.4).

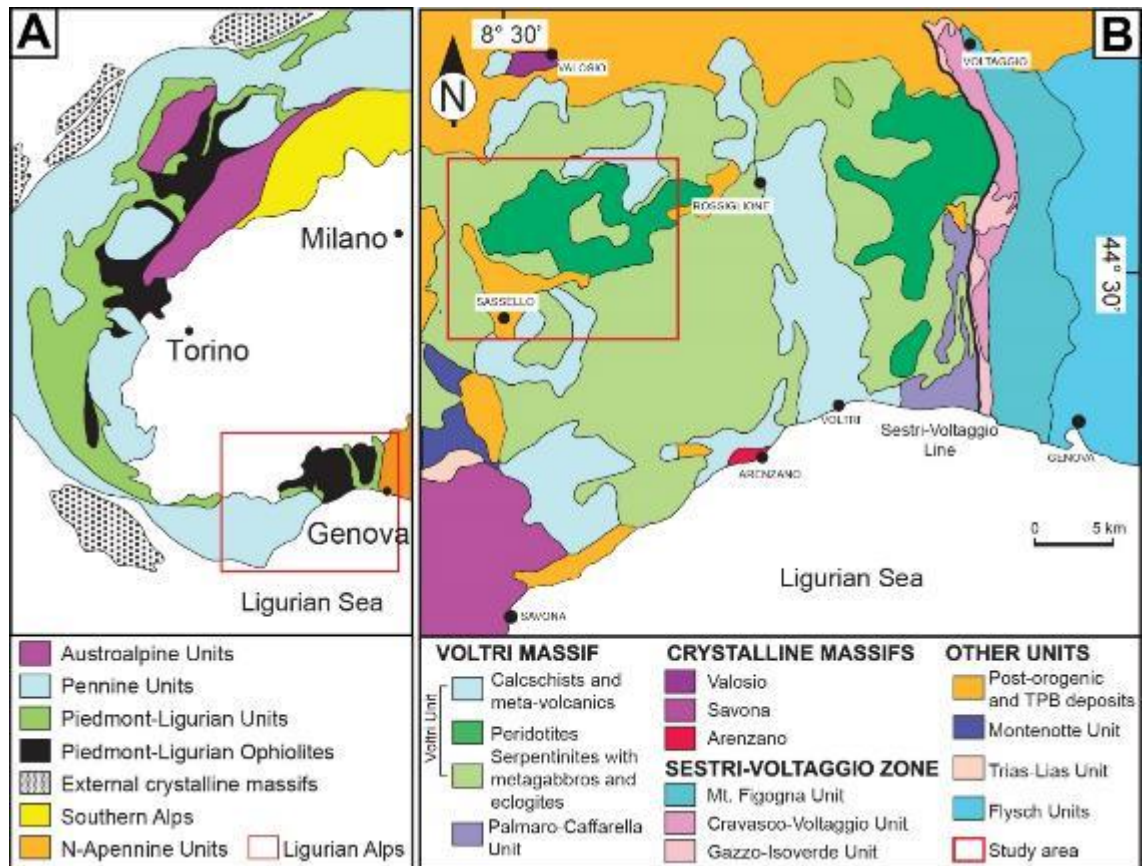


Fig. 2.4 A) Sketch of the Western Alps; B) Structural sketch map of the Voltri Massif (modified after Capponi and Crispini, 2002).

The VM represents a remnant of the Jurassic Ligurian Tethys and is composed by tectono-metamorphic units accreted during the Alpine orogenesis (e.g., Messiga and Piccardo, 1974; Piccardo, 1984; Vanossi, 1984; Capponi and Crispini, 2008 and references therein); these units consist mainly of mafic to ultramafic rocks derived from different paleogeographic domains, including subcontinental mantle, oceanic lithosphere with sedimentary covers and subordinate continental crust (Vanossi, 1984; Piccardo, 1984). These units have a polyphase tectono-metamorphic evolution with blueschist- to eclogite facies peak metamorphism and variable retrogressive overprints down to greenschist facies (e.g., Cortesogno et al., 1977; Cimmino et al., 1979; Messiga and Scambelluri, 1991; Scambelluri et al., 1995; Capponi and Crispini, 2002, 2008;

Federico et al., 2007; Vignaroli et al. 2010; Malatesta et al., 2012; Capponi et al., 2016; Scarsi et al., 2018).

In the VM ultramafic rocks are both mantle peridotite (i.e., Erro-Tobbio peridotite; Chiesa et al., 1975; Piccardo, 1977; Scambelluri et al., 1995; Piccardo and Vissers, 2007) and oceanic lithosphere serpentinite (Chiesa et al., 1975; Piccardo, 1977; Scambelluri et al., 1991). The Voltri Unit, which underwent eclogite-facies Alpine peak metamorphism, makes up the greatest part of the Voltri Massif, including the studied sites.

Peridotites (*Peridotiti Iherzolitiche del Monte Tobbio Formation*; Capponi and Crispini, 2008; Capponi et al., 2016) occur as km-scale bodies and consist mainly of spinel- and plagioclase-bearing Iherzolite, with some harzburgite, dunite lenses and pyroxenite bands, with various degree of serpentinization that develops mainly along a network of anastomosing and cross-cutting shear zones; the serpentinitic shear zones separate domains of peridotite with little or no coeval ductile deformation (Scambelluri et al., 1991). Most of the serpentinite mylonite zones shows a gradual transition from partially serpentinized peridotite to strongly foliated serpentinite mylonite. This transition reflects progressive synkinematic hydration of the peridotite within shear zones (Scambelluri et al., 1991). Even if peridotites underwent local oceanic serpentinization and HP-LT recrystallization attained during the Alpine orogeny (Chiesa et al., 1975; Rampone et al. 2005; Capponi and Crispini, 2008; Capponi et al. 2016), they still preserve textures and mineralogical associations of the pre-Alpine mantle evolution. The preserved mineralogical association includes olivine, ortho- and clino-pyroxene, spinel and plagioclase (Messiga and Piccardo, 1974; Piccardo, 1984, Capponi and Crispini, 2008). The ocean-floor metamorphism produced the partial transformation of the original mantle assemblages to mesh-textured antigorite, with minor chrysotile (after olivine), bastites and/or tremolitic amphiboles (after pyroxenes), magnetite (after spinels), and chlorite (Scambelluri et al., 1991).

The prograde Alpine evolution is instead reflected by the development of antigorite, magnetite, and brucite and later Ti-clinohumite, olivine, diopside, magnetite, and chlorite, which cross cut earlier mantle and oceanic assemblages (Scambelluri et al., 1991 and references therein). During the metamorphic peak, all the above microtextures are statically overgrown by neoblastic olivine, antigorite, Ti-clinohumite, and magnetite preferentially developed over mantle olivine, and by new diopside that replaced previous mantle pyroxenes. The early

retrograde stage is marked by the static overgrow of antigorite and Fe-oxides or antigorite and brucite on the peak assemblages, whereas the latest stages are characterized by coronitic tremolite and chrysotile rims in between mantle diopside relics and granular olivine, antigorite, and minor Ti-clinohumite aggregates (Scambelluri et al., 1991).

In the VM, antigoritic-serpentinites (*Serpentinoscisti antigoritici del Bric Del Dente* Formation; Capponi and Crispini, 2008; Capponi et al., 2016) is the most abundant lithotype, cropping out over a total area of more than 200 km² (Malatesta, 2011). They are composed of antigorite-bearing massive serpentinites and antigorite-bearing serpentine schists, sometimes with textural relics of the mantle peridotites. Gradual transitions from massive and essentially undeformed to strongly foliated serpentinite occurs over the entire area (Hoogerduijn Strating, 1991). Serpentinites are commonly characterized by a pervasive composite schistosity, with multiple folding phases of folds and shear bands (Hoogerduijn Strating, 1991; Scambelluri et al., 1991; Liou et al., 1998; Hermann et al., 2000, Crispini and Capponi, 2001; Capponi and Crispini, 2002; Malatesta et al., 2012; Federico et al. 2015; Capponi et al. 2016). In antigorite-bearing serpentine schists the main foliation is defined by the preferential orientation of antigorite, chlorite, and magnetite (Cimmino et al., 1979, Messiga et al., 1983). Along local shear bands, a composite fabric with crenulation cleavage is commonly developed and the mineralogical assemblage is replaced by fine grained of olivine, antigorite, chlorite, diopside, and Ti-clinohumite (Hoogerduijn Strating, 1991) or olivine, Ti-clinohumite, magnetite, minor antigorite and diopside (Scambelluri et al., 1991). The growth of the olivine-bearing assemblage is interpreted as a result of the progressive synkinematic dehydration of antigorite and therefore during progressively changing metamorphic conditions. Olivine-bearing assemblages (olivine, Ti-clinohumite, magnetite, antigorite, and minor diopside) also occur in small veins crosscutting the foliation and the extensional crenulation cleavage. The composite fabric and the olivine-bearing veins are deformed by small scale folds accompanied by a new crenulation cleavage that is associated with the growth of antigorite and magnetite after olivine (Hoogerduijn Strating, 1991; Scambelluri et al., 1991).

At the contact between serpentinites and other lithologies (e.g. metasediments and mafic bodies), intercalations or reaction rims of either chlorite-/talc-schist or tremolite-chlorite schists (i.e., "hybrid" rocks, Spandler et al., 2008), including

chlorite, talc, tremolite, actinolite, albite, titanite and magnetite, are common (Hoogerduijn Strating, 1991; Federico et al., 2007; Malatesta et al., 2012).

2.1.4. Study sites

Eight study sites were selected based on the following criteria (Fig. 2.5 and 2.6 and Table 2.1):

- i) degree of serpentinization (i.e., partially serpentinized lherzolites, relics-bearing serpentinite, massive serpentinites, serpentine schists);
- ii) textural feature (i.e., massive or foliated serpentinites);
- iii) structural feature (i.e., presence of one or more sets of veins or fractures, shear zones, lithological or tectonic contact with others lithology);
- iv) degree of weathering and degree of soil profile evolution.

The choice of the most suitable sampling sites was also subject to accessibility since it is commonly limited by slope acclivity and bushy vegetation. In fact, the rock cropping out in each study sites represent generally about the 30-40% of the entire area, due to the presence of bushy vegetation. The studied sites mostly occur close to road cuts, abandoned quarry, or stream banks. A detailed database of each sites is reported in *Appendix A*.

Site	Sign	Rock	Typology	Coordinate	Altitude (m a.s.l.)	Slope exposition
Bric Gippone	BG	MS/FS	Road cut	44°29'12.0"N, 8°30'51.5"E	585	S
Badia Tiglieto	BT	FS	Abandoned quarry	44°31'31.6"N, 8°36'06.7"E	380	S
Case Lavrin	CL	FS	Abandoned quarry	44°29'46.9"N, 8°35'10.4"E	668	ESE
Diga Antenna	DA	FS (TC)	Road cut	44°28'56.1"N, 8°35'45.4"E	580	SW
Strada Giusvalla	GIU	MS	Road cut	44°26'53.1"N, 8°25'32.4"E	433	SE
Rocca Grin	RG	PSP	Abandoned quarry	44°30'10.2"N, 8°32'32.5"E	626	SW
Strada Ferriera	SF	MS	Road cut	44°26'02.3"N, 8°25'27.7"E	576	SSE
Torrente Orba	TO	FS (TC)	Stream banks/Abandoned quarry	44°31'02.7"N, 8°37'22.8"E	418	W

Table 2.1 Geographical and lithological information of studied sites. PSP = partially serpentinized lherzolites; MS = massive serpentinite; FS = foliated serpentinite; TC = tremolite-chlorite hybrid rocks)

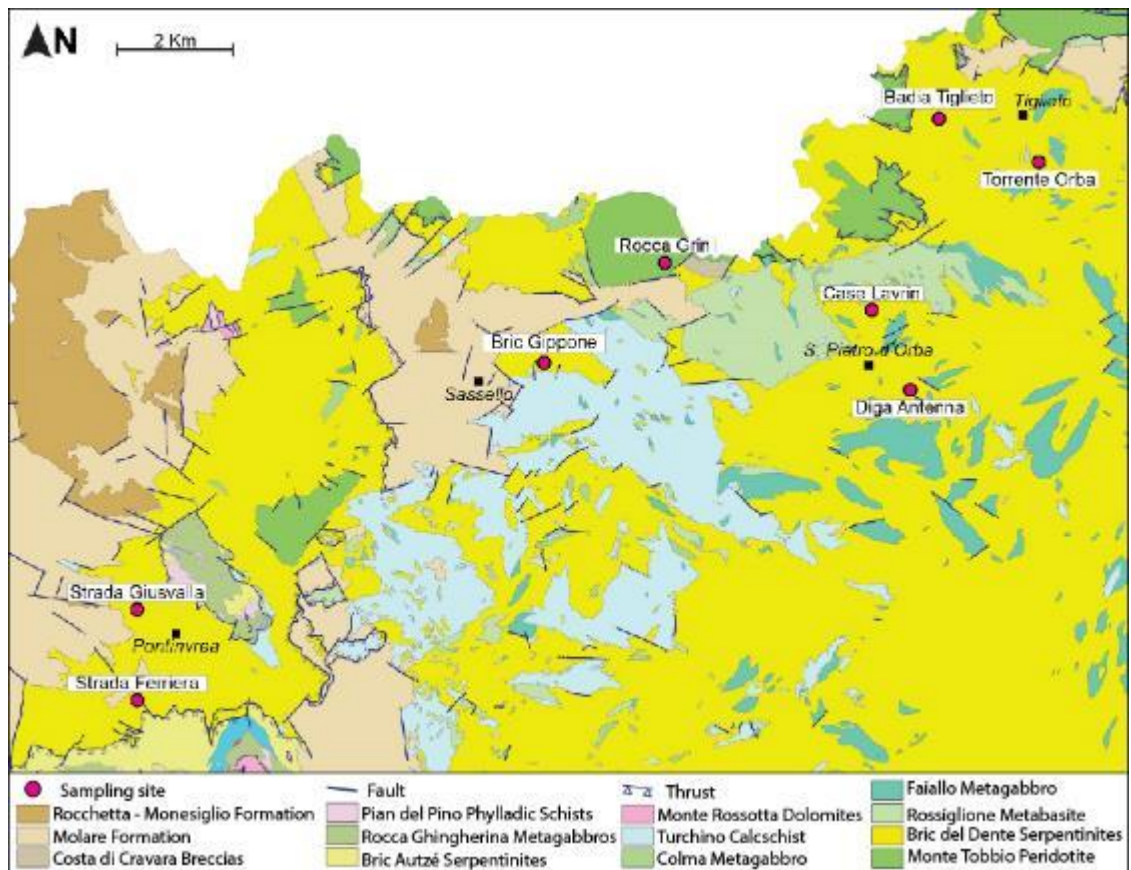


Fig. 2.5 Geological map of the study area with sampling sites location (modified after Capponi et al., 2013).

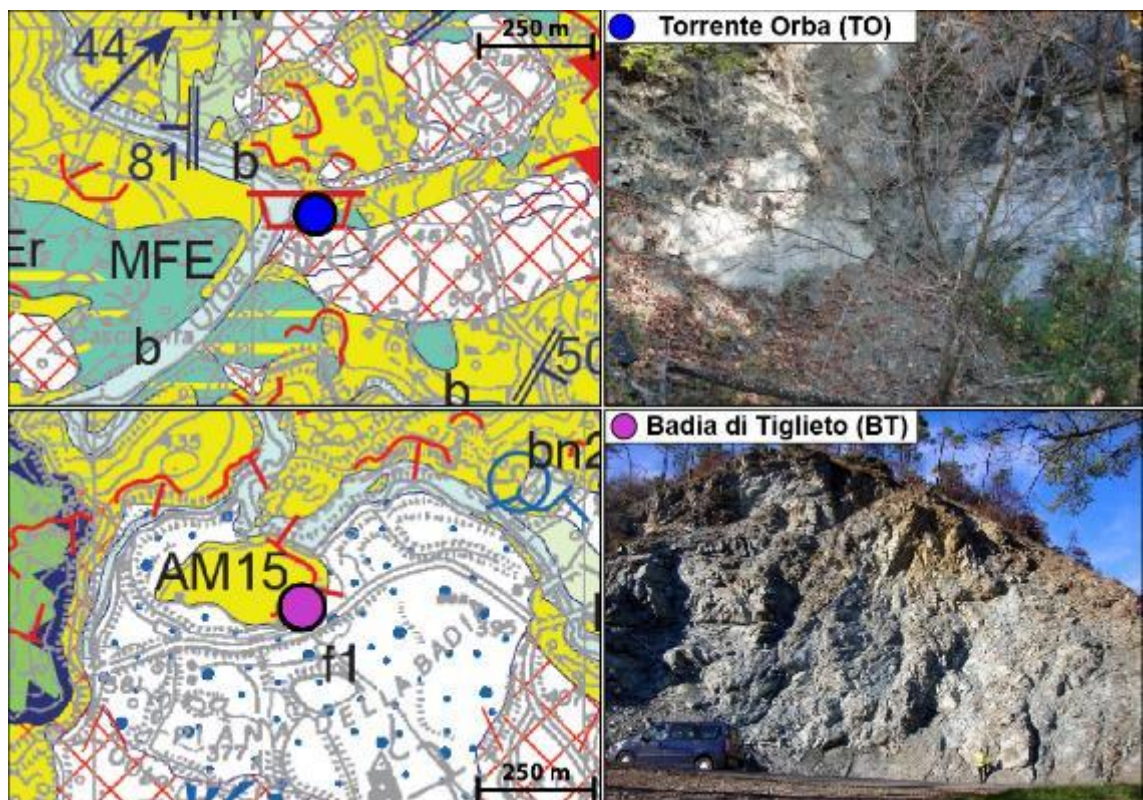


Fig. 2.6 Studied sites overview and relative geological map. See Fig. 2.5 for geological legend.

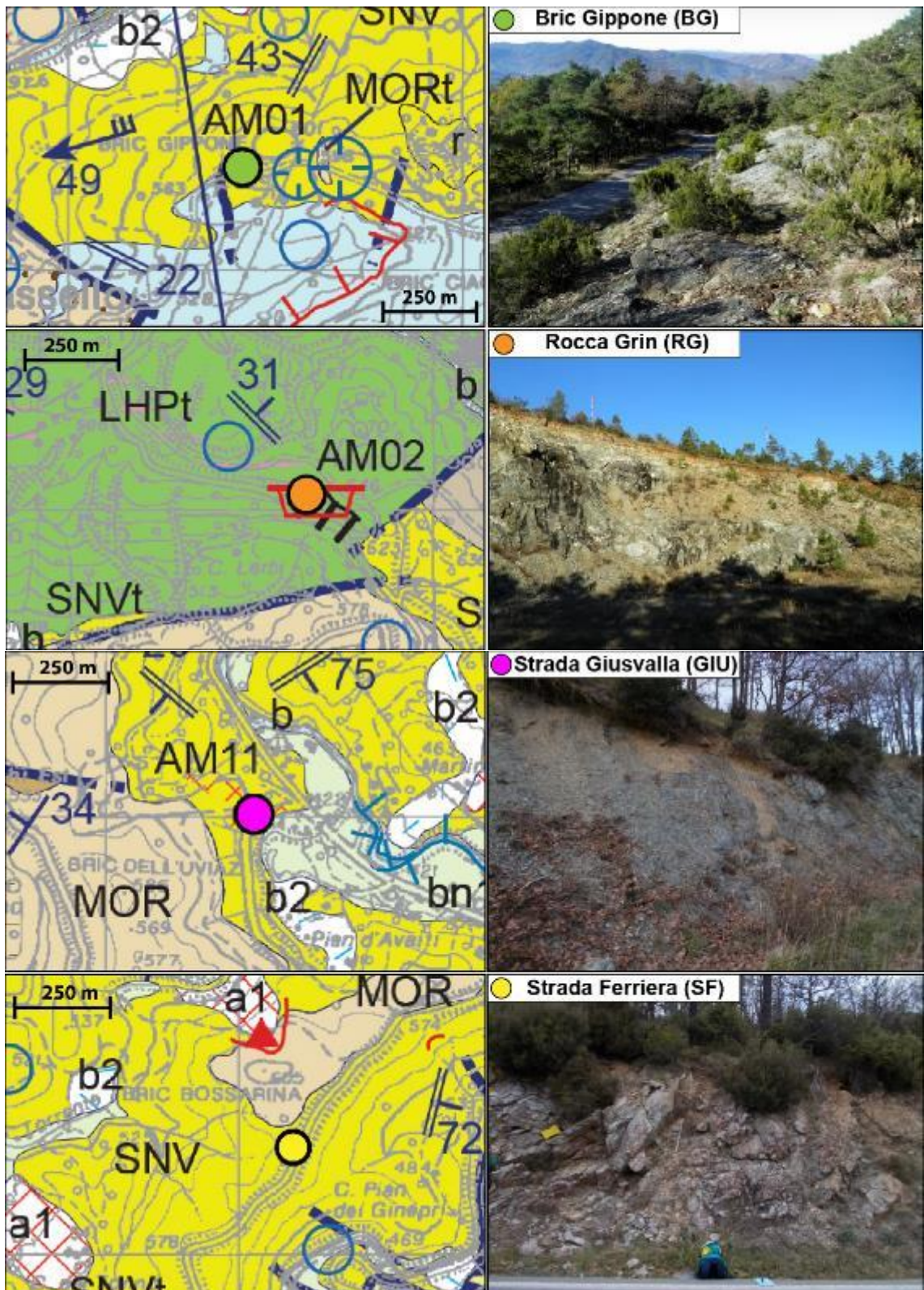


Fig. 2.6 Continued

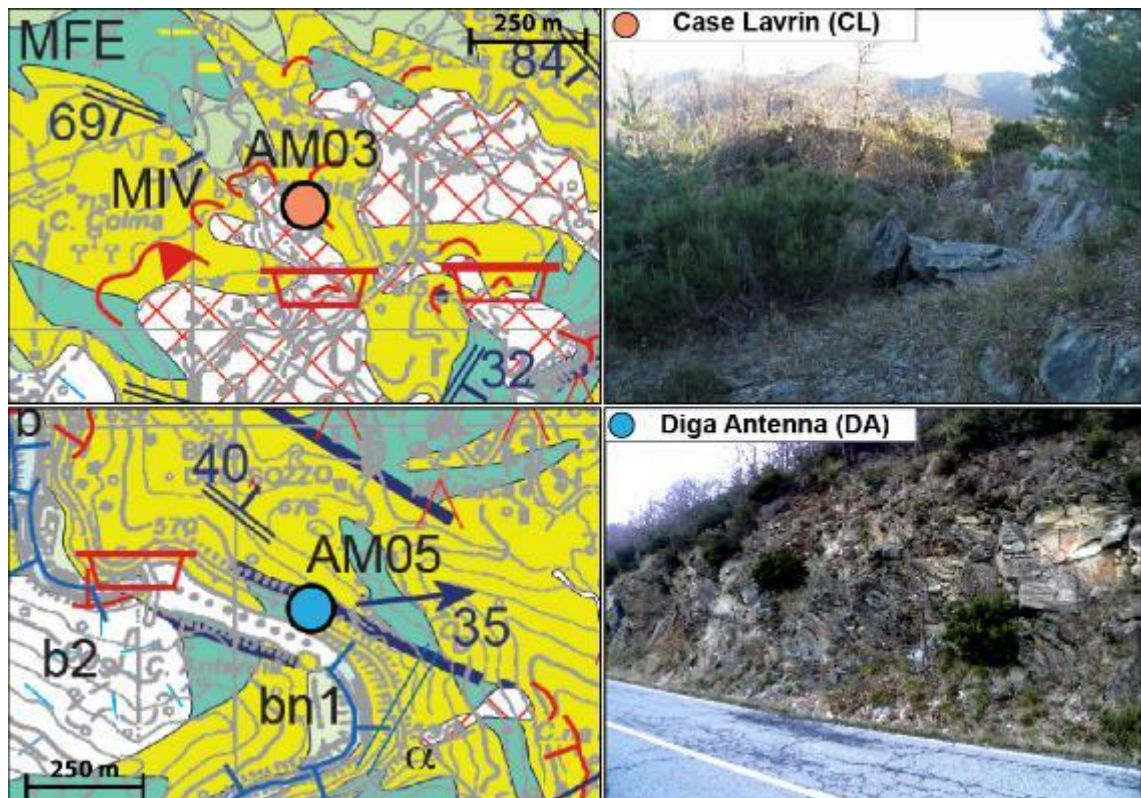


Fig. 2.6 Continued

References

- Bonifacio, E., Zanini, E., Boero, V., and Franchini-Angela, M. (1997). Pedogenesis in a soil catena on serpentinite in north-western Italy. *Geoderma*, 75(1-2), 33-51.
- Borghini, G., Rampone, E., Crispini, L., De Ferrari, R., and Godard, M. (2007). Origin and emplacement of ultramafic–mafic intrusions in the Erro-Tobbio mantle peridotite (Ligurian Alps, Italy). *Lithos*, 94(1-4), 210-229.
- Cannaò, E., Scambelluri, M., Agostini, S., Tonarini, S., and Godard, M. (2016). Linking serpentinite geochemistry with tectonic evolution at the subduction plate-interface: The Voltri Massif case study (Ligurian Western Alps, Italy). *Geochimica et Cosmochimica Acta*, 190, 115-133.
- Capponi, G., and Crispini, L. (2002). Structural and metamorphic signature of alpine tectonics in the Voltri Massif (Ligurian Alps, North-Western Italy). *Eclogae Geologicae Helvetiae*, 95(1), 31-42.
- Capponi, G., and Crispini, L. (2008). Note Illustrative della Carta Geologica d'Italia alla scala 1: 50.000 Foglio 213 Genova. SELCA, Firenze.
- Capponi, G., Crispini, L., Federico, L., (with contributions by, Cabella, R., Faccini, F., and Piazza, M. (2013). Note illustrative al Foglio 212 'Spigno Monferrato'della Carta Geologica Regionale della Liguria.
- Capponi, G., Crispini, L., Federico, L., and Malatesta, C. (2016). Geology of the Eastern Ligurian Alps: a review of the tectonic units. *Italian Journal of Geosciences*, 135(1), 157-169.
- Carobene, L., & Firpo, M. (1994). Una paleospiazzia tra Voltri e Palmaro (Genova): evidenze sedimentologiche e morfologiche. *Il Quaternario*, 7(1), 123-138.
- Carobene, L., & Firpo, M. (2002). Forme terrazzate relitte di genesi marina lungo la costa ligure tra Genova e Savona (Liguria Occidentale). *Il Quaternario*, 15(1), 53-68.
- Chiesa, S., Cortesogno, L., Forcella, F., Galli, M., Messiga, B., Pasquare, G., Pedemonte, G.M., Piccardo, G.B., and Rossi, P. M. (1975). Assetto strutturale ed interpretazione geodinamica del Gruppo di Voltri. *Bollettino della Società Geologica Italiana*, 94(3), 555-581.

- Cimmino, F., Messiga, B., and Piccardo, G.B. (1979). Ti-clinohumite-bearing assemblages within antigoritic serpentinites of the Voltri Massif (Western Liguria): inferences on the geodynamic evolution of piemontese ultramafic sections. *Ofioliti*, 4, 97-120.
- Cortesogno, L., Ernst, W.G., Galli, M., Messiga, B., Pedemonte, G.M., and Piccardo, G.B. (1977). Chemical petrology of eclogitic lenses in serpentinite, Gruppo di Voltri, Ligurian Alps. *The Journal of Geology*, 85(3), 255-277.
- Cortesogno, L., Mazzucotelli, A., and Vannucci, R. (1979). Alcuni esempi di pedogenesi su rocce ultrafemiche in clima mediterraneo. *Ofioliti*, 4, 295-312.
- Costantini, E.A.C., Urbano, F., & L'Abate, G. (2004). Soil regions of Italy. CRA-ISSDS, Firenze, 8.
- Crispini, L., and Capponi, G. (2001). Tectonic evolution of the Voltri Group and Sestri Voltaggio Zone (southern limit of the NW Alps): a review. *Ofioliti*, 26(2a), 161-164.
- IUSS, W. (2015). World Reference Base for Soil Resources 2014, update 2015. International soil classification system for naming soils and creating legends for soil maps. *World Soil Resources Reports*, (106), 153-154.
- Ernst, W.G., and Piccardo, G.B. (1979). Petrogenesis of some Ligurian peridotites - I. Mineral and bulk-rock chemistry. *Geochimica et Cosmochimica Acta*, 43(2), 219-237.
- Federico, L., Crispini, L., Scambelluri, M., and Capponi, G. (2007). Different PT paths recorded in a tectonic mélange (Voltri Massif, NW Italy): implications for the exhumation of HP rocks. *Geodinamica Acta*, 20(1-2), 3-19.
- Federico, L., Crispini, L., Malatesta, C., Torchio, S., and Capponi, G. (2015). Geology of the Pontinvrea area (Ligurian Alps, Italy): structural setting of the contact between Montenotte and Voltri units. *Journal of Maps*, 11(1), 101-113.
- Firpo, M., Guglielmin, M., and Queirolo, C. (2006). Relict blockfields in the Ligurian alps (Mount Beigua, Italy). *Permafrost and Periglacial Processes*, 17(1), 71-78.
- Geoportale Regione Liguria. Available online: <https://geoportal.regione.liguria.it> (accessed on 25 May 2018).
- Hermann, J., Müntener, O., and Scambelluri, M. (2000). The importance of serpentinite mylonites for subduction and exhumation of oceanic crust. *Tectonophysics*, 327(3-4), 225-238.
- Hoogerduijn Strating, E.H. (1991). The evolution of the Piemonte-Ligurian ocean: a structural study of ophiolite complexes in Liguria (NW Italy) (Doctoral dissertation, Instituut voor Aardwetenschappen der Rijksuniversiteit Utrecht).
- Liou, J.G., Zhang, R.Y., Ernst, W.G., Rumble, D., and Maruyama, S. (1998). High-pressure minerals from deeply subducted metamorphic rocks. *Reviews in Mineralogy and Geochemistry*, 37(1), 33-96.
- Malatesta, C. (2011). Subduction and Exhumation of Hp Ligurian-piedmontese Ophiolites: An Integrated Approach from Field to Numerical Models: Tesi Di Dottorato (Doctoral dissertation, Università degli studi di Genova, Scuola di dottorato in Scienze e tecnologie per l'ambiente e il territorio, Corso di dottorato in Scienze della terra, Ciclo 23).
- Malatesta, C., Crispini, L., Federico, L., Capponi, G., and Scambelluri, M. (2012). The exhumation of high-pressure ophiolites (Voltri Massif, Western Alps): Insights from structural and petrologic data on metagabbro bodies. *Tectonophysics*, 568, 102-123.
- Marsili, S., Roccotiello, E., Rellini, I., Giordani, P., Barberis, G., and Mariotti, M. G. (2009). Ecological studies on the serpentine endemic plant *Cerastium utriense* Barberis. *Northeastern Naturalist*, 405-421.
- Messiga, B., and Piccardo, G.B. (1974). Rilevamento geopetrografico e strutturale del Gruppo di Voltri. Il settore Nord-Orientale: la zona fra Monte Tacco e Monte Orditano. *Mem. Soc. Geol. It*, 12(2), 301-315.
- Messiga, B., and Scambelluri, M. (1991). Retrograde P-T-t path for the Voltri Massif eclogites (Ligurian Alps, Italy): Some tectonic implications. *Journal of Metamorphic Geology*, 9(1), 93-109.
- Messiga, B., Piccardo, G. B., and Ernst, W. G. (1983). High-pressure eo-Alpine parageneses developed in magnesian metagabbros, Gruppo di Voltri, western Liguria, Italy. *Contributions to Mineralogy and Petrology*, 83(1-2), 1-15.

- Padovano, M., Piccardo, G. B., and Vissers, R. L. (2014). Tectonic and magmatic evolution of the mantle lithosphere during the rifting stages of a fossil slow–ultraslow spreading basin: insights from the Erro–Tobbio peridotite (Voltri Massif, NW Italy). *Geological Society, London, Special Publications*, 413, SP413-7.
- Piccardo, G.B. (1977). Le ofioliti dell'areale ligure: petrologia ed ambiente geodinamico di formazione. *Rend. Soc. It. Min. Petr.*, 33, 221-252.
- Piccardo, G.B. (1984). Le ofioliti metamorfiche del Gruppo di Voltri, Alpi Liguri: caratteri primari ed interpretazione geodinamica. *Mem. Soc. Geol. It*, 28, 95-114.
- Piccardo, G.B., Rampone, E., Romairone, A., Scambelluri, M., Tribuzio, R., and Beretta, C. (2001). Evolution of the Ligurian Tethys: inference from petrology and geochemistry of the Ligurian Ophiolites. *Per. Mineralogy*, 70, 147-192.
- Piccardo, G.B., & Vissers, R.L.M. (2007). The pre-oceanic evolution of the Erro-Tobbio peridotite (Voltri Massif, Ligurian Alps, Italy). *Journal of Geodynamics*, 43(4-5), 417-449.
- Pinna, M. (1970). Contributo alla classificazione del clima d'Italia. *Rivista geografica italiana*, 77(2), 129-152.
- Rampone, E., Romairone, A., Abouchami, W., Piccardo, G. B., and Hofmann, A. W. (2005). Chronology, petrology and isotope geochemistry of the Erro–Tobbio peridotites (Ligurian Alps, Italy): records of Late Palaeozoic lithospheric extension. *Journal of Petrology*, 46(4), 799-827.
- Rellini, I., Trombino, L., Firpo, M., and Rossi, P.M. (2009). Extending westward the loess basin between the Alps and the Mediterranean region: micromorphological and mineralogical evidences from the northern scope of the Ligurian Alps, Northern Italy. *Geografia Fisica e Dinamica Quaternaria*, 32, 103-116.
- Rellini, I., Trombino, L., Rossi, P. M., and Firpo, M. (2014). Frost activity and ice segregation in a palaeosol in the Ligurian Alps (Beigua Massif, Italy): evidence of past permafrost? *Geografia Fisica Dinamica Quaternaria*, 37(1), 29-42.
- Sacchini, A., Ferraris, F., Faccini, F., & Firpo, M. (2012). Environmental climatic maps of Liguria (Italy). *Journal of Maps*, 8(3), 199-207.
- Scambelluri, M., Müntener, O., Hermann, J., Piccardo, G.B., and Trommsdorff, V. (1995). Subduction of water into the mantle: history of an Alpine peridotite. *Geology*, 23(5), 459-462.
- Scambelluri, M., Strating, E.H., Piccardo, G.B., Vissers, R.L.M., and Rampone, E. (1991). Alpine olivine-and titanite-bearing assemblages in the Erro-Tobbio peridotite (Voltri Massif, NW Italy). *Journal of Metamorphic Geology*, 9(1), 79-91.
- Scarsi, M., Malatesta, C., and Fornasaro, S. (2018). Lawsonite-bearing eclogite from a tectonic mélange in the Ligurian Alps: new constraints for the subduction plate-interface evolution. *Geological Magazine*, 155(2), 280-297.
- Scopesi C. (2009). *Studi pedopaesaggistici nella pianificazione territoriale del comune di Sassello: alcuni esempi e applicazioni GIS*. Unpublished BSc Thesis, University of Genoa.
- Scopesi, C., Maerker, M., Bachofer, F., Rellini, I., & Firpo, M. (2017). Assessment of flash floods in a small Mediterranean catchment using terrain analysis and remotely sensed data: a case study in the Torrente Teiro, Liguria, Italy. *Zeitschrift für Geomorphologie, Supplementary Issues*, 61(2), 137-163.
- Spandler, C., Hermann, J., Faure, K., Mavrogenes, J.A., and Arculus, R.J. (2008). The importance of talc and chlorite “hybrid” rocks for volatile recycling through subduction zones: evidence from the high-pressure subduction mélange of New Caledonia. *Contributions to Mineralogy and Petrology*, 155(2), 181-198.
- Vanossi, M. (1984). *Geologia delle Alpi liguri*. Memorie/Soc. geol. Italiana, 28.
- Vignaroli, G., Rossetti, F., Rubatto, D., Theye, T., Lisker, F., and Phillips, D. (2010). Pressure-temperature-deformation-time (P-T-d-t) exhumation history of the Voltri Massif HP complex, Ligurian Alps, Italy. *Tectonics*, 29(6).

Materials and Methods

A multidisciplinary approach combining field, analytical, and laboratory studies is necessary to evaluate the PTEs geochemistry related to the ultramafic rocks and soils and to determine whether or not ultramafic rocks and soils are sources of non-anthropogenic PTEs contamination. Moreover, the studied rock and soils samples have been analyzed using a multiscale and multi-analytical approach including:

- i) field survey and geo-structural analyses;
- ii) soil physics analyses;
- iii) mineralogical, petrographic, and micro-structural/-textural analyses by means of polarized-light optical microscopy (PLOM) and scanning electron microscopy (SEM-EDS);
- iv) mineralogical and mineralo-chemical analysis by means of electron microprobe analyzer (EMPA-WDS) and X-ray powder diffraction (XRPD);
- v) in-situ measurements of trace and ultra-trace elements by laser ablation-inductively coupled plasma-mass spectrometry (LA-ICP-MS);
- vi) bulk chemical analyses by means of energy dispersive X-ray fluorescence (EDXRF) and inductively coupled plasma – atomic emission spectroscopy (ICP-AES).

In this chapter, the materials and methods used during the main stages of this PhD thesis are listed and described.

3.1. FIELD WORK AND SAMPLING

3.1.1. Field survey and geo-structural analyses

In all study sites a detailed geo-structural survey has been performed in order to describe and classify the bedrocks according to lithological and structural-textural criteria and identify the most striking structural and textural features that characterize the area. On the basis of the geological survey data and the previous geological studies (Fornasaro, 2014; Orecchia, 2014; Cureda, 2015; Malerba, 2016), a geological sketch of all study sites is produced and reported in *Appendix A*.

3.1.2. Sampling strategy

The main objective of sampling was to account for the lithological and structural variability within ultramafic rocks (from partially serpentinized lherzolites, massive and foliated serpentinites). For each selected site 2 to 10 rock samples and 2 to 18 soil samples have been collected depending on lithological and structural variability.

Soil samples were collected with steel auger and shovel, from two soil layers: 1) the *topsoil* (0-30 cm), excluding the rhizosphere (organic horizons), and 2) the *subsoil* (30-60 cm) following the criteria of Darnley (1997), Salminen et al. (1998), and GEMAS project (Albanese et al., 2015). For each sampling point approximately one kg of soil was taken, after removing the granulometric fraction > 2 cm fraction as required by current legislation (D.M. 471/1999, abrogated and now replaced by D.Lgs 152/2006).

Rock samples were collected at the base of soil profile, from two different alteration zone: unweathered rock and weathered rock at the direct contact to subsoil where coherent rock structure is still preserved.

3.2. ANALYTICAL TECHNIQUES

3.2.1. Soil physical analyses

Soil color and other properties including grain-size, grain-morphology, texture, structure, and consistence are used to distinguish and identify soil horizons and to group soils according to the soil classification system (FAO-WRB classification; IUSS, 2015).

Colorimetric analyses

Color was used as a preliminary qualitative evaluation of Fe-oxide mineral content (e.g., goethite vs hematite) and for the other environmental conditions (e.g., anaerobic vs aerobic soil condition). Regardless of the methods used to quantitatively measure of soil color, two main systems have been applied: the Munsell Color System (Munsell Color Co. 1929) and the CIE-La*b* color space (Commission Internationale de l'Eclairage – CIE, 1931). The Munsell Color System is based on three parameters: i) hue (H; spectral color); ii) chroma (C; color intensity); iii) value (V; lightness and darkness). CIE-La*b* color space is an approximately uniform color system, based on three numerical values: L is the

metric lightness function (representing brightness or luminance), a^* and b^* are the chromatic coordinates represent opponent red–green scales ($+a^*$ = reds, $-a^*$ = greens) and opponent blue–yellow scales ($+b^*$ = yellows, $-b^*$ = blues).

The color of the all soil samples was determined by means of visual estimation, using the Munsell® Soil Color Charts (2000), either on field on moist soil sample and in laboratory on dry sample. The data obtained were also converted into CIE- $L^*a^*b^*$ color system using the *Munsell Conversion Software CMC10d*.

Granulometric analyses

The granulometric analyses were performed at the Laboratory for rock and soil analyses of DISTAV (University of Genova – Italy).

The particle size distribution of the all soil samples was obtained by wet sieving with a Controls D411 Automatic Sieve Shaker into size fractions of: ≥ 2 cm, 2 cm to 1 mm, 1 mm to 355 μm , 355-150 μm , 150-63 μm , <63 μm . All the fractions were successively dried in a stove at 50°C and weighed. Granulometric classification was obtain according to Folk classification (Folk, 1954).

Morphological analyses

A preliminary observation of all soil sample fractions was carried out by means of a stereo-microscope using a Leica Wild M8 with Dino-Eye Microscope Eye-Piece Camera. Elaboration image has been performed by means of DinoXcope 1.9.6 software (AnMo Electronics Corporation) at the Laboratory for Mineralogical Analyses of DISTAV (University of Genova – Italy).

Stereoscopic analyses have provided useful information for initial screening giving qualitative information on:

- Shape and morphology of soil grain, according to Shepard (1963) and Zingg (1935), based on roundness/sphericity ration;
- Modal estimation of opaque grains with comparative table (Baccelle & Bosellini, 1965; Ricci Lucchi, 1980);
- Presence of magnetic minerals;
- Estimation of alteration and oxidation degree.

Moreover, thanks to stereomicroscopic analyses, the granulometric fraction between 355 and 150 μm was selected for the preparation of thin section as this granulometric interval represents the best compromise between a large number

of granules in the section and the presence of polimineral granules suitable for identifying the prevailing textural and lithological characteristics.

3.2.2. Mineralogical, petrographic, and microstructural analyses

A preliminary petrographic description, micro-structural/-textural analyses, and qualitative weathering evaluation of rock and soil samples were carried out using polarized-light optical microscopy (PLOM) and scanning electronic microscopy and microanalysis (SEM-EDS).

Polarized-light optical microscopy (PLOM)

The PLOM analyses were carried out at the Laboratory for Mineralogical Analyses of DISTAV (University of Genova – Italy), using the Olympus System Microscope Model BX-41. High-resolution images were acquired using OLYMPUS COLOR VIEW II-SET cameras and processed using OLYMPUS C-VIEW II-BUND-cell ^ B software. The microscope is equipped with 2x, 4x, 10x, 20x, 40x, 50x objective magnifications and 10x and 12,5x eyepieces.

The PLOM analyses were used for a preliminary petrographic description, microstructural analysis, and qualitative weathering evaluation of rock and soil samples and for the selection of point analyses by means of SEM and EMPA.

Fifty-eight polished thin sections were prepared from twenty-seven rock samples and from thirty-one soil samples.

Twenty-seven rocks were selected and appropriately orientated for the preparation of thin section. Thin sliver of rock was cut from the sample with a diamond saw and grounded optically flat. Sample was then mounted on a glass slide and smoothed using progressively finer abrasive grit (6, 1 ed 1/4 µm) until the sample was only 30 µm thick.

Thirty-three soil thin section were prepared for the study of mineralogy of soil skeleton. After embedding in epoxy resin, the material was prepared as described for the rock samples.

Scanning Electron Microscopy and microanalyses (SEM-EDS)

SEM-EDS analyses of four rock samples and three soil samples were performed on polished thin sections at the Scanning Electron Microscopy Laboratory of DISTAV (University of Genova – Italy) using a SEM Vega3 – TESCAN type LMU system equipped with an EDS EDAX APOLLO XSDD with DPP3 analyzer.

Analyses were performed at 20 kV accelerating voltage and 1.2 nA beam current at the specimen level for 60 live second counting time with a spot size of 370 nm and working distance of 15 mm. Concentrations of major chemical components were calculated on an anhydrous basis with ZAF corrections and using natural silicates and oxides for calibration.

These analyses were functional to the preliminary chemical identification of PTEs-bearing minerals (e.g., spinel-group minerals, serpentine minerals, oxyhydroxides) in the selected soil and rock thin sections.

3.2.3. Mineralogical, mineral chemical, and crystallographic analyses

Qualitative identification of the mineral assemblages and quantitative analyses in the studied samples were performed by means of X-Ray Powder Diffraction (XRPD) and electron microprobes with wavelength dispersive spectrometers (EMPA-WDS). The selected soil and rock analyzed samples are chosen in order to represent all the four type of the investigated bedrocks.

X-Ray Powder Diffraction (XRPD)

Diffraction data with traditional technique on rock and soil samples were performed at the *Physic and Geology Department* (University of Perugia – Italy) using Philips PW1830 diffractometer, with $\text{CuK}\alpha$ ($\lambda = 1.5406 \text{ \AA}$). The analyses were recorded in the range of 2-theta angles from 5° to 80° at step size of $0,02^\circ$. Samples were crushed and then powdered using an agata mortar and pestle and spiked with a 10% wt. Si metallic standard, for amorphous phases quantification. The clay fractions were separated by gravity separation using Stokes Law determinations and centrifugation in deionized water to remove free ions and were also filtered with filter paper with $4 \mu\text{m}$ of porosity.

Nevertheless, in soil samples, data collected with traditional diffraction techniques has resulted of difficult interpretation due to the occurrence of a large number of complex mineral phases (such us serpentine minerals, spinels, Fe-oxyhydroxides, and clay minerals) often intimately mixed with amorphous phases. For these reasons the complete mineralogical characterization of soil samples has required high-quality and high-resolution X-ray diffraction patterns, obtained by means of synchrotron X-ray sources.

Synchrotron radiation X-ray powder diffraction

The synchrotron-based diffraction data was collected at Material Characterization by X-ray Diffraction (MCX) beamline at Elettra Synchrotron radiation facility located in Trieste, Italy.

A total of sixteen soil samples were analyzed at the MCX beamline. The samples were representative of 4 different soil profiles and were subdivided into three different aliquots in order to investigate the mineralogy of the sand (2 mm-63 μm), silt (63-4 μm), and clay (<4 μm) fractions. Data were collected in transmission mode on 0.3 mm boron capillaries using a wavelength radiation of 1.033 Å, in the 2–70° 2 θ angular range, 0.01 (sand and silt) and 0.005 (clay) 2 θ step-size, and 1 sec counting time.

XRD software analyses

Preliminary identification of mineral phases was carried out with “X’Pert Highscore” (University of Perugia), “PDF-4+/Minerals” (Elettra Synchrotron), and “Match!” (University of Genova).

For the quantitative analyses and for the determination of amorphous phases content, Rietveld refinements were conducted with General Structure Analysis Software (EXPGUI-GSAS software; Larson & Von Dreele, 1994). Crystallographic information file (CIF) from the American Mineralogist Crystal Structure Database (<http://ruff.geo.arizona.edu>) were used for the refinement.

Electron microprobes with wavelength dispersive spectrometers (EMPA-WDS)

Mineral chemistry of eleven rock and five soil samples was determined at the Electron Microprobe Laboratory of *Earth Science Department “Ardito Desio”* (University of Milan – Italy) using electron microprobe analyzer (WDS JEOL, JXA – 8200 WD/ED model). Operating conditions were: accelerating voltage of 15 kV and a beam current of 5 nA and a counting time of 10 s for all the elements. Calibration was performed with a set of synthetic and natural standards including olivine 154 (Mg), omphacite 154 (Na), Cr, rhodonite (Mn and Zn), k-feldspar 113 (K), anorthite 137 (Al and Ca), wollastonite (Si), V, fayalite 143 (Fe), ilmenite (Ti), Co, galena (S), niccolite (Ni).

In-situ spot analyses with a diameter of ~1 μm were focused on the potential PTEs-bearing phases (e.g., spinel-group minerals, serpentine minerals,

pyroxene, olivine, chlorite, and authigenic minerals) both on rock samples and soil samples.

Detailed compositional X-ray intensity maps were obtained for selected areas to investigate the distribution of major and minor elements (i.e., Cr, Fe, Mg, Mn, Ni, S, and Si) in spinel-group minerals. The image acquisition conditions were 15 kV accelerating voltage, 1 μm^2 pixel size, and a 30 ms dwell time.

Subsequent analyses carried out with Laser Ablation Inductively Coupled Plasma Mass Spectrometry (LA-ICP-MS) used Fe, Mg, Si, and Al values as internal standards for the quantification of minor and trace components in the selected PTEs-bearing minerals.

3.2.4. Trace and ultra-trace minero-chemical analyses

Trace and ultra-trace element of selected minerals (e.g., olivine, pyroxene, serpentine minerals, and spinel-group minerals) were determined by laser ablation-inductively coupled plasma-mass spectrometry (LA-ICP-MS) at the LA-ICP-MS Lab of the *Physic and Geology Department* (University of Perugia – Italy). Eight rock thin section, representative of the four different studied bedrocks and relative soil samples (n° 5 thin sections) were analyzed.

LA-ICP-MS system is composed by a commercial New Wave UP213 (New Wave, UK) LA system coupled with a Thermo Electron X7 (Thermo Electron Corporation, Waltham, USA) ICP-MS. The analyses were conducted using a ~30–20 μm beam diameter, 8 Hz frequency, and 0.032–0.105 mJ/pulse power, during 90 s analysis. The following trace elements were detected: Li, Na, Mg, Al, Si, P, K, Ca, Sc, Ti, V, Cr, Mn, Co, Ni, Cu, Zn, Ga, Rb, Sr, Y, Zr, Nb, Sn, Ba, Hf, Ta, Pb, Th, and U, including REEs. Other details on the instrumentation, precision and accuracy are reported in Petrelli et al. (2008, 2016).

3.2.5. Bulk chemistry (major, minor, and trace elements)

Major, minor, and trace elements for soil and rock samples were analyzed by means of EDXRF and ICP-AES.

Energy Dispersive X-ray Fluorescence (EDXRF)

EDXRF analyses were performed on forty-five rock and twenty-two soil samples; 1) for soil samples the analyses were performed on the granulometric fraction

<2mm; 2) rock samples were crushed and porphyzied. The EDXRF instrument was an EDXRF-X-MET7500, Oxford Instruments, with a Fundamental Parameter (FP) calibration built by factory (Mining & Soil). The X-ray fluorescence signal was collected for 120 s. To better detected the concentration of “light” ($12 \leq Z \leq 20$) and “heavy” ($Z > 20$) elements, two different instrument calibrations was chosen: i) *Soil LE FP* was selected to analyses Ti, Fe, Mn, Ca, V, Cr, Co, Ni, Cu, Zn, Rb, Sr, Zr, Cd, Sn, Sb, Ba, Pb; ii) *Mining LE PF* was selected to analyses Al, Si, P, S, K, Ca, Ti, Fe, Mg, Mn, Ca, V, Cr, Co, Ni, Cu, Zn, Rb, Sr, Zr, Cd, Sn, Sb, Ba, Pb, Nb, Mo. Detection limits are reported in Table 3.1.

ppm	Mg	Al	P	K	Ca	Ti	V	Cr	Mn	Co	Ni	Cu	Zn
LOD	3500	694	38	36	24	12	13	8	9	4	2	2	3

Table 3.1 XRF detection limits.

Inductively Coupled Plasma – Atomic Emission Spectroscopy (ICP – AES)

The determination of the total content by total digestion with concentrated HNO₃ and HCl (1:3, v/v) (*aqua regia*) of fourteen elements (Al, Fe, Mn, Be, V, Cr, Co, Ni, Cu, Zn, As, Cd, Ba, and Pb) in eighteen rock and seventeen soil were performed by means of an Optimal DV 2100 Perkin-Elmer at ARPAL Laboratory (Agenzia Regionale per la Protezione dell’Ambiente – Liguria, Italy). These analyses were carried out on eighteen rock samples and seventeen soil samples following the procedure recommended by D.M. 13/9/99 and D.Lgs 152/2006, and according to EPA – 3050 B e EPA – 6010 C. Detection limits are reported in Table 3.2.

ppm	Al	V	Cr	Mn	Fe	Co	Ni	Cu	Zn
LOD	0.01	0.01	0.002	0.001	0.01	0.003	0.01	0.006	0.02

Table 3.2 ICP-AES detection limits

References

- Albanese, S., Sadeghi, M., Lima, A., Cicchella, D., Dinelli, E., Valera, P., Falconi, M., Demetriades, A., De Vivo, B., and the GEMAS Project Team (2015). GEMAS: cobalt, Cr, Cu and Ni distribution in agricultural and grazing land soil of Europe. *Journal of geochemical exploration*, 154, 81-93.
- Baccelle, L., and Bosellini, A. (1965). *Diagrammi per la stima visiva: della composizione percentuale nelle rocce sedimentarie (Vol. 1)*. Università degli studi di Ferrara.
- Curedda F. (2015). *Determination of natural background values for metals of environmental concern in ultrabasic soils and rocks from Voltri Unit*. Master’s degree thesis, University of Genova. Unpublished
- Darnley, A. G., Bjorklund, A., Bolviken, B., Gustavsson, N., Koval, P. V., Steenfelt, A., and Xuejing, X. (1995). *A global geochemical database. Recommendations for international geochemical mapping. Final report of IGCP project*, 259.

- Decreto Legislativo 3/04/2006 n° 152 "Norme in materia ambientale". G.U. 88. 14/04/2006.
- Decreto Ministeriale 25/10/1999 n° 471 "Regolamento recante criteri, procedure e modalità per la messa in sicurezza, la bonifica e il ripristino ambientale dei siti inquinati, ai sensi dell'articolo 17 del decreto legislativo 5 febbraio 1997, n. 22", e successive modificazioni e integrazioni. G.U. 293, 15/12/1999.
- Folk, R.L. (1954). *The distinction between grain size and mineral composition in sedimentary-rock nomenclature. The Journal of Geology*, 62(4), 344-359.
- Fornasaro S. (2014). *Determination of natural background values for selected metals in ophiolitic soils and rocks from Voltri Massif. Master's degree thesis, University of Genova. Unpublished*
- IUSS, W. (2015). *World Reference Base for Soil Resources 2014, update 2015. International soil classification system for naming soils and creating legends for soil maps. World Soil Resources Reports*, (106), 153-154.
- Larson, A. C., and Von Dreele, R. B. (1994). *Gsas. Report IAUR*, 86-748.
- Malerba G. (2016) *Determination of ecotoxic metals in rocks and soils from Voltri Unit master's degree thesis, University of Genova. Unpublished*
- Munsell, S.C.C. (2000). *Munsell color. Grand Rapids, Michigan.*
- Orecchia M. (2014). *Determination of asbestos natural concentration values on ophiolitic soils and rocks from Voltri Massif. Master's degree thesis, University of Genova. Unpublished.*
- Petrelli, M., Morgavi, D., Vetere, F., and Perugini, D. (2016). *Elemental imaging and petro-volcanological applications of an improved laser ablation inductively coupled quadrupole plasma mass spectrometry. Periodico di Mineralogia*, 85, 25-39.
- Petrelli, M., Perugini, D., Alagna, K.E., Poli, G., and Peccerillo, A. (2008). *Spatially resolved and bulk trace element analysis by laser ablation-inductively coupled plasma-mass spectrometry (LA-ICP-MS). Periodico di Mineralogia*, 77(3).
- Ricci Lucchi, F. (1980). *Sedimentologia: Parte 1: materiali e tessiture dei sedimenti. Cooperativa Libreria Universitaria Editrice.*
- Salminen, R., Tarvainen, T., Demetriades A., Duris M., Fordyce F.M., Gregorauskiene V., Kahelin H., Kivisilla J., Klaver G., Klein H., Larson J.O., Lis J., Locutura J., Marsina K., Mjartanova H., Mouvet C., O'Connor P., Odor L., Ottonello G., Paukola T., Plant J.A., Reimann C., Schermann O., Siewers U., Steenfelt A., Van der Sluys J., de Vivo B. and Williams L. (1998). *FOREGS geochemical mapping field manual.*
- Shepard, F.P. (1963). 1. *Introduction Submarine canyons have been discussed extensively in the literature during the past 30 years. Field investigations, however, have lagged and have been confined to a very few individuals and to a few localities. This is regrettable. The Earth Beneath the Sea History Sea*, 3, 480.
- USEPA. (1996). *Method 3050B. Acid digestion of sediments, sludges, and soils. Test methods for evaluating solid waste.*
- US Environmental Protection Agency. (2006). *Method 6010: Inductively coupled plasma-atomic emission spectrometry. Test Methods for Evaluating Solid Waste, Physical/Chemical Methods, 6010C-1.*
- Zingg, T. (1935). *Beitrag zur schotteranalyse (Doctoral dissertation, ETH Zurich).*

Section Two

Investigation on the ultramafic rocks

Ultramafic rocks can store several PTEs which can be released to the environment during weathering and pedogenesis.

To determine the PTEs distribution, to evaluate their mobility and their potential bioavailability as well as to discriminate the natural geochemical background from possible source of contamination, a multidisciplinary approach is necessary to combine the bulk chemistry of outcropping rocks with their geological, structural, mineralogical, and crystallochemical data.

In the ultramafic rocks, spinel-group minerals are the main source of the PTEs which can have a significant impact on the environmental and human health once they are mobilized into soil, water or dust. Moreover, in the ultramafic rocks, PTEs-bearing phases are also represented by the other rock-forming minerals (e.g., serpentines, olivines, pyroxenes, and chlorites) and some accessory phases (e.g., ilmenite and other oxides, sulphides). Hence, the knowledge of the crystallochemical variations (including PTEs concentration) as a function of the metamorphic conditions or structural properties, other than for their petrological implications, may have a paramount environmental concern since the mode of occurrence of PTE-bearing minerals can directly affect weathering processes during pedogenesis and thus soil chemistry, PTEs mobility, and bioavailability.

This *Section* is subdivided into two chapters (*IV and V*).

Chapter IV refers to the determination of the chemistry, mineralogy, and microstructural features of ultramafic rocks from Voltri Massif (Central Liguria, Italy), in order to assess the role of meso- and micro-scale lithological, mineralogical, textural, and structural factors in the concentration and distribution of PTEs in serpentized and deformed ultramafic rocks. A description and classification of the ultramafic bedrocks according to lithological and (micro)structural-textural criteria is also provided.

Chapter V refers specifically to the mineralogy and the crystal chemistry of spinel-groups minerals. In particular, the chapter is focused on the relationships between their crystallochemical variations and their mode of occurrence with respect to the degree of serpentinization and deformation of the host rocks.

Potentially toxic elements distribution in the serpentized and deformed ultramafic rocks from the Voltri Massif (NW, Italy)

Keywords: serpentization, deformation, trace elements, nickel, chromium, cobalt, serpentine textures

4.1. INTRODUCTION

High concentrations of potentially toxic elements (PTEs) in surface and near-surface environment may be attributed both to anthropogenic sources (including industrial, agricultural, and mining activities) and to geogenic sources (natural weathering of rocks and pedogenesis).

From the environmental point of view, ultramafic rocks (e.g., dunite, peridotite, pyroxenite, and serpentinite) are, among the geogenic sources, the most critical. In fact, besides their common content of asbestos minerals (Cheshire and Guven, 2005; Alexander, 2007; Hseu et al., 2007), ultramafic rocks are characterized by high contents of Cr (up to 15300 ppm; Stueber and Goles, 1967), Ni (up to 7733 ppm; Savov et al., 2007), and Co (up to 950 ppm; Garnier et al., 2009). It is well known that weathering of ultramafic rocks produces ultramafic soils containing a high concentration of Cr, Ni, and Co (Oze et al. 2004a, b; Alexander, 2007) that can have a potentially harmful impact on ecosystems and human health when released into soils and waters. Their concentration, in suitable pedogenic conditions, can reach even economic significance (e.g. Ni-laterites; Butt and Cluzel, 2013). Although ultramafic rocks and relative soils cover approximately 1% of the Earth's surface, they are worldwide distributed, being generally associated with ophiolite complexes (Coleman, 1977; Coleman and Jove, 1992; Vaughan and Scarrow, 2003; Dilek and Furnes, 2009).

Despite a general similarity in the whole rock chemical composition, the concentration and distribution of PTEs in ultramafic rocks is highly variable worldwide: in general, PTEs content can range up to two orders of magnitude, mainly because of heterogeneities in mineralogy, texture, and structural

properties of the rock (Kierczak et al., 2016; Echevarria, 2018), that are related to different geological settings as well as metamorphic and geodynamic evolutions (Deschamps et al., 2013), which strictly influence the mineralogical assemblages and the relative mineral chemistry.

In general, the mineralogical composition of ultramafic rocks is dominated by the presence of Fe- and Mg-rich silicate minerals (e.g., olivines and pyroxenes) and spinel-group minerals (e.g., chromite and magnetite). During serpentinization a large variety of metasomatic and metamorphic minerals is formed; they are mainly represented by serpentines (lizardite, chrysotile, and antigorite), chlorites and clay minerals, amphiboles (e.g., tremolite and actinolite), talc, brucite, iron oxides, and carbonates. Most of the above minerals may incorporate varying concentrations of trace elements into their crystal structures.

Spinel-group minerals, other than Cr, can contain a wide range of PTEs because several elements, such as Zn^{2+} , Co^{2+} , and Ni^{2+} can substitute Mg^{2+} and Fe^{2+} in the tetrahedral site, whereas V^{3+} can substitute Fe^{3+} , Al^{3+} , and Cr^{3+} in the octahedral site (O'Neill and Navrotsky, 1984; Sack and Ghiorso, 1991; Burkhard, 1993; Abre et al. 2009; Colas et al., 2014; Liu et al., 2014; Canil et al., 2016). The type and degree of substitution in both sites depends on many factors, such as oxygen fugacity, magma/fluid composition, and temperature (Buddington and Lindsley, 1964; Frost and Lindsley, 1991; Lindsley, 1991; Toplis and Carroll, 1995; Dare et al., 2009, 2014; González-Jiménez et al., 2014; Liu et al., 2016).

Olivines host a limited number of trace elements, predominantly the first-row transition metals (Zanetti et al., 2004; Foley et al., 2013; Bussweiler et al., 2015). Among PTEs, only Ni and Co can be host in olivine in significant concentration (1000 to 5000 ppm and 120-120 ppm respectively; Sobolev et al., 2007; Straub et al., 2008; Herzberg et al., 2013, 2016); subordinate amounts of Zn and Cr can be also present (Foley et al., 2013; Prelević et al., 2013; Jaques and Foley, 2018). The trace element signature in olivine is mainly controlled by P-T conditions and melt composition (Prelević and Foley, 2007; Sobolev et al., 2009; De Hoog et al., 2010; Foley et al., 2013; Bussweiler et al., 2015).

Orthopyroxenes and clinopyroxenes are commonly characterized by a wide range of ionic substitutions in the octahedral site, where Fe and Mg may be replaced by several metals of environmental concern (mainly Cr, Ni, and V; Simon et al., 2007; Zhang et al., 2001; Krátký et al., 2018). In particular, augite and enstatite can incorporate significant concentration of Cr (up to 1 wt% and 0.1

wt% respectively; Von Knorring et al., 1986; Brothers and Grapes, 1989; Treloar, 1987; Sanchez-Vizcaino et al., 1995; Deer et al., 1996; Krátký et al., 2018). These variations are influenced by the composition of the magma from which the clinopyroxene crystals crystallize (e.g., Dal Negro et al., 1982, 1985, 1986, 1989; Carbonin et al., 1991) as well as by pressure and temperature of crystallization (Margarotto et al., 1993; Nimis, 1995; Nazzareni et al., 2001, 2011).

Serpentines are hydrous Mg-rich phyllosilicates, where Mg in the octahedral site can be substituted by Fe^{2+} , Fe^{3+} , Al, Cr, Ni, and Mn^{2+} (Brigatti et al., 2011). The trace metals content of serpentines is commonly strictly related to the chemical composition of the peridotite protolith since these elements have generally a conservative behavior during serpentinization (Roumejon et al., 2015). The crystal chemistry of serpentines is also dependent either on the polytype (i.e., antigorite, lizardite, and chrysotile) and on the different serpentine precursor (i.e., olivine or pyroxenes; Viti and Mellini, 1997, 1998; Deschamps et al., 2010, 2012). Ni is mainly concentrated in serpentines after olivine (up to 0.77 wt% NiO; Kodolanyi and Pettke, 2011; Kodolanyi et al., 2012), whereas serpentines deriving from pyroxenes are enriched preferentially in Cr (up to 1.37 wt% Cr_2O_3 ; Kodolanyi and Pettke, 2011; Kodolanyi et al., 2012).

Chlorite is a common rock-forming mineral found in a variety of geologic environments (i.e., diagenetic, metamorphic and hydrothermal) and in rocks with variable compositions (Laird, 1988). Chlorites are hydrous aluminosilicates with a complex chemical composition and structure. They can incorporate Cr, Ni, Mn, V, and Cu in both the octahedral sites (Bailey, 1988; Wiewiora and Weiss, 1990; Brigatti et al., 2011). This wide range of compositional variations depends on either the bulk-rock composition or the physicochemical conditions of the environment (including P-T, pH, the activities of the various metals within the fluid, and the activities of S_2 , O_2 , and CO_2 ; Hayes, 1970; Walker, 1993; Vidal et al., 2000; Inoue et al., 2009). In ultramafic rocks, Cr-chlorite is an important Cr-bearing phase where Cr_2O_3 content can vary from 0.5 to 8 wt.% (e.g., Arai et al., 2006; Khalil, 2007; Grieco et al., 2011).

Amphibole, due to their complex structure, allows a large number of isomorphous substitutions (Comodi et al., 1991; Ottonello, 2000; Schumacher, 2007; Hanley and Bray, 2009). PTEs such as Zn, Ni^{2+} , Co^{2+} , V^{3+} , Cu^{2+} , and Cr^{3+} can substitute Fe^{3+} , Mg, Al in the octahedral site (Prewitt, 1963; Klein and Ito, 1968; Della Ventura et al., 1996, 1997; Hawthorne and Oberti, 2007; Hanley and Bray, 2009).

These substitutions are enabled by a variety of structural distortions in both the octahedral strip and tetrahedral chains (e.g., bond-layer tilting, bond-length stretching, compression, and rotation; Hazen and Wones, 1972; Hawthorne and Oberti, 2007; Hanley and Bray, 2009). The extent of these cation substitutions may also be temperature-dependent (Welch et al., 2007), or controlled by the absolute metal concentrations in fluids, magmas, or metamorphic protoliths (e.g., Arai, 1986).

From the petrological point of view, the paragenesis and the mineral chemistry (in particular the trace elements) are commonly used as an efficient fingerprint to interpret the petrogenesis and the geodynamic setting of ultramafic rocks (Witt-Eickschen & O'Neill 2005; Brett et al., 2009). Moreover, considering the environmental implications, the detailed knowledge of mineralogy and crystal chemistry of the different ultramafic rocks can help to understand the distribution of PTEs and their fate during weathering processes, because element mobility, bioavailability, and mineral stability are strictly related to the mineralogical assemblages. As an example, Ni is generally more mobile than Cr because the latter is bounded in more weathering-resistant minerals (i.e., chromite and Cr-bearing magnetites) (e.g., Kierczak et al., 2007; Quantin et al., 2008; Cheng et al., 2011).

For all these reasons, the occurrence of ultramafic rocks and the knowledge of the chemical and mineralogical variations as a function of these factors may play an important role in environmental management (Kumarathilaka et al., 2014; Tashakor et al., 2014).

The aim of this study is to assess the role of meso- and micro-scale lithological, mineralogical, textural, and structural factors in the concentration and distribution of PTEs (V, Cr, Co, Ni, Cu, and Zn) in the serpentinized ultramafic rocks occurring in the high pressure-low temperature (HP-LT) ophiolites of the Voltri Massif (Central Liguria, Italy), which is one of the widest metaophiolite outcrops in the Western Alps.

4.2. MATERIAL AND METHODS

A preliminary detailed geo-structural survey has been performed in eight sites of the Voltri Massif (VM) with good exposures of ultramafic rocks (e.g. roadcut, abandoned quarries, stream banks), that were representative of significant structural and textural variations.

Forty-five rock samples have been selected according to i) the different degree of serpentinization (i.e., 50 to 90% of serpentinization), as well as to ii) textural (i.e., massive vs foliated serpentinites) and iii) structural (i.e., presence of one or more sets of veins or fractures or contact with other lithologies) criteria.

The rock samples have been analyzed using a multiscale and multi-analytical approach including: i) mineralogical, petrographic description and microstructural analysis by means of polarized-light optical microscopy and scanning electron microscopy (SEM-EDS); ii) qualitative and quantitative mineralogical analyses by means of X-ray powder diffraction (XRPD); iii) minero-chemical analysis by means of electron microprobe analyzer (EMPA-WDS) and laser ablation-inductively coupled plasma-mass spectrometry (LA-ICP-MS); iv) bulk rock chemical analyses by means of energy dispersive X-ray fluorescence (EDXRF) and ICP-AES.

SEM-EDS analyses have been performed on selected representative carbon-coated thin sections of studied rock samples at the Department for Earth, Environmental and Life Sciences (DISTAV) of the University of Genova (Italy), using a SEM Vega3 – TESCAN type LMU system equipped with an EDS EDAX APOLLO XSDD with DPP3 analyzer. Analyses were performed at the following conditions: 20 kV accelerating voltage, 1.2 nA beam current, 10-40 μm beam diameter, 15 mm working distance. Counting times were set at 60 s to prevent damage to the coated surface. Calibration for chemical analysis was accomplished with a set of synthetic and natural standards.

X-ray powder diffraction was performed on eight samples, that have been selected according to serpentinization and deformation degree. The analysis has been performed on pulverized samples at the Department of Physics and Geology, University of Perugia (Italy) and has been carried out using a Philips PW1710 diffractometer equipped with a Cu-anode ($\text{CuK}\alpha$ radiation; range 5-80° 2 θ ; step size 0.02° 2 θ). Metallic silicon (10 wt%) was added as standard for amorphous phases quantification. Rietveld refinements were conducted with General Structure Analysis Software (GSAS; Larson and Von Dreele, 2004).

The most representative samples (eleven carbon-coated metallographic sections) were analyzed by the EMPA-WDS JEOL 8200 Super Probe at the Department of Earth Sciences “Ardito Desio”, University of Milano (Italy). The working conditions were set at 15 kV accelerating voltage and 4.9 nA beam current. Calibration for chemical analysis was accomplished by using the

following standards: olivine (Mg), omphacite (Na), Cr₂O₃ (Cr), rhodonite (Mn and Zn), k-feldspar (K), anorthite (Al and Ca), wollastonite (Si), pure V, fayalite (Fe), ilmenite (Ti), CoO (Co), galena (S), niccolite (Ni).

Trace and ultra-trace elements of selected minerals (e.g., olivines, pyroxenes, serpentines, and spinel-group minerals) were determined with detection limits below ppm units by laser ablation-inductively coupled plasma-mass spectrometry (LA-ICP-MS) at the Department of Physics and Geology, University of Perugia (Italy); details on the working conditions, instrumentation, precision, and accuracy are reported in Petrelli et al. (2016).

Bulk chemical analyses were assessed by means of X-MET7500 (Oxford Instruments) EDXRF spectrometer (GeoSpectra s.r.l. - University of Genova Spin-Off company) and by ICP-AES at the Regional Agency for Environmental Protection of Liguria (ARPAL, Genova, Italy), using a Perkin Elmer - Optima 2100 DV spectrometer, on 3.5 g sample powder after total digestion of the material by melting with *aqua regia* (1 cc HNO₃ + 2 cc HCl).

4.3. RESULTS

4.3.1. Petrographic, mineralogical, and microstructural features of the studied rocks

The studied rocks can be grouped into three main groups (Fig. 4.1): i) partially serpentinized lherzolites (**PSP**) with a serpentinization overprint that ranges between 50 to 90 % (Fig. 4.1A); ii) massive serpentinites (**MS**) with a prevailing undeformed massive texture, with a serpentinization degree that ranges between 90% to 100% (Fig. 4.1B); iii) foliated serpentinites (**FS**) with a serpentinization degree between 95% to 100% (Fig. 4.1C).

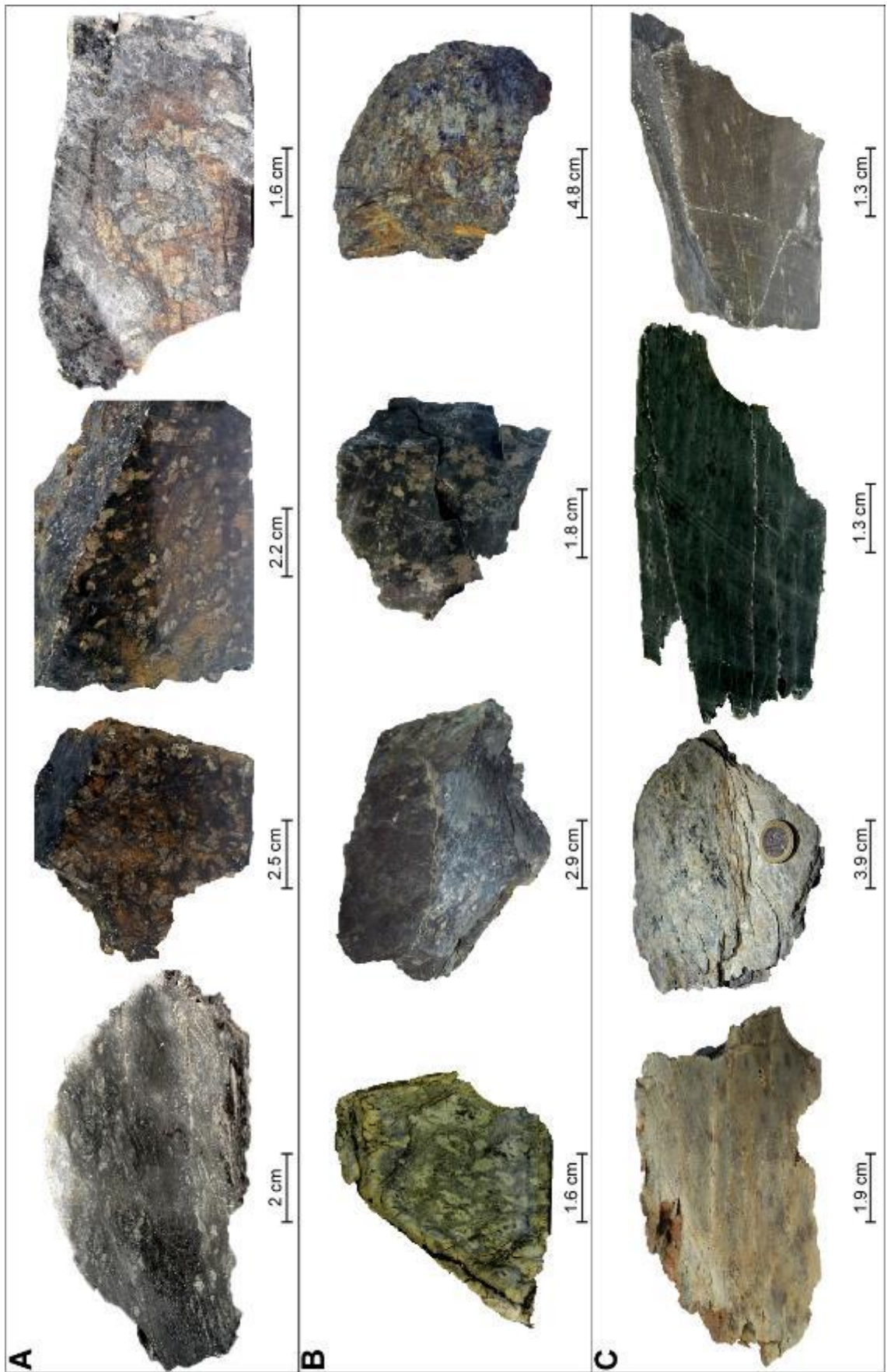


Fig. 4.1 Examples of studied ultramafic rocks from the Voltri Massif metaophiolites: A) partially serpentinized lherzolites (PSP); B) massive serpentinites (MS); C) foliated serpentinites (FS).

Partially serpentinized Iherzolites (PSP)

PSP form metric to pluri-metric bodies bordered by decametric- to metric-thick serpentinitic shear zones; they are medium (1-5 mm) to coarse- (5-10 mm) grained rocks displaying a granular to porphyroclastic texture with pyroxene crystals (up to 5 mm) that are locally oriented allowing to identify a weakly preserved magmatic foliation.

PSP show well-preserved pseudomorphic textures (i.e., mesh textures and bastites) with relics of forsteritic olivine (Fo89), clinopyroxenes (augite and diopside), enstatite (sometimes partially replaced by amphiboles), and spinel-group minerals (mainly Cr-spinel; Fig. 4.2A).

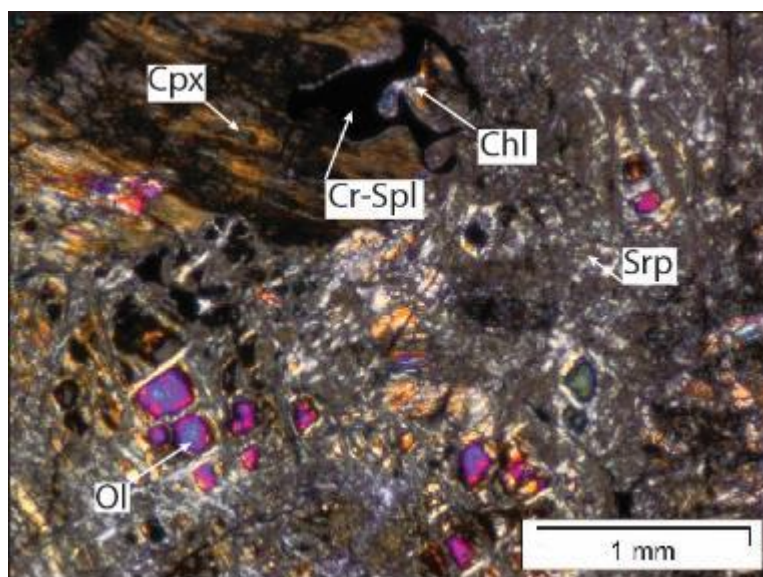


Fig. 4.2A Photomicrographs of the PSP: mesh texture with olivine relics and bastitic pyroxenes (crossed-polarized light - XPL). Mineral abbreviations are after Kretz (1998).

Antigorite and magnetite are the main minerals within mesh textures and bastites, with subordinate chrysotile and chlorite within mesh rims and along grain boundaries. Locally, mm-thick mylonitic shear zones cut the pseudomorphic textures isolating sigmoidal-shape domains where the mesh textures evolve to hourglass, ribbon and/or interpenetrating textures from the center toward the rims. The outer mylonitic shear zones are exclusively composed by synkinematic antigorite, intimately intergrown with chlorite, and fine-grained magnetite and Cr-magnetite. Along shear-zone antigorite \pm chrysotile bastites are commonly deformed and pervasively kinked.

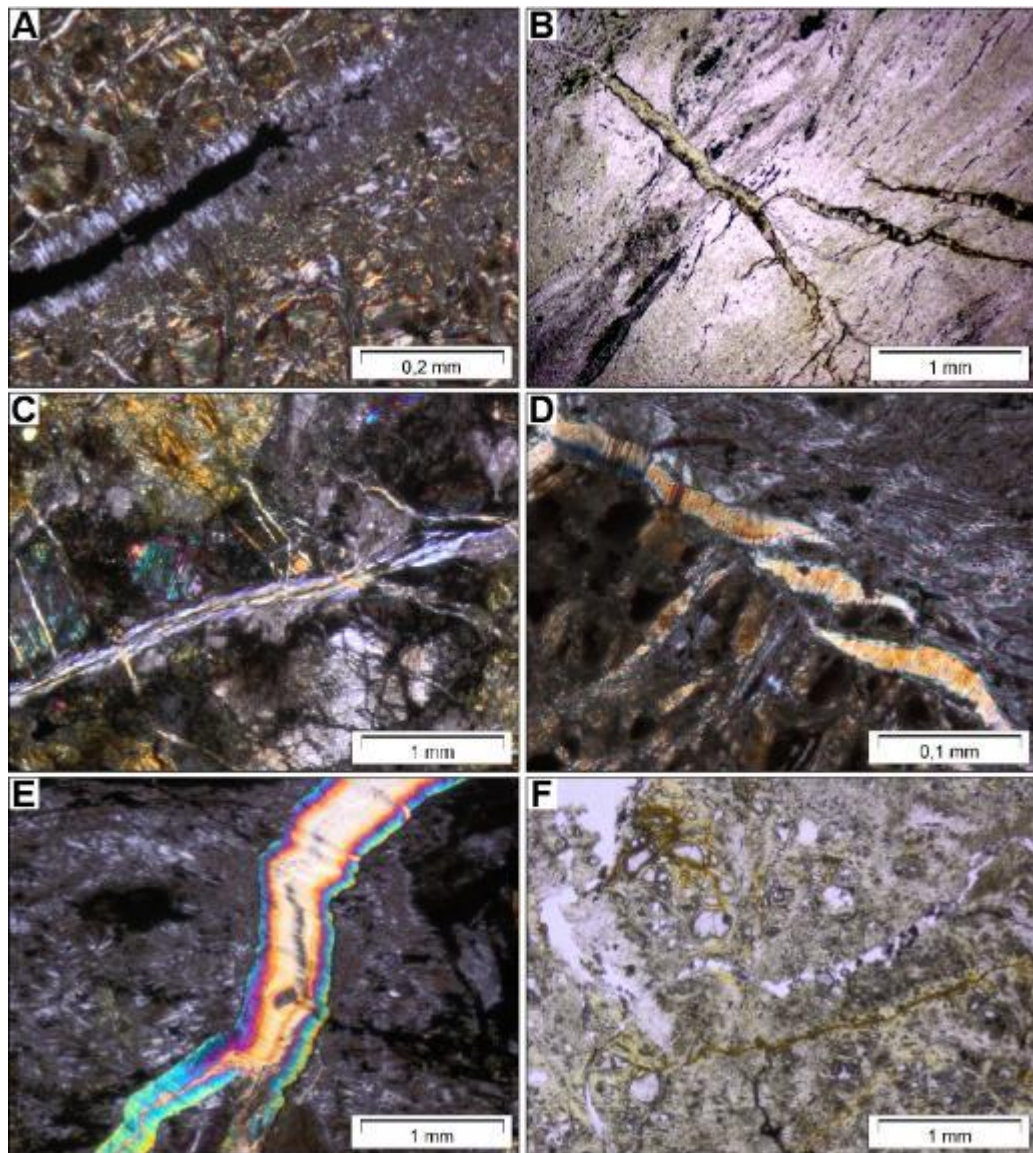


Fig. 4.3 Photomicrographs of the vein systems in the PSP: A) syntaxial veins filled by chrysotile cross-fibers and magnetite (XPL); B) stretched veins filled by chrysotile cross-fibers (PPL); C) shear veins filled by chrysotile slip-fibers (XPL); D) sigmoidal veins filled by chrysotile and chlorite (XPL); E) composite veins filled by talc and chrysotile (XPL); F) oxidized magnetite veinlets (PPL).

PSP are generally crosscut by several veins, which can be grouped as follow on the basis of spatial relationships and filling (Fig. 4.3A-E): 1) syntaxial submillimetric veins (up to ~200 μm in width) mainly occurring in the domains preserving pseudomorphic textures; these veins are filled with chrysotile cross-fibers, growing symmetrically from the vein rims, and subidiomorphic magnetite crystals along the median line (Fig. 4.3A); 2) millimetric stretched veins (up to ~2 mm in width) crosscutting the foliation and filled with chrysotile cross-fibers \pm talc \pm brucite (Fig. 4.3B); 3) shear veins (up to ~100 μm in width) parallel to foliation and connected with extensional veins at high angles; they are mainly filled with deformed slip-fibers of chrysotile with minor talc and magnetite (Fig. 4.3C); 4)

sigmoidal veins and en-échelon veins (5-70 μm in width) with a random spatial distribution, filled with fibrous chlorite and chrysotile (Fig. 4.3D); 5) composite veins (up to ~ 2 mm in width) crosscutting the foliation and the other set of veins (1-4); they are mainly filled with fibrous talc associated with minor chrysotile and magnetite (Fig. 4.3E); 6) micrometric magnetite veinlets (< 50 μm) forming an irregular network and crosscutting all the other vein sets; magnetite is commonly oxidized, with oxidation patterns along the vein rims and oxidation halos in the adjoining selvages (Fig. 4.3F).

Serpentines represent about 50 wt% of the overall mineralogical composition (Table 4.1), with dominant antigorite (ranging from 26 to 49 wt%; Fig. 4.4A) and subordinate chrysotile (ranging from 8 to 27 wt%), which reach the higher concentration in the highly fractured samples.

Clinochlore (7-25 wt%), augite, (16-33 wt%), enstatite (5-7 wt%), and spinel-group minerals (mainly magnetite and subordinate Cr-spinels; up to 5 wt%) are diffuse but always subordinate. Forsterite and actinolite-tremolite amphibole occur locally and generally vary from 1 to 3 wt% (Table 4.1 and Fig. 4.4A).

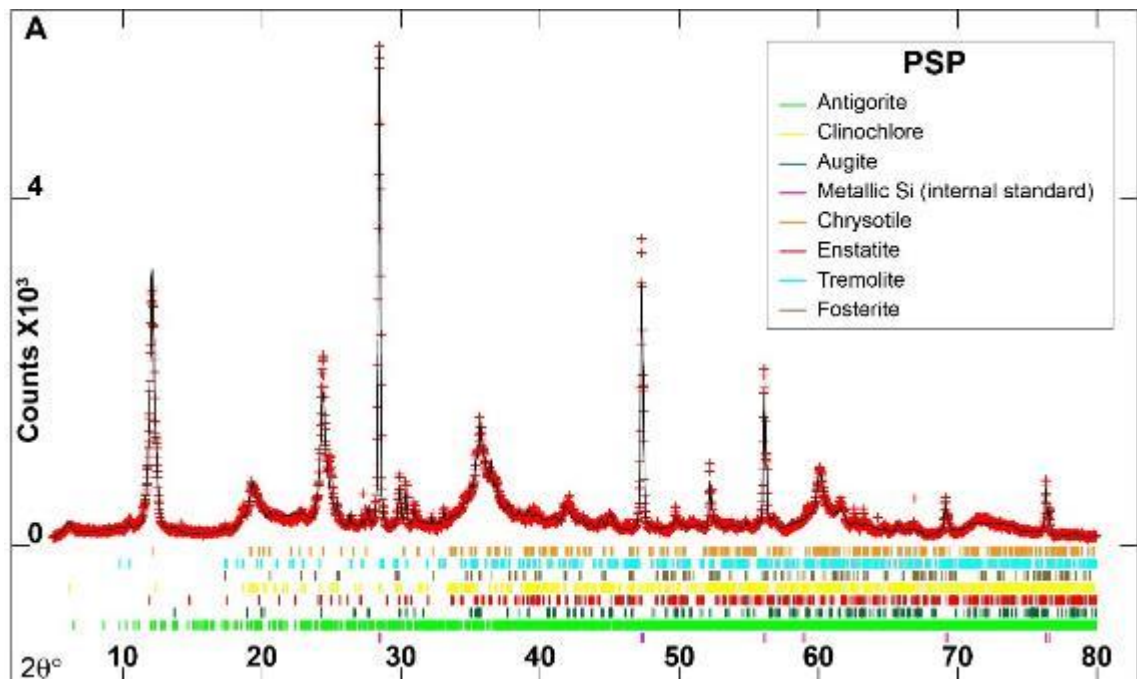


Fig. 4.4A Rietveld refinement patterns of powder XRPD data for the selected samples representative of PSP. Experimental data and calculated profiles are shown as red crosses and black solid lines, respectively. The colored thick lines at the bottom of the spectra represent the theoretical Bragg positions of recognized mineral phases.

Cryptocrystalline authigenic Fe-oxide and oxyhydroxides form oxidation halos around fractures, mylonitic zones and grain boundaries (mostly around olivine

and magnetite). These authigenic minerals correspond mostly to the amorphous phases quantified by Rietveld refinement (1-11 wt%).

The most common accessory minerals are talc and brucite, occurring associated with chrysotile within veins.

Rock	PSP	MS	FS
Antigorite	xxx	xxx	xxx
Chrysotile	xx	-	-
Augite	xx	-	-
Enstatite	x	-	-
Clinocllore	xx	-	-
Fosterite	(x)	-	-
Magnetite s.l.	-	x	(x)
Cr-spinels s.l.	(x)	-	-
Plagioclase	(x)	-	-
Tremolite	(x)	-	-
Amorphous phases	(x)	x	x
Accessory minerals*	Magnetite s.l., Ti, Di, Fe-ox, Bc, clay	Cr-spinels s.l., Chl, Ctl, Fe-ox, clay	Ilm, Ctl, Chl, Di, Ap, Zrn, Fe-ox, clay

Table 4.1 Mineralogy of selected rock samples determined by XRPD and Rietveld refinement. Legend: xxx = abundant (>30 wt%); xx intermediate = (10-30 wt%); x = minor (5-10 wt%); (x) = trace (1-5 wt%). *Accessory minerals have been detected by other techniques (e.g., PLOM, SEM, EMPA) and are supposed to be <1 wt%. Mineral abbreviations are after Kretz (1998). Cr-spinel s.l. comprises Cr-spinel, Al-chromite, and ferrian chromite; magnetite s.l. comprises magnetite and Cr-magnetite.

Massive serpentinites (MS)

MS occur as metric lenses wrapped by decimetric- to metric-thick cataclastic or mylonitic areas; they are medium- (1-5 mm) to fine-grained (<1 mm) serpentinite and display a massive texture with rare spinel-group minerals porphyroclasts (up to 5 mm).

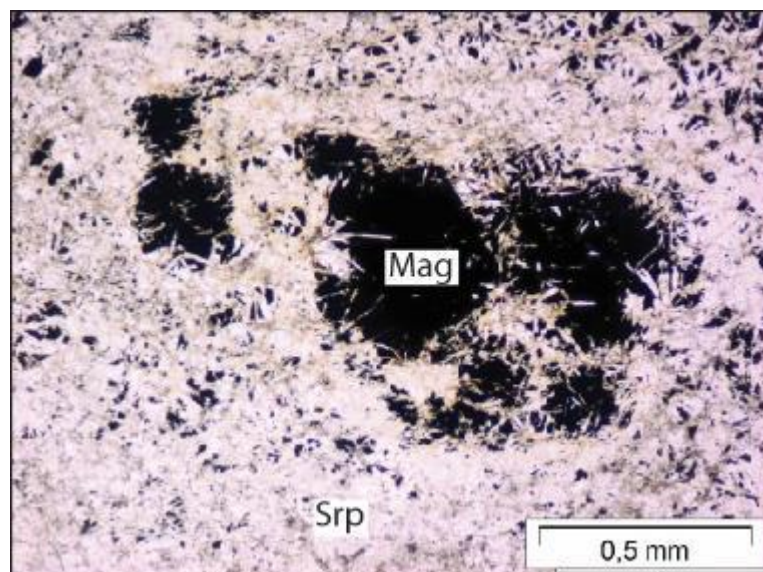


Fig. 4.2B Photomicrographs of the MS: magnetite and serpentine minerals aggregates within interpenetrating texture (PPL). Mineral abbreviations are after Kretz (1998).

Non-pseudomorphic interpenetrating textures are predominant although pseudomorphic textures (such as mesh, hourglass, ribbon, and bastitic textures) occur locally (Fig. 4.2B).

Antigorite and subordinate magnetite are the main minerals within the above-mentioned textures. Antigorite shows lamellar, acicular, and less frequently pseudo-fibrous habit, according to the different textures. Magnetite together with Cr-magnetite occurs also as scattered isolated porphyroclasts, in trails of micrometric crystals or in pseudo-rounded aggregates associated with antigorite. Fine-grained magnetite forms coronas around bastites or occurs along the mineralogical cleavage of former pyroxene. Magnetite and chrysotile are also the more common minerals within veins.

MS are generally crosscut by several veins, which can be grouped as follow on the basis of spatial relationships and filling: 1) stretched millimetric veins (up to ~1 mm in width) filled with chrysotile cross-fibers \pm talc \pm magnetite sometimes replaced by secondary Fe-oxyhydroxides (Fig. 4.3G); 2) antitaxial submillimetric veins (up to ~500 μm in width) filled with elongated magnetite crystals arranged symmetrically at the vein rims and chrysotile cross-fibers along the median line (Fig. 4.3H); 3) syntaxial submillimetric veins (up to ~200 μm in width) filled with chrysotile cross-fibers growing symmetrically from the vein rims and subidiomorphic magnetite crystals along the median line (Fig. 4.3I); 4) micrometric magnetite veinlets (<50 μm) forming an irregular network and crosscutting all the other vein sets; magnetite is commonly oxidized, with oxidation patterns along the vein rims and oxidation halos in the adjoining selvages.

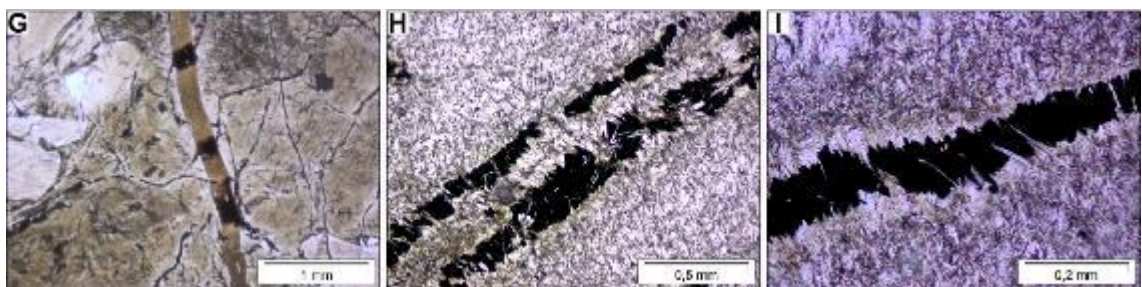


Fig. 4.3 Photomicrographs of the vein systems in the MS. G) stretched veins filled by chrysotile cross-fibers (PPL); H) antitaxial veins filled by magnetite and chrysotile cross-fibers (PPL); I) syntaxial veins filled by magnetite and chrysotile cross-fibers (PPL).

The main mineralogical phase of MS is antigorite (ranging from 88 to 98 wt%), with subordinate magnetite (up to 10 wt%), chrysotile (<1 wt%), talc (<1 wt%),

and chlorite (<1 wt%; Table 4.1 and Fig. 4.4B). Authigenic Fe-oxide and oxyhydroxides form commonly oxidation halos around fractures and grain boundaries (mostly around magnetite); they are generally cryptocrystalline and correspond mostly to the amorphous phases quantified by Rietveld refinement (2-11 wt%).

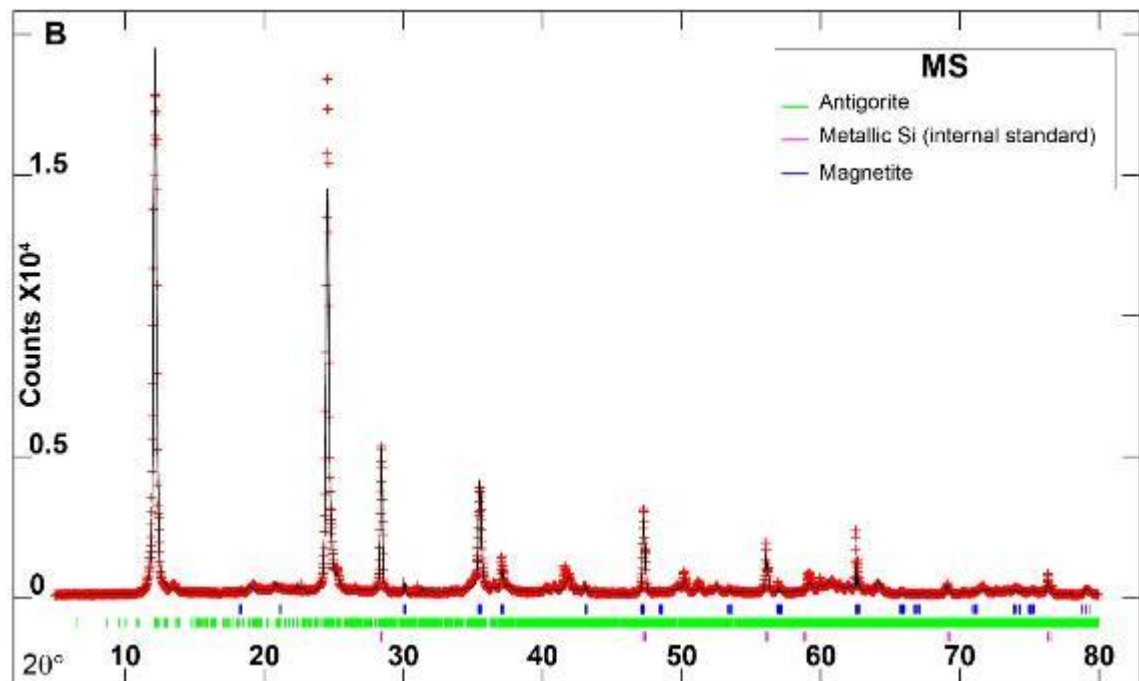


Fig. 4.4B Rietveld refinement patterns of powder XRPD data for the selected samples representative of MS. Experimental data and calculated profiles are shown as red crosses and black solid lines, respectively. The colored thick lines at the bottom of the spectra represent the theoretical Bragg positions of recognized mineral phases.

Foliated serpentinites (FS)

FS occur as decimetric- to metric-thick layers that wrap massive serpentinite domains, as a result of a variable strain partitioning in the most deformed zones. FS are fine- (<1mm) to medium-grained (1-5 mm) rocks with rare scattered subidiomorphic magnetite porphyroclasts (3–5 mm; Fig. 4.2C). FS generally show a pervasive foliation that is locally deformed by open folds.

This pervasive foliation, that is the main structural feature of FS, is defined by syn-kinematic lamellar or prismatic antigorite, acicular chlorite, microcrystalline magnetite, and minor apatite ± zircon. Rootless hinges of intrafoliar folds, with axial surfaces parallel to the main foliation, are preserved and define a composite fabric. The composite fabric is deformed by a later crenulation cleavage with an axial surface at a high angle with respect to the foliation. Locally, sigmoidal boudins along the foliation preserve domains with antigorite-rich pseudomorphic (ribbon and bastite textures) and non-pseudomorphic textures. Syn-kinematic

mm-sized magnetite often borders sigmoidal boudins together with ilmenite. Magnetite occurs also as mm-sized porphyroclasts along the foliation, showing brittle deformation patterns (i.e. *bookshelf structures*). Clinopyroxenes (mostly diopside) occur locally as relics along the foliation.

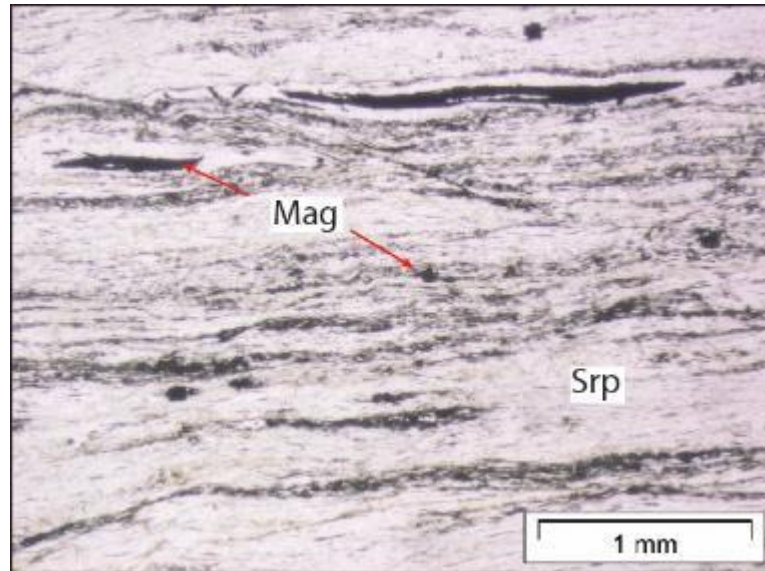


Fig. 4.2C Photomicrographs of the FS: fine-grained magnetite-rich layers within an antigorite-rich domain characterized by a pervasive schistosity (FS; PPL). Mineral abbreviations are after Kretz (1998).

FS are generally crosscut by several vein systems, which can be grouped as follow on the basis of spatial relationships and filling: 1) shear veins (up to ~100 μm in width) parallel to the foliation and mainly filled with deformed slip-fibers of chrysotile with minor talc and magnetite (Fig. 4.3L); 2) sigmoidal veins (100-300 μm in width) arranged parallel to the foliation and filled with microcrystalline magnetite mostly oxidized along the vein rims from which oxidation halos spread toward the adjoining selvages (Fig. 4.3M); 3) micrometric magnetite veinlets (<50 μm) forming an irregular network and crosscutting all the other vein sets (Fig. 4.3N).

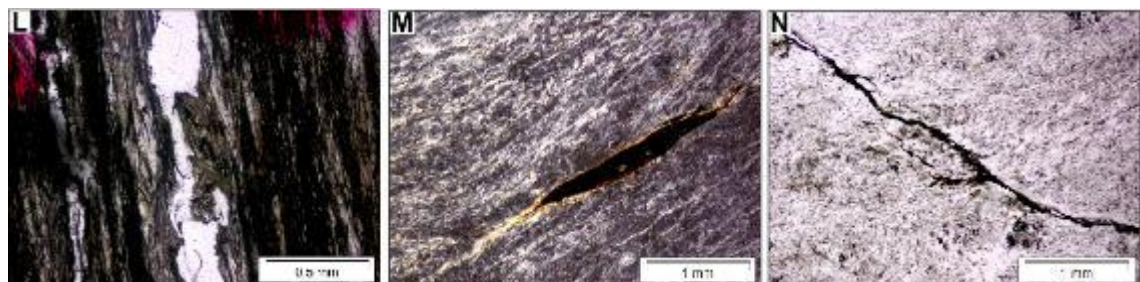


Fig. 4.3 Photomicrographs of the vein systems in the FS: L) shear veins filled by chrysotile slip-fibers (PPL); M) sigmoidal veins filled by magnetite (XPL); N) oxidized magnetite veinlets (PPL).

Antigorite represents about the 92 wt% of the overall mineralogical composition (ranging from 91 to 94 wt%; Table 4.1 and Fig. 4.4C), with subordinated magnetite (up to 5 wt%), chrysotile (<1 wt%), and chlorite (<1 wt%). Cryptocrystalline authigenic Fe-oxide and oxyhydroxides form oxidation halos around foliation, fractures, mylonitic zones, and grain boundaries. They correspond mostly to the amorphous phases quantified by Rietveld refinement (3-7 wt%). The most common accessory minerals are ilmenite, diopside, apatite, and zircon.

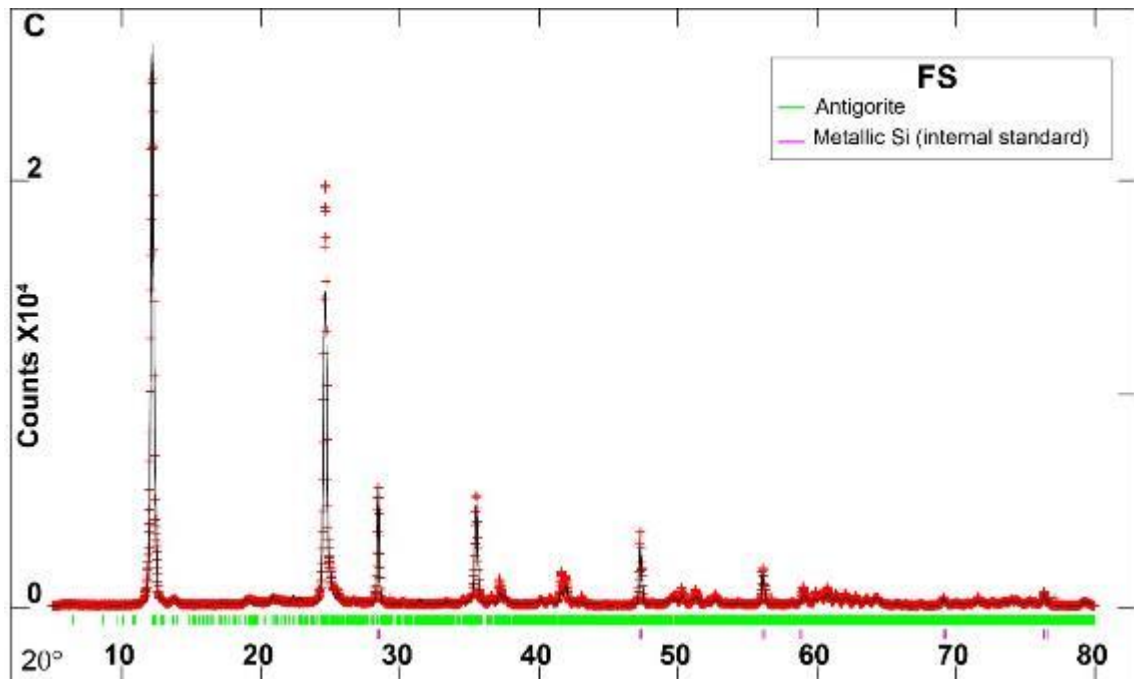


Fig. 4.4C Rietveld refinement patterns of powder XRPD data for the selected samples representative of FS. Experimental data and calculated profiles are shown as red crosses and black solid lines, respectively. The colored thick lines at the bottom of the spectra represent the theoretical Bragg positions of recognized mineral phases.

Locally, tremolite-chlorite hybrid rocks (TC; Fig. 4.5) are present within FS and MS where they are in contact with mafic rocks (mainly eclogitic gabbros and metabasites) or metasediments (mainly calcschists). TC occur as variable-sized and discontinuous lenses in MS or as irregular layers (millimetric to metric in thickness) within foliated serpentinite (Fig. 4.5A).

Within MS, elongated chlorite grows together with antigorite mainly in interpenetrating textures; post-kinematic chlorite ± tremolitic amphibole form clusters probably replacing former pyroxene.

Within FS tremolite-chlorite layers are characterized by a pervasive mylonitic foliation, that consist of a rhythmic alternance of amphibole-rich and chlorite-rich layers (100-500 μm), deformed by isoclinal folds. Amphibole-rich layers are made

by syn-kinematic fine-grained Ca-amphibole (mainly actinolite-tremolite), chlorite, rare carbonate, and apatite. Ilmenite and Ti-rich spinel are scattered in both layers. Locally acicular post-kinematic actinolite-tremolite grows in chlorite-rich layers. Tremolite-chlorite mylonites associated with foliated serpentinites are folded together producing a sequence of alternating serpentinite-rich (Fig. 4.5B), amphibole-rich and chlorite-rich layers. The serpentinite-rich layers include syn-kinematic antigorite growing together with chlorite and scattered opaque minerals (mainly magnetite and ilmenite).

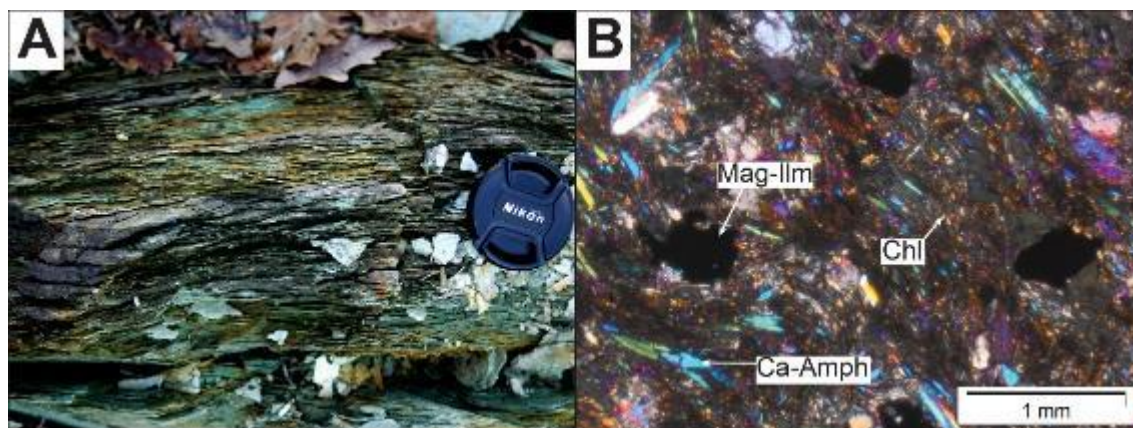


Fig. 4.5 A) Outcrop photo of tremolite-chlorite hybrid rocks associated to foliated serpentinites. B) Photomicrographs of the tremolite-chlorite-rich deformed layers with scattered magnetite and ilmenite crystals in foliated serpentinites (crossed-polarized light). Mineral abbreviations are after Kretz (1998).

4.3.2. Mineral chemistry of the PTEs-bearing minerals

The PTEs considered in this work are mainly hosted in serpentines (Cr, Ni, and Co), spinel-group minerals (Cr, Ni, and Co), pyroxenes (mainly Cr and subordinately V and Ni), olivines (mainly Ni), chlorites (Cr and Ni), tremolite (V, Co, and Ni), talc (Ni and Cr), ilmenite (V), and weathering products (mainly Fe-oxides and -oxyhydroxides which are strongly enriched in Ni, Cr, and subordinately Co) (Fig. 4.6 and Table 4.2). The complete EMPA-WDS and LA-ICP-MS database, using for the statistical analyses, is available on the electronic support (*Appendix B1 and B3*).

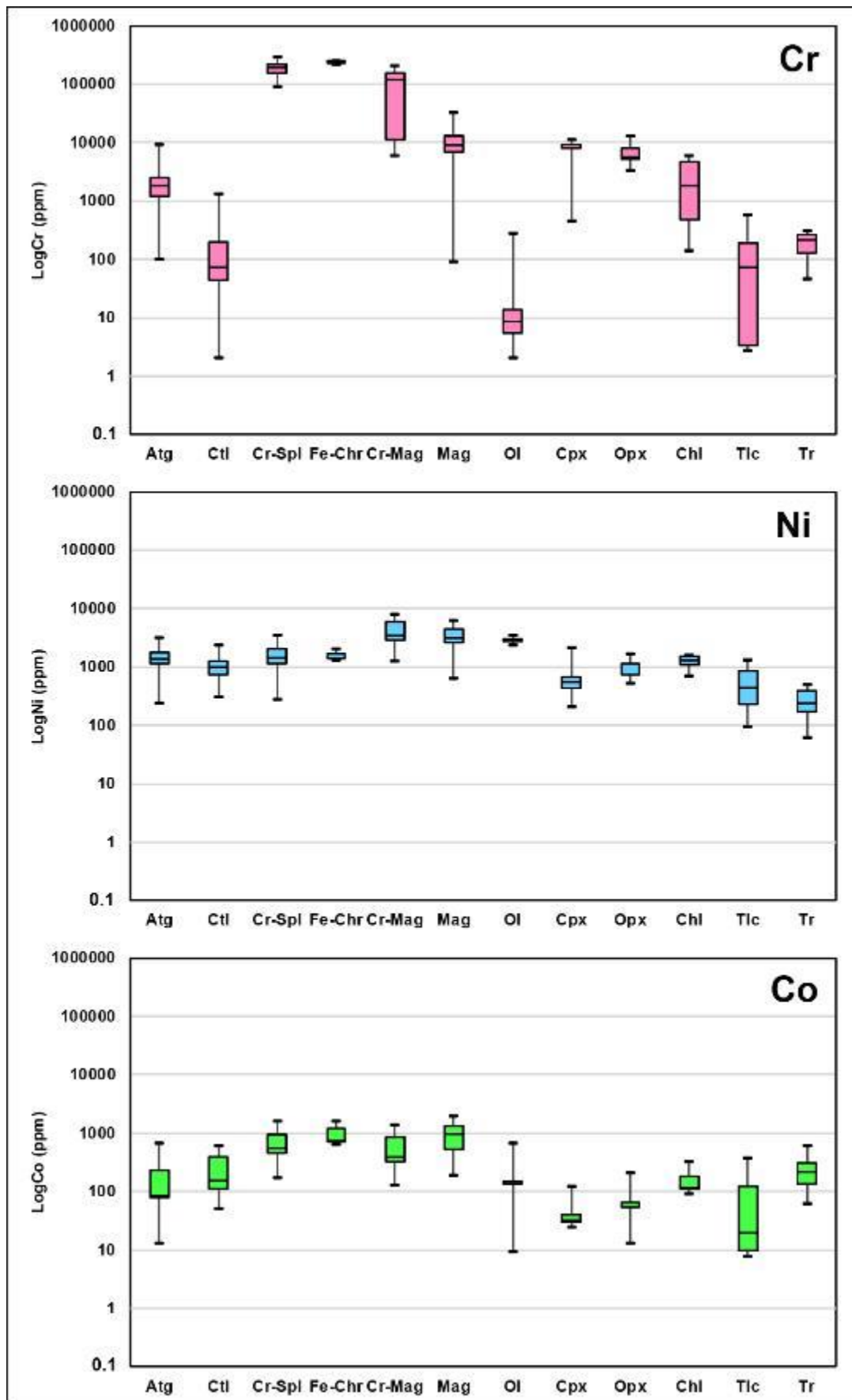


Fig. 4.6 Box plots showing statistical parameters of concentrations (in ppm) of Cr, Ni, Co, V, Cu, and Zn in the different minerals (EMPA-WDS and LA-ICP-MS data). Vertical lines show the range in concentrations, the boxes are bounded by the 1st and 3th quartile values, and the horizontal line inside the box represents the median value.

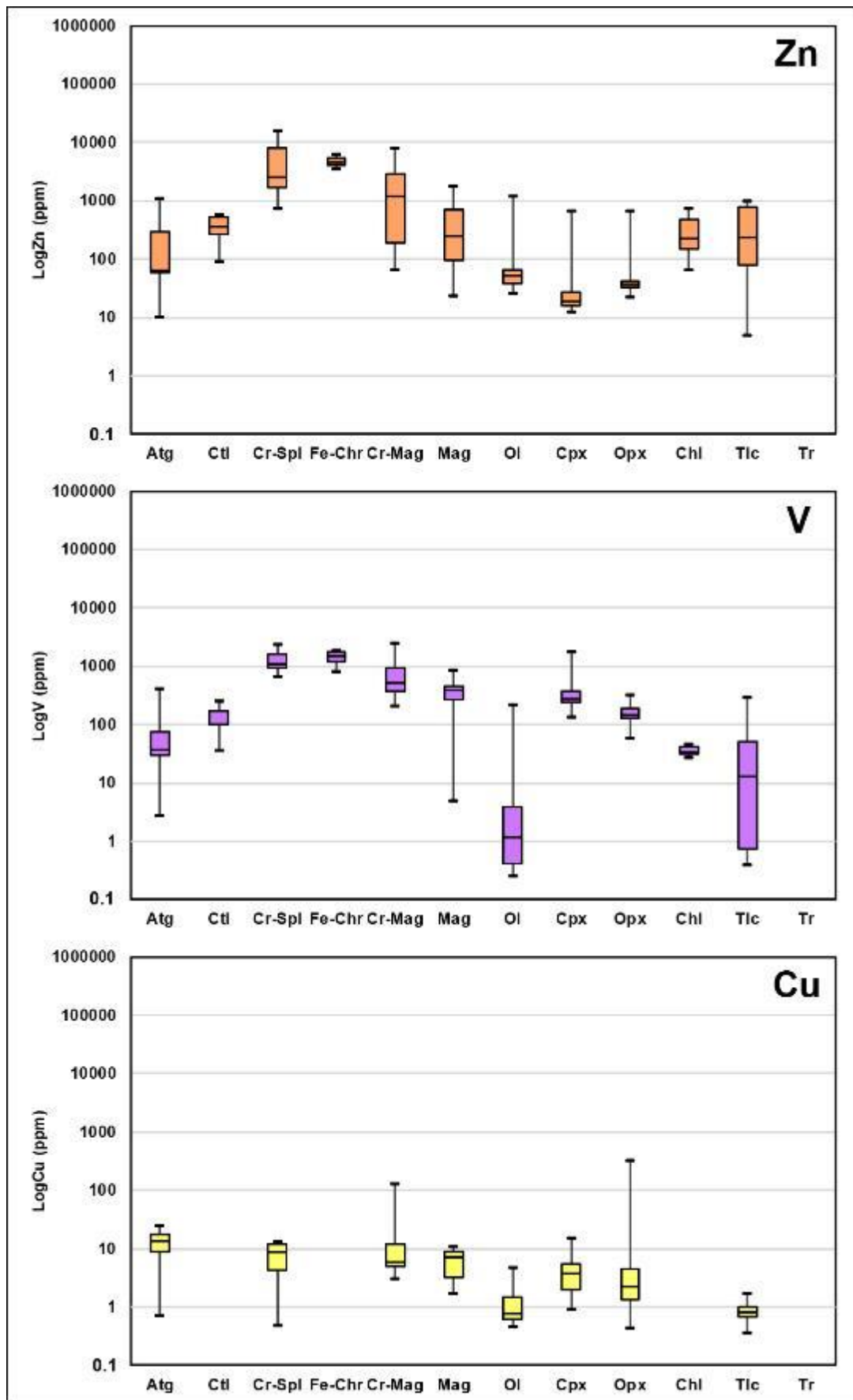


Fig. 4.6 Continued

Serpentines

Serpentines (antigorite and subordinately chrysotile) are the main mineral species in the three rock groups (PSP, MS, and FS) and in all textural (i.e., pseudomorphous and non-pseudomorphous textures) and structural domains (i.e., veins and fractures). The main PTEs hosted in serpentines are Cr and Ni, and subordinately Co, Zn, V, and Cu (Fig. 4.6 and Table 4.2). Among the serpentines, antigorite is the main PTEs-bearing mineral showing the highest concentration and the widest ranges of Cr (101-9397 ppm), Ni (244-3131 ppm), Zn (10-1113 ppm), Co (13-673 ppm), and V (3-415 ppm). The wide variations in Cr and Ni do not evidence correlation with the different serpentinite groups or textural/structural domain both for antigorite and chrysotile (Fig. 4.7). Nevertheless, antigorite occurring in mesh textures after olivine are invariably enriched in Ni (up to 3198 ppm) with respect to those occurring in bastites (up to 1283 ppm), which on the contrary evidence the highest Cr content (up to 9397 ppm) and not-negligible amount of other PTEs (Co, V, Zn, and Cu). Chrysotile in veins is characterized by low and quite homogeneous Cr and Ni contents (up to 727 and 1168 ppm, respectively).

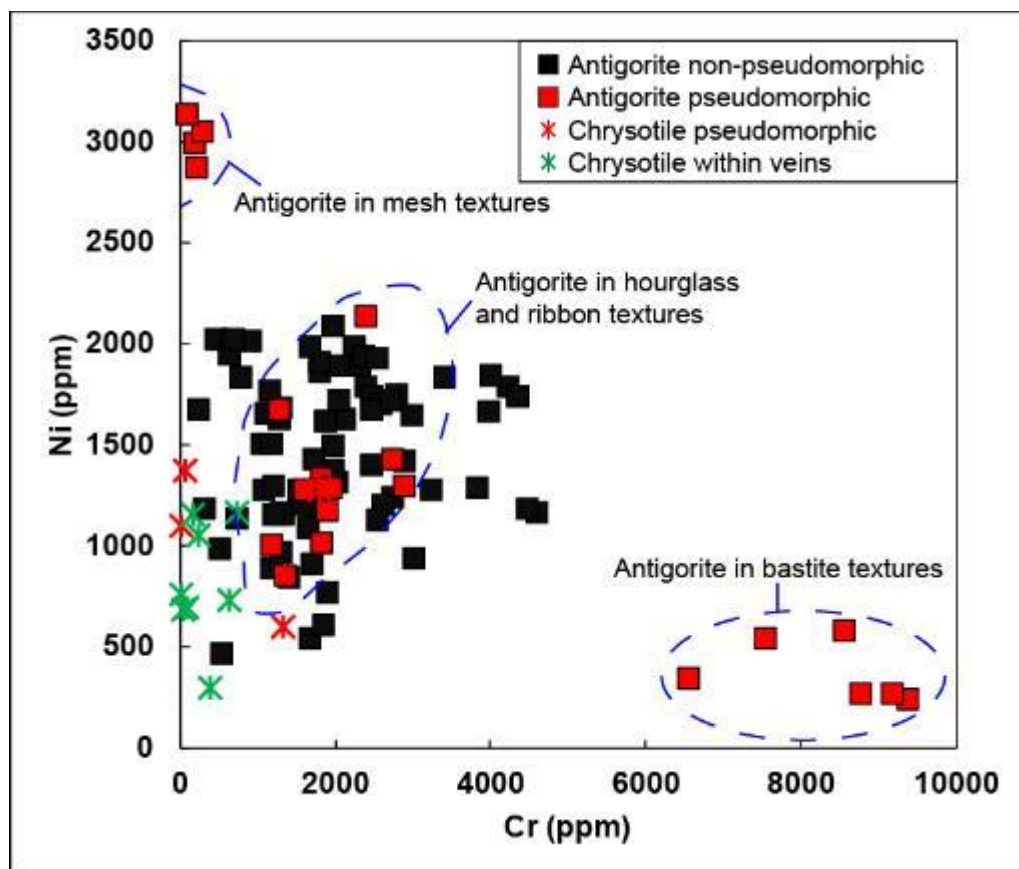


Fig. 4.7 Cr vs Ni contents (ppm) of antigorite and chrysotile in the studied rocks grouped according to the micro-structural or -textural location (EMPA-WDS and LA-ICP-MS data).

Minerals	Antigorite			Chrysotile	
	Rock	PSP	MS	FS	PSP
SiO ₂	37.90	43.27	43.17	40.38	42.80
TiO ₂	bdl	0.02	0.02	0.07	0.03
Al ₂ O ₃	0.56	1.30	1.65	0.54	1.33
Cr ₂ O ₃	bdl	0.32	0.29	0.23	0.23
FeO _{tot}	9.46	2.90	4.44	8.09	2.36
MgO	33.27	37.30	36.21	33.64	37.06
MnO	0.09	0.07	0.08	0.15	0.05
NiO	0.25	0.15	0.17	0.17	0.12
CaO	0.05	0.01	0.02	0.32	0.02
Na ₂ O	0.02	0.01	0.03	0.02	0.01
K ₂ O	bdl	0.01	0.01	0.02	0.01
V ₂ O ₅	0.02	0.02	0.02	0.03	0.03
CoO	0.06	0.03	0.03	0.04	0.08
SO ₂	0.15	0.03	0.03	0.06	0.02
ZnO	0.03	0.06	0.06	0.04	0.05
Sum	81.79	85.42	86.15	83.42	84.11
Structural formula calculated basis on 14 oxygens					
Si	3.93	4.19	4.18	4.10	4.19
Ti	0.00	0.00	0.00	0.00	0.00
Al _{tot}	0.07	0.15	0.19	0.04	0.15
Cr	0.00	0.02	0.02	0.01	0.02
Mg	5.14	5.38	5.22	5.09	5.41
Mn	0.01	0.01	0.01	0.01	0.00
Ni	0.02	0.01	0.01	0.01	0.01
Ca	0.01	0.00	0.00	0.04	0.00
Na	0.00	0.00	0.00	0.00	0.00
K	0.00	0.00	0.00	0.00	0.00
V	-	-	-	-	-
Co	-	-	-	-	-
Zn	-	-	-	-	-
S	-	-	-	-	-
Fe _{tot}	0.82	0.23	0.36	0.69	0.19
Fe ³⁺	-	-	-	-	-
Fe ²⁺	-	-	-	-	-
Sum	10.00	10.00	10.00	10.00	10.00

Table 4.2A Representative analysis of the serpentines (EMPA-WDS data) and calculated formulas.

Spinel-group minerals

Spinel-group minerals occur in all the rock groups and have a wide compositional range covering the fields of Cr-spinel (in PSP), ferrian chromite and Cr-magnetite (both in PSP and in MS), and magnetite (in all three rock groups; Fig. 4.6). These crystallochemical variations appear to be strictly related to the degree of serpentinization. The main PTEs hosted in spinel-group minerals are Cr, Zn, and

Ni, and subordinately Co, V, and Cu (Fig. 4.6 and Table 4.2). As a general rule, other than Cr, V and Zn content decreases from Cr-spinel (median Cr 202660 ppm, V 1132 ppm, Zn 2680 ppm) toward magnetite (median Cr 9201, Zn 258 ppm, V 407 ppm); conversely, Ni and Co increase from Cr-spinels (median Ni 1480 ppm and Co 579 ppm) to magnetite (median Ni 3133 ppm and Co 1032 ppm). In general, Cu is present in a negligible amount in all spinel-group minerals (up to 131 ppm) (see Chapter V).

Minerals	Cr-Spinel	Ferrrian chromite		Cr-Magnetite		Magnetite		
	PSP	PSP	MS	PSP	MS	PSP	MS	FS
SiO ₂	0.04	0.04	0.02	0.32	0.05	0.46	0.06	0.07
TiO ₂	0.19	0.46	0.62	0.39	0.61	0.01	0.14	0.21
Al ₂ O ₃	37.22	5.54	0.09	2.01	0.07	0.03	0.02	0.01
Cr ₂ O ₃	27.11	33.99	36.20	23.47	21.43	0.02	1.29	1.71
FeO _{tot}	23.23	53.60	57.37	67.17	69.84	91.69	90.36	90.94
MgO	11.81	1.55	0.83	1.20	1.61	0.58	0.66	0.23
MnO	0.23	0.46	1.66	0.35	1.53	0.12	0.29	0.16
NiO	0.15	0.21	0.18	0.33	0.47	0.12	0.60	0.35
CaO	0.00	0.00	bdl	0.01	0.01	0.01	0.01	0.01
Na ₂ O	0.03	0.04	0.01	0.02	0.02	bdl	0.03	0.02
K ₂ O	0.00	bdl	0.01	0.00	bdl	0.01	0.00	0.00
V ₂ O ₅	0.20	0.31	0.14	0.23	0.09	bdl	0.05	0.06
CoO	0.10	0.09	0.21	0.09	0.12	0.15	0.14	0.16
SO ₂	bdl	bdl	bdl	bdl	bdl	bdl	bdl	bdl
ZnO	0.52	0.61	0.57	0.26	0.38	0.03	0.04	0.04
Sum	100.83	96.89	97.92	95.85	96.23	93.23	93.68	93.98
Structural formula calculated basis on 3 cations								
Si	0.00	0.00	0.00	0.01	0.00	0.02	0.00	0.00
Ti	0.00	0.01	0.02	0.01	0.02	0.00	0.00	0.01
Al_{tot}	1.27	0.23	0.00	0.09	0.00	0.00	0.00	0.00
Cr	0.63	0.98	1.06	0.69	0.63	0.00	0.04	0.05
Mg	0.51	0.08	0.05	0.07	0.09	0.03	0.04	0.01
Mn	0.01	0.01	0.05	0.01	0.05	0.00	0.01	0.01
Ni	0.00	0.01	0.01	0.01	0.01	0.00	0.02	0.01
Ca	0.00	0.00	-	0.00	0.00	0.00	0.00	0.00
Na	0.00	0.00	0.00	0.00	0.00	-	0.00	0.00
K	0.00	-	0.00	0.00	-	0.00	0.00	0.00
V	0.00	0.01	0.00	0.01	0.00	-	0.00	0.00
Co	0.00	0.00	0.01	0.00	0.00	0.00	0.00	0.00
Zn	0.01	0.02	0.02	0.01	0.01	0.00	0.00	0.00
S	-	-	-	-	-	-	-	-
Fe_{tot}	-	-	-	-	-	-	-	-
Fe³⁺	0.09	0.74	0.89	1.16	1.32	1.96	1.95	1.93
Fe²⁺	0.48	0.90	0.90	0.93	0.85	0.97	0.93	0.97
Sum	3.00	3.00	3.00	3.00	3.00	3.00	3.00	3.00

Table 4.2B Representative analysis of the spinel-group minerals (EMPA-WDS data) and calculated formulas.

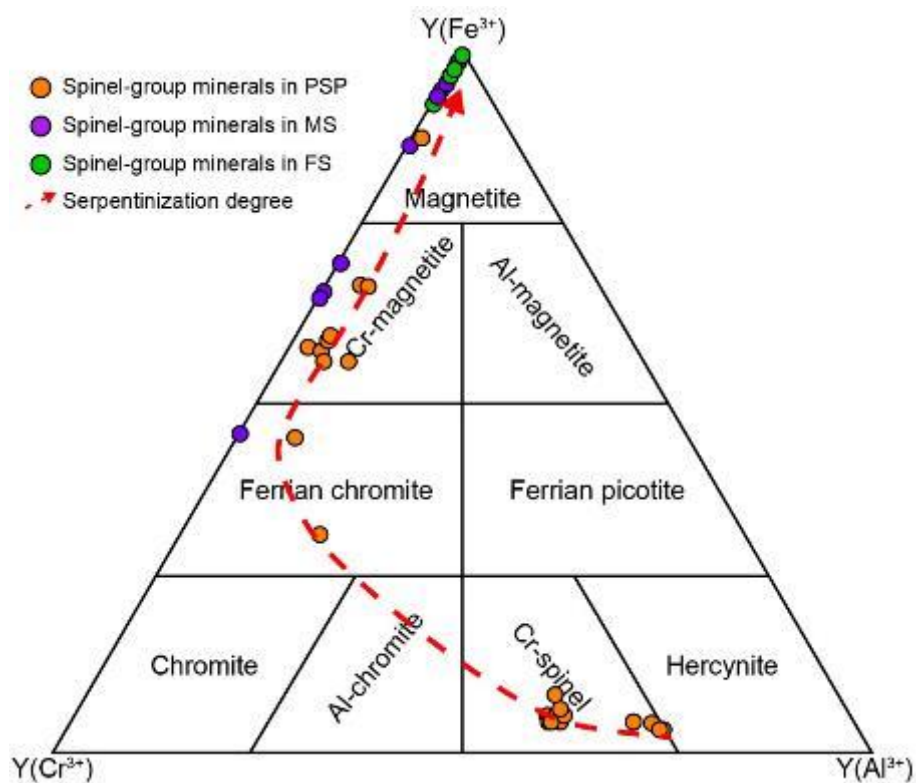


Fig. 4.8 Spinel-group minerals classification diagram (Al^{3+} , Cr^{3+} , and Fe^{3+}); compositional fields are from Stevens, 1944; Haggerty, 1991; Zussman et al., 1992; Gargiulo et al., 2013).

Olivines and pyroxenes

Olivines (Fo89) occur as relic only in mesh-textures of PSP. They contain a very high concentration of Ni (2326-3514 ppm; median 2921 ppm) and non-negligible amounts of Co (9-661 ppm; median 141 ppm) (Fig. 4.6B-C and Table 4.2).

Among the silicates, enstatite is the main Cr-bearing phase (3344-13000 ppm; median 5830 ppm); clinopyroxenes (augites and diopside) have the highest concentration and the widest ranges of Ni (207-2200 ppm; median 580 ppm) and V (135-1793 ppm; median 300 ppm). Zn, Cu, and Co are always present in a negligible amount (Fig. 4.6 and Table 4.2).

Chlorites, tremolite, and talc

Chlorites (mainly clinochlore) occur in PSP as coronas around Cr-spinel porphyroclasts whereas they form cryptocrystalline to microcrystalline aggregates intimately associated with antigorite in pseudomorphic and non-pseudomorphic textures or with chrysotile in several vein types. Clinochlore in PSP is an important carrier of PTEs (Fig. 4.6 and Table 4.2), showing high contents and a wide range of Cr (141-5916 ppm), Ni (717-1626 ppm), and subordinately Zn (66-731 ppm) and Co (90-326 ppm).

Talc mainly occurs as vein filling associated with magnetite and chrysotile in the three rock groups. Talc shows a wide range of Ni (97-1334 ppm) and Zn (5-1005 ppm), and subordinately of Cr (3-580 ppm) and Co (8-377 ppm; Fig. 4.6 and Table 4.2).

Tremolite is mainly concentrated in the salband of MS and FS developing close tremolite-chlorite hybrid rocks. Tremolite is generally characterized by significant and quite homogeneous concentrations of Cr, Co, and Ni (up to 312, 617, and 512 ppm, respectively) (Fig. 4.6 and Table 4.2).

Accessory phases

Ilmenite is a widespread accessory mineral in FS where it occurs associated with magnetite both in trails developed along the main foliation and in aggregates. Other than Ti, ilmenite is an important carrier of V (up to 20391 ppm) and Zn (up to 1880) (Table 4.2).

Minerals	Olivine	Enstatite	Augite	Diopside		Chlorite	Talc	Tremolite	Ilmenite
Rock	PSP	PSP	PSP	PSP	FS	PSP	PSP	MS	FS
SiO ₂	40.66	55.34	51.14	50.96	50.42	34.41	42.29	59.13	0.07
TiO ₂	0.01	0.09	0.18	0.40	0.43	0.00	0.03	0.08	52.94
Al ₂ O ₃	0.01	3.68	3.05	5.16	6.29	13.71	0.21	0.12	0.01
Cr ₂ O ₃	bdl	0.74	0.79	1.31	0.95	0.37	0.01	0.01	0.10
FeO _{tot}	9.90	6.49	3.11	2.74	2.72	2.94	7.86	2.79	39.76
MgO	48.09	32.07	20.29	15.28	15.68	33.34	32.33	21.68	1.48
MnO	0.17	0.16	0.31	0.06	0.22	0.02	0.17	0.08	2.85
NiO	0.37	0.10	0.06	0.05	0.20	0.16	0.08	0.04	0.07
CaO	0.01	0.75	16.72	23.22	22.95	0.01	0.06	13.14	0.01
Na ₂ O	bdl	0.04	0.51	0.30	0.74	0.01	0.02	0.24	bdl
K ₂ O	bdl	0.01	0.01	bdl	0.03	bdl	0.01	0.02	bdl
V ₂ O ₅	bdl	0.02	0.03	0.06	0.12	0.00	0.00	0.00	3.49
CoO	bdl	0.01	0.01	0.01	bdl	0.01	bdl	0.03	bdl
SO ₂	bdl	0.02	0.01	bdl	bdl	0.01	bdl	bdl	bdl
ZnO	bdl	0.03	0.00	0.03	bdl	0.02	bdl	bdl	0.09
Sum	99.22	99.55	96.22	99.58	100.48	85.02	83.07	97.35	100.86
Structural formula calculated basis on n⁺:									
	4 oxygens	6 oxygens				14 oxygens	22 oxygens	24 oxygens	4 cations
Si	1.01	1.93	1.90	1.87	1.82	1.15	6.64	8.11	0.00
Ti	0.00	0.00	0.00	0.01	0.01	0.40	0.00	0.02	1.98
Al _{tot}	0.00	0.15	0.13	0.22	0.27	0.00	0.04	0.01	0.00
Cr	-	0.02	0.02	0.04	0.03	0.01	0.00	0.00	0.00
Mg	1.77	1.67	1.12	0.84	0.84	0.83	7.57	4.43	0.11
Mn	0.00	0.00	0.01	0.00	0.01	0.00	0.02	0.01	0.12
Ni	0.01	0.00	0.00	0.00	0.00	0.00	0.01	0.00	0.00
Ca	0.00	0.03	0.67	0.91	0.89	0.00	0.01	1.93	0.00
Na	-	0.00	0.04	0.02	0.05	0.00	0.01	0.06	-
K	-	0.00	0.00	-	0.00	-	0.00	0.00	-
V	-	0.00	0.00	0.00	0.00	0.00	-	0.00	0.11
Co	-	0.00	0.00	0.00	-	0.00	-	0.00	-
Zn	-	0.00	0.00	0.00	-	0.00	-	-	0.00
S	-	0.00	0.00	-	-	-	-	-	-
Fe _{tot}	-	-	-	-	-	0.04	1.03	0.32	1.66
Fe ³⁺	-	-	0.03	0.01	0.08	-	-	-	-
Fe ²⁺	0.20	0.19	0.06	0.08	0.00	-	-	-	-
Sum	2.99	4.00	4.00	4.00	4.00	2.43	15.34	14.91	4.00

Table 4.2 Representative analysis of the main PTEs-bearing minerals (EMPA-WDS data) and calculated formulas.

Authigenic minerals

The main authigenic phases forming by oxidation and weathering of primary minerals are Fe-oxides (hematite) and -oxyhydroxides (goethite) which occur as partial to complete replacement after magnetite or form cryptocrystalline aggregates within veins or in the surrounding oxidation halos. Although the chemical analyses of these minerals systematically refer to the bulk chemistry of the aggregates, the PTEs concentration of Fe-oxides and oxyhydroxides is generally very high (Ni up to 51000 ppm, Cr up to 8370 ppm, Co up to 1924 ppm, and V up to 376 ppm) reflecting their ability to scavenge several metals from the weathering fluids (e.g., Schwertmann and Taylor, 1989; Manceau et al., 2000; Quantin et al., 2002; Becquer et al., 2003; Fander et al., 2009; Ho et al., 2013).

4.3.3. Bulk chemistry

The three groups of ultramafic rocks under investigation are characterized by significant variations of Mg, Si, and, subordinately, Fe (Fig. 4.9).

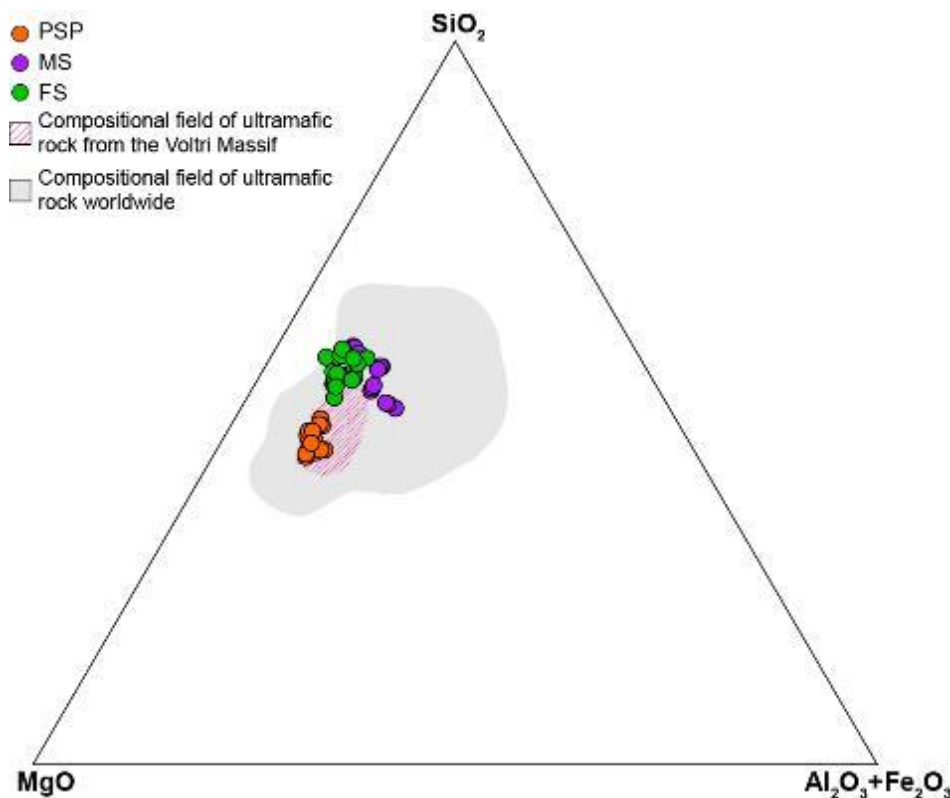


Fig. 4.9 Compositional variations of ultramafic rocks on the $\text{MgO-SiO}_2-(\text{Al}_2\text{O}_3+\text{Fe}_2\text{O}_3)$ diagram. Pink dashed areas refer to the composition of the Erro-Tobbio peridotites (Rampone et al., 2005; Piccardo & Visser, 2007; Borghini et al., 2007; Padovano et al., 2014; Cannaò et al., 2016; Cortesogno et al., 1979); gray fields refer to the composition of ultramafic rocks worldwide (Alexander, 1988; Andreani et al., 2013; Angeloni et al., 1993; Baumeister et al., 2015; Bonifacio et al., 2010; Burgess et al., 2009; Caillaud et al., 2006; Deschamps et al., 2013 and reference therein; De Hoog et al., 2009; Kierczak et al., 2016; Oze et al., 2004; Quantin et al., 2008).

The MgO/SiO₂ ratio falls in the range of subduction-related serpentinites (1.3-0.7; Deschamps et al., 2013) and systematically decrease with the increasing serpentinization degree (from about 1 in PSP to about 0.7 in MS and FS).

Although also the other major elements define quite large compositional range (Al₂O₃ = 0.9-3.52 wt%; FeO_{tot} = 4.2-11.49 wt%; CaO = 0.05-2.67 wt%; TiO₂ = 0.02-1.30 wt%; MnO_{tot} = 0.06-0.2 wt%), these variations are not related to the degree of serpentinization. The only exception is represented by FeO_{tot}, which reach the highest concentration in the MS (which have the highest content of magnetite and oxidation products) and by TiO₂ which systematically reach the highest concentration in FS and MS associated with tremolite-chlorite hybrid rocks.

Among the minor and trace elements, Cr, Co, and Ni, and subordinately Cu, V, and Zn are systematically present in significant concentrations (Table 4.3).

Cr and Ni have always the highest concentrations and widest range of variability. Cr and Ni vary systematically with the rock types (i.e. with the degree of serpentinization) and show opposite trends with negative and positive correlations with MgO, respectively (Fig. 4.10A-B). Cr reaches the highest concentration (4183 ppm) in MS and decreases to 884 ppm with increasing MgO content in PSP (Table 4.3 and Fig. 4.10A). On the other hand, Ni has the highest concentration in PSP (3900 ppm) and lowest in MS (1051 ppm; Table 4.3 and Fig. 4.10B). Co content is very homogeneous in PSP whereas shows a wider variation range in FS and, particularly, in MS where it reaches the highest concentrations (334 ppm; Fig. 4.10C). Cu, with a variation range between 2 to 75 ppm, has a similar behavior to Co (Fig. 4.10D).

The other PTEs (i.e., Zn, and V) do not show clear correlations to the degree of serpentinization, although there are sometimes significant differences in the three different groups considered. V content is very similar in the three rock groups (varying from 13 to 58 ppm) with the lowest concentrations occurring systematically in FS, whereas zinc content appears to be randomly distributed, although in a narrow range of variation (30-63 ppm) (Fig. 4.10E-F).

Rock	PSP				
Sample	Average	Median	Min	Max	St.Dev.
MgO	39.55	39.90	36.01	42.60	1.95
Al ₂ O ₃	1.67	1.58	1.01	3.52	0.54
SiO ₂	39.94	40.05	38.42	41.09	0.79
CaO	1.80	2.00	1.02	2.67	0.48
TiO ₂	0.07	0.07	0.07	0.08	0.01
MnO _t	0.09	0.09	0.08	0.09	0.00
Fe ₂ O _{3t}	7.99	8.06	6.60	9.75	0.96
V	39	36	27	96	17
Cr	1327	1257	884	2700	425
Co	84	81	73	103	9
Ni	2767	2700	1663	3900	811
Cu	13	11	2	27	7
Zn	45	44	33	60	9
Rock	MS				
Sample	Average	Median	Min	Max	St.Dev.
MgO	27.94	28.25	26.60	28.88	0.81
Al ₂ O ₃	1.66	1.64	0.90	2.51	0.60
SiO ₂	44.87	43.66	41.22	49.30	2.86
CaO	0.35	0.15	0.12	1.24	0.41
TiO ₂	0.08	0.08	0.04	0.10	0.02
MnO _t	0.14	0.15	0.06	0.20	0.05
Fe ₂ O _{3t}	9.33	10.31	5.53	12.77	2.33
V	50	52	33	58	8
Cr	2899	2603	1473	4183	1038
Co	211	212	74	334	74
Ni	1902	2057	1051	2212	430
Cu	27	22	11	58	15
Zn	46	44	38	63	8
Rock	FS				
Sample	Average	Median	Min	Max	St.Dev.
MgO	31.34	31.06	28.30	35.75	2.33
Al ₂ O ₃	1.38	1.40	1.01	1.60	0.17
SiO ₂	47.33	46.80	45.84	49.01	1.06
CaO	0.47	0.38	0.05	1.26	0.42
TiO ₂	0.04	0.03	0.02	0.07	0.02
MnO _t	0.12	0.13	0.07	0.15	0.03
Fe ₂ O _{3t}	7.00	7.21	4.67	8.57	1.16
V	26	31	13	48	13
Cr	2057	2106	1305	3020	397
Co	107	105	57	190	44
Ni	1350	1370	1093	1730	183
Cu	24	13	7	75	21
Zn	40	37	30	54	9

Table 4.3 Main descriptive statistic parameters (average, standard deviation, median, and maximum and minimum values) for major, minor element, and selected PTEs in the bulk rock (ICP-AES and XRF data).

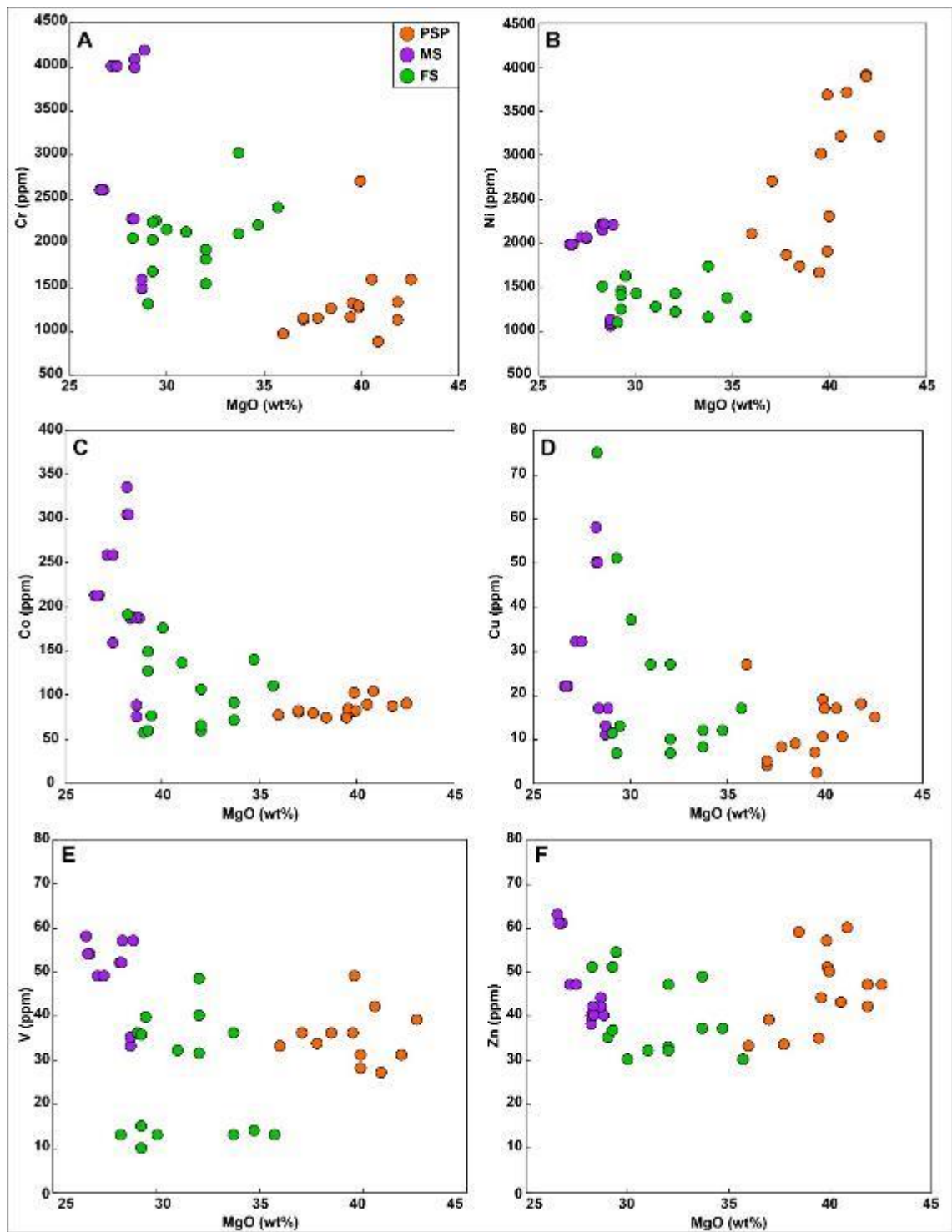


Fig. 4.10 Correlation plots of MgO vs Cr (A), Ni (B), Co (C), Cu (D), Zn (E), and V (F).

The general picture of PTEs distribution evidence that only Cr and Ni systematically exceed (up to one order of magnitude) the residential and industrial threshold values (CSC) according to Italian law (Fig. 4.11A-B; D.M. 471/1999; D.Lgs 152/2006). Among the other elements, only Co evidence concentration of environmental concern, since they are always above the residential CSC in the three rock groups and above the industrial CSC in MS.

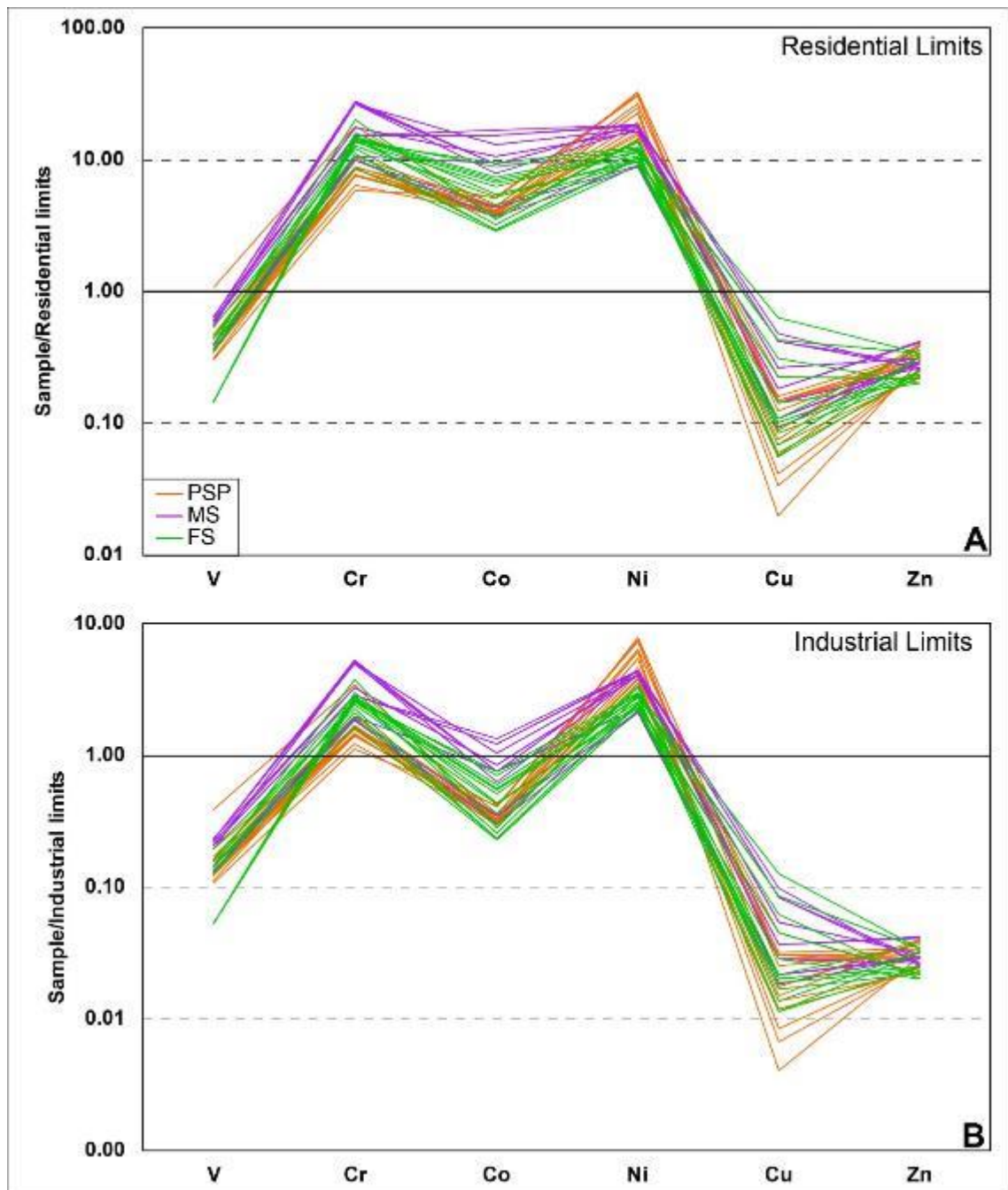


Fig. 4.11 PTEs concentration normalized to Italian threshold values for residential (A) and industrial (B) sites according to Italian law (D.M. 471/1999; D.Lgs 152/2006).

4.4. DISCUSSION

Our results evidenced that Cr, Ni, and, subordinately, Co are invariably the PTEs with the highest concentrations; in addition, V, Cu, and Zn are generally found in high concentrations. These results fall in the compositional fields obtained from several authors either in the studied area (Cortesogno et al., 1979; Ernst and Piccardo, 1979; Bonifacio et al., 1997; Rampone et al., 2005; Rampone and Borghini, 2008) and in other ultramafic complexes worldwide (Deschamps et al., 2013 and reference therein).

The main factors controlling the trace element distribution within the studied ultramafic rocks appeared to be the serpentinization degree and the deformation style and intensity which, in turn, strictly control the mineral assemblages and the mineral chemistry (Stueber and Goals, 1965; Gulacar and Delaloye, 1975).

Serpentinization is one of the most important processes that influence the mineralogy and the physico-chemical properties of ultramafic rocks (Shervais et al., 2005) and, consequently, the distribution of trace elements, including PTEs. The mobility of elements during serpentinization has been discussed for a long time (Deschamps et al., 2013 and references therein), and the debate is still open. Generally, the process of serpentinization is considered essentially isochemical for Si, Mg, and Fe elements, that are essentially redistributed within the rock (Iyer et al., 2008; Debret et al., 2013a,b); other elements (i.e., Ca, Al, Cr, Ni, and REE) are released to the fluids circulating during serpentinization (Janecky and Seyfried, 1986; Douville et al., 2002; Shervais et al., 2005; Paulick et al., 2006; Augustin et al., 2012; Barnes et al., 2013). Concerning Ni and Co, Gulaçar and Delaloye (1976) noted an isochemical behavior of the ultramafic rocks during serpentinization on a kilometer scale, with relative remobilization of these elements on a smaller scale (centimetric to metric). On the other side, other authors have mentioned that the process of serpentinization has no evident effect on the abundances of Cr, Ni, and Co in ultramafic rocks (Stueber and Goles 1965; Govindaraju, 1995; Aziz et al., 2011).

Our results highlighted that Cr and, subordinately Co and Cu, tend to significantly increase with the serpentinization degree in good agreement with several works (e.g., Gahlan and Arai, 2007; Li and Lee, 2006; Paulick et al., 2006). In fact, although Cr-spinel, Al-chromite, and ferrian-chromite are rarely preserved with the increasing serpentinization (i.e., from PSP to MS; Fig. 4.8), the significant chromium enrichment observed in MS can be explained by the progressive increase in Cr-bearing magnetite, which can represent up to 10% of the rock-forming minerals. These minerals tend to pseudomorphically replace primary spinels, to concentrate along rims of the mesh-textures or along cleavage planes of bastites as well as to fill several veins.

In the foliated serpentinites, the deformation style and intensity appear to be the main control in distribution and concentration of the new-forming Cr-bearing magnetites. In fact, in FS, most of these minerals tend to concentrate in millimetric layers or linear trails parallel to the main foliation representing on average up to

5% of the rock-forming minerals. Both in MS and FS the Cr contents of magnetite is generally high (more than 10000 ppm on average) reaching the highest concentration in pseudomorphs after spinel porphyroclasts (up to 32600 ppm; Fig. 4.6) in MS. In MS, the Cr-bearing magnetites represent up to 10% of the rock-forming minerals (mean value 5%).

Other than spinel-group minerals, non-negligible amounts of chromium are incorporated either in clinocllore (mean value = 2550 ppm; Fig. 4.6) and in antigorite both in pseudomorphic textures of MS (where it reaches the highest values in bastites after pyroxenes; up to 9397 ppm; Fig. 4.6; as also observed by Debret et al., 2013a in the Lanzo Massif and Roumèjon et al., 2015 in the Southwest Indian Ridge) and non-pseudomorphic texture (mean value 1960 ppm; Fig. 4.6).

Contrary to what is shown by Cr, the highest concentration and the widest range of Ni was found in the less serpentinized rocks, in good agreement to what observed by Li and Lee (2006) in the Feather River Ophiolites (Sierra Nevada Metamorphic Belt – California), but in contrast to the results of Gahlan and Arai (2007) in Bou-Azzer ophiolites (Anti-Atlas, Morocco) and Aziz et al. (2011) in the northwestern Zagros Suture Zone (Kurdistan Region – Iraq). The decreasing of the Ni concentrations from PSP to FS is in agreement with the progressive disappearance of olivine (the main Ni-bearing minerals in the studied rocks) with the increasing serpentinization. Only antigorite after olivine within mesh texture in MS have significant and comparable Ni content (up to 3131 ppm) whereas the other serpentine minerals occurring in MS and FS contains about 1400 ppm of Ni on average with the lowest concentrations recorded on chrysotile occurring within veins (< 302 ppm) and antigorite within bastites (< 500 ppm).

Similar to the Cr behavior, Co significantly increase from PSP to FS to MS (from 84 to 107 to 221 ppm, respectively; mean values) since the main minerals hosting high cobalt amounts are magnetites and antigorite occurring within pseudomorphic textures (up to 1879 ppm and 602 ppm, respectively; Fig. 4.6).

V, Zn, and Cu seem to have a conservative behavior since the concentrations of these elements remain almost unchanged and do not show clear correlations to either the degree of serpentinization or deformation style and intensity.

During the serpentinization, Zn and V are mainly released from olivine and spinel-group minerals and incorporated in the hydrous silicates (mainly antigorite, chlorite, and talc) or in some accessory phases (e.g., V in ilmenites).

The anomalous high bulk concentration of copper in some MS and FS samples (Fig. 4.10) is presumably due to the presence of sulfides (locally observed as micrometric inclusions within Fe-oxides) as also observed by Alt et al. (2012) and Malatesta et al. (2017) in other serpentinites of the Voltri Massif.

4.5. CONCLUSIONS

The multidisciplinary approach used in this work allowed to associate the potentially toxic elements variation to the progressive evolution of the ultramafic rocks, from partially serpentinized lherzolites to highly deformed and foliated serpentinites.

The highest controlling factors in PTEs variation appear to be the degree of serpentinization and the style and intensity of deformation, which in turn controls the mineralogical assemblage. Our study highlights that in the studied ultramafic rocks, spinel-group minerals are the main source of the PTEs. Moreover, PTEs-bearing phases are also represented by the other rock-forming minerals (such as serpentines, olivines, pyroxenes, and chlorites) and some accessory phases (e.g., ilmenite and other oxides, sulphides).

Although the chemical and mineralogical variation due to serpentinization are known in the literature, to the best of my knowledge, few studies are focused on the distribution and variation of elements of environmental concerns due to the mineralogical, textural, and micro-structural feature of similar ultramafic rocks (e.g., Kierczak et al., 2016). A study of this kind that combine the bulk chemistry of outcropping rocks with their geological, structural, mineralogical, and crystallochemical data, can be a useful tool in environmental concerns to determine the PTEs distribution, to evaluate their mobility and their potential bioavailability as well as to discriminate the natural geochemical background from possible source of contamination.

In the light of the results obtain, it is evident that it is necessary to apply the same type of approach not only to the primary minerals of the rock but also to the authigenic phases, formed in the early stages of rock weathering, because of they can significantly contribute to the total PTE budget and affect their fate during the weathering and pedological evolution.

Moreover, this multidisciplinary approach will be extended to the complete ultramafic soil profile (from bedrock to topsoil), whose the studied rocks in this

work represented the bedrocks and to similar ophiolites complexes (e.i., Vara supergroup ophiolite – Northern Apennine; *Chapter VI*).

References

- Abre, P., Cingolani, C., Zimmermann, U., and Cairncross, B. (2009). Detrital chromian spinels from Upper Ordovician deposits in the Precordillera terrane, Argentina: a mafic crust input. *Journal of South American Earth Sciences*, 28(4), 407-418.
- Alexander, E.B. (1988). Morphology, fertility, and classification of productive soils on serpentinized peridotite in California (USA). *Geoderma*, 41(3-4), 337-351.
- Alexander, E.B. (2007). *Serpentine geocology of western North America: geology, soils, and vegetation*. Oxford University Press, New York.
- Alt, J.C., Shanks III, W.C., Crispini, L., Gaggero, L., Schwarzenbach, E.M., Früh-Green, G.L., and Bernasconi, S.M. (2012). Uptake of carbon and sulfur during seafloor serpentinization and the effects of subduction metamorphism in Ligurian peridotites. *Chemical Geology*, 322, 268-277.
- Andreani, M., Munoz, M., Marcaillou, C., and Delacour, A. (2013). μ XANES study of iron redox state in serpentine during oceanic serpentinization. *Lithos*, 178, 70-83.
- Angelone, M., Vaselli, O., Bini, C., and Coradossi, N. (1993). Pedogeochemical evolution and trace elements availability to plants in ophiolitic soils. *Science of the total environment*, 129(3), 291-309.
- Arai, S. (1986). K/Na variation in phlogopite and amphibole of upper mantle peridotites due to fractionation of the metasomatizing fluids. *The Journal of Geology*, 94(3), 436-444.
- Arai, S., Shimizu, Y., Ismail, S.A., and Ahmed, A.H. (2006). Low-T formation of high-Cr spinel with apparently primary chemical characteristics within podiform chromitite from Rayat, northeastern Iraq.
- Augustin, N., Paulick, H., Lackschewitz, K. S., Eisenhauer, A., Garbe-Schönberg, D., Kuhn, T., Botz, R., and Schmidt, M. (2012). Alteration at the ultramafic-hosted Logatchev hydrothermal field: Constraints from trace element and Sr-O isotope data. *Geochemistry, Geophysics, Geosystems*, 13(3).
- Aziz, N. R., Aswad, K. J., and Koyi, H. A. (2011). Contrasting settings of serpentinite bodies in the northwestern Zagros Suture Zone, Kurdistan Region, Iraq. *Geological Magazine*, 148(5-6), 819-837.
- Bailey, S.W. (1988). X-ray diffraction identification of the polytypes of mica, serpentine, and chlorite. *Clays and Clay minerals*, 36(3), 193-213.
- Barnes, J.D., Eldam, R., Lee, C.T.A., Errico, J.C., Loewy, S., and Cisneros, M. (2013). Petrogenesis of serpentinites from the Franciscan Complex, western California, USA. *Lithos*, 178, 143-157.
- Baumeister, J.L., Hausrath, E.M., Olsen, A.A., Tschauer, O., Adcock, C.T., and Metcalf, R. V. (2015). Biogeochemical weathering of serpentinites: an examination of incipient dissolution affecting serpentine soil formation. *Applied Geochemistry*, 54, 74-84.
- Becquer, T., Quantin, C., Sicot, M., and Boudot, J.P. (2003). Chromium availability in ultramafic soils from New Caledonia. *Science of the Total Environment*, 301(1-3), 251-261.
- Bonifacio, E., Falsone, G., and Piazza, S. (2010). Linking Ni and Cr concentrations to soil mineralogy: does it help to assess metal contamination when the natural background is high? *Journal of Soils and Sediments*, 10(8), 1475-1486.
- Bonifacio, E., Zanini, E., Boero, V., and Franchini-Angela, M. (1997). Pedogenesis in a soil catena on serpentinite in north-western Italy. *Geoderma*, 75(1-2), 33-51.
- Borghini, G., Rampone, E., Crispini, L., De Ferrari, R., and Godard, M. (2007). Origin and emplacement of ultramafic–mafic intrusions in the Erro-Tobbio mantle peridotite (Ligurian Alps, Italy). *Lithos*, 94(1-4), 210-229.
- Brett, R.C., Russell, J.K., and Moss, S. (2009). Origin of olivine in kimberlite: Phenocryst or

impostor? *Lithos*, 112, 201-212.

Brigatti, M.F., Malferrari, D., Laurora, A., Elmi, C., and Mottana, A. (2011). Structure and mineralogy of layer silicates: recent perspectives and new trends. *Layered Mineral Structures and their Application in Advanced Technologies*, 11, 1-71.

Brothers, R.N., and Grapes, R.H. (1989). Clastic lawsonite, glaucophane, and jadeitic pyroxene in Franciscan metagraywackes from the Diablo Range, California. *Geological Society of America Bulletin*, 101(1), 14-26.

Buddington, A.F., and Lindsley, D.H. (1964). Iron-titanium oxide minerals and synthetic equivalents. *Journal of petrology*, 5(2), 310-357.

Burgess, J.L., Lev, S., Swan, C.M., and Szlavecz, K. (2009). Geologic and edaphic controls on a serpentine forest community. *Northeastern Naturalist*, 366-384.

Burkhard, D.J. (1993). Accessory chromium spinels: Their coexistence and alteration in serpentinites. *Geochimica et Cosmochimica Acta*, 57(6), 1297-1306.

Busweiler, Y., Foley, S.F., Prelević, D., and Jacob, D.E. (2015). The olivine macrocryst problem: new insights from minor and trace element compositions of olivine from Lac de Gras kimberlites, Canada. *Lithos*, 220, 238-252.

Butt, C.R., and Cluzel, D. (2013). Nickel laterite ore deposits: weathered serpentinites. *Elements*, 9(2), 123-128.

Caillaud, J., Proust, D., and Righi, D. (2006). Weathering sequences of rock-forming minerals in a serpentinite: influence of microsystems on clay mineralogy. *Clays and Clay Minerals*, 54(1), 87-100.

Canil, D., Grondahl, C., Lacourse, T., and Pisiak, L. K. (2016). Trace elements in magnetite from porphyry Cu–Mo–Au deposits in British Columbia, Canada. *Ore Geology Reviews*, 72, 1116-1128.

Cannaò, E., Scambelluri, M., Agostini, S., Tonarini, S., and Godard, M. (2016). Linking serpentinite geochemistry with tectonic evolution at the subduction plate-interface: The Voltri Massif case study (Ligurian Western Alps, Italy). *Geochimica et Cosmochimica Acta*, 190, 115-133.

Carbonin, C., Dal Negro, A., Ganeo, S., and Piccirillo, E.M. (1991). Influence of magma composition and oxygen fugacity on the crystal structure of C2/c clinopyroxenes from a basalt-pantellerite suite. *Contributions to Mineralogy and Petrology*, 108(1-2), 34-42.

Cheng, C.H., Jien, S.H., Iizuka, Y., Tsai, H., Chang, Y.H., and Hseu, Z.Y. (2011). Pedogenic chromium and nickel partitioning in serpentine soils along a toposequence. *Soil Science Society of America Journal*, 75(2), 659-668.

Cheshire, M., and Güven, N. (2005). Conversion of chrysotile to a magnesian smectite. *Clays and Clay Minerals*, 53(2), 155-161.

Colás, V., González-Jiménez, J. M., Griffin, W.L., Fanlo, I., Gervilla, F., O'Reilly, S. Y., Pearson, N.J., Kerestedjian, T., and Proenza, J.A. (2014). Fingerprints of metamorphism in chromite: New insights from minor and trace elements. *Chemical Geology*, 389, 137-152.

Coleman, R.G. (1977). What is an Ophiolite? In *Ophiolites* (pp. 1-7). Springer, Berlin, Heidelberg.

Coleman, R.G., and Jove, C. (1992). Geological origin of serpentinites. *The vegetation of ultramafic (serpentine) soils*, 1-17.

Comodi, P., Mellini, M., Ungaretti, L., and Zanazzi, P.F. (1991). Compressibility and high pressure structure refinement of tremolite, pargasite and glaucophane. *European Journal of Mineralogy*, 3(3), 485-499.

Cortesogno, L., Mazzucotelli, A., and Vannucci, R. (1979) Alcuni esempi di pedogenesi su rocce ultrafemiche in clima mediterraneo. *Ofioliti* 4:295–312.

Dal Negro, A., Carbonin, S., Molin, G.M., Cundari, A., and Piccirillo, E.M. (1982). Intracrystalline cation distribution in natural clinopyroxenes of tholeiitic, transitional, and alkaline basaltic rocks. In *Advances in physical geochemistry* (pp. 117-150). Springer, New York, NY.

Dal Negro, A., Carbonin, S., Salviulo, G., Piccirillo, E.M., and Cundari, A. (1985). Crystal Chemistry and Site Configuration of the Clinopyroxene from Leucite-bearing Rocks and Related

- Genetic Significance: the Sabatini Lavas, Roman Region, Italy. Journal of Petrology, 26(4), 1027-1040.*
- Dal Negro, A., Cundari, A., Piccirillo, E.M., Molin, G.M., and Uliana, D. (1986). Distinctive crystal chemistry and site configuration of the clinopyroxene from alkali basaltic rocks. *Contributions to Mineralogy and Petrology, 92(1), 35-43.*
- Dal Negro, A., Manoli, S., Secco, L., and Piccirillo, E.M. (1989). Megacrystic clinopyroxenes from Victoria (Australia): crystal chemical comparisons of pyroxenes from high- and low-pressure regimes. *European Journal of Mineralogy, 105-122.*
- Dare, S.A., Barnes, S.J., Beaudoin, G., Méric, J., Boutroy, E., and Potvin-Doucet, C. (2014). Trace elements in magnetite as petrogenetic indicators. *Mineralium Deposita, 49(7), 785-796.*
- Dare, S.A., Pearce, J.A., McDonald, I., and Styles, M.T. (2009). Tectonic discrimination of peridotites using fO₂-Cr# and Ga-Ti-Fe^{III} systematics in chrome-spinel. *Chemical Geology, 261(3-4), 199-216.*
- De Hoog, J.C., Janák, M., Vrabec, M., and Froitzheim, N. (2009). Serpentinised peridotites from an ultrahigh-pressure terrane in the Pohorje Mts. (Eastern Alps, Slovenia): geochemical constraints on petrogenesis and tectonic setting. *Lithos, 109(3-4), 209-222.*
- De Hoog, J.C., Gall, L., and Cornell, D.H. (2010). Trace-element geochemistry of mantle olivine and application to mantle petrogenesis and geothermobarometry. *Chemical Geology, 270(1), 196-215.*
- Debret, B., Andreani, M., Godard, M., Nicollet, C., Schwartz, S., and Lafay, R. (2013a). Trace element behavior during serpentinization/de-serpentinization of an eclogitized oceanic lithosphere: A LA-ICPMS study of the Lanzo ultramafic massif (Western Alps). *Chemical Geology, 357, 117-133.*
- Debret, B., Nicollet, C., Andreani, M., Schwartz, S., and Godard, M. (2013b). Three steps of serpentinization in an eclogitized oceanic serpentinization front (Lanzo Massif–Western Alps). *Journal of Metamorphic Geology, 31(2), 165-186.*
- Decreto Legislativo 3/04/2006 n° 152 “Norme in materia ambientale”. G.U. 88. 14/04/2006.
- Decreto Ministeriale 25/10/1999 n° 471 “Regolamento recante criteri, procedure e modalità per la messa in sicurezza, la bonifica e il ripristino ambientale dei siti inquinati, ai sensi dell’articolo 17 del decreto legislativo 5 febbraio 1997, n. 22”, e successive modificazioni e integrazioni. G.U. 293, 15/12/1999.
- Deer, W. Howie, R.A., and Zussman, J. (1996) *An Introduction to the rock Forming Minerals*, 696 p.
- Della Ventura, G., Robert, J.L., and Hawthorne, F.C. (1996). Infrared spectroscopy of synthetic (Ni, Mg, Co)-potassium-richterite (Vol. 5, pp. 55-63).
- Della Ventura, G., Robert, J.L., Raudsepp, M., Hawthorne, F.C., and Welch, M.D. (1997). Site occupancies in synthetic monoclinic amphiboles: Rietveld structure refinement and infrared spectroscopy of (nickel, magnesium, cobalt)-richterite. *American Mineralogist, 82(3-4), 291-301.*
- Deschamps, F., Godard, M., Guillot, S., and Hattori, K. (2013). Geochemistry of subduction zone serpentinites: A review. *Lithos, 178, 96-127.*
- Deschamps, F., Godard, M., Guillot, S., Chauvel, C., Andreani, M., Hattori, K., Wunder, B., and France, L. (2012). Behavior of fluid-mobile elements in serpentines from abyssal to subduction environments: Examples from Cuba and Dominican Republic. *Chemical Geology, 312, 93-117.*
- Deschamps, F., Guillot, S., Godard, M., Chauvel, C., Andreani, M., and Hattori, K. (2010). In situ characterization of serpentinites from forearc mantle wedges: timing of serpentinization and behavior of fluid-mobile elements in subduction zones. *Chemical Geology, 269(3-4), 262-277.*
- Dilek, Y., and Furnes, H. (2009). Structure and geochemistry of Tethyan ophiolites and their petrogenesis in subduction rollback systems. *Lithos, 113(1-2), 1-20.*
- Douville, E., Charlou, J.L., Oelkers, E.H., Bienvenu, P., Colon, C.J., Donval, J.P., and Appriou, P. (2002). The rainbow vent fluids (36° 14' N, MAR): the influence of ultramafic rocks and phase separation on trace metal content in Mid-Atlantic Ridge hydrothermal fluids. *Chemical Geology, 184(1-2), 37-48.*
- Echevarria, G. (2018). Genesis and behaviour of ultramafic soils and consequences for nickel

- biogeochemistry. In *Agromining: Farming for Metals* (pp. 135-156). Springer, Cham.
- Ernst, W.G., and Piccardo, G.B. (1979). Petrogenesis of some Ligurian peridotites—I. Mineral and bulk-rock chemistry. *Geochimica et Cosmochimica Acta*, 43(2), 219-237.
- Fandeur, D., Juillot, F., Morin, G., Olivi, L., Cognigni, A., Ambrosi, J.P., Guyot, F., and Fritsch, E. (2009). Synchrotron-based speciation of chromium in an Oxisol from New Caledonia: Importance of secondary Fe-oxyhydroxides. *American Mineralogist*, 94(5-6), 710-719.
- Foley, S.F., Prelevic, D., Rehfeldt, T., and Jacob, D.E. (2013). Minor and trace elements in olivines as probes into early igneous and mantle melting processes. *Earth and Planetary Science Letters*, 363, 181-191.
- Frost, B.R., and Lindsley, D.H. (1991). Occurrence of iron-titanium oxides in igneous rocks. *Reviews in Mineralogy and geochemistry*, 25(1), 433-468.
- Gahlan, H.A., and Arai, S. (2006). Genesis of peculiarly zoned Co, Zn and Mn-rich chromian spinel in serpentinite of Bou-Azzer ophiolite, Anti-Atlas, Morocco. *Journal of Mineralogical and Petrological Sciences*, 0612070013-0612070013.
- Gargiulo, M.F., Bjerg, E.A., and Mogessie, A. (2013). Spinel group minerals in metamorphosed ultramafic rocks from Río de Las Tunas belt, Central Andes, Argentina. *Geologica Acta: an international earth science journal*, 11(2).
- Garnier, J., Quantin, C., Guimarães, E., Garg, V.K., Martins, E.S., and Becquer T. (2009) Understanding the genesis of ultramafic soils and catena dynamics in Niquelândia, Brazil. *Geoderma* 151 (2009) 204–214.
- Gonzalez-Jimenez, J.M., Griffin, W.L., Proenza, J.A., Gervilla, F., O'Reilly, S.Y., Akbulut, M., Pearson N.J. and Arai, S. (2014). Chromitites in ophiolites: How, where, when, why? Part II. The crystallization of chromitites. *Lithos*, 189, 140-158.
- Govindaraju, K. (1994). 1994 compilation of working values and sample description for 383 geostandards. *Geostandards newsletter*, 18, 1-158.
- Grieco, G., Pedrotti, M., and Moroni, M. (2011). Metamorphic redistribution of Cr within chromitites and its influence on chromite ore enrichment. *Minerals Engineering*, 24(2), 102-107.
- Gülaçar, O.F., and Delaloye, M. (1976). Geochemistry of nickel, cobalt and copper in alpine-type ultramafic rocks. *Chemical Geology*, 17, 269-280.
- Haggerty, S.E. (1991). Oxide textures; a mini-atlas. *Reviews in Mineralogy and Geochemistry*, 25(1), 129-219.
- Hanley, J.J., and Bray, C.J. (2009). The trace metal content of amphibole as a proximity indicator for Cu-Ni-PGE mineralization in the footwall of the Sudbury Igneous Complex, Ontario, Canada. *Economic Geology*, 104(1), 113-125.
- Hawthorne, F.C., and Oberti, R. (2007). Amphiboles: crystal chemistry. *Reviews in Mineralogy and Geochemistry*, 67(1), 1-54.
- Hayes, J.B. (1970). Polytypism of chlorite in sedimentary rocks. *Clays and Clay minerals*, 18, 285-306.
- Hazen, R.M., and Wones, D.R. (1972). The effect of cation substitutions on the physical properties of trioctahedral micas. *American Mineralogist: Journal of Earth and Planetary Materials*, 57(1-2), 103-129.
- Herzberg, C., Asimow, P.D., Ionov, D.A., Vidito, C., Jackson, M.G., and Geist, D. (2013). Nickel and helium evidence for melt above the core–mantle boundary. *Nature*, 493(7432), 393.
- Herzberg, C., Vidito, C., and Starkey, N.A. (2016). Nickel–cobalt contents of olivine record origins of mantle peridotite and related rocks. *American Mineralogist*, 101(9), 1952-1966.
- Ho, C.P., Hseu, Z.Y., Iizuka, Y., and Jien, S.H. (2013). Chromium speciation associated with iron and manganese oxides in serpentine mine tailings. *Environmental Engineering Science*, 30(5), 241-247.
- Hseu, Z.Y., Tsai, H., Hsi, H.C., and Chen, Y.C. (2007). Weathering sequences of clay minerals in soils along a serpentinitic toposequence. *Clays and Clay Minerals*, 55(4), 389-401.
- Inoue, A., Meunier, A., Patrier-Mas, P., Rigault, C., Beaufort, D., and Vieillard, P. (2009). Application of chemical geothermometry to low-temperature trioctahedral chlorites. *Clays and*

Clay Minerals, 57(3), 371-382.

Iyer, K., Jamtveit, B., Mathiesen, J., Malthes-Sørensen, A., and Feder, J. (2008). Reaction-assisted hierarchical fracturing during serpentinization. *Earth and Planetary Science Letters*, 267(3-4), 503-516.

Janecky, D.R., and Seyfried Jr, W.E. (1986). Hydrothermal serpentinization of peridotite within the oceanic crust: Experimental investigations of mineralogy and major element chemistry. *Geochimica et Cosmochimica Acta*, 50(7), 1357-1378.

Jaques, A.L., and Foley, S.F. (2018). Insights into the petrogenesis of the West Kimberley lamproites from trace elements in olivine. *Mineralogy and Petrology*, 1-19.

Khalil, K.I. (2007). Chromite mineralization in ultramafic rocks of the Wadi Ghadir area, Eastern Desert, Egypt: mineralogical, microchemical and genetic studies. *Neues Jahrbuch für Mineralogie-Abhandlungen: Journal of Mineralogy and Geochemistry*, 183(3), 283-296.

Kierczak, J., Neel, C., Bril, H., and Puziewicz, J. (2007). Effect of mineralogy and pedoclimatic variations on Ni and Cr distribution in serpentine soils under temperate climate. *Geoderma*, 142(1-2), 165-177.

Kierczak, J., Pędziwiatr, A., Waroszewski, J., and Modelska, M. (2016). Mobility of Ni, Cr and Co in serpentine soils derived on various ultrabasic bedrocks under temperate climate. *Geoderma*, 268, 78-91.

Klein Jr, C., and Ito, J. (1968). Zincian and manganoan amphiboles from Franklin, New Jersey. *American Mineralogist: Journal of Earth and Planetary Materials*, 53(7-8), 1264-1275.

Kodolányi, J., and Pettke, T. (2011). Loss of trace elements from serpentinites during fluid-assisted transformation of chrysotile to antigorite—an example from Guatemala. *Chemical Geology*, 284(3), 351-362.

Kodolányi, J., Pettke, T., Spandler, C., Kamber, B.S., and Gméling, K. (2011). Geochemistry of ocean floor and fore-arc serpentinites: constraints on the ultramafic input to subduction zones. *Journal of Petrology*, 53(2), 235-270.

Krátký, O., Rappich, V., Racek, M., Míková, J., and Magna, T. (2018). On the Chemical Composition and Possible Origin of Na–Cr-Rich Clinopyroxene in Silicocarbonatites from Samalpattí, Tamil Nadu, South India. *Minerals*, 8(8), 355.

Kumarathilaka, P., Dissanayake, C., and Vithanage, M. (2014). Geochemistry of serpentinite soils: A brief overview. *Journal of Geological Society of Sri Lanka Vol. 16*, 53-63

Laird, J. (1988). Chlorite: metamorphic petrology. Pp. 405-453 in: *Hydrous Phyllosilicates* (SW Bailey, editor). *Reviews in Mineralogy*, 19.

Larson, A.C. and Von Dreele, R.B. (1994). *General Structure Analysis System (GSAS)*. Los Alamos National Laboratory Report LAUR 86-748.

Li, Z.X.A., and Lee, C.T.A. (2006). Geochemical investigation of serpentinized oceanic lithospheric mantle in the Feather River Ophiolite, California: implications for the recycling rate of water by subduction. *Chemical Geology*, 235(1-2), 161-185.

Lindsley, D.H. (1991). Experimental studies of oxide minerals. *Reviews in Mineralogy and Geochemistry*, 25(1), 69-106.

Liu, P.P., Zhou, M.F., Chen, W.T., Gao, J.F., and Huang, X.W. (2015). In-situ LA-ICP-MS trace elemental analyses of magnetite: Fe–Ti–(V) oxide-bearing mafic–ultramafic layered intrusions of the Emeishan Large Igneous Province, SW China. *Ore Geology Reviews*, 65, 853-871.

Malatesta, C., Federico, L., Crispini, L., and Capponi, G. (2017). Fluid-controlled deformation in blueschist-facies conditions: plastic vs brittle behaviour in a brecciated mylonite (Voltri Massif, Western Alps, Italy). *Geological Magazine*, 155(2), 335-355.

Malgarotto, C., Molin, G., and Zanazzi, P.F. (1993). Crystal chemistry of clinopyroxenes from Filicudi and Salina (Aeolian Islands, Italy). *Geothermometry and barometry. European Journal of Mineralogy*, 915-924.

Manceau, A., Schlegel, M.L., Musso, M., Sole, V.A., Gauthier, C., Petit, P.E., and Trolard, F. (2000). Crystal chemistry of trace elements in natural and synthetic goethite. *Geochimica et Cosmochimica Acta*, 64(21), 3643-3661.

- Nazzareni, S., Molin, G., Peccerillo, A., and Zanazzi, P. (2001). Volcanological implications of crystal-chemical variations in clinopyroxenes from the Aeolian Arc, Southern Tyrrhenian Sea (Italy). *Bulletin of Volcanology*, 63(1), 73-82.
- Nazzareni, S., Skogby, H., and Zanazzi, P.F. (2011). Hydrogen content in clinopyroxene phenocrysts from Salina mafic lavas (Aeolian arc, Italy). *Contributions to Mineralogy and Petrology*, 162(2), 275-288.
- Nimis, P. (1995). A clinopyroxene geobarometer for basaltic systems based on crystal-structure modeling. *Contributions to Mineralogy and Petrology*, 121(2), 115-125.
- O'Neill, H.S.C., and Navrotsky, A. (1984). Cation distributions and thermodynamic properties of binary spinel solid solutions. *American Mineralogist*, 69(7-8), 733-753.
- Ottoneo, G. (2000). *Principles of geochemistry*. Columbia University Press.
- Oze, C., Fendorf, S., Bird, D. K., and Coleman, R. G. (2004). Chromium geochemistry in serpentized ultramafic rocks and serpentine soils from the Franciscan complex of California. *American Journal of Science*, 304(1), 67-101.
- Oze, C., Fendorf, S., Bird, D.K., and Coleman, R.G. (2004a) Chromium geochemistry in serpentized ultramafic rocks and serpentine soils from the Franciscan complex of California. *American Journal of Sciences* 304:67–101.
- Padovano, M., Piccardo, G.B., and Vissers, R.L. (2014). Tectonic and magmatic evolution of the mantle lithosphere during the rifting stages of a fossil slow–ultraslow spreading basin: insights from the Erro–Tobbio peridotite (Voltri Massif, NW Italy). *Geological Society, London, Special Publications*, 413, SP413-7.
- Paulick, H., Bach, W., Godard, M., De Hoog, J.C.M., Suhr, G., and Harvey, J. (2006). Geochemistry of abyssal peridotites (Mid-Atlantic Ridge, 15 20' N, ODP Leg 209): implications for fluid/rock interaction in slow spreading environments. *Chemical Geology*, 234(3), 179-210.
- Petrelli, M., Morgavi, D., Vetere, F., and Perugini, D. (2016). Elemental imaging and petro-volcanological applications of an improved laser ablation inductively coupled quadrupole plasma mass spectrometry. *Periodico di Mineralogia*, 85, 25-39.
- Piccardo G.B. and Vissers R.L.M. (2007). The pre-oceanic evolution of the Erro-Tobbio peridotite (Voltri Massif, Ligurian Alps, Italy). *Journal of Geodynamics* 43, 417–449.
- Prelević, D., and Foley, S.F. (2007). Accretion of arc-oceanic lithospheric mantle in the Mediterranean: evidence from extremely high-Mg olivines and Cr-rich spinel inclusions in lamproites. *Earth and Planetary Science Letters*, 256(1), 120-135.
- Prelević, D., Jacob, D.E., and Foley, S.F. (2013). Recycling plus: a new recipe for the formation of Alpine–Himalayan orogenic mantle lithosphere. *Earth and Planetary Science Letters*, 362, 187-197.
- Prewitt, C.T. (1963). Crystal structures of two synthetic amphiboles. In *Geological Society of America Annual Meeting, New York, Program*, 132A–133A.
- Quantin, C., Becquer, T., and Berthelin, J. (2002). Mn-oxide: a major source of easily mobilisable Co and Ni under reducing conditions in New Caledonia Ferralsols. *Comptes Rendus Geoscience*, 334(4), 273-278.
- Quantin, C., Ettler, V., Garnier, J., and Šebek, O. (2008). Sources and extractibility of chromium and nickel in soil profiles developed on Czech serpentinites. *Comptes Rendus Geoscience*, 340(12), 872-882.
- Rampone, E., and Borghini, G. (2008). Melt migration and intrusion in the Erro-Tobbio peridotites (Ligurian Alps, Italy): Insights on magmatic processes in extending lithospheric mantle. *European Journal of Mineralogy*, 20(4), 573-585.
- Rampone, E., Romairone, A., Abouchami, W., Piccardo, G.B., and Hofmann A.W. (2005) Chronology, Petrology and Isotope Geochemistry of the Erro–Tobbio Peridotites (Ligurian Alps, Italy): Records of Late Palaeozoic Lithospheric Extension *Journal of Petrology* 46(4) April 2005.
- Rouméjon, S., Cannat, M., Agrinier, P., Godard, M., and Andreani, M. (2015). Serpentinization and fluid pathways in tectonically exhumed peridotites from the Southwest Indian Ridge (62–65 E). *Journal of Petrology*, 56(4), 703-734.
- Sack, R.O., and Ghiorso, M.S. (1991). Chromian spinels as petrogenetic indicators;

- thermodynamics and petrological applications. *American Mineralogist*, 76(5-6), 827-847.
- Sanchez Vizcaino, V.L., Franz, G., and Gomez Pugnaire, M.T. (1995). The behavior of Cr during metamorphism of carbonate rocks from the Nevado-Filabride complex, Betic Cordilleras, Spain. *The Canadian Mineralogist*, 33(1), 85-104.
- Savov, I.P., Ryan, J.G., D'Antonio, M., and Fryer, P. (2007). Shallow slab fluid release across and along the Mariana arc-basin system: Insights from geochemistry of serpentinized peridotites from the Mariana fore arc. *Journal of Geophysical Research: Solid Earth*, 112(B9).
- Schumacher, J.C. (2007). Metamorphic amphiboles: composition and coexistence. *Reviews in Mineralogy and Geochemistry*, 67(1), 359-416.
- Schwertmann, U.T.R.M., and Taylor, R.M. (1989). Iron oxides. *Minerals in soil environments, (mineralsinsoile)*, 379-438.
- Shervais, J.W., Kolesar, P., and Andreasen, K. (2005). A field and chemical study of serpentinization—Stonyford, California: chemical flux and mass balance. *International Geology Review*, 47(1), 1-23.
- Simon, S.B., Sutton, S.R., and Grossman, L. (2007). Valence of titanium and vanadium in pyroxene in refractory inclusion interiors and rims. *Geochimica et Cosmochimica Acta*, 71(12), 3098-3118.
- Sobolev, A.V., Hofmann, A.W., Kuzmin, D.V., Yaxley, G.M., Arndt, N.T., Chung, S.L., Danyushevsky, L.V., Elliott, T., Frey, F.A., Garcia, M.O, Gurenko, A.A, Kamenetsky, V.S., Kerr, A.C., Krivolutsкая, N.A., Matvienkov, V.V., Nikogosian, I.K., Rocholl, A., Sigurdsson, I.A., Sushchevskaya, N.M., and Teklay, M. (2007). The amount of recycled crust in sources of mantle-derived melts. *science*, 316(5823), 412-417.
- Sobolev, N.V., Logvinova, A.M., Zedgenizov, D.A., Pokhilenko, N.P., Malygina, E.V., Kuzmin, D.V., and Sobolev, A.V. (2009). Petrogenetic significance of minor elements in olivines from diamonds and peridotite xenoliths from kimberlites of Yakutia. *Lithos*, 112, 701-713.
- Stevens, R.E. (1944). Composition of some chromites of the western hemisphere. *American Mineralogist: Journal of Earth and Planetary Materials*, 29(1-2), 1-34.
- Straub, S. M., LaGatta, A.B., Pozzo, M.D., Lillian, A., and Langmuir, C.H. (2008). Evidence from high-Ni olivines for a hybridized peridotite/pyroxenite source for orogenic andesites from the central Mexican Volcanic Belt. *Geochemistry, Geophysics, Geosystems*, 9(3).
- Stueber, A.M., and Goles, G.G. (1967). Abundances of Na, Mn, Cr, Sc and Co in ultramafic rocks. *Geochimica et Cosmochimica Acta*, 31(1), 75-93.
- Tashakor, M., Yaacob, W.Z.W., Mohamad, H., and Ghani, A.A. (2014). Geochemical characteristics of serpentinite soils from Malaysia. *Malaysian Journal of Soil Science*, 18, 35-49.
- Toplis, M.J., and Carroll, M.R. (1995). An experimental study of the influence of oxygen fugacity on Fe-Ti oxide stability, phase relations, and mineral—melt equilibria in ferro-basaltic systems. *Journal of Petrology*, 36(5), 1137-1170.
- Treloar, P.J. (1987). The Cr-minerals of Outokumpu—Their chemistry and significance. *Journal of Petrology*, 28(5), 867-886.
- Vaughan, A.P., and Scarrow, J.H. (2003). Ophiolite obduction pulses as a proxy indicator of superplume events? *Earth and Planetary Science Letters*, 213(3-4), 407-416.
- Vidal, O., and Parra, T. (2000). Exhumation paths of high-pressure metapelites obtained from local equilibria for chlorite—phengite assemblages. *Geological Journal*, 35(3-4), 139-161.
- Viti, C., and Mellini, M. (1997). Contrasting chemical compositions in associated lizardite and chrysotile in veins from Elba, Italy. *European Journal of Mineralogy*, 9(3), 585-596.
- Viti, C., and Mellini, M. (1998). Mesh textures and bastites in the Elba retrograde serpentinites. *European Journal of Mineralogy*, 10(6), 1341-1359.
- Von Knorring, O., Condliffe, E., and Tong, Y.L. (1986). Some mineralogical and geochemical aspects of chromium-bearing skarn minerals from northern Karelia, Finland. *Bulletin of Geological Society of Finland*, 58, 277-292.
- Walker, J.R. (1993). Chlorite polytype geothermometry. *Clays and Clay minerals*, 41, 260-260.

- Welch, M.D., Cámara, F., Ventura, G.D., and Iezzi, G. (2007). Non-ambient in situ studies of amphiboles. *Reviews in Mineralogy and Geochemistry*, 67(1), 223-260.
- Whitney, D.L., and Evans, B.W. (2010). Abbreviations for names of rock-forming minerals. *American mineralogist*, 95(1), 185-187.
- Wiewióra, A., and Weiss, Z. (1990). Crystallochemical classifications of phyllosilicates based on the unified system of projection of chemical composition: II. The chlorite group. *Clay Minerals*, 25(1), 83-92.
- Witt-Eickschen, G., and O'Neill, H.S.C. (2005). The effect of temperature on the equilibrium distribution of trace elements between clinopyroxene, orthopyroxene, olivine and spinel in upper mantle peridotite. *Chemical Geology*, 221(1-2), 65-101.
- Zanetti, A., Tiepolo, M., Oberti, R., and Vannucci, R. (2004). Trace-element partitioning in olivine: modelling of a complete data set from a synthetic hydrous basanite melt. *Lithos*, 75(1-2), 39-54.
- Zhang, J., Zhang, Z., Xu, Z., Yang, J., and Cui, J. (2001). Petrology and geochronology of eclogites from the western segment of the Altyn Tagh, northwestern China. *Lithos*, 56(2-3), 187-206.
- Zussman, J., Howie, R.A., and Deer, W.A. (1992). *An introduction to the rock forming minerals*. Longman Group Ltd, New York, p 698.
- Defant MJ, Drummond MS (1990) Derivation of some modern arc magmas by melting of young subducted lithosphere. *Nature*, 347, 662-665.
- Della.

Potentially toxic elements compositional variation in spinel-group minerals of serpentized and deformed ultramafic rocks from the Voltri Massif (NW Italy)

Keywords: magnetite, Laser-ablation ICP-MS, trace elements, deformation, serpentization, ophiolite, hydrothermal alteration, serpentine textures

5.1. INTRODUCTION

Spinel-group minerals occur widely in igneous, metamorphic, and sedimentary rocks, as well as in several types of ore-deposits (Dupuis and Beaudoin, 2011); these minerals form under a wide variety of genetic conditions ranging from high temperature crystallization from silicate and sulfide melts (Dare et al., 2014), to relatively low-temperature precipitation from hydrothermal fluids (Dare et al., 2014), and to prograde or retrograde metamorphic recrystallization in ultramafic rocks (Evans and Frost, 1974).

Spinel-group minerals are cubic closest packing oxides (space group Fd3m) with general formula XY_2O_4 . The X site is occupied by Mg^{2+} and Fe^{2+} in tetrahedral coordination and the Y site is usually occupied by Fe^{3+} , Cr^{3+} , and Al^{3+} in octahedral coordination. They are subdivided according to whether the trivalent ion is Al^{3+} (spinel series s.s.), Fe^{3+} (magnetite series), or Cr^{3+} (chromite series). Pure end-members of the spinel-group minerals are rare in nature. Spinel-group minerals have a wide range of composition because several elements, such as Zn^{2+} , Co^{2+} , Mn^{2+} , and Ni^{2+} can substitute Mg^{2+} and Fe^{2+} in the X site, whereas V^{3+} , Sc^{3+} , Ga^{3+} , and Ti^{4+} can substitute Fe^{3+} , Al^{3+} , and Cr^{3+} in the Y site (O'Neill and Navrotsky, 1984; Sack and Ghiorso, 1991; Burkhard, 1993; Abre et al. 2009; Colas et al., 2014; Liu et al., 2014; Canil et al., 2015). The type and degree of substitution in both sites depends on many parameters, including the similarity of the ionic radii and the valence of the cations, oxygen fugacity, magma/fluid composition, and temperature (Buddington and Lindsley, 1964; Frost and Lindsley, 1991; Lindsley, 1991; Toplis and Carroll, 1995; Dare et al., 2009; González-Jiménez et al., 2014; Liu et al., 2016).

From the petrological point of view, the variations of the composition of spinel-group minerals are commonly used as an efficient fingerprint to interpret the petrogenesis and the geodynamic setting of ultramafic rocks formation: the chemical composition of spinel-group minerals is in fact mainly controlled by the mantle melting processes occurring in the different tectonic settings (Irvine, 1967; Dick and Bullen, 1984; Arai, 1992; Stowe, 1994; Zhou and Robinson, 1994; Barnes and Roeder, 2001; Kamenetsky et al., 2001; Ahmed and Arai, 2002; Ahmed et al., 2005; Mondal et al., 2006; Rollinson, 2008; Pagé and Barnes, 2009; Mukherjee et al., 2010; Colas et al., 2014). In spite of their highly refractory behavior, textural and chemical changes may occur in spinel-group minerals during post-magmatic metamorphic, metasomatic and/or hydrothermal events in many rock types (Müller et al., 2003; Carew, 2004; Singoyi et al., 2006; Rusk et al., 2009; Dupuis and Beaudoin, 2011; Dare et al., 2012; Grieco and Merlini, 2012; Huang et al., 2014; Hu et al., 2014; Dare et al., 2015; Liu et al., 2015; Nadoll et al., 2015; Huang et al., 2016, 2017).

Spinel-group minerals, and in particular those hosted in ultramafic rocks, are also the main source of some elements, defined as *potentially toxic elements* (PTEs), which can have a significant impact on the environmental and human health once they are mobilized into soil, water or dust.

Hence, the knowledge both of spinel-group mineral content in ultramafic rocks and of their compositional variations (including PTEs concentration) as a function of metamorphic or structural parameters, other than for their petrological implications, results to be a paramount environmental concern. This information may have also an important application on the determination of the PTEs geochemical background values in natural and anthropogenic soils.

In this study we have focused our attention on spinel-group minerals hosted in serpentinites and serpentinitized lherzolites of the Voltri Massif meta-ophiolites (Ligurian Alps, NW Italy), in order to define how their textures, microstructures, as well as the degree of serpentinitization, can affect the compositional variations in spinel-group minerals and therefore their content of PTEs (mainly Cr, Ni, and Co).

5.2. ANALYTICAL METHODS

Forty-five samples of ultramafic rocks were collected from eight sites of the VM, according to their degree of serpentinization as well as to textural and structural criteria.

The rock specimens were analyzed using a multiscale and multi-analytical approach including: i) mineralogical, petrographic, and micro-structural/-textural analyses by means of polarized-light optical microscopy (PLOM) and scanning electron microscopy (SEM-EDS); ii) mineralogical and mineral-chemical analyses by means of X-ray powder diffraction (XRPD) and electron microprobe analyzer (EMPA-WDS); iii) in-situ measurements of trace and ultra-trace elements by laser ablation-inductively coupled plasma-mass spectrometry (LA-ICP-MS).

Preliminary mineralogical and micro-structural/-textural studies were carried out at the DISTAV, University of Genoa (Italy), using a SEM Vega3 – TESCAN type LMU system equipped with an EDS EDAX APOLLO XSDD with DPP3 analyzer. Single spot EDS analyses were performed at 20 kV accelerating voltage and 1.2 nA beam current at the specimen level for 60 live second counting time with a spot size of 370 nm and a working distance of 15 mm.

Major (i.e. Mg, Al, Cr, and Fe) and minor (i.e. Ti, V, Mn, Zn, Si, Co, K, Ca, and Ni) elements in spinel minerals were analyzed using the electron microprobe with wavelength-dispersive spectroscopy JEOL 8200 Super Probe at the “Ardito Desio” Department of Earth Sciences, University of Milano (Italy). The analytical conditions were set at 15 kV accelerating voltage and 4.9 nA beam current. Calibration for chemical analysis was accomplished using the following standards: olivine (Mg), omphacite (Na), Cr₂O₃ (Cr), rhodonite (Mn and Zn), k-feldspar (K), anorthite (Al and Ca), wollastonite (Si), pure V, fayalite (Fe), ilmenite (Ti), CoO (Co), galena (S), niccolite (Ni). Detailed compositional X-ray intensity maps were obtained for selected areas to investigate the distribution of major and minor elements (i.e. Cr, Fe, Mg, Mn, Ni, S, and Si) in spinel-group minerals. The image acquisition conditions were 15 kV accelerating voltage, 1 μm² pixel size, and a 30 ms dwell time.

The major-, minor- (detected with both EMPA and LA-ICP-MS; i.e. Al, Ca, Co, Cr, Cu, K, Mg, Mn, Na, Ni, Si, Ti, V, and Zn), and trace- (detected only by LA-ICP-MS; REE, Ba, Cs, Ga, Hf, Li, Nb, P, Pb, Rb, Sc, Sn, Sr, Ta, Th, U, Y, and Zr) element compositions of spinel-group minerals were determined using a Thermo Fisher Scientific iCAP Q quadrupole mass spectrometer coupled with a

Teledyne/Photon Machine ArF Excimer G2 laser ablation system at the Department of Physics and Geology, University of Perugia (Italy). The analyses were conducted using a ~30-20 μm beam diameter, 8 Hz frequency, and 0.032–0.105 mJ/pulse power, during 90 s analysis (50 s for the gas blank and 40 s on the grain). Details on the working conditions, instrumentation, precision, and accuracy are reported in Petrelli et al. (2016).

The structural formula of spinels was calculated assuming stoichiometry, following the procedure of Droop (1987); spinel-group minerals were classified using Stevens (1944), Haggerty (1991) and Zussman et al. (1992) classification fields (see Gargiulo et al., 2013).

5.3. RESULTS

5.3.1 Spinel-group minerals in the studied rocks: a crystallochemical classification

The composition of spinel-group minerals occurring in the three rock-groups (*described in the chapter IV*) is shown in Table 5.1 and Fig. 5.1. Spinel-group minerals classified according to Site Y vicariances (Fig. 5.1A), have a wide compositional range covering the fields of Cr-spinel, ferrian chromite, Cr-magnetite, and magnetite (Fig. 5.1).

Spinel-group minerals in the studied rocks are mainly: i) Cr-spinel with $\text{Fe}\# = [\text{Fe}^{3+}/(\text{Fe}^{3+}+\text{Fe}^{2+})] = 0.1\text{-}0.22$, $\text{Mg}\# = [\text{Mg}/(\text{Mg}+\text{Fe}^{2+})] = 0.3\text{-}0.7$, $\text{Cr}\# = [\text{Cr}/(\text{Cr}+\text{Al})] = 0.2\text{-}0.4$; ii) rare ferrian chromite with $\text{Fe}\# = 0.4\text{-}0.6$, $\text{Mg}\# = 0.15\text{-}0.2$, $\text{Cr}\# = 0.75\text{-}0.9$; iii) Cr-magnetite with $\text{Fe}\# = 0.68\text{-}0.4$, $\text{Mg}\# = 0.01\text{-}0.2$, $\text{Cr}\# = 0.7\text{-}0.97$, and $\text{Fe}\# = 0.6\text{-}0.68$, $\text{Mg}\# = 0\text{-}0.2$, $\text{Cr}\# = 0.9\text{-}1$, in PSP and MS, respectively; iv) magnetite with $\text{Fe}\# = 0.68\text{-}0.69$, $\text{Mg}\# = 0.01\text{-}0.02$, and a significant amount of Cr (i.e. $\text{Cr}\# = 0.27\text{-}0.38$).

Rock	Partially serpentinized peridotites						Massive serpentinites						Foliated serpentinites										
	Porphyroclasts			Serpentine texture			Porphyroclasts			Recrystallized porphyroclasts			Serpentine texture			Recrystallized porphyroclasts			Serpentine texture				
Microstructure	Cr-SPL	Fe-CHR	Cr-MAG	Fe-CHR	Cr-MAG	MAG	Fe-CHR	Cr-MAG	Cr-MAG	MAG	Fe-CHR	Cr-MAG	MAG	Fe-CHR	Cr-MAG	MAG	Fe-CHR	Cr-MAG	MAG	Fe-CHR	Cr-MAG	MAG	
Minerals																							
SiO ₂	0.04	0.04	0.32	0.46	0.02	0.05	0.02	0.05	0.05	0.03	0.02	0.05	0.03	0.02	0.05	0.03	0.02	0.05	0.03	0.02	0.05	0.03	0.02
TiO ₂	0.19	0.46	0.39	0.01	0.01	0.61	0.62	0.61	0.16	0.16	0.10	0.13	0.16	0.10	0.13	0.16	0.10	0.13	0.16	0.10	0.13	0.16	0.10
Al ₂ O ₃	37.22	5.54	2.01	0.03	0.03	0.07	0.09	0.07	0.02	0.02	0.01	0.02	0.02	0.01	0.02	0.02	0.01	0.02	0.01	0.02	0.01	0.02	0.01
Cr ₂ O ₃	27.11	33.99	23.47	0.02	0.02	21.43	36.20	21.43	1.77	1.77	0.88	1.03	1.77	0.88	1.03	1.77	0.88	1.03	1.77	0.88	1.03	1.77	0.88
FeO	23.23	53.60	67.17	91.69	91.69	69.84	57.37	69.84	90.63	90.63	89.71	90.47	90.63	89.71	90.47	90.63	89.71	90.47	90.63	89.71	90.47	90.63	89.71
MgO	11.81	1.55	1.20	0.58	0.58	1.61	0.83	1.61	0.57	0.57	0.58	0.81	0.57	0.58	0.81	0.57	0.58	0.81	0.57	0.58	0.81	0.57	0.58
MnO	0.23	0.46	0.35	0.12	0.12	1.53	1.66	1.53	0.21	0.21	0.31	0.35	0.21	0.31	0.35	0.21	0.31	0.35	0.21	0.31	0.35	0.21	0.31
NiO	0.15	0.21	0.33	0.12	0.12	0.47	0.18	0.47	0.50	0.50	0.61	0.69	0.50	0.61	0.69	0.50	0.61	0.69	0.50	0.61	0.69	0.50	0.61
CaO	0.00	0.00	0.01	0.01	0.01	0.01	0.00	0.01	0.01	0.01	0.01	0.02	0.01	0.01	0.02	0.01	0.01	0.02	0.01	0.01	0.02	0.01	0.01
Na ₂ O	0.03	0.04	0.02	0.00	0.00	0.02	0.01	0.02	0.02	0.02	0.01	0.04	0.02	0.02	0.04	0.02	0.02	0.04	0.02	0.02	0.04	0.02	0.02
K ₂ O	0.00	0.00	0.00	0.01	0.01	0.00	0.01	0.00	0.00	0.00	0.01	0.00	0.00	0.00	0.00	0.00	0.01	0.00	0.00	0.00	0.00	0.00	0.00
V ₂ O ₅	0.20	0.31	0.23	0.00	0.00	0.09	0.14	0.09	0.07	0.07	0.14	0.05	0.07	0.04	0.05	0.07	0.04	0.05	0.07	0.04	0.05	0.07	0.04
CoO	0.10	0.09	0.09	0.15	0.15	0.12	0.21	0.12	0.13	0.13	0.14	0.16	0.13	0.14	0.16	0.13	0.14	0.16	0.13	0.14	0.16	0.13	0.14
ZnO	0.52	0.61	0.26	0.03	0.03	0.38	0.57	0.38	0.04	0.04	0.01	0.05	0.04	0.01	0.05	0.04	0.01	0.05	0.04	0.01	0.05	0.04	0.01
Sum	100.83	96.89	95.85	93.23	93.23	96.23	97.92	96.23	94.15	94.15	92.56	93.86	94.15	92.56	93.86	94.15	92.56	93.86	94.15	92.56	93.86	94.15	92.56
Si	0.00	0.00	0.01	0.02	0.02	0.00	0.00	0.00	0.00	0.00	0.01	0.00	0.00	0.01	0.00	0.00	0.01	0.00	0.00	0.01	0.00	0.00	0.00
Ti	0.00	0.01	0.01	0.00	0.00	0.02	0.02	0.02	0.00	0.00	0.00	0.00	0.00	0.00	0.00	0.00	0.00	0.00	0.00	0.01	0.00	0.00	0.00
Al	1.27	0.23	0.09	0.00	0.00	0.00	0.00	0.00	0.00	0.00	0.00	0.00	0.00	0.00	0.00	0.00	0.00	0.00	0.00	0.00	0.00	0.00	0.00
Cr	0.63	0.98	0.69	0.00	0.00	1.06	1.06	1.06	0.05	0.05	0.03	0.05	0.05	0.03	0.05	0.05	0.03	0.05	0.05	0.03	0.05	0.05	0.03
Mg	0.51	0.08	0.07	0.03	0.03	0.09	0.05	0.09	0.03	0.03	0.03	0.05	0.03	0.03	0.05	0.03	0.03	0.05	0.03	0.03	0.05	0.03	0.03
Mn	0.01	0.01	0.01	0.00	0.00	0.05	0.05	0.05	0.01	0.01	0.01	0.01	0.01	0.01	0.01	0.01	0.01	0.01	0.01	0.01	0.01	0.01	0.01
Ni	0.00	0.01	0.01	0.00	0.00	0.01	0.01	0.01	0.02	0.02	0.02	0.02	0.02	0.02	0.02	0.02	0.02	0.02	0.02	0.02	0.02	0.02	0.02
Ca	0.00	0.00	0.00	0.00	0.00	0.00	0.00	0.00	0.00	0.00	0.00	0.00	0.00	0.00	0.00	0.00	0.00	0.00	0.00	0.00	0.00	0.00	0.00
Na	0.00	0.00	0.00	0.00	0.00	0.00	0.00	0.00	0.00	0.00	0.00	0.00	0.00	0.00	0.00	0.00	0.00	0.00	0.00	0.00	0.00	0.00	0.00
K	0.00	0.00	0.00	0.00	0.00	0.00	0.00	0.00	0.00	0.00	0.00	0.00	0.00	0.00	0.00	0.00	0.00	0.00	0.00	0.00	0.00	0.00	0.00
V	0.00	0.01	0.01	0.00	0.00	0.01	0.01	0.01	0.00	0.00	0.00	0.00	0.00	0.00	0.00	0.00	0.00	0.00	0.00	0.00	0.00	0.00	0.00
Co	0.00	0.00	0.00	0.00	0.00	0.00	0.01	0.00	0.00	0.00	0.00	0.00	0.00	0.00	0.00	0.00	0.00	0.00	0.00	0.00	0.00	0.00	0.00
Zn	0.01	0.02	0.01	0.00	0.00	0.01	0.02	0.01	0.00	0.00	0.01	0.00	0.00	0.01	0.00	0.00	0.01	0.00	0.00	0.01	0.00	0.00	0.00
Fe ³⁺	0.09	0.74	1.16	1.96	1.96	1.32	0.89	1.32	1.93	1.93	1.95	1.96	1.93	1.95	1.96	1.93	1.95	1.96	1.93	1.95	1.96	1.93	1.95
Fe ²⁺	0.48	0.90	0.93	0.97	0.97	0.85	0.90	0.85	0.95	0.95	0.94	0.92	0.95	0.94	0.92	0.95	0.94	0.92	0.95	0.94	0.92	0.95	0.94

Table 5.1 Representative point analysis of spinel-group minerals, chosen in order to acquire a representative selection of the different textures (Formula calculated basis on four cations).

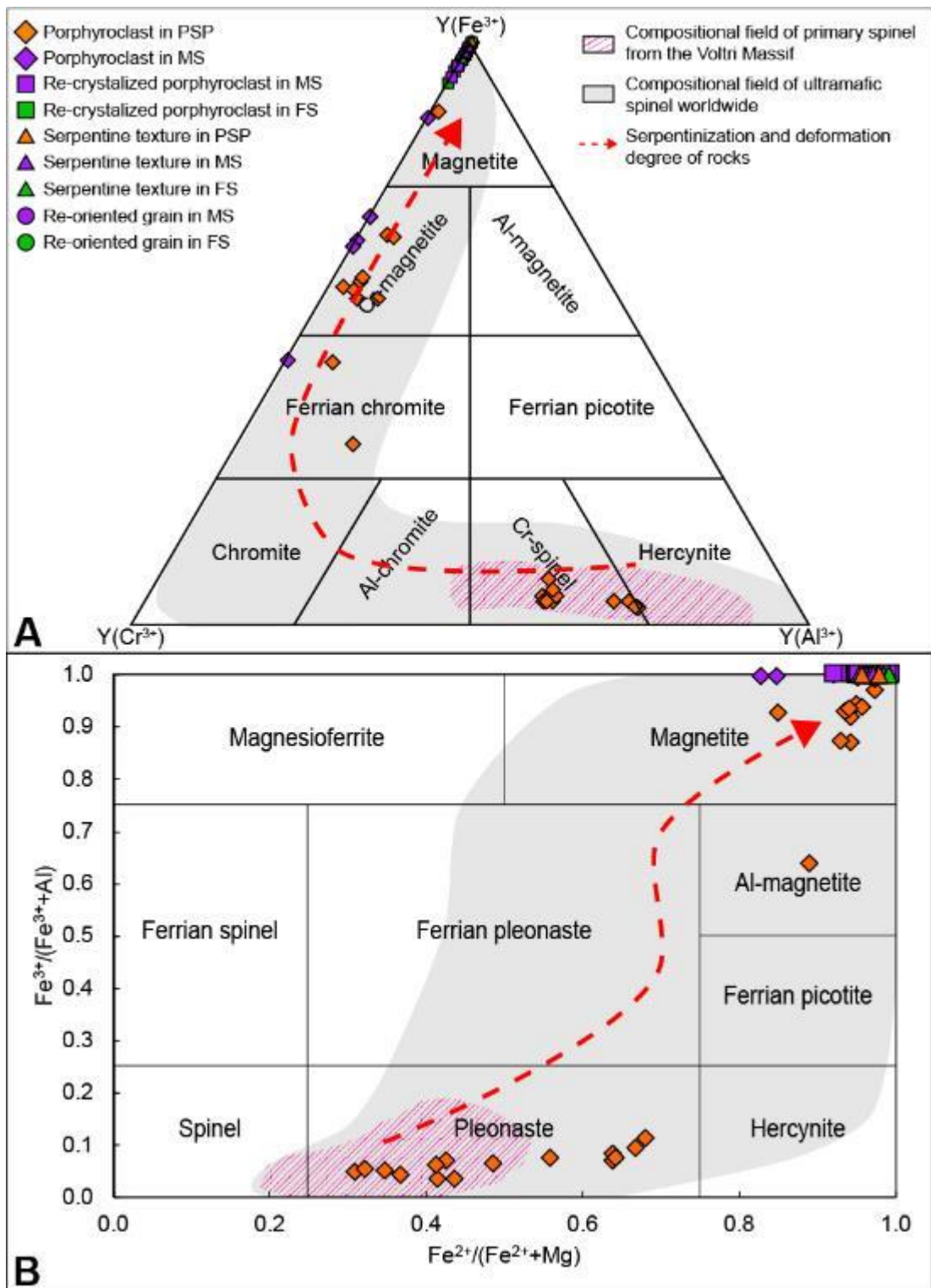


Fig. 5.1 Classification diagrams of spinel-group minerals; spinel-group minerals are grouped according to their microstructure and texture (see paragraph 2); pink dashed areas refer to the composition of primary spinel from the Voltri Massif (mainly Erro-Tobbio primary spinels; Rampone et al., 2005; Piccardo & Visser, 2007; Borghini et al., 2007; Padovano et al., 2005); gray fields refer to the composition of ultramafic spinel worldwide (see Barnes & Roeder, 2001 and reference therein). A) Ternary diagram considering the Al^{3+} , Cr^{3+} and Fe^{3+} exchange in "Y" structural site (field-contours are after Stevens, 1944; Haggerty, 1991; Zussman et al., 1992). B) Binary diagram considering the Mg^{2+} - Fe^{2+} exchange in the "X" structural site (field-contours are after Stevens, 1944; Haggerty, 1991; Deer et al., 1992).

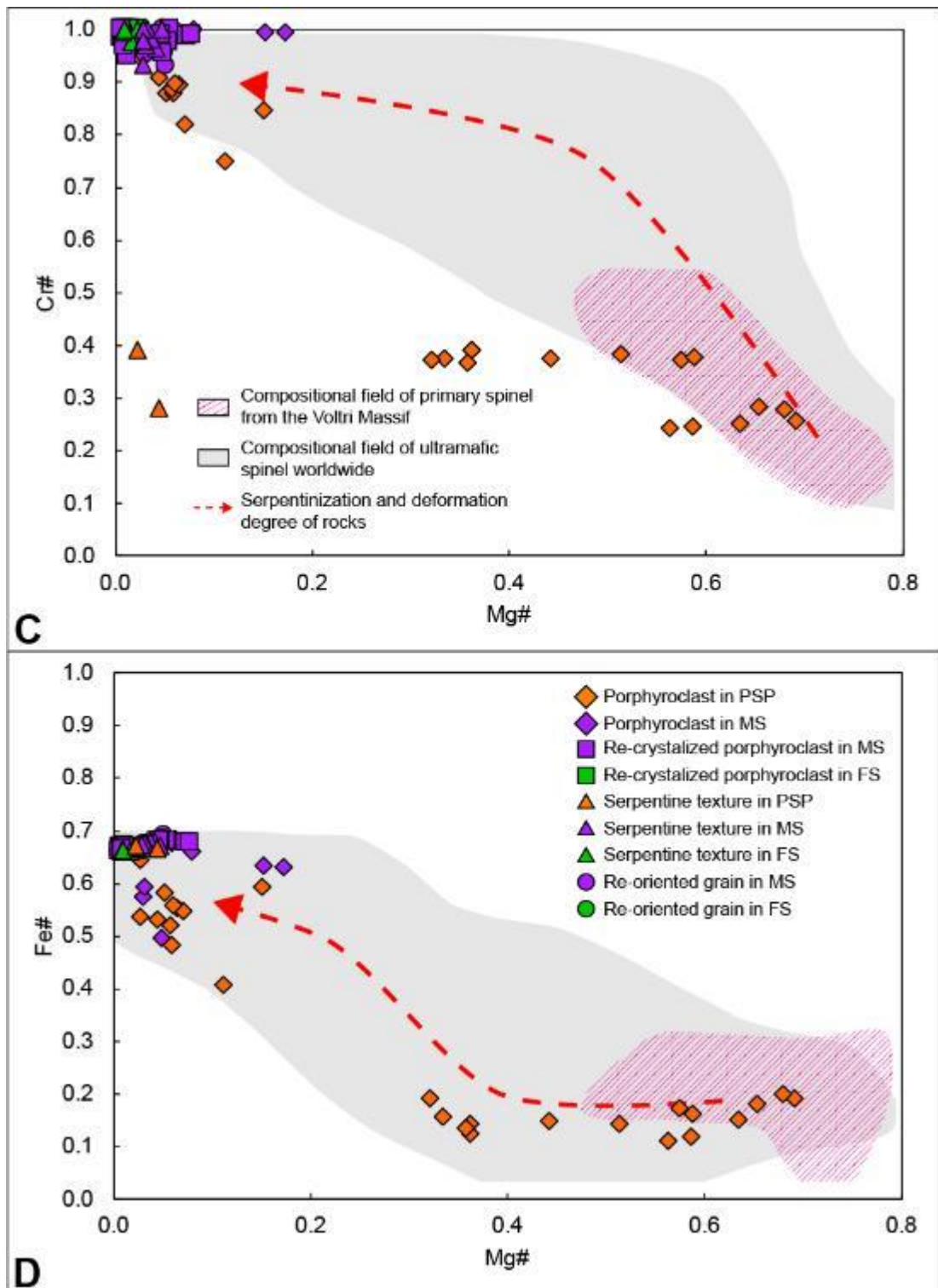


Fig. 5.1 C) $Mg\# = [Mg / (Mg + Fe^{2+})]$ vs $Cr\# = [Cr / (Cr + Al)]$ diagram of spinel-group minerals. D) $Mg\# = [Mg / (Mg + Fe^{2+})]$ vs $Fe\# = [Fe^{3+} / (Fe^{3+} + Al)]$ diagram of spinel-group minerals.

5.3.2 Microstructures and textures of spinel-group minerals

In the three rock-groups, spinel-group minerals can be grouped in the following classes (Fig. 5.2), according to their different microstructures and textures.

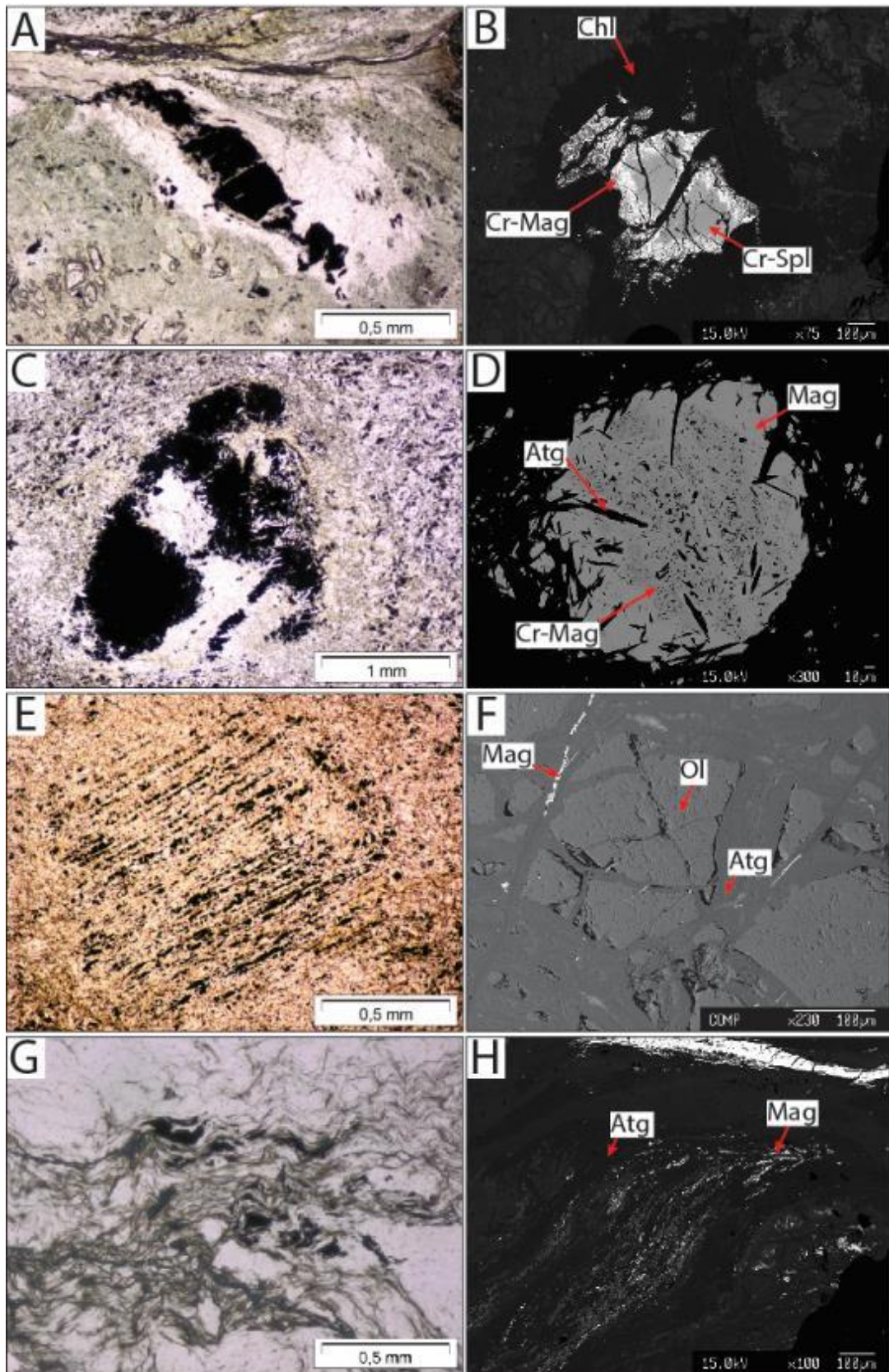


Fig. 5.2 Spinel-group mineral microstructures: a-b) spinel-group mineral porphyroclasts surrounded by chlorite coronas, in PSP; c-d) recrystallized spinel-group minerals porphyroclasts intergrowing with serpentine minerals in MS; e) spinel-group minerals within bastite in MS; f) spinel-group minerals within mesh texture in PSP; g-h) spinel-group minerals re-oriented along the foliation in FS. Mineral abbreviations after Kretz (1983): Chl = chlorite, Cr-Mag = chromian magnetite, Cr-Spl = chromian spinel, Atg = antigorite, Mag = magnetite, Ol = olivine.

Spinel-group mineral porphyroclasts with various degree of recrystallization

Spinel porphyroclasts mainly consist of scattered sub-euhedral crystals, varying in size between 0.1 and 2 mm. Porphyroclasts occurring in the studied rocks show various degrees of recrystallization, evolving from pristine mantle spinels.

Mantle spinels porphyroclasts are Cr-spinel and are found in PSP (Fig. 5.2A-B); these porphyroclasts mainly occur with a characteristic holly-leaf texture (as defined by Mercier and Nicolas, 1975), in which Cr-spinel is surrounded by Cr-chlorite coronas that have a content of Cr up to 5900 ppm. Replacement of Cr-spinel by ferrian chromite/Cr-magnetite spongy rims starts along rims and fractures and progressively affects the Cr-spinel.

In MS, porphyroclasts are mainly represented by Cr-magnetite relics at the core with rims having a magnetite composition; this substitution is visible also along microfractures and veins cutting porphyroclasts (Fig. 5.2C-D).

In FS, pseudomorphs of almost “pure” magnetite after Cr-magnetite occur along the foliation.

Spinel-group minerals within pseudomorph and non-pseudomorph textures

Idiomorphic to sub-idiomorphic spinel-group mineral crystals (10 to 40 μm in size) occur in trails (Fig. 5.2E-F) within: i) bastites texture, with very fine magnetite arranged along the cleavage planes of former mantle pyroxene; or ii) along the rims of the mesh, hourglass, and ribbon textures, regardless of the degree of serpentinization of the rock (i.e., PSP vs MS). In interpenetrating textures, spinels may occur as sub-mm scattered crystals. In general, all these spinel-group minerals have magnetite composition (e.g. $\text{Fe}\# = 0.68\text{-}0.69$, $\text{Mg}\# = 0.01\text{-}0.02$, $\text{Cr}\# = 0.27\text{-}0.38$).

Spinel-group minerals re-oriented along the foliation

In FS and in mm-thick shear zones cutting MS, spinel-group minerals occur either as porphyroclasts made of aggregates of allotriomorphic crystals (60 to 130 μm), or as micron-size crystals, oriented along the folded composite fabric (Fig. 5.2G-H). Their composition is close to magnetite, but substantial differences exist according to the rock class in which they occur: in shear zones cutting MS, magnetite has higher Mg and less Cr than magnetite in FS.

5.3.3 Trace and ultra-trace element variation in spinel-group minerals

The analysis of trace and ultra-trace elements in spinel-group minerals highlighted that the most important carrier of these elements in the studied rocks are porphyroclasts.

In general Al, V, Cr, Zn, and Mg content decreases from porphyroclasts in PSP to those in MS and FS (Fig. 5.1C-D, 5.3 and 5.4); conversely, Ni, Co, and Mn increase from spinels in PSP to those in MS (Fig. 5.3A-B-C). Nevertheless, porphyroclasts in MS are richer in Ni than porphyroclasts in FS (Fig. 5.3A).

In mesh-hosted spinel-group minerals (i.e., magnetite), a significant amount of Ni (~0.03 apfu) and Co (~0.008 apfu) occurs, whereas bastites-hosted spinel-group minerals (i.e., magnetite) have a significant amount of Cr (~0.05 apfu), regardless of the rock in which they occur.

Re-oriented spinel-group minerals (i.e. magnetite), in shear zones cutting MS, include more Mg (~0.05 apfu), Ni (~0.02 apfu), and Mn (~0.014 apfu) compared to spinels in FS. On the other hand, FS spinel-group minerals can host higher content of Cr (~0.08 apfu) and Ti (~0.01 apfu) compared to MS spinels in shear zones cutting MS.

Our analyses (Fig. 5.5) moreover highlighted that in general Mn and Ti in MS porphyroclasts, and V and Zn in PSP porphyroclasts are strongly positively correlated with Cr; Ni and Co content in all the spinels classes is independent of Cr variations.

Figure 5.6, providing an overview of the concentration of a wide range of elements within spinel-group minerals, shows a high content of Cr, Ni, V, Co, Ti, Mn, and Ga which are compatible into magnetite, and low Zr, Hf, Sc, Ta, and Nb values, which are incompatible into magnetite.

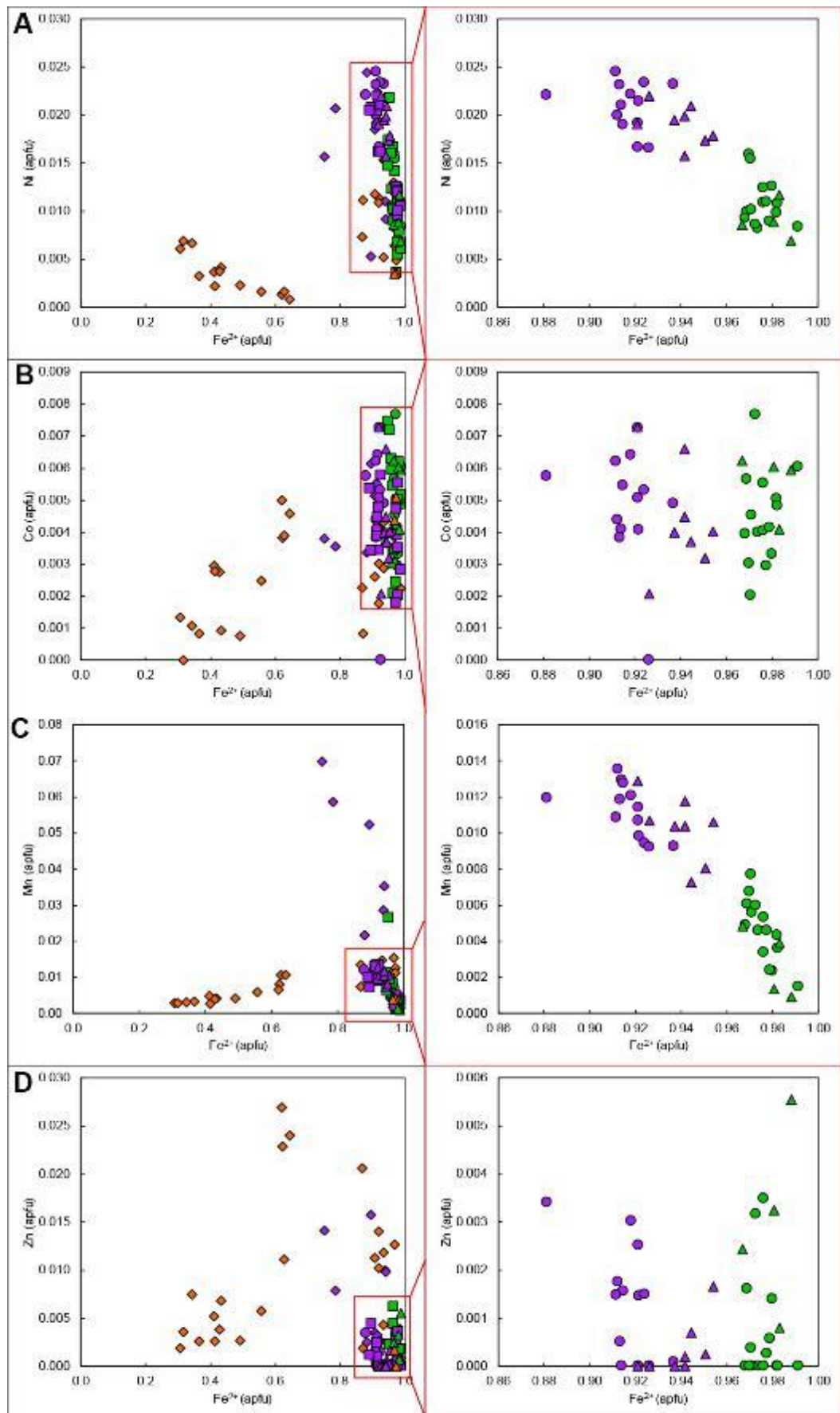


Fig. 5.3 Correlation plots of Fe^{2+} (structural site "X") vs Ni (A), Co (B), Mn (C), and Zn (D). Values are in atoms per formula unit (apfu). Diagram on the right are the zoomed area of left diagram (red box) report only spinel-group minerals within serpentine textures and re-oriented along the foliation. For the legend of symbols please refer to Fig. 5.1.

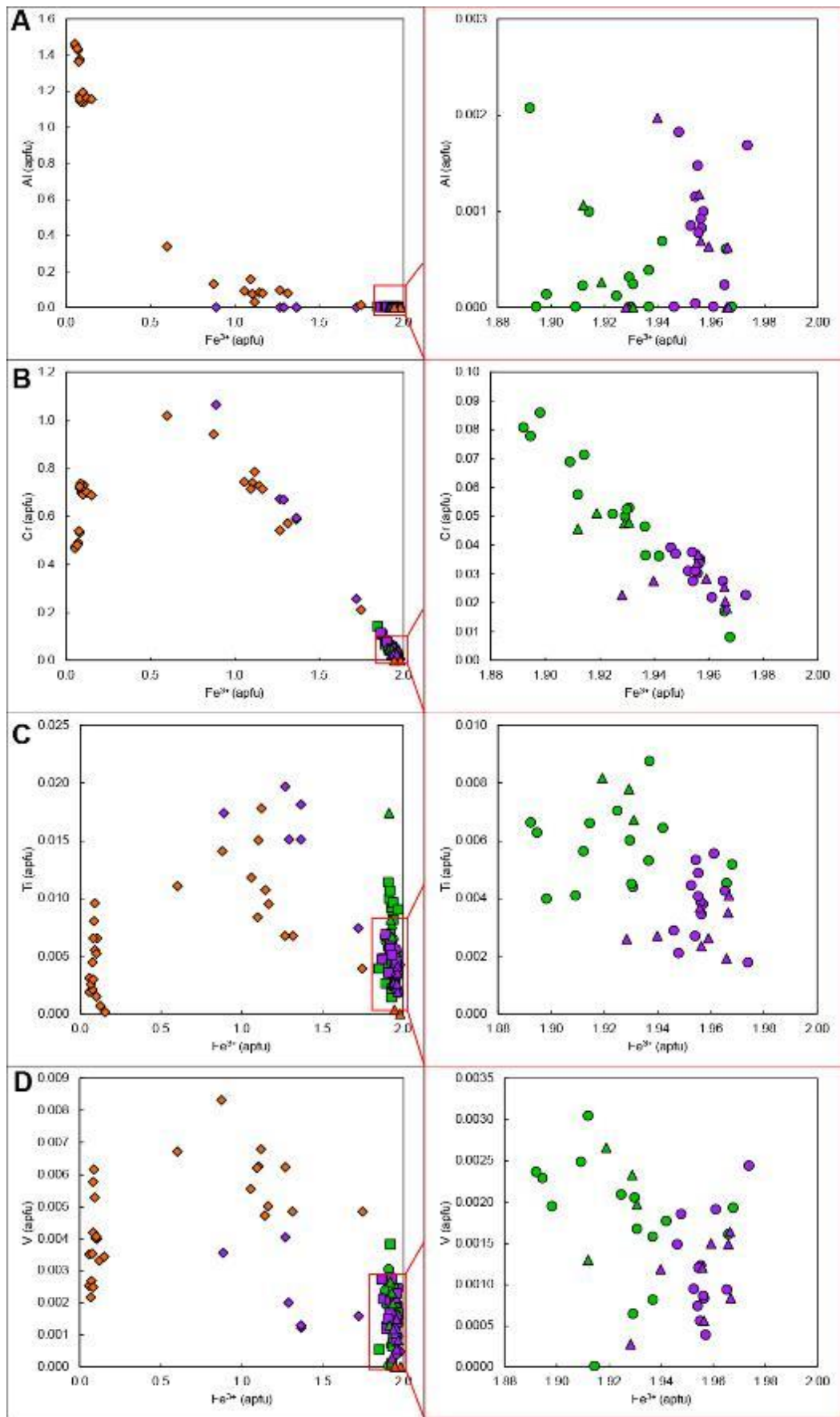


Fig. 5.4 Correlation plots of Fe^{3+} (structural site "Y") vs Al (A), Cr (B), Ti (C), and V (D). Values are in atoms per formula unit (apfu). Diagram on the right are the zoomed area of left diagram (red box) report only spinel-group minerals within serpentine textures and re-oriented along the foliation. For the legend of symbols please refer to Fig. 5.1.

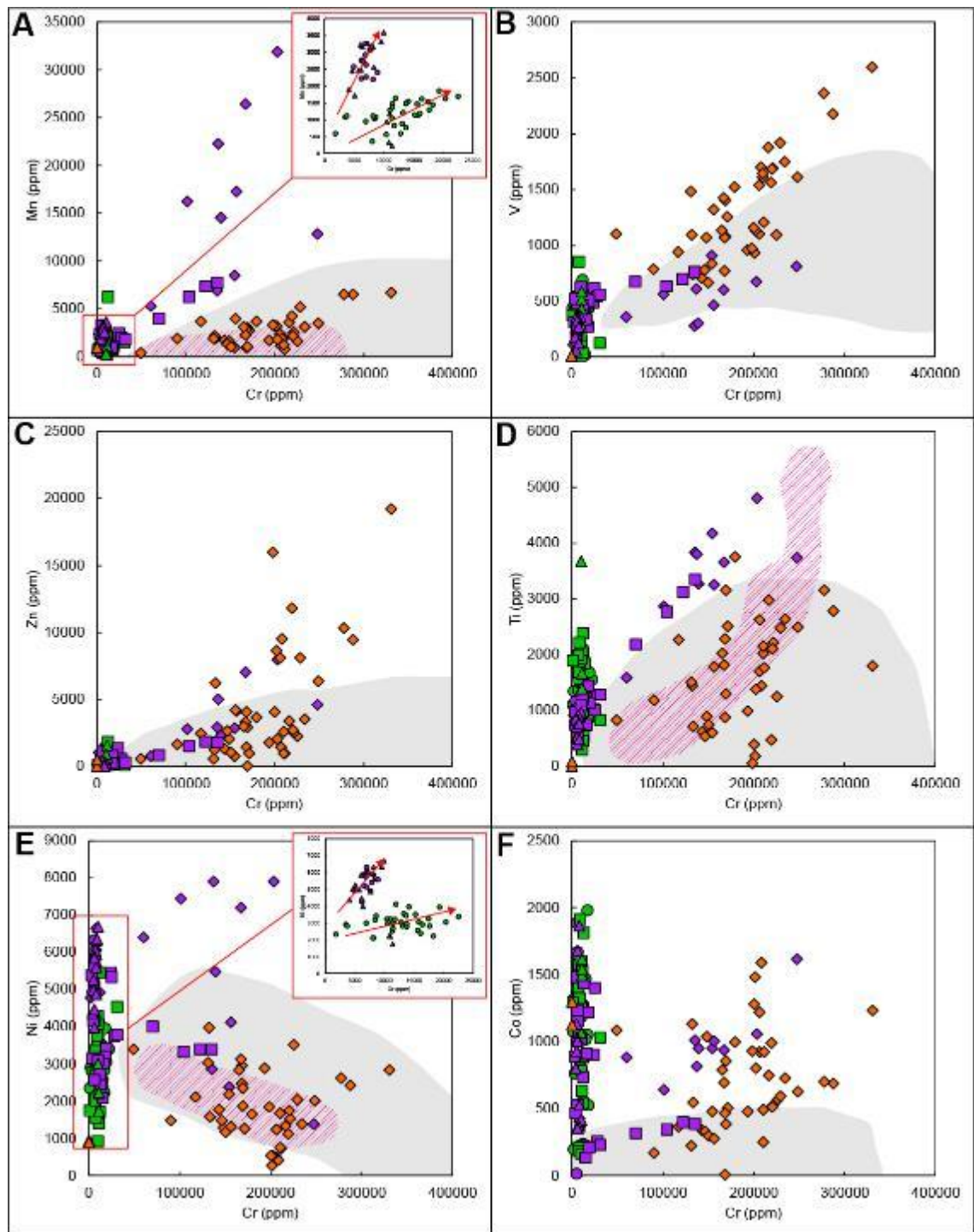


Fig. 5.5 Correlation diagram of Cr vs Mn, V, Zn, Ti, Ni, and Co, respectively (EMPA-WDS and LA-ICP-MS data). Values in ppm. Pink dashed areas refer to the composition of primary spinel from the Voltri Massif (mainly Erro-Tobbio primary spinels; Rampone et al., 2005; Piccardo & Visser, 2007; Borghini et al., 2007; Padovano et al., 2005); gray fields refer to the composition of ultramafic spinel worldwide (see Barnes & Roeder, 2001 and reference therein). For the legend of symbols please refer to Fig. 3.

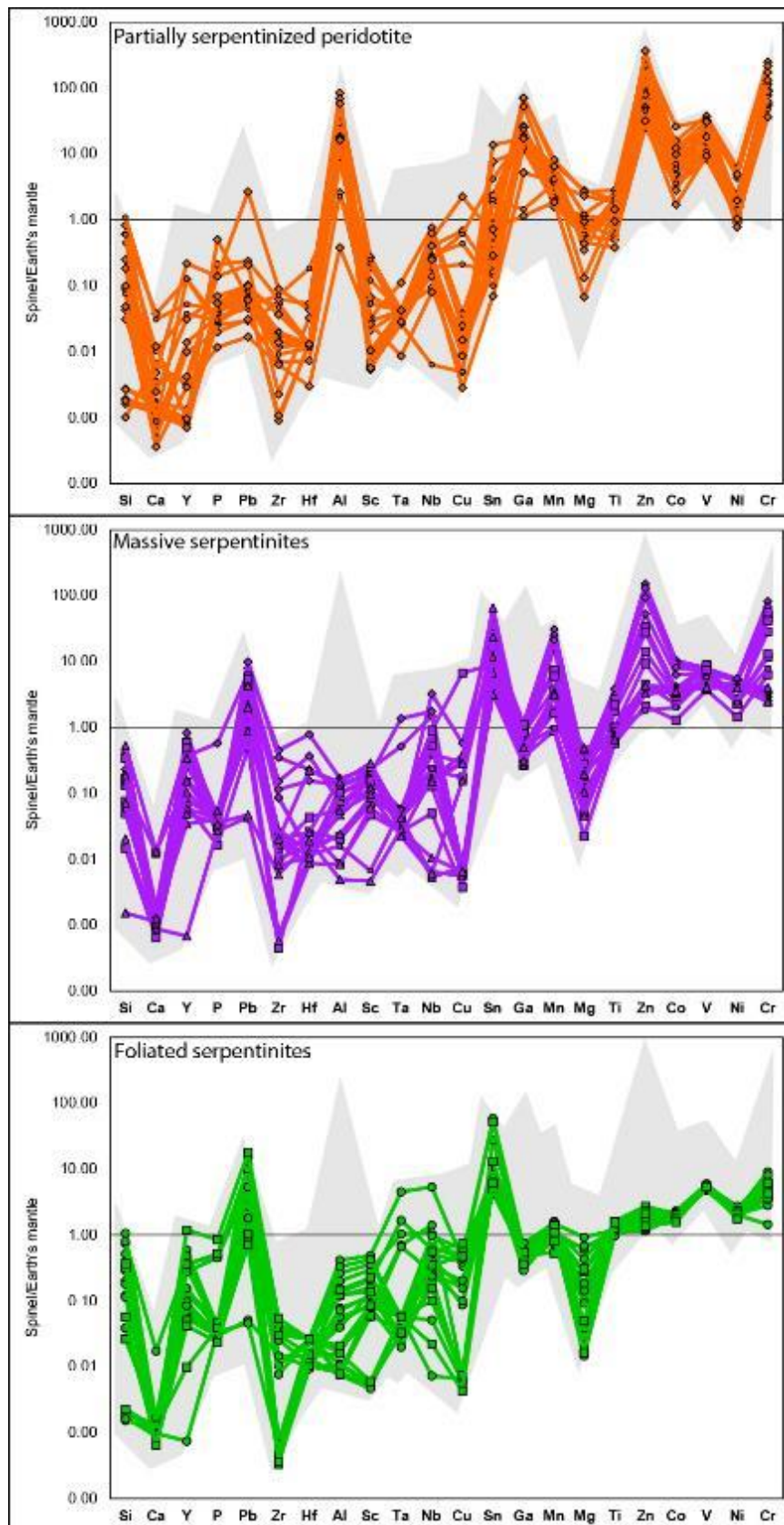


Fig. 5.6 Multi-element variation diagrams of the analyzed spinel-group minerals after in situ laser ablation analysis (LA-ICP-MS data). The values have been normalized to the Earth's mantle average composition (Palms & O'Neill, 2014). Diamonds represent porphyroclasts analyses, squares re-crystallized porphyroclasts, circles re-oriented magnetite, triangles are magnetite within pseudomorphic textures. The shaded grey area marks the sum of the ranges of the three different lithologies. The 22 trace elements are

plotted in order of increasing compatibility into magnetite, as suggested by Dare et al. (2014).

5.4. DISCUSSION

The chemistry and microstructure of spinel-group minerals in ultramafic rocks can be significantly modified both during oceanic serpentinization and/or prograde and retrograde metamorphism (Barnes, 1998, 2000). Spinel-group minerals occurring in the studied rocks have similar chemical characteristics as those described by Evans and Frost (1975), Barnes and Roeder (2001) and Gargiulo et al. (2013) for spinel-group minerals related to metamorphosed ultramafic rocks from alpine-type complexes (Fig. 5.1). The analyzed spinels however recorded several stages of the multiphase evolution experienced by the VM, as sketched in Fig. 5.7. In the following, we will discuss the effects of serpentinization and deformation on both texture, microstructure, and chemistry of spinel-group minerals.

5.4.1 Textural and microstructural evolution

In the early stage of oceanic serpentinization of the lithospheric mantle rocks (Fig. 5.7, stage A), peridotites were affected by the formation of pseudomorphic textures (mainly mesh texture and bastite) with crystallization of microcrystals of magnetite within mesh-rims. Cr-spinels were altered by hydrothermal fluids that promoted the reaction with silicates (i.e., olivine and pyroxene), forming rims and veins of ferrian chromite and/or Cr-magnetite, and Cr-chlorite coronas (Cr-clinochlore), at temperature probably higher than 200°–300°C (as suggested by Auzende et al. 2006; Hajjalioghli et al. 2007; Grieco and Merlini, 2012). After this reaction, olivine and spinel were residually respectively enriched in Fe²⁺ and Cr by a loss of MgO (olivine) and Al₂O₃ (spinel) (Piccardo et al., 2001; Colas et al., 2014).

The compositional map (Fig. 5.8) of porphyroclasts clearly shows that they are depleted in Cr and other metals starting from veins, as observed by Barnes (2000) for the serpentinization process. Therefore, the spongy alteration texture of the rims and areas close to cracks of the Cr-spinel can be attributed to the dissolution of several elements (i.e. Al, Cr, Ti, Mg, Zn, and Co) from these crystals during the serpentinization processes (Garuti et al., 2007; Teixeira et al., 2012).

In literature, only a few hypotheses have been formulated on the general conditions at which ferrian chromite and Cr-chlorite formation occurred. Barnes (2000) proposed that the growth of ferrian chromite is to be attributed to an Mg–Fe exchange between the magnetite rim and spinel. Cr-clinochlore formation has been instead closely associated with ferrian chromite formation after the reaction of silicates (i.e. olivine and pyroxene) with primary spinels as indicated by textural evidence (e.g., holly-leaf texture) and Cr₂O₃ content of chlorite (Barnes and Roeder 2001; Piccardo et al., 2001; Grieco and Merlini, 2012).

The reactions producing ferrian chromite and Cr-clinochlore have been already assessed in several studies (e.g. Christofides et al. 1994; Barnes and Roeder 2001; Piccardo et al., 2001; Grieco and Merlini, 2012; Colas et al., 2014); not all the authors, however, agree on the timing of this reactions, suggesting that they occurred during either i) a pre-oceanic serpentinization process, but after all deep magmatic events (Grieco and Merlini, 2012), ii) during the oceanic serpentinization process (Bliss and MacLean, 1975), iii) after the main serpentinization of the rock (Kimball, 1990; Mellini et al., 2005), either during prograde metamorphism of serpentinized ultramafic rocks (Evans and Frost, 1975; Bliss and MacLean, 1975; Barnes and Roeder, 2001), or during the retrograde evolution of the rock from high-pressure conditions (Gervilla et al., 2012; Colas et al., 2014) or during regional metamorphism of ultramafic rocks, after the reactions of spinel with silicates and metamorphic fluids (Barnes and Roeder, 2001).

According to what we observed in massive serpentinites we suggest that, during the ongoing oceanic serpentinization of the mantle rocks (Fig. 5.7, Stage B-C), mantle spinel was later progressively replaced by magnetite, as attested by the occurrence of Cr-rich core relics (where eventually relic magmatic chromite can still be found), surrounded by Cr-poor magnetite rims (Diella et al., 1994; Fontana et al., 2009). With the progressive intensification of serpentinization, mesh texture becomes hourglass texture and, at the early stage of deformation, ribbon texture (with an enrichment in trace elements).

The progressive deformation, locally affecting serpentinites during subduction and exhumation (Scambelluri et al., 1991), caused both the formation of magnetite porphyroclasts and the grain-size reduction of re-crystallized porphyroclasts of magnetite (Fig. 5.7, Stage D1), with the alignment of micron size magnetite as trails along the foliation (Fig. 5.7, Stage D2).

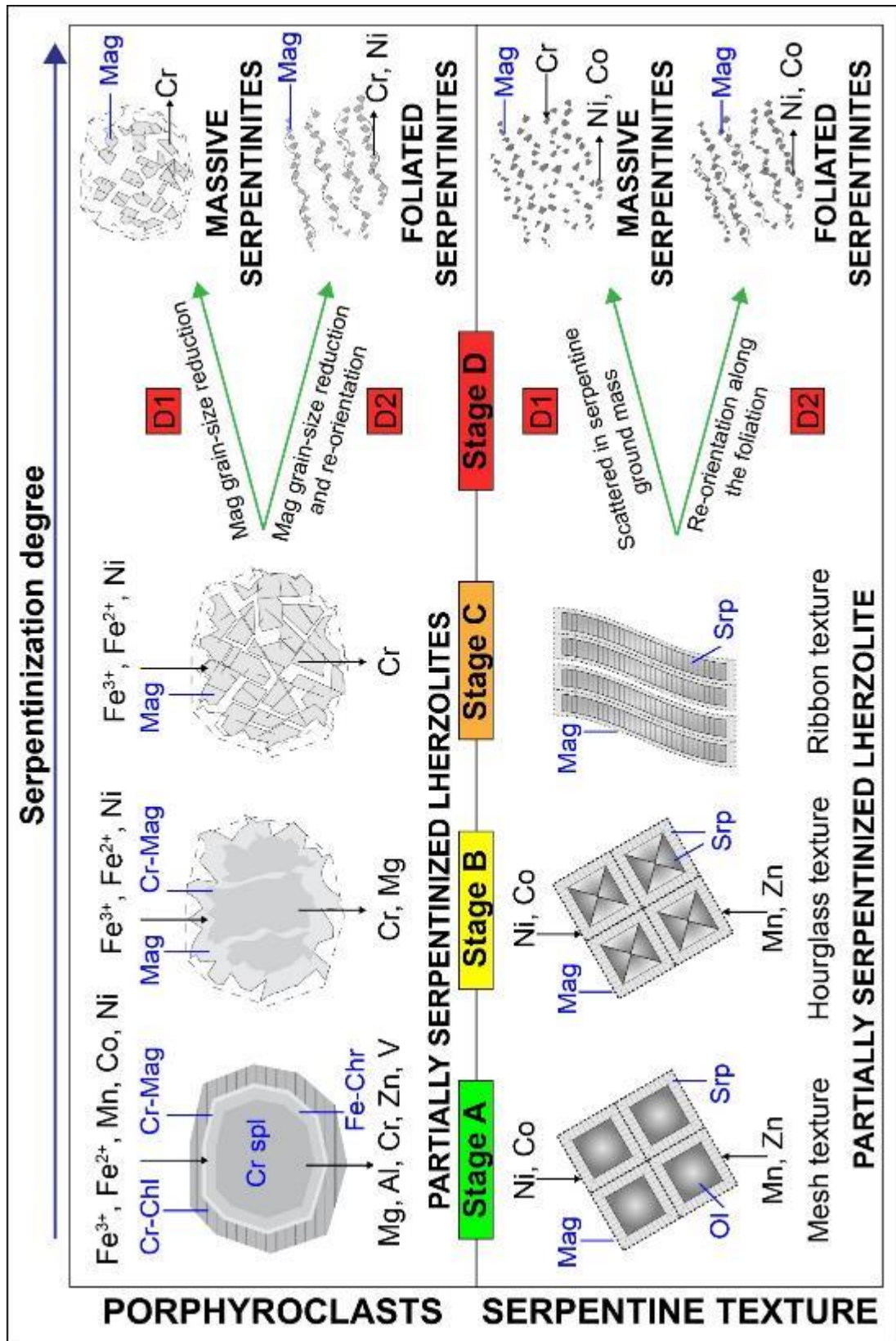


Fig. 5.7 Sketch of spinel-group minerals variation: Stage A. early oceanic alteration stage in partially serpentinized lherzolites, with the development of mesh texture; Stage B. the ongoing oceanic alteration triggers the first stage of Al-spinel substitution by Cr-magnetite, with intergrowing of serpentine minerals, and the progressive evolution of pseudomorphic texture (hourglass); Stage C. complete replacement of Cr-magnetite by magnetite and development of ribbon texture; Stage D1. grain-size reduction of magnetite in massive serpentinites; Stage D2. grain-size reduction and re-orientation of magnetite along the foliation in foliated serpentinites.

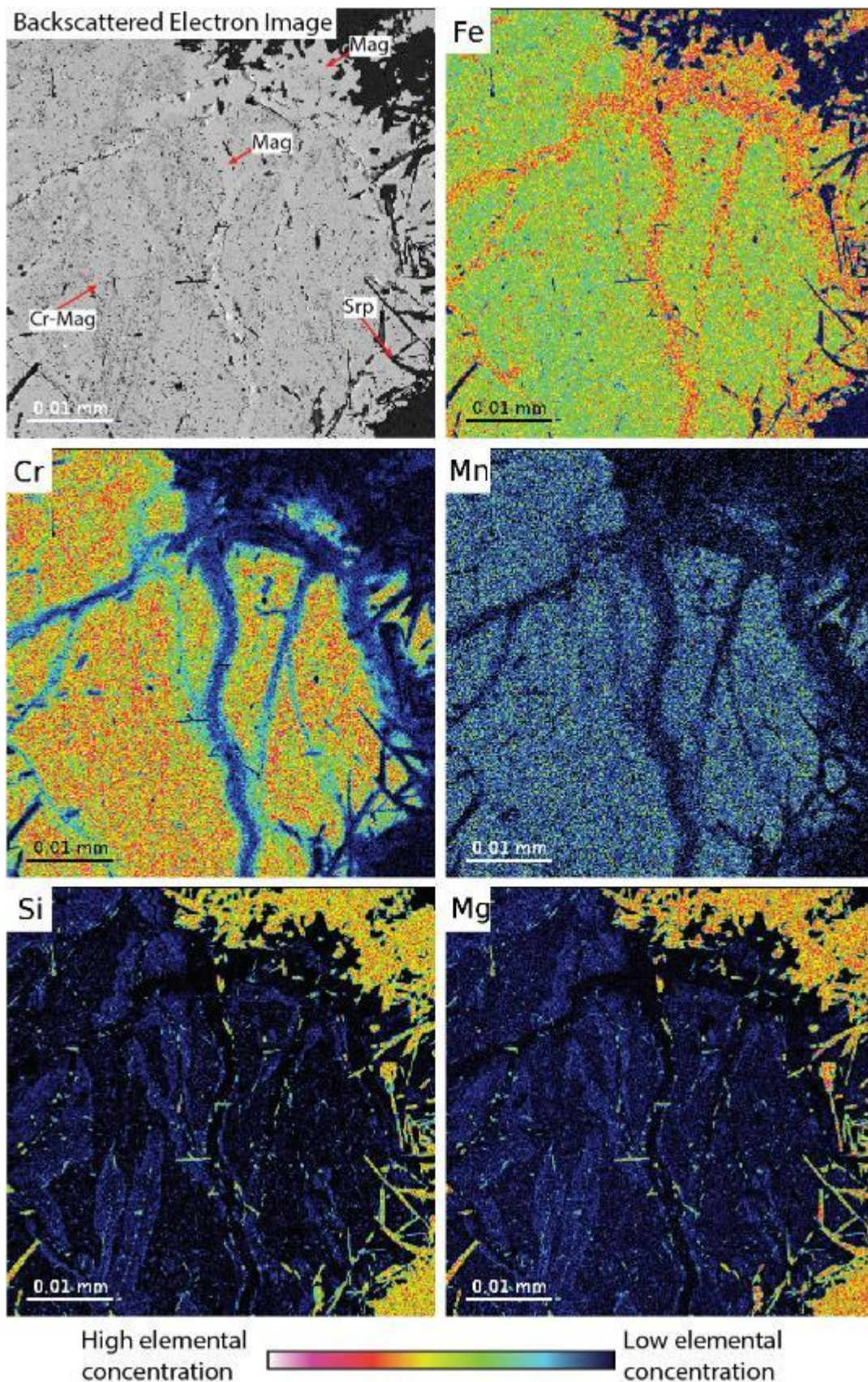


Fig. 5.8 WDS compositional maps of Fe, Cr, Mn, Si, and Mg showing the complete removal of chromium during chromian-spinel partially replacement by secondary magnetite along edges and microfractures

5.4.2 Trace element variation in spinel-group minerals

We observed that the wide compositional variations in trace elements of spinel-group minerals are mainly correlated with the degree of serpentinization and deformation.

In general in the studied spinel-group minerals, the serpentinization degree affects the composition of spinel-group minerals since olivine is the major repository of Mn, Zn, Ni, and Co in ultramafic rocks and the availability of these elements in solution, after olivine breakdown, is the main factor controlling their incorporation in the lattice of chromian spinel (Gahlan and Arai, 2007); it should be therefore expected that the complete alteration of olivine after serpentinization would provide the necessary Mn, Zn, Ni, and Co amounts that have been detected in the analyzed spinels and in worldwide chromian spinels (Barnes and Roeder, 2001). Mn, Zn, Co, and Ni, released after the alteration of olivine, are in fact incompatible with serpentine minerals structure and they are dissolved in hydrothermal solution involved in serpentinization (Singh and Singh, 2013) and later incorporated in spinels crystal structure. Porphyroclasts in MS are richer in Ni than porphyroclasts in PSP, as confirmed by Barnes (1998, 2000), who notes that Ni incorporation within chromite is complicated by crystal-chemical effects and that it is more stable in magnetite due to the inverse spinel cation distribution (Hodel et al, 2017; Beckett-Brown and McDonald, 2018). The above processes are strongly confirmed by the increase, that we observed in our samples, of Ni, Co, and Zn from PSP- to MS-porphyroclasts and by the high content of Ni and Co in mesh-hosted magnetite, suggesting a strong influence of the serpentinization process on the mobility of trace and ultra-trace elements and in particular of PTEs. In general, compared to other ultramafic massifs worldwide, the relative abundance of Ni, Zn, and Co in magnetite of our samples can also be linked to the poor concentrations of sulfide (not detected in rock sample of present work; Ramdohr, 1967; Alansari et al., 2015). A high Zn content in Cr-spinel core is common in metamorphosed ultramafic rocks, (e.g. Barnes, 2000; Saumur et al., 2013). Compositional variations between cores and rims suggest that Zn behaves like Mg and is liberated from Cr-spinel during initial-stage reactions with serpentine or Mg- and Si-rich fluids, as suggested by Gonzalez-Jimenez et al. (2009).

The significant amount of Cr (~0.05 apfu) in bastite-hosted spinel-group minerals (i.e. magnetite), regardless of the rock in which they occur, is to be correlated

with the high Cr content of pyroxene that is, among silicates, the main Cr repository.

5.5. CONCLUSIONS

In this study, we have investigated the mineralogy and the mineral chemistry of spinel-groups minerals in ultramafic rocks (e.g., partially serpentinized lherzolites, massive serpentinites, and foliated serpentinites) from the Voltri Massif metaophiolites (Ligurian Alps). In particular, we focused on variations of the spinel-group mineral composition in relation to different textures, microstructures and various degree of serpentinization and deformation.

In the analyzed rocks, the spinel-group minerals occur with particular textural and microstructural features that can be grouped into three classes: i) spinel-group mineral porphyroclasts with various degree of recrystallization, scattered within partially serpentinized lherzolite and massive serpentinite; ii) spinel-group minerals within pseudomorphic and non-pseudomorphic textures; iii) spinel-group minerals re-oriented along the foliation.

The results highlighted a significant variation in trace metal concentrations in spinel-group minerals during the serpentinization and deformation evolution of the studied ultramafic rocks. In particular, Cr, Ni, and Co concentrations progressively decrease with the serpentinization of the rocks.

At a general scale, the PTEs variability is primarily related to the petrologic and tectonic evolution but, at a local scale, also the mineralogical, lithological, structural, and textural features correlated to the degree of serpentinization and/or deformation significantly influence their distribution and concentration in trace elements.

These variations have also strong environmental implications since some of these trace elements are potential toxic elements which can be released to soil and circulating water during weathering and pedogenic processes. Furthermore, this study should be the preliminary step for the evaluation of background concentrations for naturally occurring contaminants.

References

Abre, P., Cingolani, C., Zimmermann, U., and Cairncross, B. (2009) Detrital chromian spinels from Upper Ordovician deposits in the Precordillera terrane, Argentina: a mafic crust input. *J S AM EARTH SCI.*, 28(4), 407-418. <https://doi.org/10.1016/j.jsames.2009.04.005>

- Ahmed, A.H., Arai, S., Abdel-Aziz, Y.M., Rahimi, A. (2008) Spinel composition as a petrogenetic indicator of the mantle section in the Neoproterozoic Bou Azzer ophiolite, Anti-Atlas, Morocco. *PRECAMBRIAN RES*, 2008, 138(3-4), 225-234. <https://doi.org/10.1016/j.precamres.2005.05.004>
- Ahmed, A., and Arai, S. (2002) Unexpectedly high-PGE chromitite from the deeper mantle section of the northern Oman ophiolite and its tectonic implications. *Contrib Mineral Petrol*, 2002, 143(3), 263-278. <https://doi.org/10.1007/s00410-002-0347-8>
- Arai, S. (1992). Chemistry of chromian spinel in volcanic rocks as a potential guide to magma chemistry. *Mineralogical Magazine*, 56(383), 173-184.
- Auzende A.L., Guillot G., Devouard B., and Baronnet A. (2006) Behaviour of serpentinites in convergent context: microstructural evidences. *Eur J Mineral* 18:21–33.
- Barnes, S.J. (1998). Chromite in komatiites, I. Magmatic controls on crystallization and composition. *Journal of Petrology*, 39(10), 1689-1720.
- Barnes S.J. (2000) Chromite in komatiites, II modification during Greenschist to mid-amphibolite facies metamorphism. *J Petrol* 41:387–409.
- Barnes, S.J., and Roeder, P.L. (2001). The range of spinel compositions in terrestrial mafic and ultramafic rocks. *Journal of petrology*, 42(12), 2279-2302.
- Beckett-Brown, C. E., and McDonald, A. M. (2018). The Crystal-chemistry of Ni-bearing Spinel-group Minerals: Chemical, Geological, and Exploration Implications. *The Canadian Mineralogist*, 56(1), 77-94.
- Bliss, N.W., and MacLean, W.H. (1976). The paragenesis of zoned chromite from central Manitoba. In *Chromium: its Physicochemical Behavior and Petrologic Significance* (pp. 973-990).
- Borghini, G., Rampone, E., Crispini, L., De Ferrari, R., and Godard, M. (2007). Origin and emplacement of ultramafic–mafic intrusions in the Erro-Tobbio mantle peridotite (Ligurian Alps, Italy). *Lithos*, 94(1-4), 210-229.
- Buddington, A.F., and Lindsley, D.H. (1964). Iron-titanium oxide minerals and synthetic equivalents. *Journal of petrology*, 5(2), 310-357.
- Burkhard, D.J. (1993). Accessory chromium spinels: Their coexistence and alteration in serpentinites. *Geochimica et Cosmochimica Acta*, 57(6), 1297-1306.
- Candia, M.A.F., and Gaspar, J.C. (1997). Chromian spinels in metamorphosed ultramafic rocks from Mangabal I and II complexes, Goiás, Brazil. *Mineralogy and Petrology*, 60(1-2), 27-40.
- Cannaò, E., Scambelluri, M., Agostini, S., Tonarini, S., and Godard, M. (2016). Linking serpentinite geochemistry with tectonic evolution at the subduction plate-interface: The Voltri Massif case study (Ligurian Western Alps, Italy). *Geochimica et Cosmochimica Acta*, 190, 115-133.
- Capponi G., Crispini L., Federico L., and Malatesta C. (2016). Geology of the Eastern Ligurian Alps: a review of the tectonic units. *Ital J Geosci* 135:157–169.
- Capponi, G. and Crispini, L. 2008. Note Illustrative della Carta Geologica d'Italia alla scala 1:50.000 Foglio 213 Genova. Firenze: SELCA.
- Capponi, G., and L. Crispini. 2002. Structural and metamorphic signature of alpine tectonics in the Voltri Massif (Ligurian Alps, northwestern Italy). *Eclogae Geologicae Helvetiae* 95:31–32.
- Capponi, G., Crispini, L., Silvestri, R., and Vigo, E. (1999). The role of Early Miocene thrust tectonics in the structural arrangement of the Voltri Group (Ligurian Alps, Italy): evidence from the Bandita area. *Ofioliti*, 24(1a), 13-19.
- Carew, M.J. (2004). Controls on Cu-Au mineralisation and Fe oxide metasomatism in the Eastern Fold Belt, NW Queensland, Australia (Doctoral dissertation, James Cook University).
- Chiesa, S., Cortesogno, L., Forcella F., Galli M., Messiga B., Pasquare G., Pedemonte G.M., Piccardo G.B., and Rossi P.M. (1975). Assetto strutturale ed interpretazione geodinamica del Gruppo di Voltri. *Bollettino Società Geologica Italiana* 94:555–581.
- Christofides G., Thimiatis G., Koroneos A., Sklavounos S.N.S, and Eleftheriadis G. (1994) Mineralogy and chemistry of Cr-chlorites associated with chromites from Vavdos and Vasilika ophiolite complexes (Chalikidiki, Macedonia, N. Greece). *Chemie der Erde* 54:151–166.

- Cimmino, F., Messiga, B., Piccardo, G.B., and Zeda, O., (1979). Titanian clinohumite-bearing assemblage within antigoritic serpentines of the Voltri Massif (Western Liguria): inferences on the geodynamic evolution of Piemontese ultramafic section. *Ophioliti* 4 (2), 97–120.
- Colás, V., González-Jiménez, J.M., Griffin, W.L., Fanlo, I., Gervilla, F., O'Reilly, S.Y., and Proenza, J.A. (2014). Fingerprints of metamorphism in chromite: New insights from minor and trace elements. *Chemical Geology*, 389, 137-152.
- Dare, S.A., Barnes, S.J., and Beaudoin, G. (2012). Variation in trace element content of magnetite crystallized from a fractionating sulfide liquid, Sudbury, Canada: Implications for provenance discrimination. *Geochimica et Cosmochimica Acta*, 88, 27-50.
- Dare, S.A., Barnes, S.J., Beaudoin, G., Méric, J., Boutroy, E., and Potvin-Doucet, C. (2014). Trace elements in magnetite as petrogenetic indicators. *Mineralium Deposita*, 49(7), 785-796.
- Dare, S.A., Pearce, J.A., McDonald, I., and Styles, M.T. (2009). Tectonic discrimination of peridotites using fO_2 -Cr# and Ga-Ti-FeIII systematics in chrome-spinel. *Chemical Geology*, 261(3-4), 199-216.
- Dick, H.J., and Bullen, T. (1984). Chromian spinel as a petrogenetic indicator in abyssal and alpine-type peridotites and spatially associated lavas. *Contributions to mineralogy and petrology*, 86(1), 54-76.
- Diella V., Ferrario A. and Rossetti P., 1994. The magnetite ore deposits of the southern Aosta valley: chromitite transformed during an Alpine metamorphic event. *Ophioliti*, 19 (2a): 247-256.
- Droop, G.T.R. (1987). A general equation for estimating Fe³⁺ concentrations in ferromagnesian silicates and oxides from microprobe analyses, using stoichiometric criteria. *Mineralogical magazine*, 51(361), 431-435.
- Dupuis, C., and Beaudoin, G. (2011). Discriminant diagrams for iron oxide trace element fingerprinting of mineral deposit types. *Mineralium Deposita*, 46(4), 319-335.
- Evans B. and Frost R.B. (1975) Chrome spinel in progressive metamorphism: a preliminary analysis. *Geochim et Cosmochim Acta* 39:959–972.
- Federico L., Crispini L., Malatesta C., Torchio S. and Capponi G. (2015) Geology of the Pontinvrea area (Ligurian Alps, Italy): structural setting of the contact between Montenotte and Voltri units. *Journal of Maps*, 2015 Vol. 11, No. 1, 101 –113, <http://dx.doi.org/10.1080/17445647.2014.945749>.
- Federico, L., Capponi, G., Crispini, L., Scambelluri, M., and Villa, I.M., (2005). ³⁹Ar/⁴⁰Ar dating of high-pressure rocks from the Ligurian Alps: evidence for a continuous subduction–exhumation cycle. *EPSL* 240, 668–680.
- Federico, L., Crispini, L., Scambelluri, M., and Capponi, G. (2007). Different PT paths recorded in a tectonic mélange (Voltri Massif, NW Italy): implications for the exhumation of HP rocks. *Geodinamica Acta*, 20(1-2), 3-19.
- Fontana, E., Panseri, M., and Tartarotti, P. (2008). Oceanic relict textures in the Mount Avic serpentinites, Western Alps. *Ophioliti*, 33(2), 105-118.
- Frost, B.R., and Lindsley, D.H. (1991). Occurrence of iron-titanium oxides in igneous rocks. *Reviews in Mineralogy and geochemistry*, 25(1), 433-468.
- Gargiulo, M.F., Bjerg, E.A., and Mogessie, A. (2013). Spinel group minerals in metamorphosed ultramafic rocks from Río de Las Tunas belt, Central Andes, Argentina. *Geologica Acta: an international earth science journal*, 11(2).
- Garuti G., Proenza J.A., and Zaccarini F. (2007). Distribution and mineralogy of platinum-group elements in altered chromitites of the Campo Formoso layered intrusion (Bahia State, Brazil): Control by magmatic and hydrothermal processes. *Mineralogy and Petrology*, 89, 159-188.
- González-Jiménez, J.M., Griffin, W.L., Proenza, J.A., Gervilla, F., O'Reilly, S.Y., Akbulut, M., and Arai, S. (2014). Chromitites in ophiolites: How, where, when, why? Part II. The crystallization of chromitites. *Lithos*, 189, 140-158.
- Grieco, G., and Merlini, A. (2012). Chromite alteration processes within Vourinos ophiolite. *International Journal of Earth Sciences*, 101(6), 1523-1533.

- Hajialioghli R., Moazzen M., Droop G.T.R., Oberhansli R., Bousquet R., Jhngri A., and Ziemann M. (2007). Serpentine polymorphs and P-T evolution of metaperidotites and serpentinite in the Takab area, NW Iran. *Mineral Mag* 71:203–222.
- Haggerty, S.E. (1991). Oxide mineralogy of the upper mantle. *Reviews in Mineralogy and Geochemistry*, 25(1), 355-416.
- Hermann, J., Muntener, O., and Scambelluri, M., (2000). The importance of serpentinite melonite for subduction and exhumation of oceanic crust. *Tectonophysics* 327, 225–238.
- Hodel, F., Macouin, M., Triantafyllou, A., Carlut, J., Berger, J., Rousse, S., ... and Trindade, R. I. F. (2017). Unusual massive magnetite veins and highly altered Cr-spinels as relics of a Cl-rich acidic hydrothermal event in Neoproterozoic serpentinites (Bou Azzer ophiolite, Anti-Atlas, Morocco). *Precambrian Research*, 300, 151-167.
- Hu, H., Li, J.W., Lentz, D., Ren, Z., Zhao, X.F., Deng, X.D., and Hall, D. (2014). Dissolution – reprecipitation process of magnetite from the Chengchao iron deposit: insights into ore genesis and implication for in-situ chemical analysis of magnetite. *Ore Geology Reviews*, 57, 393-405.
- Huang, X., Qi, L., and Meng, Y. (2014). Trace Element Geochemistry of Magnetite from the Fe (-Cu) Deposits in the Hami Region, Eastern Tianshan Orogenic Belt, NW China. *Acta Geologica Sinica-English Edition*, 88(1), 176-195.
- Huang, X.W., Gao, J.F., Qi, L., Meng, Y.M., Wang, Y.C., and Dai, Z.H. (2016). In-situ LA-ICP-MS trace elements analysis of magnetite: the Fenghuangshan Cu-Fe-Au deposit, Tongling, Eastern China. *Ore Geology Reviews*, 72, 746-759.
- Huang, R., Lin, C.T., Sun, W., Ding, X., Zhan, W., and Zhu, J. (2017). The production of iron oxide during peridotite serpentinitization: Influence of pyroxene. *Geoscience Frontiers*, 8(6), 1311-1321.
- Irvine, T.N. (1967). Chromian spinel as a petrogenetic indicator: Part 2. Petrologic applications. *Canadian Journal of Earth Sciences*, 4(1), 71-103
- Gonzalez-Jiménez, J.M., Kerestedjian, T., Fernández, J.A.P., and Linares, F.G. (2009). Metamorphism on chromite ores from the Dobromirski ultramafic massif, Rhodope mountains (SE Bulgaria). *Geologica Acta*, 7(4), 413-429.
- Kamenetsky, V.S., Crawford, A.J., and Meffre, S. (2001). Factors controlling chemistry of magmatic spinel: an empirical study of associated olivine, Cr-spinel and melt inclusions from primitive rocks. *Journal of Petrology*, 42(4), 655-671.
- Kimball K.L. (1990) Effects of hydrothermal alteration on the composition of chromian spinels. *Contrib Mineral Petrol* 105:337–346.
- Kretz, R. (1983) Symbols of rock-forming minerals. *American Mineralogist*, 68, 277–279
- Li X.-P., Rahn M., and Bucher K. (2004). Serpentinites of the Zermatt-Saas ophiolite complex and their texture evolution: Zermatt serpentinites. *J Metamorph Geol* 22:159–177. doi: 10.1111/j.1525-1314.2004.00503.x.
- Lindsley, D.H. (1991). Experimental studies of oxide minerals. *Reviews in Mineralogy and Geochemistry*, 25(1), 69-106.
- Liou, J.G., Zhang, R., Ernst, W.G., Liu, J., and McLimans, R., (1998). Mineral parageneses in the Piampaludo eclogitic body, Gruppo di Voltri, Western Ligurian Alps. *Schweizer Mineralogische und Petrographische Mitteilungen* 78, 317–335.
- Liu, P.P., Zhou, M.F., Chen, W.T., Gao, J.F., and Huang, X.W. (2015). In-situ LA-ICP-MS trace elemental analyses of magnetite: Fe-Ti-(V) oxide-bearing mafic-ultramafic layered intrusions of the Emeishan Large Igneous Province, SW China. *Ore Geology Reviews*, 65, 853-871.
- Malatesta, C., Crispini, L., Federico, L., Capponi, G., and Scambelluri, M. (2012). The exhumation of high-pressure ophiolites (Voltri Massif, Western Alps): Insights from structural and petrologic data on metagabbro bodies. *Tectonophysics*, 568, 102-123.
- Mellini, M., Rumori, C., and Viti, C. (2005). Hydrothermally reset magmatic spinels in retrograde serpentinites: formation of “ferritchromit” rims and chlorite aureoles. *Contributions to Mineralogy and Petrology*, 149(3), 266-275.
- Mercier J.C., and Nicolas A. (1975) Textures and fabrics of upper-mantle peridotites as illustrated by xenoliths from basalts. *J Petrol* 16:454–487.

- Merlini, A., Tartarotti, P., Grieco, G., Sansone, M., Rizzo, G., and Prosser, G. (2012). Coupled ferritchromite and chromian-chlorite in mantle rocks: a comparison from circum-mediterranean ophiolites. *RENDICONTI DELLA SOCIETÀ GEOLOGICA ITALIANA*, 21(1), 305-307.
- Messiga, B., and Scambelluri, M. (1991). Retrograde P-T-t path for the Voltri Massif eclogites (Ligurian Alps, Italy): Some tectonic implications. *Journal of Metamorphic Geology*, 9(1), 93-109.
- Messiga, B., Piccardo, G.B., and Ernst, W.G., (1983). High pressure Eo-Alpine parageneses developed in magnesian metagabbros, Gruppo di Voltri, Western Liguria, Italy. *Contributions to Mineralogy and Petrology* 83, 1–15.
- Mondal, S.K., Ripley, E.M., Li, C., and Frei, R. (2006). The genesis of Archaean chromitites from the Nuasahi and Sukinda massifs in the Singhbhum Craton, India. *Precambrian Research*, 148(1-2), 45-66.
- Mukherjee, R., Mondal, S.K., Rosing, M.T., and Frei, R. (2010). Compositional variations in the Mesoarchean chromites of the Nuggihalli schist belt, Western Dharwar Craton (India): potential parental melts and implications for tectonic setting. *Contributions to Mineralogy and Petrology*, 160(6), 865-885.
- Müller, B., Axelsson, M.D., and Öhlander, B. (2003). Trace elements in magnetite from Kiruna, northern Sweden, as determined by LA-ICP-MS. *Gff*, 125(1), 1-5.
- Nadoll, P., Mauk, J.L., Leveille, R.A., and Koenig, A.E. (2015). Geochemistry of magnetite from porphyry Cu and skarn deposits in the southwestern United States. *Mineralium Deposita*, 50(4), 493-515.
- O'Neill, H.S.C., and Navrotsky, A. (1984). Cation distributions and thermodynamic properties of binary spinel solid solutions. *American Mineralogist*, 69(7-8), 733-753.
- Pagé, P., and Barnes, S.J. (2009). Using trace elements in chromites to constrain the origin of podiform chromitites in the Thetford Mines ophiolite, Québec, Canada. *Economic Geology*, 104(7), 997-1018.
- Palme, H., and O'Neill, H. (2014). Cosmochemical estimates of mantle composition. In *Treatise on Geochemistry*, 2nd Edition. Elsevier.
- Petrelli, M., Morgavi, D., Vetere, F., and Perugini, D. (2016). Elemental imaging and petro-volcanological applications of an improved laser ablation inductively coupled quadrupole plasma mass spectrometry. *Periodico di Mineralogia*, 85(1), 25-39.
- Piccardo G.B. and Vissers R.L.M. (2007). The pre-oceanic evolution of the Erro-Tobbio peridotite (Voltri Massif, Ligurian Alps, Italy). *Journal of Geodynamics* 43, 417–449.
- Piccardo, G.B., Messiga, B., and Cimmino, F. (1980). Antigoritic serpentinites and rodingites of the Voltri Massif: some petrological evidences for their evolutive history. *Ofioliti*, 5(1), 11-114.
- Piccardo, G.B. (1977). Le ofioliti dell'areale ligure: petrologia ed ambiente geodinamico di formazione: *Rendiconti Società Italiana di Mineralogia e Petrologia*, v. 33.
- Piccardo, G.B. (1984). Le ofioliti metamorfiche del Gruppo di Voltri, Alpi Liguri: caratteri primari ed interpretazione geodinamica. *Mem. Soc. Geol. It*, 28, 95-114.
- Piccardo, G.B., Rampone, E., Romairone, A., Scambelluri, M., Tribuzio, R., and Beretta, C. (2001). Evolution of the Ligurian Tethys: inference from petrology and geochemistry of the Ligurian Ophiolites. *Per. Mineralogy*, 70, 147-192.
- Piccardo, G.B., Zanetti, A., Spagnolo, G., and Poggi, E. (2005). Recent researches on melt-rock interaction in the Lanzo South peridotite. *Ofioliti*, 30(2), 115-124.
- Rampone E., Romairone A., Abouchami W., Piccardo G.B., and Hofmann A.W. (2005) *Chronology, Petrology and Isotope Geochemistry of the Erro–Tobbio Peridotites (Ligurian Alps, Italy): Records of Late Palaeozoic Lithospheric Extension. Journal Of Petrology Volume 46 Number 4 April 2005.*
- Rollinson, H. (2008). The geochemistry of mantle chromitites from the northern part of the Oman ophiolite: inferred parental melt compositions. *Contributions to Mineralogy and Petrology*, 156(3), 273-288.
- Rusk, B., Oliver, N., Cleverley, J., Blenkinsop, T., Zhang, D., Williams, P., and Habermann, P. (2010). Physical and chemical characteristics of the Ernest Henry iron oxide copper gold deposit, Australia; implications for IOGC genesis. *PGC Publishing*.

- Sack, R.O., and Ghiorso, M.S. (1991). Chromian spinels as petrogenetic indicators; thermodynamics and petrological applications. *American Mineralogist*, 76(5-6), 827-847.
- Scambelluri, M., Hoogerduijn Strating, E.H., Piccardo, G.B., Vissers, R.L.M., Rampone, E. (1991). Alpine olivine- and titanian clinohumite-bearing assemblages in the Erro–Tobbio peridotite (Voltri Massif, NW Italy). *Journal of Metamorphic Geology* 9, 79–91.
- Scambelluri, M., Müntener, O., Hermann, J., Piccardo, G.B., and Trommsdorff, V. (1995). Subduction of water into the mantle: history of an Alpine peridotite. *Geology*, 23(5), 459-462.
- Scarsi, M., Malatesta, C., and Fornasaro, S. (2018). Lawsonite-bearing eclogite from a tectonic mélange in the Ligurian Alps: new constraints for the subduction plate-interface evolution. *Geological Magazine* 155 (2), 280-297.
- Shen P., Hwang S., Chu H., and Jeng R. (1988). STEM study of “ferritchromit” from the Heng-Chun chromitite. *American Mineralogist*, 73, 383-388.
- Singoyi, B., Danyushevsky, L., Davidson, G.J., Large, R., and Zaw, K. (2006). Determination of trace elements in magnetites from hydrothermal deposits using the LA ICP-MS technique. In *Oral and Poster Presentations from the SEG 2006 Conference Society of Economic Geologists*, Keystone, USA (pp. 367-368).
- Stevens, R.E. (1944). Composition of some chromites of the western hemisphere. *American Mineralogist: Journal of Earth and Planetary Materials*, 29(1-2), 1-34.
- Stowe, C.W. (1994). Compositions and tectonic settings of chromite deposits through time. *Economic Geology*, 89(3), 528-546.
- Strating, E.H.H., 1991. The evolution of the Piemonte–Ligurian Ocean. A structural study of ophiolite complexes in Liguria (NW Italy). *Geology Ultraiectina* 74 145 p.
- Teixeira, R.J., Neiva, A.M., and Gomes, M.E. (2012). Chromian spinels and magnetite of serpentinites, steatitic rocks, tremolite asbestos and chloritites from Bragança massif, northeastern Portugal. *Periodico di Mineralogia*, 81(2).
- Toplis, M.J., and Carroll, M.R. (1995). An experimental study of the influence of oxygen fugacity on Fe-Ti oxide stability, phase relations, and mineral–melt equilibria in ferro-basaltic systems. *Journal of Petrology*, 36(5), 1137-1170.
- Ulmer G.C. (1974) Alteration of chromite during serpentinization in the Pennsylvania-Maryland district. *American Mineralogist*, 59, 1236-1241.
- Vanossi, M., Cortesogno, L., Galbiati, B., Messiga, B., Piccardo, G., and Vannucci, R., (1984). *Geologia delle Alpi Liguri: dati, problemi, ipotesi*. Mem. Soc. Geol. It. 28, 5–75.
- Vignaroli, G., Rossetti, F., Rubatto, D., Theye, T., Lisker, F., and Phillips, D. (2010). Pressure-temperature-deformation-time (P-T-d-t) exhumation history of the Voltri Massif HP complex, Ligurian Alps, Italy. *Tectonics*, 29(6).
- Zhou, M.F., and Robinson, P.T. (1997). Origin and tectonic environment of podiform chromite deposits. *Economic Geology*, 92(2), 259-262.
- Zussman, J., Howie, R.A., and Deer, W.A. (1992). *An introduction to the rock forming minerals*. Longman Group Ltd, New York, p 698
- Defant MJ, Drummond MS (1990) Derivation of some modern arc magmas by melting of young subducted lithosphere. *Nature*, 347, 662-665
- Della.

Section Three

Investigations on the ultramafic soil profiles

The ultramafic soils of the study area are poorly developed and occur in sites without significant allochthonous inputs as well as where contamination from anthropogenic sources is very unlikely. These are the ideal conditions to correlate the soil mineralogy and chemistry to the primary fingerprint of the bedrock and test a multidisciplinary approach that might be useful in establishing the natural background for PTEs.

In this section, the mineralogical, crystallochemical, and chemical variations occurring in ultramafic soil profiles during weathering processes under temperate climatic condition are defined in order to understand the role of the primary and authigenic mineral phases on the mobility of PTEs (particularly Cr, Ni, and Co). The chapter reports: i) a general characterization of soils properties; ii) the chemical and mineralogical compositions and their variation along the soil profiles; iii) the characterization of PTEs-bearing minerals by distinguishing between primary- (e.g., serpentine minerals, spinel-group minerals, and magmatic relicts) and authigenic-minerals (e.g., clay minerals and Fe- and Mn-oxides).

The collected data are also discussed and compared with a database realized for this work by collecting bibliographic data related to the ultramafic soils occurring in the ophiolitic complexes worldwide (see *Appendix B*), in order to assess the PTEs levels in studied soils with respect to the world average soil composition. Moreover, an environmental evaluation based on the threshold limits lead down by international and national agencies is reported.

Source and distribution of potentially toxic elements in ultramafic soil profiles from the Voltri Massif (NW Italy)

Keywords: clay minerals, Fe-oxyhydroxides, authigenic minerals, lherzolites, serpentinite, PTEs mobility, weathering, serpentine soil, trace elements

6.1. INTRODUCTION

Natural weathering of ultramafic rocks may cause several environmental issues associated to the natural release of either asbestos fibers and potentially toxic elements (PTEs) into soil, groundwater, and air (Bales et al., 1985; Schreier et al., 1987; Schreier, 1989; Roberts and Proctor, 1991; Shtiza et al., 2005; Oze et al., 2007; Alexander, 2007; Dublet et al., 2012; Holmes et al., 2012; Ratiè et al., 2013).

Concerning PTEs, the distribution and mineral speciation strongly depend on the mineralogy of the bedrock (Garnier et al., 2006, 2009; Raous et al., 2013), as well as on climatic conditions (e.g., Angelone et al., 1993; Amir and Pineau, 2003; Massoura et al., 2006), on the position in the toposequence (Cheng et al., 2011), granulometry (Tashakor et al., 2015), thermodynamic conditions of the soils (Antic-Mladenovic et al., 2011), and on soil characteristics such as pH, Eh, organic matter, and clay content (Baker and Walker, 1989; Nyamangara and Mzezewa, 1999). However, the degree of serpentinization is known to be a major discriminant factor in ultramafic pedogenesis (Alexander, 2004, 2009; Oze et al., 2004a; Kierczak et al., 2016; Echevarria, 2018; Pędziwiatr et al., 2018) as well as lithological, textural, and structural characteristics of the bedrock have an important role in the distribution and mobility of PTEs (Alexander, 2004; Alexander and DuShey, 2011; Caillaud et al., 2006, 2009; Lessovaia et al., 2014a,b; Baumeister et al., 2015; Kierczak et al., 2007, 2008, 2016; Pędziwiatr et al., 2017; Van der Ent et al., 2018; Echevarria, 2018).

6.1.1. Authigenic phases in the ultramafic soils

The PTEs mobility and distribution during weathering of ultramafic bedrocks is controlled either by the alteration of primary minerals and by the formation of authigenic phases (clay minerals and oxyhydroxides), that can represent both a source or a trap for PTEs. The weathering of ultramafic rocks leads to the formation of different authigenic minerals (mainly clay minerals and oxyhydroxides; Lee et al., 2003, 2004), which are dependent, in particular, on the nature of the bedrock and on the climate condition (e.g., Ducloux et al., 1976; Gasser et al., 1995; Velde, 1995; Caillaud et al., 2004, 2006, 2009; Hseu et al., 2007; Nguyen-Thanh et al., 2017).

The oxidation and hydrolysis of the primary minerals lead to the formation of Fe- and Mn-oxides *s.l.* which are extremely poorly soluble and very stable in supergenic condition (Schwertmann and Taylor, 1989; Manceau et al., 2000; Quantin et al., 2002; Becquer et al., 2003; Fander et al., 2009; Ho et al., 2013). Fe-oxides *s.l.* are originated from the oxidation of Fe²⁺-bearing minerals (spinel, olivine, pyroxene and amphibole).

Fe-oxides *s.l.* include Fe-oxides *s.s.* (such as hematite) and Fe-oxyhydroxides (such as goethite, ferrihydrite and lepidocrocite) and generally occur as microcrystalline-, nanocrystalline- and/or amorphous phases (Schwertmann and Taylor, 1989; Manceau et al., 2000).

Hematite (α -Fe₂O₃) has the corundum structure (α -Al₂O₃) which is based on hexagonal close packing of anions. It is extremely stable under ambient conditions and is often the end member of transformation of other Fe-oxides (Cornell and Schwertmann, 2003). Hematite is favored in soils with poor drainage condition, with a low organic matter, and is more common in tropical climates (Alloway, 2010).

Goethite (α -FeOOH) has the diasporite structure (α -AlOOH) which is based on hexagonal close packing of anions. It is thermodynamically the most stable Fe-oxyhydroxide at ambient temperature and is either the first oxide to form or the end member of several transformation (Cornell and Schwertmann, 2003). Commonly, it occurs mainly in temperate soils with good drainage conditions where it is commonly found in intragranular porosity (Vepraskas and Guertel, 1992; Vepraskas et al., 1995; Quantin et al., 2002).

Lepidocrocite (γ -FeOOH) has a boehmite structure (γ -AlOOH) which is based on cubic close packing of anions (Cornell and Schwertmann, 2003). It is common in soils affected by poor drainage, commonly under humid temperate regions. Acidic pH and low temperature are favorable conditions for its formation (Kabata-Pendias, 2011).

Ferrihydrite ($\text{Fe}_2\text{O}_3 \cdot n\text{H}_2\text{O}$) consists of hexagonal close packing of anions and is a mixture of defect-free and defective structural units (Cornell and Schwertmann, 2003). Despite it is weakly stable and poorly crystalline it is relatively widespread in natural environments. Ferrihydrite can play an important role as an active sorbent owing to its very high surface area (Cornell and Schwertmann, 2003; Alloway, 2010). Unlike the other Fe-oxides it exists exclusively as nano-crystals and unless stabilized in some way, transforms with time into the more stable Fe-oxide, mainly hematite (in warm regions) and goethite (in humid temperate zones; Kabata-Pendias, 2011).

A characteristic feature of the Fe-oxides is the variety of the possible interconversion between the different phases. These interconversions can be due to several type of transformation (e.g., thermal and hydrothermal transformations, mechanical dehydroxylation, dissolution and reprecipitation, reduction/oxidation). Goethite, ferrihydrite, and lepidocrocite can transform hematite by thermal, hydrothermal, or mechanical dehydroxylation. Lepidocrocite and ferrihydrite can transform into goethite by reprecipitation. Hematite can transform into magnetite in reducing conditions.

In general, Fe-oxides can host several metals into the structure via isochemical substitution for Fe^{3+} by other cations. Trivalent cations (e.g., Cr, Al, Ga, and Sc) are the most suitable species that isomorphically replace Fe^{3+} , but also some bivalent (e.g., Co, Mn^{2+} , Zn, Ni, and Pb) and tetravalent cations (e.g., Mn^{4+}) can enter the Fe-oxide structure (Burns and Burns, 1977; Kuhnelt et al., 1975). Moreover, Fe-oxides s.s. are important sink for PTEs (e.g., As, Co, Cu, Ni, Cr, V, and Zn; McKenzie, 1989; Singh and Gilkes, 1992) which can be scavenged from the solution through sorption and/or coprecipitation processes, thus playing an important role in controlling their bioavailability (Francis and Dodge 1990; Quantin et al., 2002; Hooda, 2010; Kabata-Pendias, 2011).

Regarding the Mn-oxides *s.l.*, they are generally amorphous, but crystalline forms, such as pyrolusite and birnessite, can be commonly present (Kim et al., 2002). In the soil, most of the Mn-oxide and -oxyhydroxide quickly precipitates

from solutions in oxidizing conditions. The ability of Mn-oxides to sorb preferentially PTEs (mainly Co and Ni) and to act as oxidants means that they play significant roles in soils. In the Mn-oxides *s.l.*, the most important isomorphic substitution occurs between Mn^{2+} and Co^{2+} and for this reason the soil with high concentrations of Co are often associated with the presence of the Mn-oxides and oxyhydroxides (Gerth, 2005). Sometimes though their role as oxidants of As and Cr may be deemed good (oxidation of As^{3+} to As^{5+}) or bad (oxidation of Cr^{3+} to Cr^{6+}) (Quantin et al., 2002; Oze et al., 2007; Alloway, 2010; Rajapaksha et al., 2013).

The clay formation in ultramafic soils are often complex and are mainly determined by the climate and the degree of serpentinization of the bedrock, as well as other factor including depth, age, drainage, and topographic position (Kirkman, 1975).

Typically clay minerals species in ultramafic soils are those mainly derived from the leaching of Mg and Si from the olivine, pyroxenes and subordinately serpentines (Cortesogno et al. 1979; Lee et al., 2003; Caillaud et al., 2006, 2004) and are commonly smectites and vermiculite (Rabenhorst et al., 1982; Alexander, 1988; Bulmer and Lavkulich, 1992; Lee et al., 2001, 2004; Bani et al., 2015). Despite the low concentration of Al in the bedrocks, the neof ormation of Al-rich clay minerals (such as illite) is not unusual (Cortesogno et al., 1979; Chardot et al., 2007; Bani et al., 2014).

A large number of clay minerals are observed in literature. Clay minerals reported in serpentine soils *s.s.* of Cornwall (England) forming under a cool, humid, temperate climate, include chlorite (70%), illite (15%), and small amounts of montmorillonite, kaolinite, and talc (Butler, 1953). On the other hand, serpentine soils *s.s.*, forming under similar conditions, contained chlorite and montmorillonite (Veniale and Van der Marel, 1963; Northern Apennine – Italy). In serpentine soils *s.s.* occurring in Albania under temperate climates the dominant clay mineral is nontronite (Bogatyrev, 1958). Nontronite also dominates similar soils occurring in California (Wildman et al. 1968). According to de Kimpe and Zizka (1973) the clay mineralogy of peridotite soils (mainly dunite) of Quebec province are composed by interstratified minerals of vermiculite, montmorillonite, and chlorite. Ultramafic soils, widely distributed throughout New Zealand, may contain montmorillonite, vermiculite, mica, kaolinite, or gibbsite (Swindale, 1966).

The type or the clay minerals and the thickness of soil profiles also depended on the drainage soil conditions (Bonifacio et al., 1997; Ducloux et al., 1976; Istok and Harward, 1982). The well-drained soils are characterized by a poorly developed C horizon and consisted mainly of 7 Å clay minerals including serpentinite and chlorite (Istok and Harward, 1982) or normal to low charged vermiculite (Bonifacio et al., 1997). Otherwise, in poorly drained soils characterized by a saprock and a well-developed saprolite (Caillaud et al., 2004), other clay minerals, such as beidellite (Berre et al., 1974), nontronite, chlorite, chlorite-vermiculite interstratifications (Ducloux et al., 1976), or low-charged smectite (Bonifacio et al., 1997), could be formed.

Because of their complex crystal structure, clay minerals may incorporate a large number of elements of different ionic sizes and charges by a variety of isomorphic substitutions (Bergaya and Lagaly, 2006). These substitutions may occur in tetrahedral and octahedral sites or in the interlayer sheet. Regarding PTEs in clay minerals, they can host in octahedral site (e.g. Cr) or, more likely, in interlayer sheet by sorption (Kabata-Pendias, 2011). Adsorption and desorption of PTEs onto clay minerals are one of the most important processes that can determine the bioavailability and ecotoxicological effects of the elements in the environment (Shirvani et al., 2006; Abollino et al., 2008). As an example, Cr is mainly incorporated into smectite (after mesh-texture serpentine) and vermiculite (after chlorite; Caillaud et al., 2006). Van der Ent (2018) reports high concentration of Ni in smectite under temperate condition. Abollino et al. (2008) notes that vermiculite and smectite (mainly montmorillonite) can absorb significant amount of Cd^{2+} , Pb^{2+} , Zn^{2+} , Mn^{2+} , Cu^{2+} , and Zn^{2+} .

6.1.2. Aims of study

Due to the potential toxicity of Ni and Cr in soils and to their economic significance in lateritic paleosols (Golightly and Arancibia, 1979; Becquer et al., 2006; Wells et al., 2009), most studies about weathering of ultramafic rocks and relative soils have already been performed in different ophiolitic complex, focusing on climatic and pedogenetic factors (Oze et al., 2007; Schwertmann and Latham, 1986; Ulven et al., 2017). Furthermore, numerous authors present the detailed studies of PTEs mobility and their relationships between mineralogy and other soil properties (e.g., Vithanage et al., 2014; Alves et al., 2011; Caillaud et al., 2009). Nevertheless, only few studies (Burgess et al., 2009; Lessovaia et al., 2016a,b;

Kierzack et al., 2016; Pędziwiatr et al., 2017) have provided detailed information about the PTEs content and the influence of rock texture and microstructure on PTEs geochemistry and authigenic mineral formation in the ultramafic soils.

The general aim of this chapter is, therefore, to characterize soil profiles developed from various ultramafic bedrocks in the Voltri Massif (VM) from the physical, chemical, mineralogical, and micromorphological point of view and to correlate their properties with bedrock characterized by different serpentinization degree and the deformation style and intensity (see *Chapter IV*). Moreover, an environmental evaluation based on the threshold limits lead down by international and national agencies and other environmental indexes is reported.

The specific aim of this chapter is to define the mineralogical variations occurring in ultramafic soil profile during weathering processes under the temperate climatic condition in order to understand the role of the primary and authigenic mineral phases on the mobility of PTEs (particularly Cr, Ni, and Co). In particular, the study is focused on the mineralogical and mineralo-chemical variation along the soil profile (bedrock → subsoil → topsoil) according to i) soil granulometry (sand → silt → clay) and ii) different degree of serpentinization of the bedrock (PSP, MS, and FS – *Chapter IV*).

6.2. MATERIAL AND METHODS

6.2.1. Sampling strategy

Soil profiles come from eight sites located within the VM and developed on a variety of ultramafic rocks, from partially serpentinized lherzolites (PSP), through massive serpentinites (MS), and foliated serpentinites (FS). These sites were chosen because of spatially isolated from urban centers as well as any factory. The soil profiles chosen for this study were located in the stable upper parts of quarries or road cuts far from potential input of allochthonous debris materials by runoff or landslides. For each site, 1 to 4 soil profiles have been selected depending on lithological and structural variability and have been sampled by collecting the topsoil, the subsoil and the bedrock.

Soil samples were collected with steel auger and shovel, from two soil layers: 1) the *topsoil* (0-30 cm), excluding the rhizosphere, and 2) the *subsoil* (30-60 cm) following the criteria of Darnley (1997), Salminen et al. (1998), and GEMAS project (Albanese et al., 2015). For each sampling point approximately one kg of

soil was taken, after removing the granulometric fraction > 2 cm fraction as required by current legislation (D.M. 471/1999, abrogated and now replaced by D.Lgs 152/2006).

Rock samples were collected at the base of soil profile, from two different zone: weathered rock (saprolite) at the direct contact to subsoil and unweathered rock. The complete description of each profiles and samples are reported in *Appendix A*.

6.2.2. Analytical techniques

Soil color and other properties including grain-size, grain-morphology, texture, structure, and consistence were determined either in situ and in laboratory and used to distinguish and identify soil horizons as well as to group soils according to the soil classification system (FAO-WRB classification; IUSS, 2015). The color of the all soil samples was determined using the Munsell® Soil Color Charts (2000). The particle size distribution of all soil samples was obtained by wet sieving and granulometric classification was obtain according to Folk classification (Folk, 1954).

Micromorphological analyses for qualitative weathering evaluation (Delvigne, 1998; Stoops et al., 2011) as well as mineralogical and petrographic determination of rock and soil samples were carried out using polarized-light optical microscopy (PLOM) and scanning electronic microscopy and microanalysis (SEM-EDS).

Mineralogical and crystallographic analyses were performed by means of synchrotron radiation X-ray powder diffraction with Rietveld refinement on the three different granulometric fraction (sand fraction: 2 mm – 63 µm; silt fraction: 63 µm – 4 µm, and clay fraction: <4 µm).

Minero-chemical analyses by means of i) electron microprobe with wavelength dispersive spectrometers (EMPA-WDS; major and minor elements) and ii) laser ablation-inductively coupled plasma-mass spectrometry (LA-ICP-MS; trace and ultra-trace elements), were performed on the skeleton of the sand fraction.

The bulk chemistry of soil and rock samples (major, minor, and trace elements) were determined by means of EDXRF and ICP-AES.

6.3. RESULT

6.3.1. The early stage of weathering in ultramafic bedrocks

The soil profiles selected for this study developed on ultramafic bedrocks characterized by different degree of serpentinization, i.e. partially serpentinized lherzolites, massive serpentinites, and foliated serpentinites (PSP, MS, and FS, as defined and described in *Section II, Chapter IV*).

All these bedrocks are variably weathered close to the contact with the subsoil (C horizon); the thickness of the weathered zone vary from 2 cm to 15 cm depending mainly on the bedrock type (i.e., PSP, MS, and FS). In particular, the difference in weathering intensity is much higher in PSP than in the most serpentinized rocks (both MS and FS).

PSP bedrocks are typically capped by weathering rinds of variable thickness (0.5 cm – 3 cm; Fig. 6.1A). These weathered surfaces are reddish brown to orange and has a few millimetric knobby relief with unaltered or weakly altered pyroxene highs and strongly weathered olivine lows. Spinel-group minerals generally appear unaltered without any evidence of weathering reactions.

The weathering rind is separated from the unweathered rock by irregularly undulated interface. Only in the more weathered sample, oxidation halos are also developed, with reddish-orange fronts extending into the unaltered rock, along microfractures, grain boundary, and other intergrain porosity.

FS bedrocks are moderately to weakly altered (Fig. 6.1B). Millimetric to centimetric oxidation halos developed from fractures and joints or along foliation planes. In these structural sites the rock color varies from greenish-grey to ochreous-reddish.

MS bedrocks are generally weakly altered showing evidence of alteration only along fracture from which centimetric oxidation layers commonly developed (Fig. 6.1C). Generally, the rock-surface is fresh with dark green to olive green colors; local yellowish-brown oxidation patches form around oxidized magnetite aggregates.

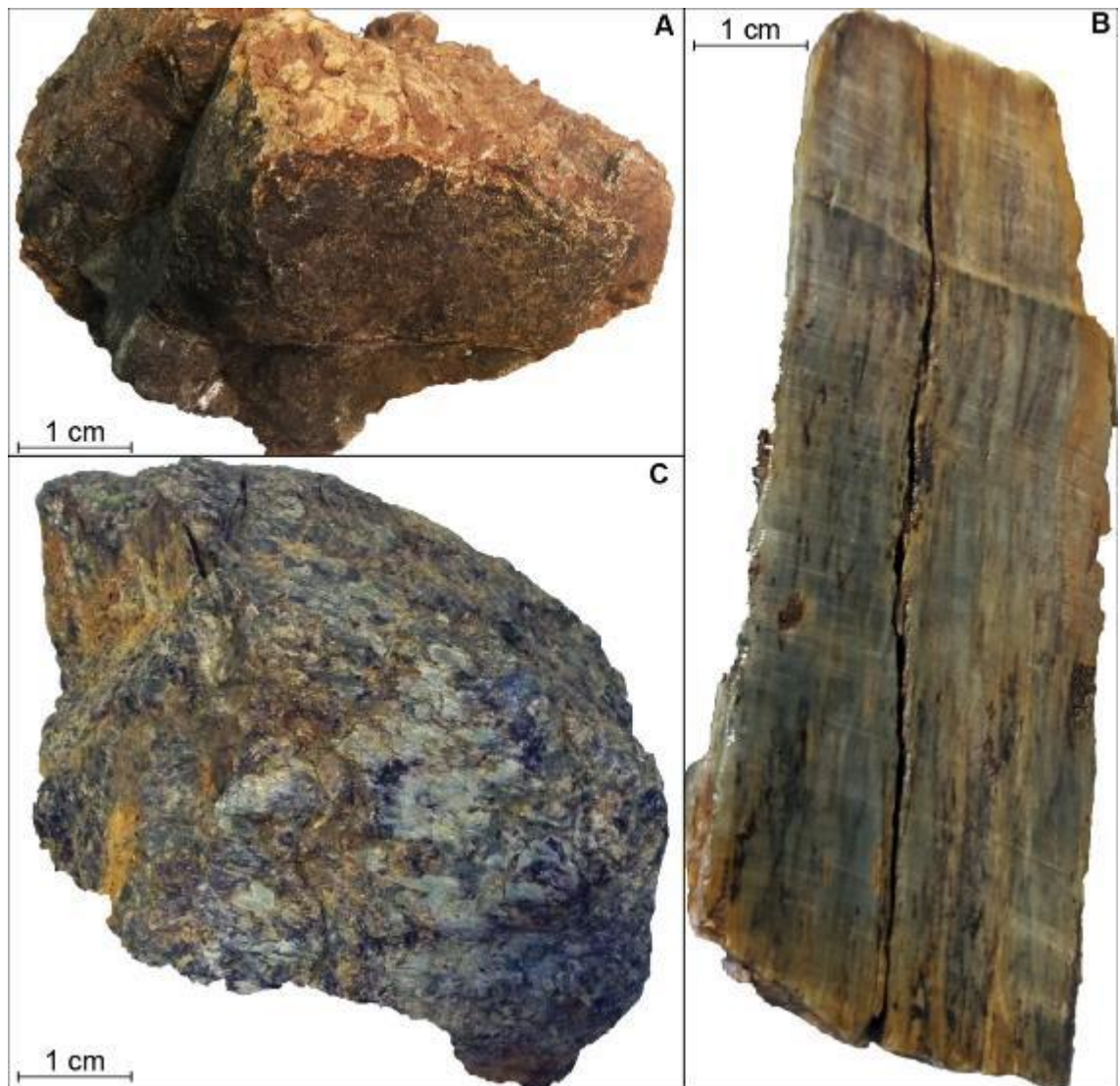


Fig. 6.1 Weathering bedrock at the macroscale: A) Sample of partially serpentinized Iherzolites from VM, showing weathering crust ranging from 1 to 10 mm in thickness. The thickness of the brown rind is visibly influenced by small fractures providing enhanced permeability. Particularly prominent are occasional large (>2 mm) grains of pyroxene in the weathered brown surface; B) Sample of massive serpentinites from VM. Alteration is not uniform and visible on the surface and along fractures; C) Sample of foliated serpentinites from MV. Weathering starts on the sample surface and affected the sample core through the foliation plane.

In PSP the primary rock textures (e.g., pseudomorphic texture after olivines and pyroxenes) are preserved even if the primary minerals are partial to totally replaced by authigenic products (*alteromorphosis*; Delvigne, 1998).

Olivine typically underwent iddingsitization which produces a complex pattern of alteration starting from crystal edges and intracrystalline fractures. Iddingsite is a red/brown mixture of poorly crystalline minerals (mainly clay minerals and Fe-oxides s.s.) that typically forms in oxidizing conditions (Fig. 6.2A). Even in the more altered olivine pseudomorphs, the magnetite trails within the mesh-texture rims, remained unaltered.

The weathering of pyroxene develops mainly from crystal edges, cleavage planes or intracrystalline fractures (Fig. 6.2B and C). The alteration products are mainly represented by brownish-orange iddingsitic mixtures and subordinately smectitic clays.

Spinel-group mineral, with the exception of magnetite are generally unaltered. Magnetite is commonly oxidized in particular when it occurs as microcrystals in trails and aggregates. Magnetite grains are variably martitized to hematite with increasing intensity towards the crystal edge. Magnetite oxidation typically produces intense pigmentation of the serpentine matrix in FS and subordinately MS (Fig. 6.2D).

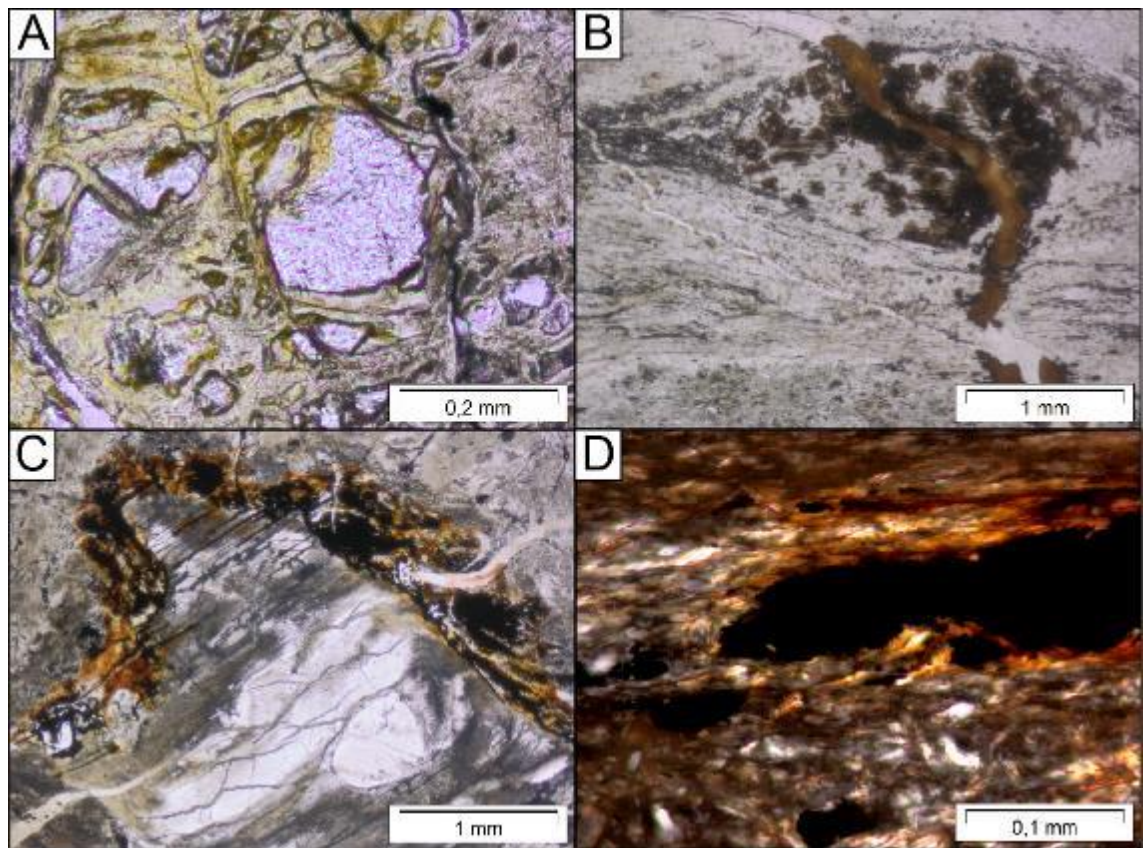


Fig. 6.2 Weathering of bedrock at the microscale: A) a complex pattern of alteration of a crystal of olivine, which at first is replaced by yellow-colored iddingsite along its periphery and along the original fractures (cross-polarized light image - XPL); B) inter-crystalline micro-crack filled by a mixture of clay minerals and oxyhydroxide, cut pyroxene minerals in massive serpentinites. Alteration developed also through cleavage plane (plane-polarized light image - PPL); C) pyroxene relicts surrounded by a regular rim of secondary magnetite (PPL); D) magnetite grain partially replaced by oxyhydroxides and weathered antigorite with iron stains in massive serpentinites (XPL).

6.3.2. Soil profile characteristics

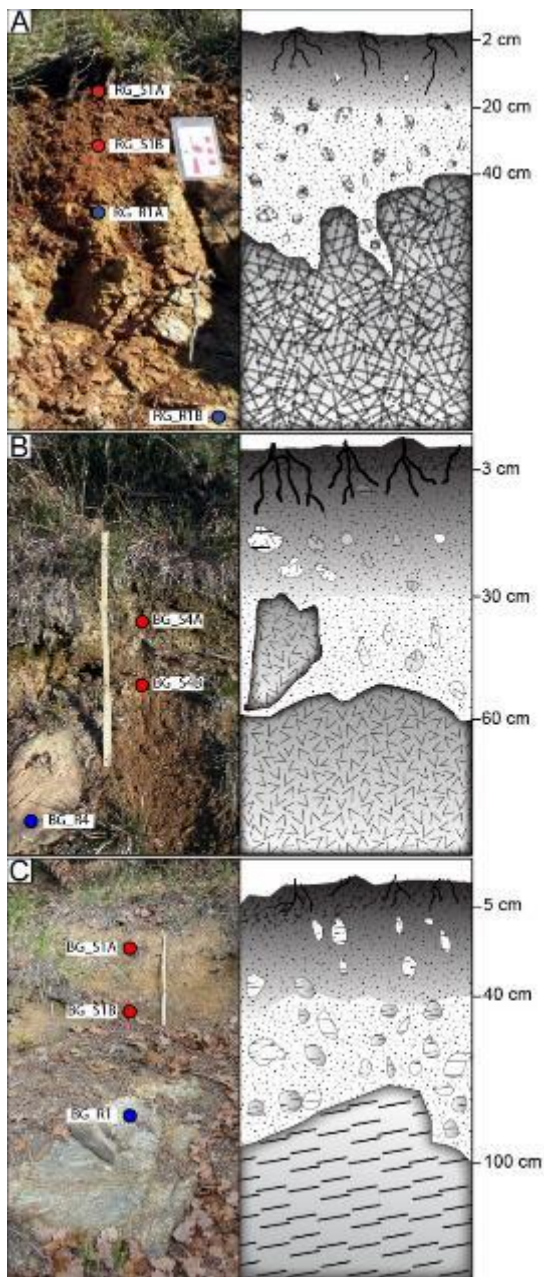


Fig. 6.3 Photograph and schematic sketch of soil profiles developed on: a) PSP; b) MS; c) FS. The red and the blue circles represent the position of the soil and bedrock samples, respectively.

In general, soil profiles, vary in thickness from 35 to 80 cm and are characterized by weakly developed A and C horizons and a very thin O horizon (up to 5-10 cm) (Fig. 6.3).

Soils developed on serpentinite bedrocks (MS and FS) have been classifiable as *Magnesian Leptic Skeletic Cambisols*, whereas those developed on peridotites as *Chromic Magnesian Leptic Skeletic Cambisols* (FAO-WRB classification; IUSS, 2015).

All the soils display heterogeneous granulometry, ranging from gravelly mud, muddy gravel, to sandy muddy gravel (Fig. 6.4; Folk, 1954) with no clear relationships to the different bedrock types. The granulometric curve has a uniform and homogeneous distribution in all the soils.

The soil is constituted for approximately 29% of organic matter, mostly concentrated in the first centimeters (1-5 cm). The highest content (up to 38 %) was always found in FS soil.

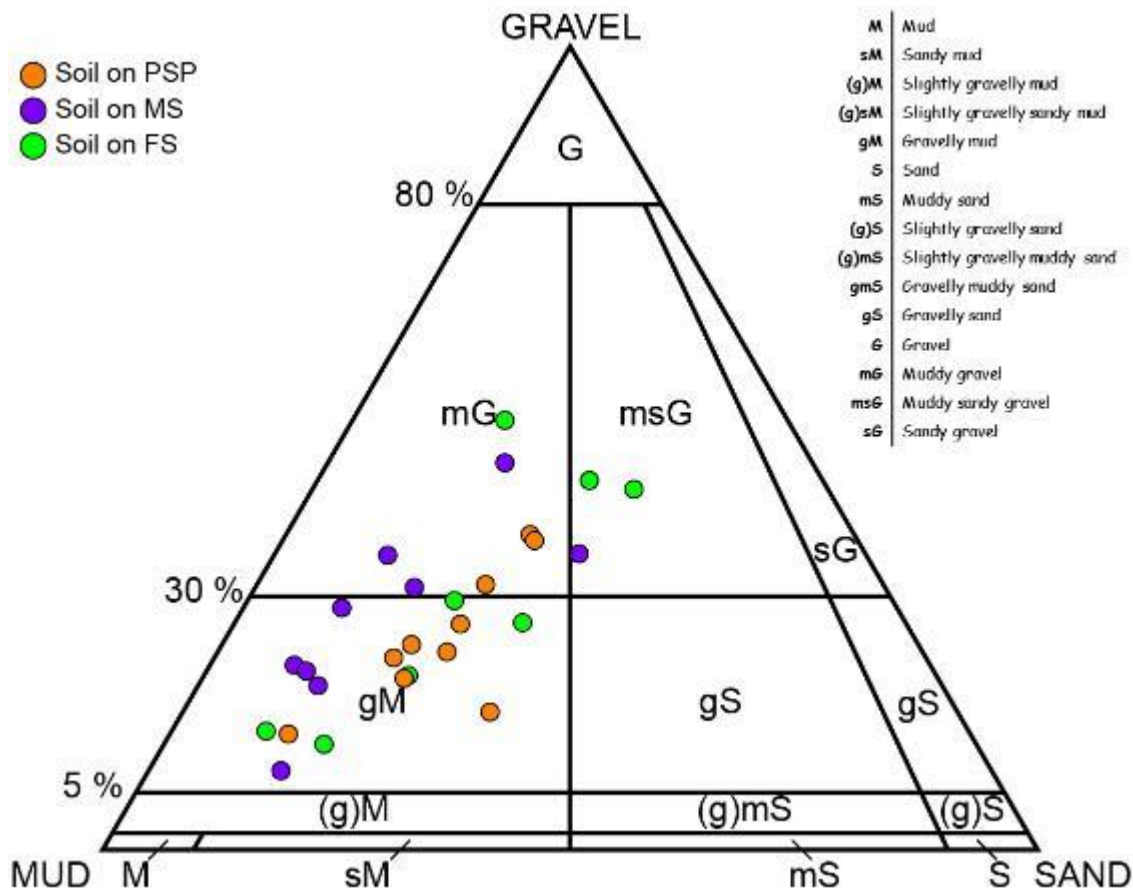


Fig. 6.4 Particle size distribution of studied soil, according to Folk classification (Folk, 1952).

Conversely, soil color is strongly influenced by the bedrock nature (Fig. 6.5). PSP soils vary in color from "strong brown" (Munsell 7.5 YR 4/6) to "reddish brown" (10 YR 5/4). FS soils cover the widest range of the color varying from "light grey" (5 Y 7/2) to "brown" (7.5 YR 4/6), MS soil ranges in color from "yellowish brown" (10 YR 5/4) to dark brown (10 YR 3/3). These variations are strictly related to the weathering intensity and in particular to the abundance of iron oxides, as described in the following chapters.

Rock		● PSP								
Munsell Color		7.5 YR 4/6			2.5 Y 3/4		2.5 Y 5/4		2.5 Y 5/4	
Cie	L*	42.3	42.3	42.3	40.6	40.6	40.6	31.3	31.3	
	a*	18.6	18.6	18.6	6.7	6.7	6.7	6.5	6.5	
	b*	33.2	33.2	33.2	29.1	29.1	29.1	29.2	29.2	

Rock		● MS								
Munsell Color		10 YR 4/3		10 YR 3/3		10 YR 4/4		10 YR 5/4		7.5 YR 5/4
Cie	L*	41	41	30.5	31.7	41.7	51.2	51.2	51.6	
	a*	5	5	5.6	10.1	10.5	10.6	10.6	9.1	
	b*	13.3	13.3	12.9	24.4	27.2	25.1	25.1	22.6	

Rock		● FS								
Munsell Color		Gley1 5/5GY	Gley1 6/5GY	5 Y 7/2	2.5 Y 6/3	10 YR 6/4	2.5 Y 6/4	7.5 YR 4/6	10 YR 4/6	
Cie	L*	42	56	72.1	62	63.1	61.7	41.2	41.5	
	a*	-9	-6.2	0.2	8.5	9.3	1.5	13.9	14.1	
	b*	3.3	5.7	15.8	9.4	26.4	27.5	34.4	39.5	

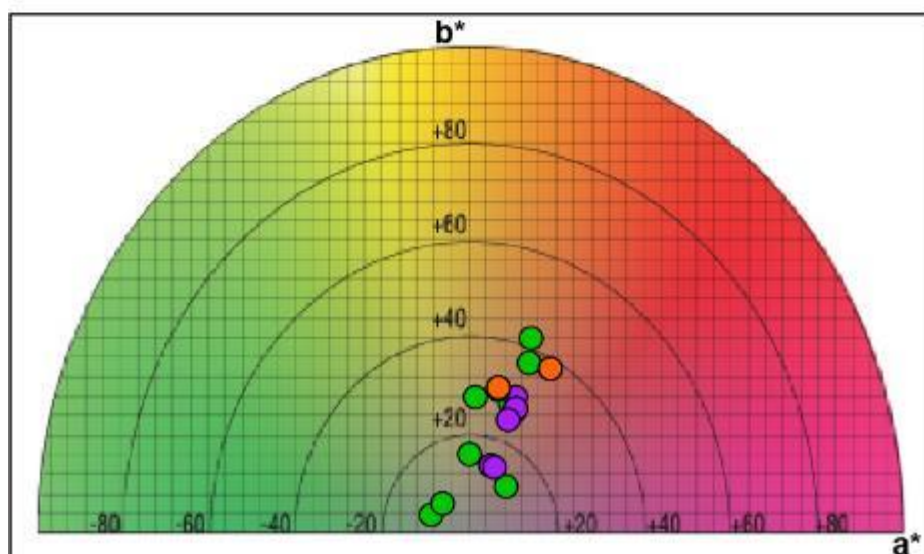


Fig. 6.5 Colorimetric properties (CIE L-a*b* classification and Munsell color soil chart).

6.3.3. Soil Micromorphology

Micromorphological analyses are a useful tool to evaluate the weathering intensity basing on the alteration patterns developed on the soil skeleton. These analyses have been performed following the criteria and the nomenclature proposed by Delvigne (1998).

The soil skeleton is heterogeneous in every studied profile. It is composed by polycrystalline aggregates of: i) unweathered to slightly weathered primary mineral inherited from bedrock (*lithorelics or alterorelics*); ii) weathering products (*alteromorphs, nodules, or iron crusts*); iii) allochthonous clasts (mainly quartz).

Lithorelics (Fig. 6.6A) are generally slightly weathered or unweathered clasts with well preserve bedrock mineralogy, microstructure (e.g., micro-folds, veins, cleavages), and microtexture (e.g., pseudomorphic and non-pseudomorphic texture). In all the studied soils, they represent about of 50 vol.% of the soil skeleton in subsoil and the 40 vol.% in topsoil.

The mineralogical composition of the lithorelics varies slightly from soil profile on PSP to those on MS and FS. In PSP they are mainly composed by antigorite, chrysotile, olivine, pyroxene, magnetite, and Cr-magnetite (in order of decreasing abundance). In MS and FS serpentine minerals (antigorite and chrysotile), chlorite and magnetite significantly increase, olivine is absent, and pyroxenes are scarce. Spinel-group minerals, other than magnetite, decrease from MS toward FS soils, where also ilmenite is present in non-negligible amounts. The lithorelic clasts containing oxides (spinel and ilmenite) are widespread in all the soil profile with a slight increase in concentration with depth.

Alterorelics (Fig. 6.6B) are highly weathered clasts that preserve bedrock microstructure and texture, but the primary minerals are partially to completely replaced by secondary authigenic products. They represent about 10 % of the soil skeleton in subsoil and the 5% in topsoil.

Alterorelics develops mainly on magnetite-rich clasts and, the alteration starts from magnetite edges or intracrystalline fractures producing yellowish-brown to reddish-orange oxidation patches. In the more altered clasts magnetite oxidation typically determines intense pigmentation of the serpentinite matrix.

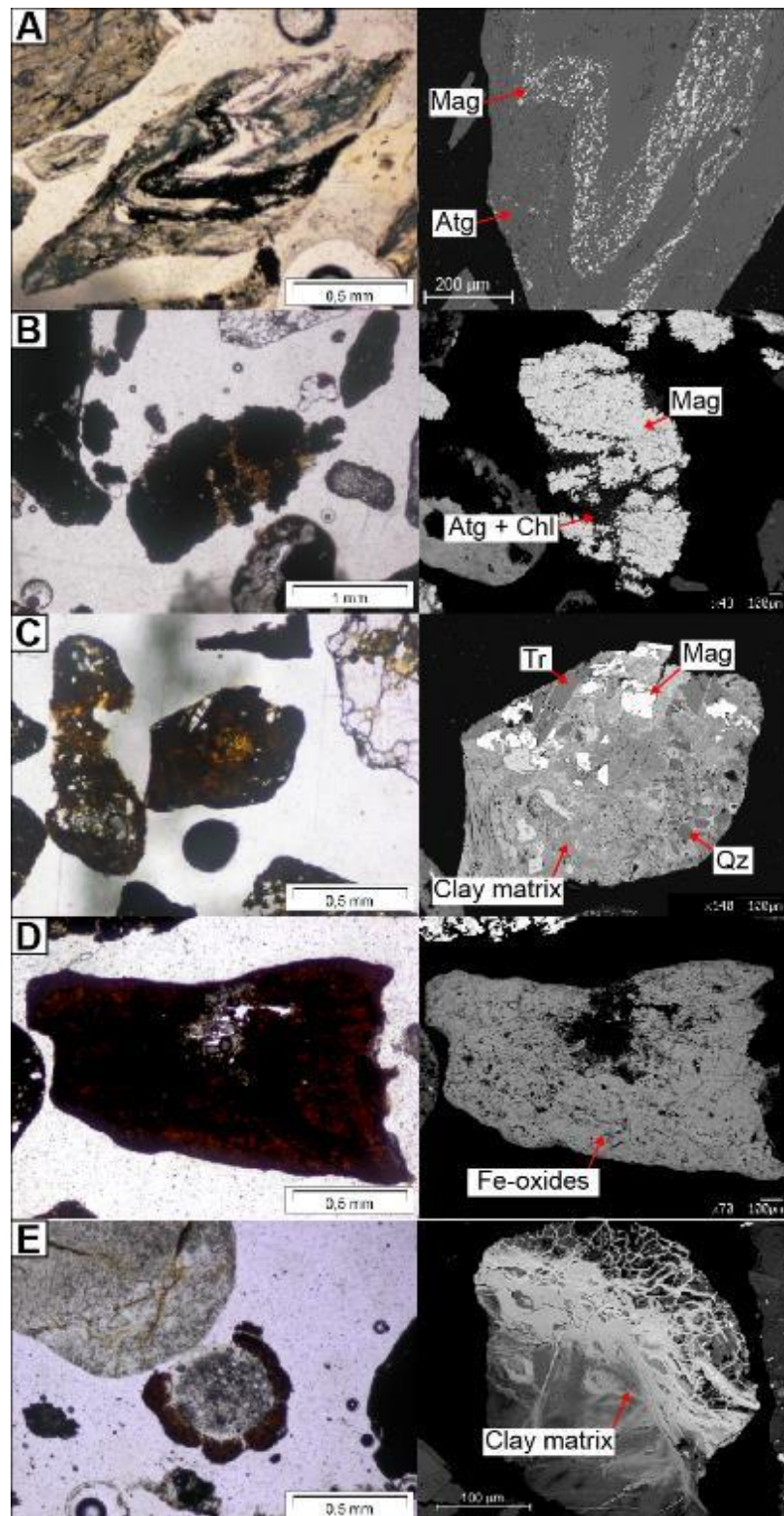


Fig 6.6. Micromorphological feature: A) Lithorelics of FS with microfold marker by microcrystalline magnetite alignment (left image is PPL and right image is BEI); B) Alterorelics aggregate of magnetite and mixture of serpentine minerals and chlorite, slightly altered and replaced by clay and oxyhydroxide in topsoil of FS soil profile (left image is PPL and right image is BEI); C) Alteromorph (left image is PPL and right image is BEI): Aggregate of magnetite, tremolite, and quartz with clay-rich matrix in subsoil of FS soil profile; D) Iron crust compact grain entirely composed by Fe-oxyhydroxide; E) Red nodules grain formed by Fe-oxyhydroxides matrix in FS topsoil (left image is XPL and right image is BEI).

Alteromorphs (Fig. 6.6C) are clasts with rounded morphology and medium sphericity consisting of aggregate of clayey matrix and primary minerals (e.g., magnetite, serpentines, chlorites), which are partially replaced by alteration products. The clayey matrix is composed either by iron oxides (Fe-oxides and oxyhydroxides) or iddingsitic mixtures which precipitates within porosity cementing together two or more individual clasts. Their modal abundance generally increases from subsoil (up to 15%) toward topsoil (about 20%).

Iron crusts are clast mainly or exclusively composed of Fe-oxyhydroxides, which can develop mainly due to 1) precipitation around clast edge according to peripheral cortification process (in this case the clast core is preserved due to a shield effect; Fig. 6.6D) and 2) precipitation within soil porosity giving rise to concentric layered crusts also called "*red nodules*" (Fig. 6.6E). The modal abundance of iron crusts generally increases from subsoil (up to 5%) toward topsoil (about 10%).

Allochthonous clasts are mainly represented by quartz generally in subangular monomineralic or polimineralic aggregates, sometimes associated with oxides and micas. Due to the ultramafic nature of the bedrocks, quartz-bearing clasts are allochthonous elements mainly related to the metasedimentary rocks occurring in the surroundings (quartz-schist or calc-schist). Locally amphibole-rich clasts occur in soil profiles developed close to tremolite-chlorite hybrid rocks. The modal abundance of allochthonous clasts always increase from subsoil (<5%) toward topsoil (up to 10%).

6.3.4. Soil Mineralogy

Soil samples were subdivided into three different aliquots in order to investigate the mineralogy of the sand (2 mm-63 μm), silt (63-4 μm), and clay (<4 μm) fractions.

The mineralogical variations have been evaluated for PSP, MS, and FS soil profiles from the subsoil toward the topsoil.

Rock	PSP		MS		FS	
Sand fraction (2 mm - 63 μm)						
Horizon	Topsoil	Subsoil	Topsoil	Subsoil	Topsoil	Subsoil
Antigorite	xxx	xxx	xxx	xxx	xxx	xxx
Clinochlore	xx	xx	x	xx	(x)	(x)
Quartz	-	-	(x)	x	x	(x)
Enstatite	xx	xx	-	-	x	-
Talc	-	-	(x)	-	(x)	-
Magnetite	xx	x	x	(x)	(x)	x
Tremolite	-	-	(x)	(x)	(x)	x
Plagioclase	-	-	-	-	x	x
Goethite	-	-	-	-	-	xx
Rutile	-	-	-	(x)	-	-
White mica	-	-	-	x	-	-
Amorphous	xx	x	xx	(x)	xxx	xx
Accessory minerals*	<i>Tr. ol, augite</i>	<i>Cr-mag, pen, tr. ol</i>	<i>Cr-mag, ilm, pen</i>	<i>Cr-mag, ilm, pen</i>	<i>Fe-chr</i>	<i>Cr-Mag</i>
Silt fraction (63 μm - 4 μm)						
Horizon	Topsoil	Subsoil	Topsoil	Subsoil	Topsoil	Subsoil
Antigorite	xxx	xxx	xxx	xxx	xxx	xxx
Chrysotile	(x)	-	-	-	-	-
Clinochlore	(x)	x	x	(x)	-	(x)
Quartz	(x)	(x)	xx	xx	xx	xx
Plagioclase	-	(x)	x	xx	x	(x)
Goethite	-	(x)	(x)	-	-	(x)
Illite/smectite	-	-	x	(x)	xx	x
Tremolite	-	-	(x)	x	x	x
Rutile	-	-	-	-	-	(x)
Ilmenite	-	-	-	(x)	-	-
Augite	(x)	-	-	-	-	-
Enstatite	-	xx	-	-	-	-
Tremolite	(x)	(x)	-	-	-	-
Magnetite	(x)	(x)	-	-	-	-
Amorphous	xxx	xx	(x)	(x)	x	(x)
Clay fraction (<4 μm)						
Horizon	Topsoil	Subsoil	Topsoil	Subsoil	Topsoil	Subsoil
Antigorite	xx	xx	xx	xx	(x)	-
Clinochlore	(x)	(x)	-	xx	(x)	x
Quartz	(x)	(x)	(x)	(x)	(x)	x
Illite	xx	-	-	xx	(x)	xxx
Goethite	x	(x)	-	x	(x)	xx
Vermiculite	-	-	-	(x)	-	-
Amorphous	xxx	xxx	xxx	xxx	xxx	xxx

Table 6.1 Mineralogy of the three soil granulometric fractions (sand 2 mm - 63 μ m; silt 63 μ m - 4 μ m; clay < 4 μ m) determined by XRD with Synchrotron radiation and Rietveld refinement. Legend: xxx = abundant (>30 wt%); xx intermediate = (10-30 wt%); x = minor (5-10 wt%); (x) = trace (1-5 wt%). *Accessory minerals have been detected by other techniques (e.g., PLOM, SEM, EMPA) and are supposed to be <1 wt%. Mineral abbreviations are after Kretz (1998).

In PSP soils, the mineralogy of the sandy fraction (that represent up to 50% of the soil constituents) is closely related to bedrock mineralogy. Serpentes represent about 50 wt% of the overall mineralogical composition (Table 6.1), with dominant antigorite (> 95 wt%) and subordinate chrysotile. Chlorite (mainly clinochlore and subordinate penninite; 19-11 wt%), enstatite (10-12 wt%), and

spinel-group minerals (mainly magnetite and subordinate Cr-spinels; up to 10 wt%) are diffuse but always subordinate with respect to serpentines. The authigenic minerals (8-10 wt%), correspond mostly to the low-crystalline or amorphous Fe-oxides *s.l.* occurring as oxidation products of primary minerals (mainly magnetite). Trace amount of quartz, augite, olivine, and tremolite also occur.

The silty fraction represents 40-45% of the soil constituents; its mineralogical composition does not differ significantly from that of the sandy fraction (Fig. 6.7B). The only clear difference is the significant increase of the low-crystalline or amorphous Fe-oxides that, in this case, range from 27 wt% in the subsoil to 41 wt% in the topsoil.

The clay fraction (that represent only the 5-10 % of the soil constituents) is mainly composed by amorphous or low-crystalline Fe-oxyhydroxides (up to 73 wt%), serpentines (mainly antigorite and subordinate chrysotile; 23-21 wt%), smectite and illite/smectite mixed-layer clay (<12 wt%), and clinochlore (<5 wt%).

In *MS soils*, the mineralogy of the sandy fraction (that represent up to 40% of the soil constituents) is closely related to bedrock mineralogy (Fig. 6.7A). Serpentines represent about 60 wt% of the overall mineralogical composition (Table 6.1), with dominant antigorite (>95 wt%) and subordinate chrysotile (<5 wt%). Chlorite (mainly clinochlore and subordinate penninite; 6-13 wt%), quartz (3-6 wt%), magnetite (6-7 wt%), and tremolite (2-3 wt%) are the main subordinate minerals. The authigenic minerals (4-14 wt%), correspond mostly to the low-crystalline or amorphous Fe-oxides *s.l.* occurring as oxidation products of primary minerals (mainly magnetite). Trace amount of talc, Cr-magnetite, rutile, ilmenite, and white mica also occur.

The silty fraction represents 50-55 wt% of the soil constituents and its mineralogical composition does not differ significantly from that of the sandy fraction although significant concentrations of plagioclase (7-12 wt%) and clay minerals (4-5 wt%) occurs. These last are mainly present in the matrix of serpentinite clasts or within veins, commonly intimately intermixed with chlorite. The only clear difference is the significant increase of the low-crystalline or amorphous Fe-oxides that, in this case, range from 27 wt% in the subsoil to 41 wt% in the topsoil. Trace amount of goethite and ilmenite are also present.

The clay fraction (that represent only the 5 wt% of the soil constituents) is mainly composed by amorphous or low-crystalline Fe-oxyhydroxides (up to 82 wt% in

the topsoil and up to 34 wt% in the subsoil). Antigorite (16-27 wt%), smectite and illite/smectite mixed-layer clay (up to 17 wt%), clinochlore (up to 14 wt%), subordinate goethite (<5 wt%), quartz (<3 wt%) and vermiculite (<1 wt%) are the most common subordinate minerals.

In *FS soils*, the mineralogy of the sandy fraction (that represent up to 50% of the soil constituents) is closely related to bedrock mineralogy. Serpentes represent about 60 wt% of the overall mineralogical composition (Table 6.1), with dominant antigorite (>95 wt%) and subordinate chrysotile (<5 wt%). Plagioclase (9-10 wt%), clinochlore (1-4 wt%), quartz (3-8 wt%), magnetite (1-7 wt%) and tremolite (2-3 wt%) are diffuse but always subordinate with respect to serpentes. The authigenic minerals (20-30 wt%), correspond mostly to the low-crystalline or amorphous Fe-oxides *s.l.* occurring as oxidation products of primary minerals (mainly magnetite). Trace amount of talc, Cr-magnetite, ferrian chromite, and enstatite also occur.

The silty fraction represents 40-45% of the soil constituents; its mineralogical composition does not differ significantly from that of the sandy fraction. The only clear difference is the presence of significant amount of smectite and illite/smectite mixed-layer clay (9-10 wt%) as well as minor amounts of rutile (<1 wt%).

The clay fraction (that represent only the 5-10% of the soil constituents; Fig. 6.7C) is mainly composed by amorphous or low-crystalline Fe-oxyhydroxides (up to 89 wt%), smectite and illite/smectite mixed-layer clay (up to 36 wt%), clinochlore (up to 7 wt%), quartz (>5 wt%), and trace amount of antigorite (<2 wt%).

In general, in all the soils related to the three bedrock groups, the mineralogy of the skeleton (sandy and silty fractions) is closely related to bedrock mineralogy as expected for primitive A-C soils. A general trend observed in the three groups is the progressive increase of the clay fractions from the subsoils toward the topsoils. Nevertheless, two different behavior are evident for the mineralogical constituents of this granulometric fraction (Fig. 6.8); in soils developed on PSP a constant increase of clay minerals (smectite and illite/smectite mixed-layer clay) is observed from the subsoil toward the topsoil, which is inversely proportional to the gradual decrease of authigenic Fe-oxides *s.l.* This trend is opposite in soils from both the serpentinitic bedrocks (MS and FS) presumably due to the lower rate of weathering of serpentine minerals with respect to olivine and pyroxenes

occurring in partially serpentinized lherzolites bedrocks (PSP). Micromorphological evidences in MS and FS soils suggest that in these cases the most significant weathering processes are those involving oxidation of spinels group minerals, mostly magnetite. As a matter of fact, antigorite and, subordinately, clinochlore are the only primary minerals residually present in significant amount in the clay fraction of the topsoils (Fig. 6.8).

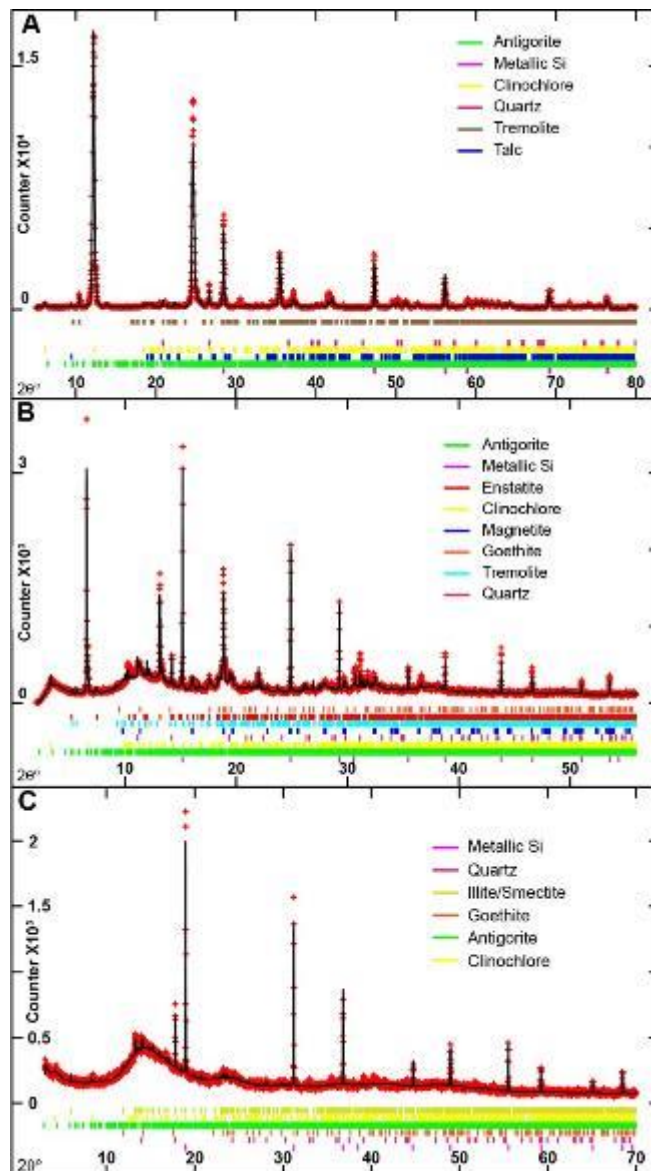


Fig. 6.7 Rietveld refinement patterns of powder Synchrotron X-ray diffraction data for the representative soil fractions and bedrocks: a) sand fraction of subsoil of MS soil; b) silt fraction of topsoil of PSP soil; c) clay fraction of topsoil of FS soil. Experimental data and calculated profiles are shown as red crosses and black solid lines, respectively. The colored thick lines at the bottom of the spectra represent the theoretical Bragg positions of recognized mineral phases.

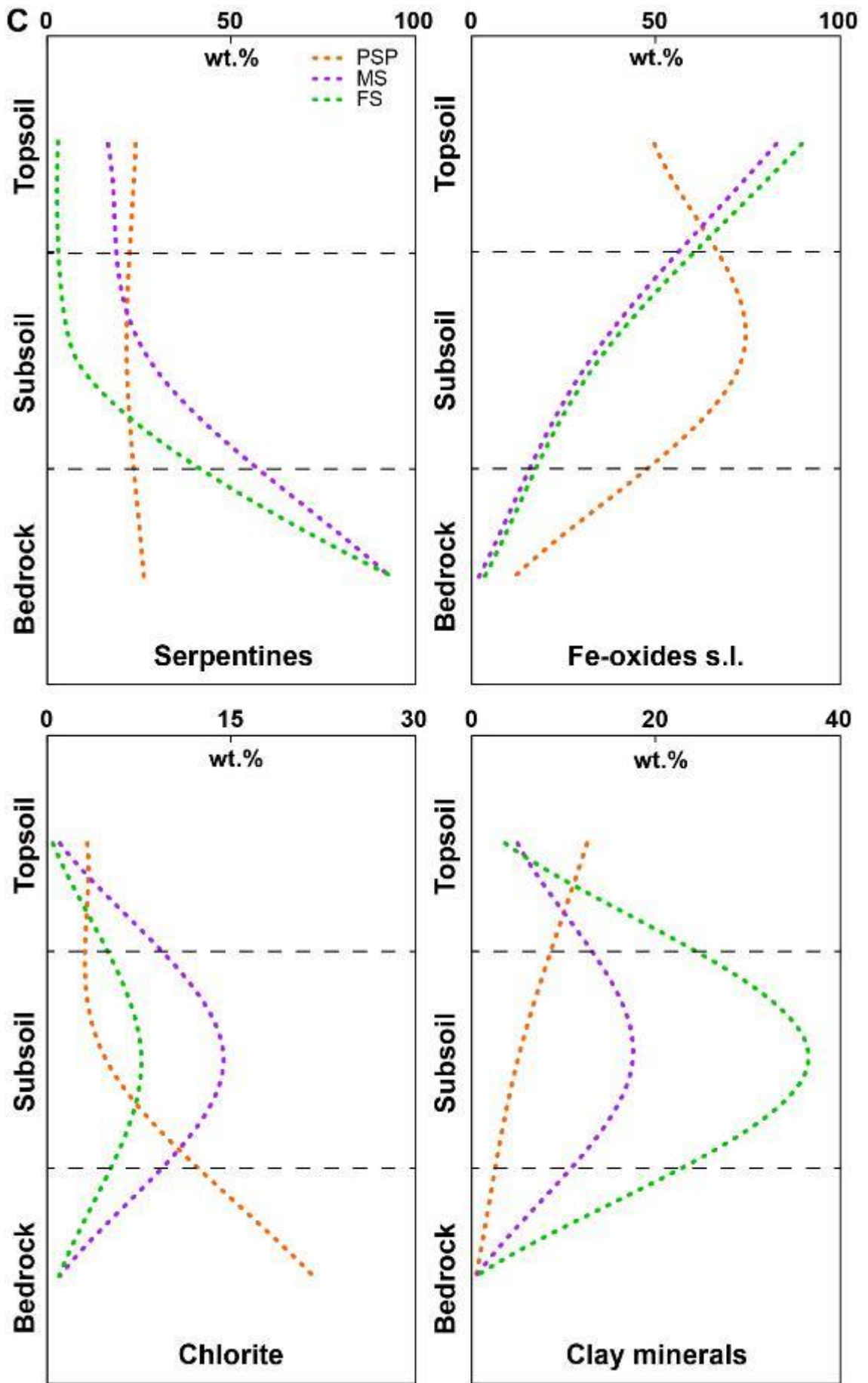


Fig. 6.8 Distribution of minerals along the soil profiles in the clay fraction.

6.3.5. Mineral chemistry

The PTEs considered in this work are hosted both in primary and authigenic minerals. In the primary minerals they are mainly present in serpentines (Ni, Cr, and subordinately Co), spinel-group minerals (Cr, and subordinately Ni and Co), pyroxenes (Cr and subordinately V and Ni), olivines (mainly Ni), chlorites (Cr and Ni), tremolite (V, Co, and Ni), talc (Ni and Cr), ilmenite (V). Both the main authigenic minerals (i.e. Fe-oxides *s.l.* and clay minerals) are able to scavenge significant amounts of Cr, Ni, and Co (Fig. 6.9-10, Table 6.2 and *Appendix B2-3*). In particular, in goethite alteromorphs after spinel-group minerals and goethite/hematite-rich iron crusts, the average Cr-content is higher than 10000 ppm and the average Ni contents is higher than 1800 ppm. Also, the clay minerals occurring in *alteromorphs* or in veins evidences very high PTEs contents ranging from 2800 ppm of Cr, 3100 ppm for Ni and 800 ppm for Co.

Considering the high stability of goethite, hematite and clay minerals in supergenic environment, it is evident that this mineral species are effective and often permanent traps for the most important PTEs of ultramafic soils and bedrocks, thus reducing its bioavailability (Francis and Dodge 1990; Quantin et al., 2002; Hooda, 2010; Kabata-Pendias, 2011).

Among the primary minerals, Cr is mainly contained within spinel-group minerals (ferrian chromite ~210000 ppm, Cr-magnetite ~175000 ppm, and magnetite ~35000 ppm), pyroxenes (~6600 ppm), chlorite (~3500 ppm), and serpentines (~2300 ppm; Fig. 6.11, Table 6.2). Spinel-group minerals in FS soil contain much Cr respect to those in the two other soil groups. Others primary minerals do not show significant variation in Cr content depending on the type of bedrock.

Among the primary minerals, Ni is mainly contained within spinel-group minerals (Cr-magnetite ~3800 ppm and magnetite ~1900 ppm), serpentines (~1700 ppm), chlorite (~1400 ppm), and ilmenite (~500; Fig. 6.11). Significant Ni concentration was also detected in authigenic minerals which thus represented effective traps for Ni leached through mineral weathering to the soil solution. In the oxyhydroxide matrix, Ni content reaches up to 19000 ppm (average ~1600 ppm). In the clay matrix, nickel distribution is irregular and reaches up to 30700 ppm (average ~1700 ppm).

In the primary minerals, Co is mainly contained within spinel-group minerals (Cr-magnetite ~800 ppm and magnetite ~720 ppm) and ilmenite (~500 ppm; Fig. 6.11). Co content does not vary sensitively according to the nature of the bedrock.

Authigenic phases (both clay and oxyhydroxides) are can host up to 82000 ppm and 52100 ppm respectively of Co.

Sample Mineral	Antigorite		Tremolite		Ilmenite		Clinocllore			Penninite			Fe-Chr			Cr-Magnetite			Magnetite		Talc	
	MS	FS	MS	FS	MS	FS	PSP	MS	FS	PSP	MS	FS	PSP	MS	FS	PSP	MS	FS	MS	FS	MS	FS
SiO ₂	41.68	42.18	57.50	58.23	0.06	0.25	31.28	31.51	30.94	34.12	33.83	0.03	0.13	0.30	0.04	0.09	0.06	0.09	0.06	0.06	60.17	
TiO ₂	0.03	0.02	0.02	0.03	50.72	49.81	0.01	0.00	0.01	0.03	0.03	0.44	0.48	0.59	0.67	0.12	0.22	0.12	0.22	0.03	0.03	
Al ₂ O ₃	1.47	1.67	0.26	0.10	0.00	0.15	17.66	16.52	16.84	13.08	13.16	5.18	0.40	0.17	0.08	0.07	0.04	0.07	0.04	0.04	0.42	
Cr ₂ O ₃	0.33	0.30	0.15	0.02	0.00	0.17	0.52	0.01	0.57	0.63	0.47	31.79	23.75	24.59	25.72	1.75	3.44	1.75	3.44	0.03	0.03	
FeO	6.23	4.99	3.27	2.74	45.15	45.01	3.16	7.16	7.36	3.40	6.81	55.64	68.36	66.89	66.19	91.10	90.08	91.10	90.08	3.95	3.95	
MgO	36.29	37.68	22.55	23.07	1.08	0.59	31.60	30.63	32.52	34.73	29.79	2.15	0.75	1.48	1.53	0.25	0.33	0.25	0.33	27.89	27.89	
MnO	0.10	0.11	0.15	0.12	2.51	2.69	0.15	0.10	0.08	0.01	0.07	1.57	0.45	1.56	1.69	0.09	0.19	0.09	0.19	0.05	0.05	
CaO	0.02	0.01	13.25	13.22	0.04	0.03	0.03	0.04	0.03	0.03	0.41	0.01	0.01	0.02	0.00	0.01	0.02	0.01	0.02	0.03	0.03	
Na ₂ O	0.02	0.02	0.18	0.25	0.00	0.00	0.02	0.01	0.00	0.00	0.01	0.04	0.05	0.10	0.02	0.01	0.05	0.01	0.05	0.04	0.04	
NiO	0.24	0.13	0.09	0.05	0.04	0.05	0.28	0.03	0.14	0.18	0.23	0.23	0.30	0.31	0.30	0.27	0.21	0.27	0.21	0.10	0.10	
K ₂ O	0.00	0.01	0.02	0.04	0.00	0.00	0.01	0.00	0.01	0.01	0.00	0.01	0.01	0.01	0.00	0.01	0.01	0.01	0.01	0.02	0.02	
V ₂ O ₅	0.01	0.02	0.03	0.00	3.32	3.30	0.03	0.00	0.01	0.07	0.01	0.15	0.27	0.11	0.08	0.06	0.09	0.06	0.09	0.01	0.01	
CoO	0.02	0.02	0.04	0.03	0.00	0.00	0.04	0.00	0.02	0.00	0.02	0.14	0.16	0.10	0.13	0.15	0.13	0.15	0.13	0.00	0.00	
SO ₂	0.03	0.05	0.00	0.00	0.00	0.00	0.02	0.04	0.00	0.06	0.02	0.00	0.00	0.00	0.00	0.00	0.00	0.00	0.00	0.00	0.00	
ZnO	0.04	0.07	0.01	0.01	0.09	0.12	0.04	0.01	0.09	0.07	0.09	0.74	0.37	0.43	0.34	0.12	0.09	0.12	0.09	0.00	0.00	
Sum	86.45	87.17	97.36	97.89	103.01	102.17	84.83	86.05	86.61	86.41	84.95	98.09	95.46	96.50	96.78	94.02	94.66	94.02	94.66	92.75	92.75	
Structural formula calculated basis on n⁺:																						
14 oxygens																						
Si	4.00	3.98	7.92	7.96	0.00	0.01	6.05	6.12	5.88	6.49	6.65	0.00	0.01	0.01	0.00	0.00	0.00	0.00	0.00	0.00	7.96	
Ti	0.00	0.00	0.00	0.00	1.86	1.85	0.00	0.00	0.00	0.00	0.00	0.01	0.01	0.02	0.02	0.00	0.01	0.00	0.01	0.00	0.00	
Al	0.17	0.19	0.04	0.02	0.00	0.01	4.03	3.78	3.77	2.93	3.05	0.22	0.02	0.01	0.00	0.00	0.00	0.00	0.00	0.00	0.06	
Cr	0.02	0.02	0.01	0.00	0.00	0.01	0.08	0.00	0.09	0.09	0.07	0.90	0.71	0.72	0.76	0.05	0.10	0.05	0.10	0.00	0.00	
Fe _{tot}	0.50	0.39	0.38	0.31	1.84	1.86	0.51	1.16	1.17	0.54	1.12	1.67	2.16	2.08	2.06	2.90	2.85	2.90	2.85	0.44	0.44	
Mg	5.18	5.30	4.63	4.70	0.08	0.04	9.12	8.87	9.21	9.85	8.73	0.11	0.04	0.08	0.08	0.01	0.02	0.01	0.02	5.50	5.50	
Mn	0.01	0.01	0.02	0.01	0.10	0.11	0.02	0.02	0.01	0.00	0.01	0.05	0.01	0.05	0.05	0.00	0.01	0.01	0.01	0.01	0.01	
Ca	0.00	0.00	1.95	1.94	0.00	0.00	0.01	0.01	0.01	0.01	0.09	0.00	0.00	0.00	0.00	0.00	0.00	0.00	0.00	0.00	0.00	
Na	0.00	0.00	0.05	0.07	0.00	0.00	0.01	0.00	0.00	0.00	0.00	0.00	0.00	0.00	0.00	0.00	0.00	0.00	0.00	0.01	0.01	
K	0.00	0.00	0.00	0.01	0.00	0.00	0.00	0.00	0.00	0.00	0.00	0.00	0.00	0.00	0.00	0.00	0.00	0.00	0.00	0.00	0.00	
Ni	0.02	0.01	0.01	0.01	0.00	0.00	0.04	0.01	0.02	0.03	0.04	0.01	0.01	0.01	0.01	0.01	0.01	0.01	0.01	0.01	0.01	
V	0.00	0.00	0.00	0.00	0.11	0.11	0.01	0.00	0.00	0.03	0.01	0.00	0.01	0.00	0.00	0.00	0.00	0.00	0.00	0.00	0.00	
Co	0.00	0.00	0.00	0.00	0.00	0.00	0.01	0.00	0.00	0.00	0.00	0.00	0.00	0.00	0.00	0.00	0.00	0.00	0.00	0.00	0.00	
S	0.00	0.00	0.00	0.00	0.00	0.00	0.00	0.00	0.00	0.00	0.00	0.00	0.00	0.00	0.00	0.00	0.00	0.00	0.00	0.00	0.00	
Zn	0.00	0.00	0.00	0.00	0.00	0.00	0.01	0.00	0.02	0.01	0.02	0.02	0.01	0.01	0.01	0.02	0.01	0.01	0.01	0.00	0.00	
Sum	9.91	9.91	15.02	15.03	4.00	4.00	19.90	19.99	20.19	20.00	19.79	3.00	3.00	3.00	3.00	3.00	3.00	3.00	3.00	14.01	14.01	
Fe ²⁺	-	-	0.24	0.25	-	-	-	-	-	-	-	0.82	0.95	0.87	0.86	0.98	0.97	0.98	0.97	-	-	
Fe ³⁺	-	-	0.14	0.07	-	-	-	-	-	-	-	0.85	1.22	1.22	1.20	1.93	1.88	1.93	1.88	-	-	

Table 6.2 Representative analysis of the main PTEs-bearing minerals (EMPA-WDS) and calculated formulas.

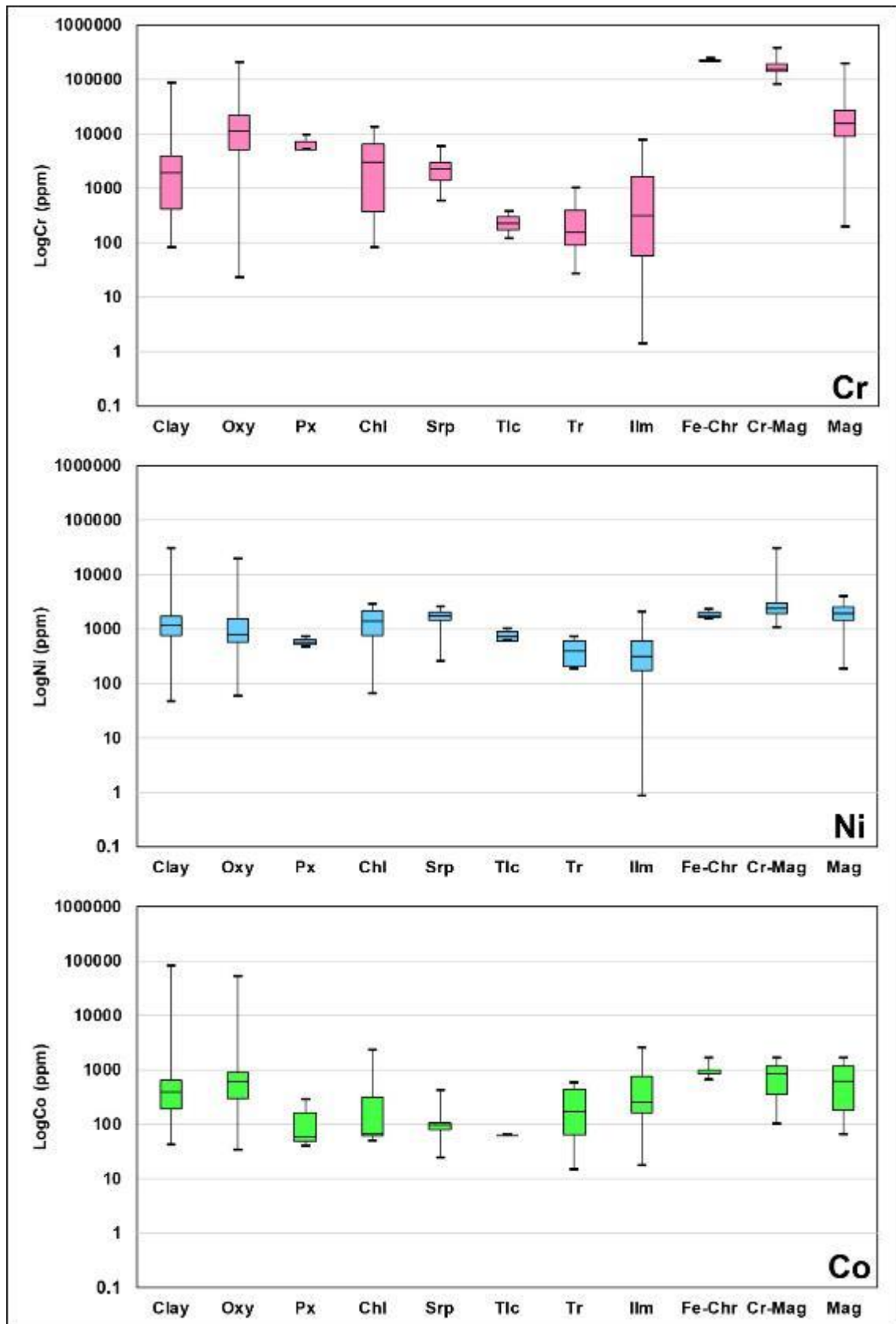


Fig. 6.9 Box plots showing statistical parameters of concentrations (in ppm) of Cr, Ni, and Co in the different minerals (EMPA-WDS and LA-ICP-MS data). Vertical lines show the range in concentrations, the boxes are bounded by the 1st and 3th quartile values, and the horizontal line inside the box represents the median value.

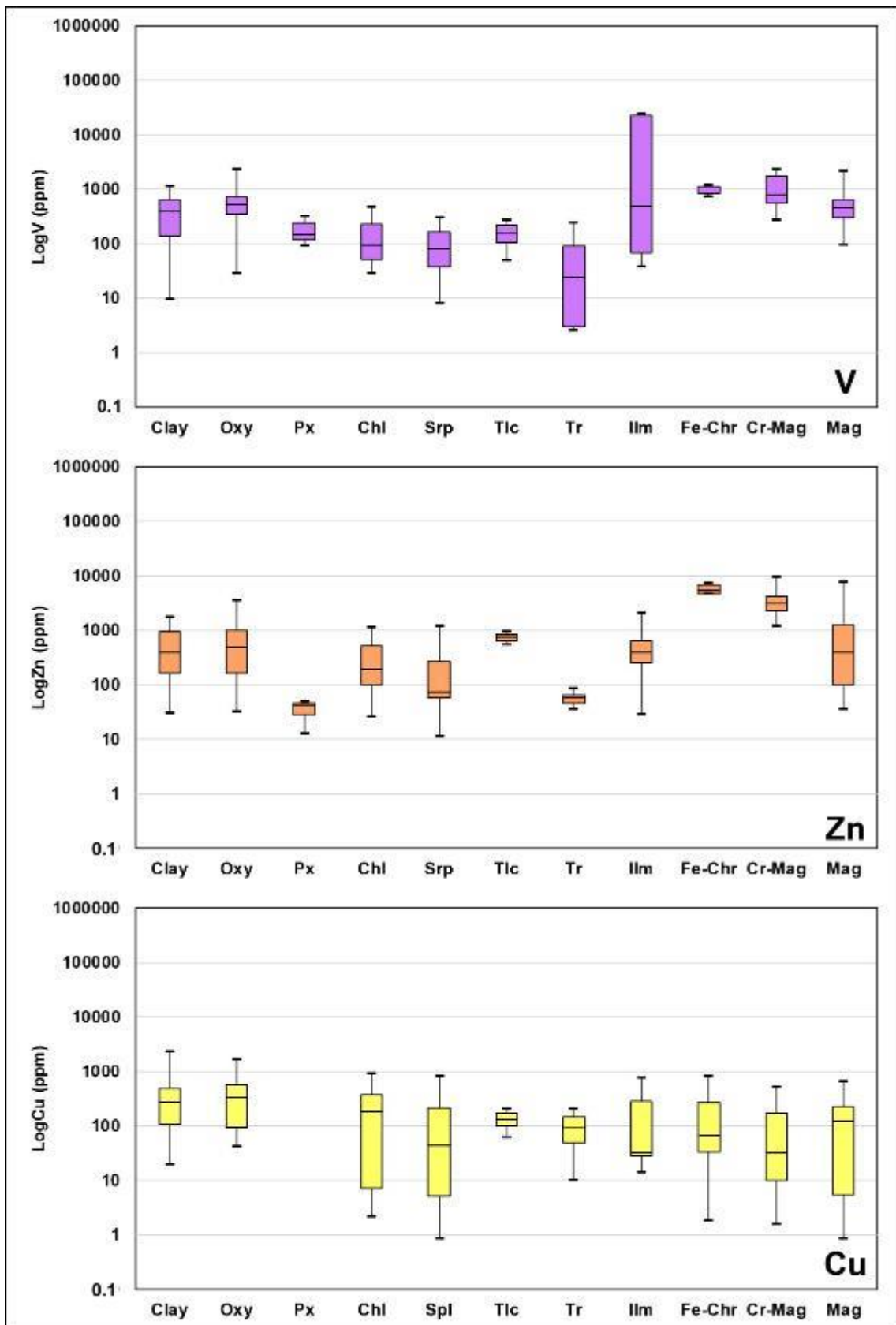


Fig. 6.10 Box plots showing statistical parameters of concentrations (in ppm) of V, Cu, and Zn in the different minerals (EMPA-WDS and LA-ICP-MS data). Vertical lines show the range in concentrations, the boxes are bounded by the 1st and 3th quartile values, and the horizontal line inside the box represents the median value.

V is mainly host in ilmenite (~10000 ppm), in Cr-magnetite (~1000 ppm), magnetite (~600 ppm), and their authigenic products (Fe-oxyhydroxide ~600 ppm), clay minerals can be carrier a significant amount of V (~400 ppm; Fig. 6.10).

As discussed in *Chapter IV*, local high concentration of Zn and Cu can be explained by the presence of these elements either in primary or authigenic minerals. The main Zn-bearing minerals are represented by spinel minerals (~2500 ppm), ilmenite (~580 ppm), as well as in goethite ± clay minerals *alteromorphs* after these minerals (~720 ppm and 570 ppm, respectively; Fig. 6.10). Minor but significant concentration of Zn can also be present in serpentines and chlorite (~200 and 340 ppm respectively). The main Cu-bearing minerals are represented by the authigenic phases (clay minerals ~440 ppm and goethite ~400 ppm). Among the primary minerals also chlorite (~240 ppm), ilmenite (~190 ppm), serpentines (~180 ppm), and spinel-group minerals (~149 ppm) have significant amount in Cu (Fig. 6.10).

6.3.6. Bulk chemistry

The chemical composition of the studied soils is strongly influenced by the bedrock chemical composition (Fig. 6.11). SiO₂ (34-52 wt%) and MgO (12-23 wt%) are the major components of the studied soils. FeO_{tot} (7-10 wt%), Al₂O₃ (8-3 wt%), and subordinate CaO (1.1-1.4 wt%) and MnO (0.7-2 wt%) are the minor components of all soils.

The three groups of ultramafic soils are characterized by significant variations of Mg, Si, Fe, and Al (Fig. 6.11). In general, it notes a systematic decrease of MgO and enrichment in Si, Fe, and subordinate Al from bedrock to soil. These variations are not related to the nature of the bedrocks.

Among the minor and trace elements, Cr, Co, and Ni, and subordinately Cu, V, and Zn are systematically present in significant concentrations (Fig. 6.12).

Cr and Ni have always the highest concentrations and widest range of variability. Cr and Ni (Fig. 6.12A-B) decrease according to the serpentinization of the bedrock, from PSP (Cr 2000 ppm and Ni 2200 ppm), through MS (Cr 1650 ppm and Ni 1400 ppm), and FS (Cr 1400 ppm and Ni 900 ppm).

V increase with the serpentinization of the bedrock: in FS ranges from 170 to 14 ppm and in PSP from 75 to 25 ppm (Fig. 6.12D).

Co, Cu, and Zn (Fig. 6.12C-E-F) not shows a clear correlation with bedrock serpentinization.

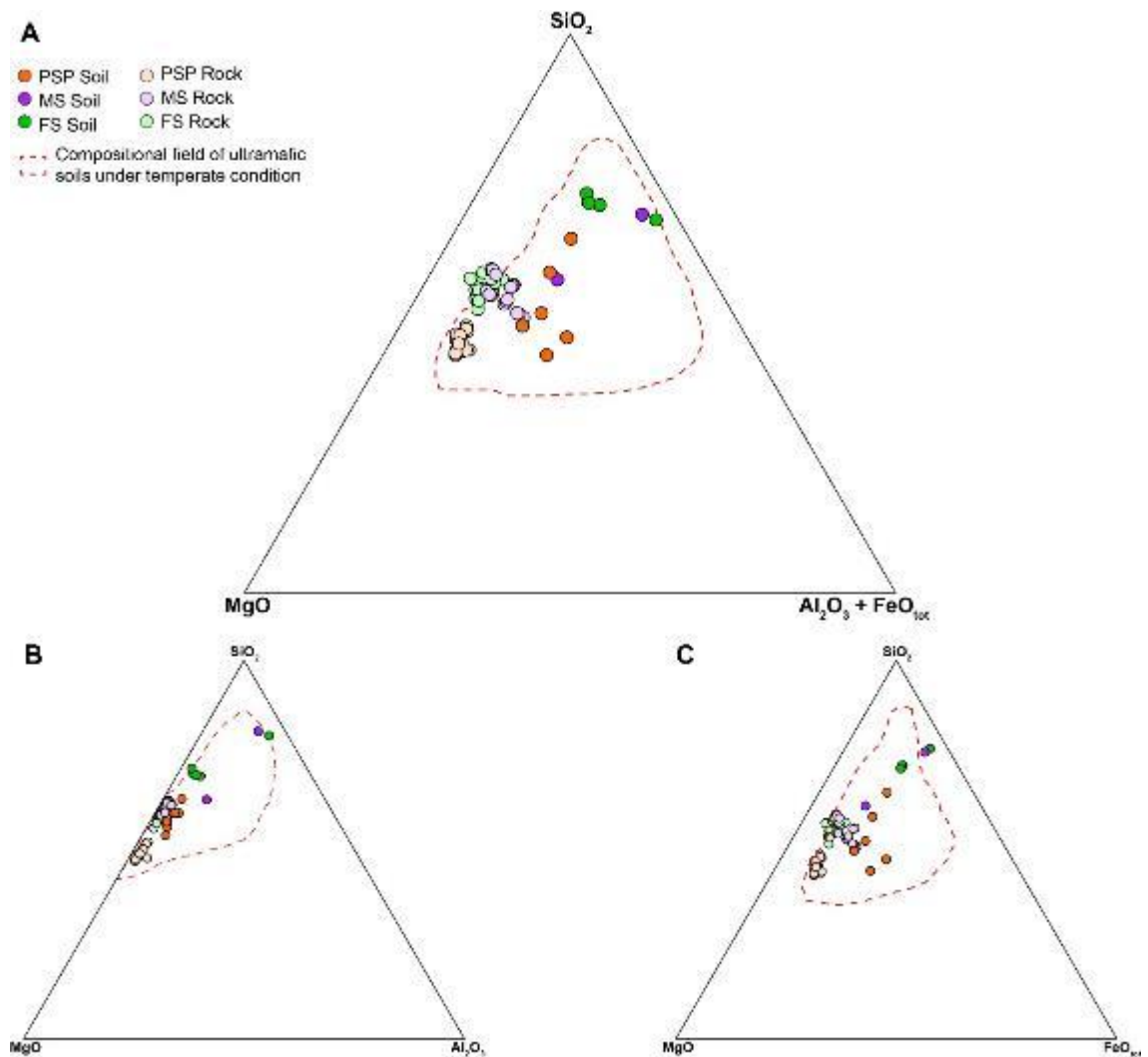


Fig. 6.11 A) Compositional variations of ultramafic soils on the MgO-SiO₂-(Al₂O₃+FeO_{tot}) diagram. B) Compositional variations of ultramafic soils on the MgO-SiO₂-Al₂O₃ diagram. C) Compositional variations of ultramafic soils on the MgO-SiO₂-FeO_{tot} diagram. Gray fields refer to the composition of ultramafic rocks under temperate climate worldwide (Cortesogno et al., 1979; Angelone et al., 1993; Venturelli et al., 1997; Bonifacio et al., 1997; D'Amico et al., 2008; Quantin et al., 2008; Cailaud et al., 2009; Kelepertizis et al., 2013; Bani et al., 2014; Baumeister et al., 2015; Kierczak et al., 2016).

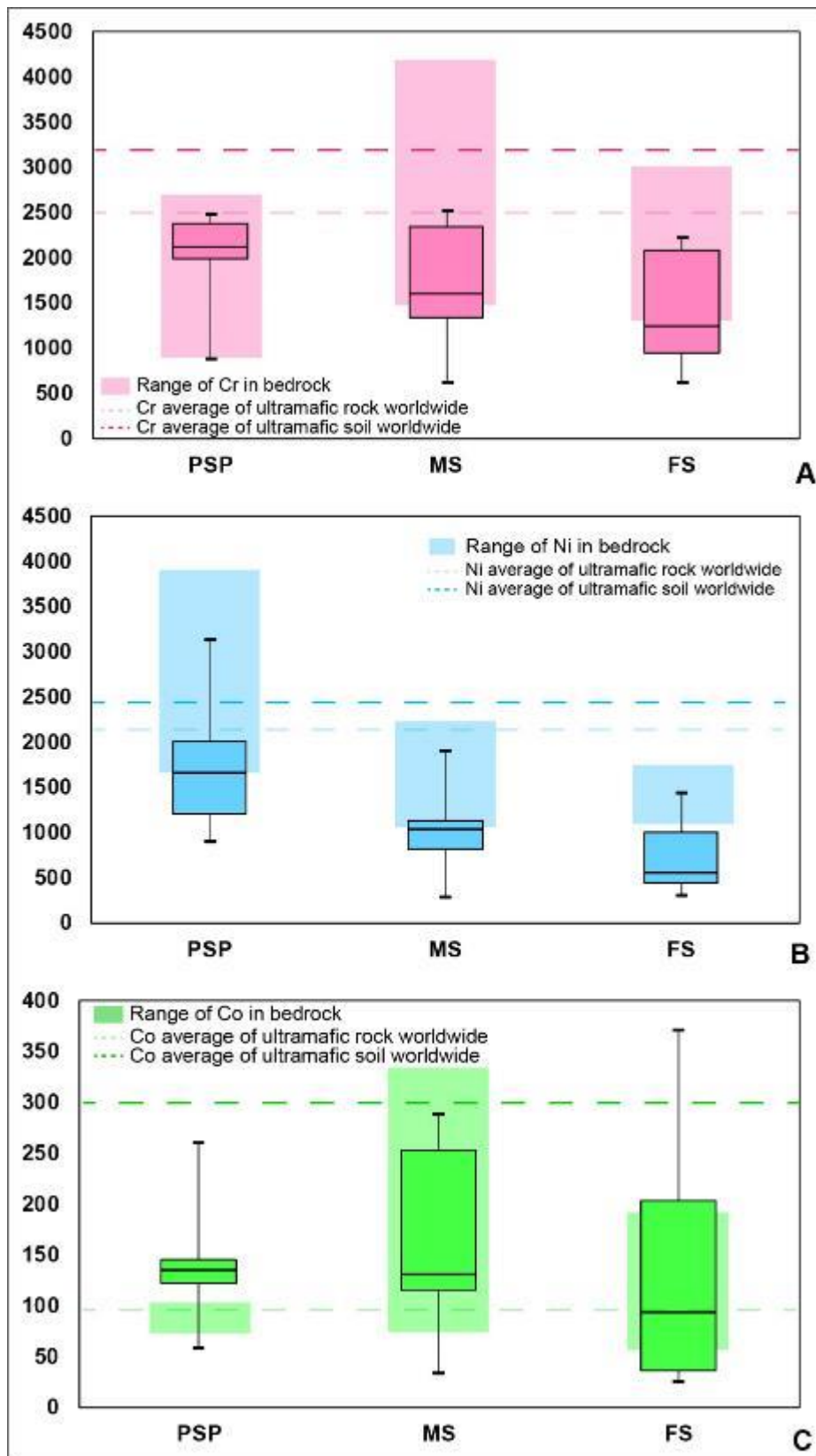


Fig 6.12 Box plots showing statistical parameters of concentrations (in ppm) of Cr, Ni, Co, V, Cu, and Zn in the different ultramafic soil (XRF and ICP-AES data). Vertical lines show the range in concentrations, the boxes are bounded by the 1st and 3th quartile values, and the horizontal line inside the box represents the median value.

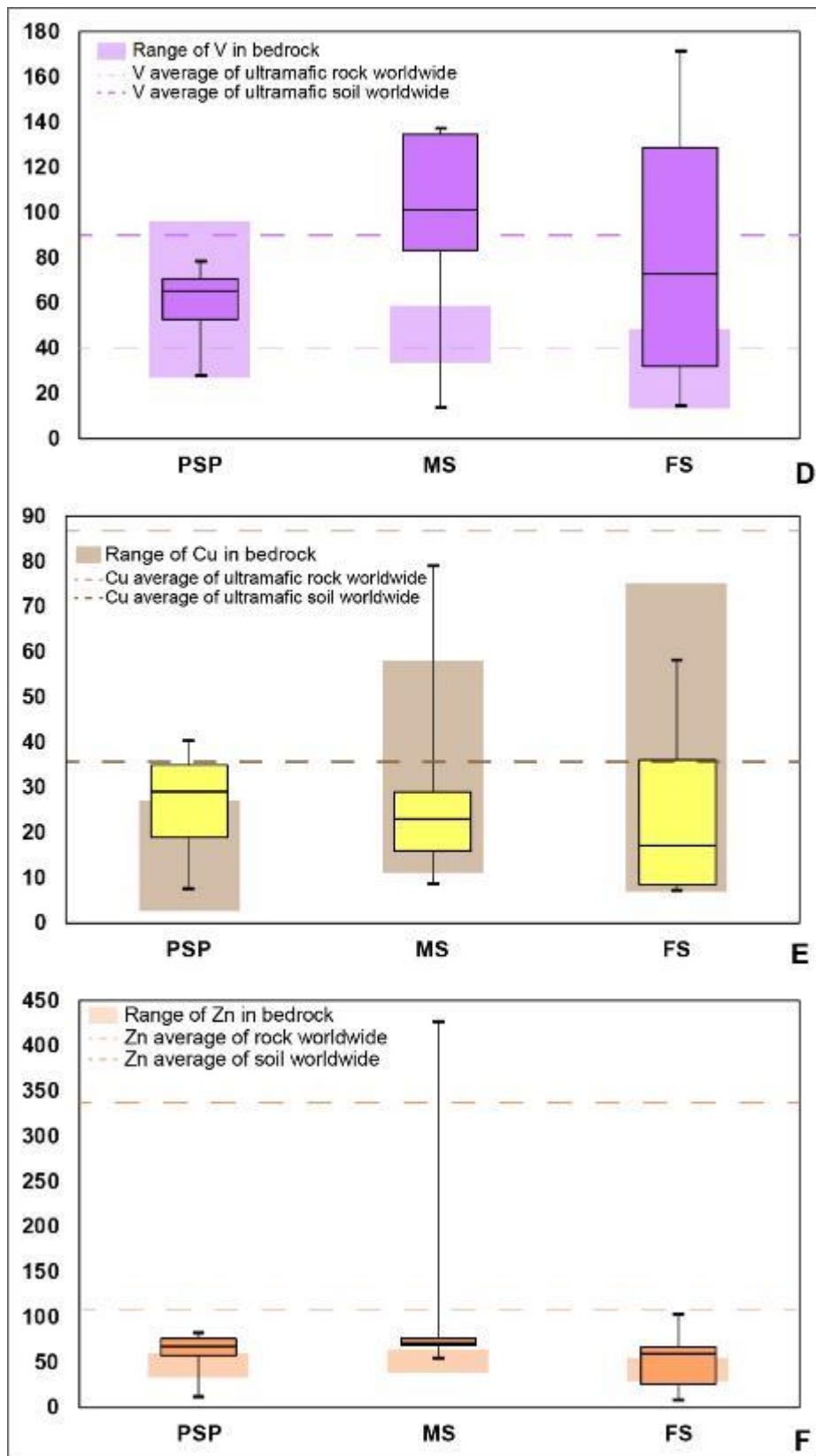


Fig. 6.12 Continued

The chemical variation of the major elements along soil profile (from unaltered toward saprolite, subsoils, and topsoils; Table 6.3) do not differ significantly depending on the nature of the bedrocks.

In general, Fe, Al, and Mn show a systematic enrichment from unaltered bedrock toward topsoil, on the other hand Mg has the opposite behavior (Fig. 6.13).

Bedrock	Description	Depth	wt%						ppm							
			MgO	Al ₂ O ₃	CaO	TiO ₂	MnO	FeO _{tot}	V	Cr	Co	Ni	Cu	Zn	As	Pb
PSP	Topsoil	2-20 cm	22.64	3.05	1.30	0.15	0.18	12.15	71	2183	145	1648	31	76	3	24
	Subsoil	20-40	21.13	2.66	1.06	0.12	0.20	14.66	63	2301	165	2090	30	65	2	11
	Weathered bedrock	40-45	39.96	1.88	2.10	0.07	0.09	8.61	48	1461	87	3150	12	49	0.4	1
	Unweathered bedrock	>45 cm	39.53	1.65	1.59	0.07	0.09	7.77	38	1287	82	2550	16	44	0.2	1
MS	Topsoil	3-30 cm	14.94	8.14	1.52	0.89	0.16	9.33	118	1374	125	743	22	79	17	43
	Subsoil	30-60	15.91	7.54	0.90	0.71	0.21	11.74	103	2071	223	1497	41	64	bdl	25
	Weathered bedrock	60-65 cm	26.90	1.76	0.12	0.06	0.16	11.78	54	3307	235	2019	27	55	bdl	8
	Unweathered bedrock	>65 cm	28.63	1.58	0.51	0.09	0.13	7.67	47	2645	198	1821	29	41	4	1
FS	Topsoil	5-40 cm	11.08	9.46	1.26	0.92	0.25	10.82	135	1651	181	990	29	70	bdl	30
	Subsoil	40-100 cm	12.12	8.82	1.18	1.06	0.32	14.05	140	2167	286	982	47	60	bdl	38
	Weathered bedrock	100-105 cm	29.10	1.30	0.38	0.03	0.07	5.53	36.1	1305	57	1093	11.3	35	2.66	0.48
	Unweathered bedrock	>105 cm	29.93	1.27	0.64	0.05	0.10	6.76	34	1856	121	1344	32	38	2	1

Table 6.3 Chemical bulk composition of the soil profiles (XRF and ICP-AES data).

Although in the complex, the soils are generally depleted in Cr, Ni, and Co and enriched in Cu, Zn, and V with respect to the bedrocks, locally some profiles show enrichment only in subsoil in contact with the bedrock, with a progressive impoverishment towards the surface.

Cr shows a systematic depletion on the topsoil in serpentine soil s.s. (MS and FS), whereas on PSP soil there is a significant increase in Cr content (Fig. 6.14). Ni shows, with some minor exceptions, a systematic decrease in concentration from bedrock to the topsoil (Fig. 6.14). Co does not follow a systematic trend of distribution correlate to the nature of the bedrock; however, most profiles show slight subsoil enrichment (Fig. 6.14). Cu shows the tendency to concentrate in the subsoil, whereas Zn and V tend to accumulate in the topsoil.

From an environmental point of view, the general picture of PTEs distribution evidence that only Cr, Ni, and, partially, Co systematically exceed (up to one order of magnitude) the residential and industrial threshold values (CSC) according to Italian law (Fig. 6.15; D.M. 471/1999; D.Lgs 152/2006). Among the other elements, only V evidence concentration of environmental concern, since they are above the residential CSC in MS and FS soils.

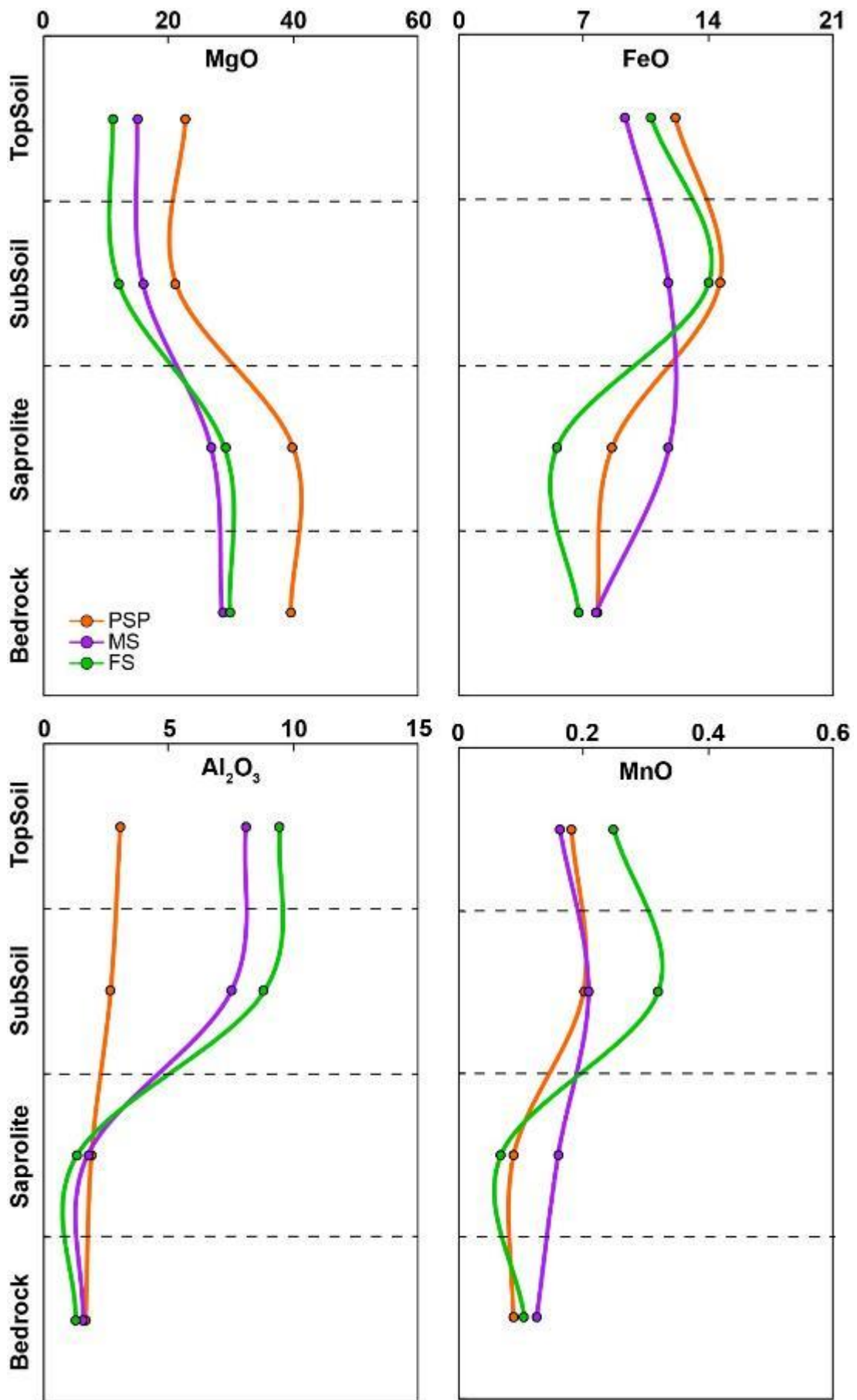


Fig. 6.13 Distribution of major and minor elements (MgO, FeO_{tot}, Al₂O₃, and MnO) along the soil profile (XRF and ICP-AES data). Values are in wt%.

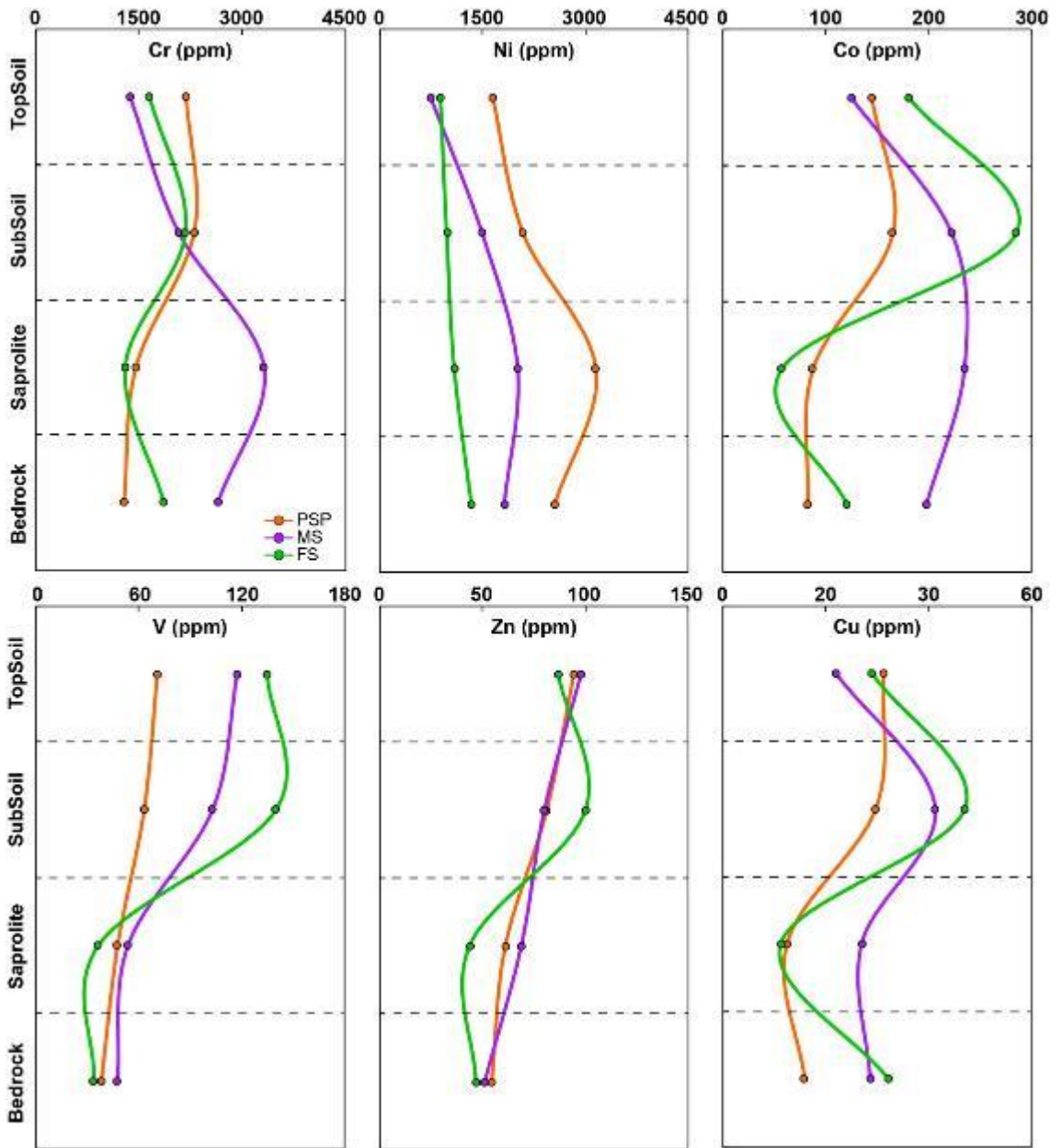


Fig. 6.14 Distribution of PTEs (Cr, Ni, Co, V, Zn, and Cu) along the soil profile (XRF and ICP-AES data). Values are in ppm.

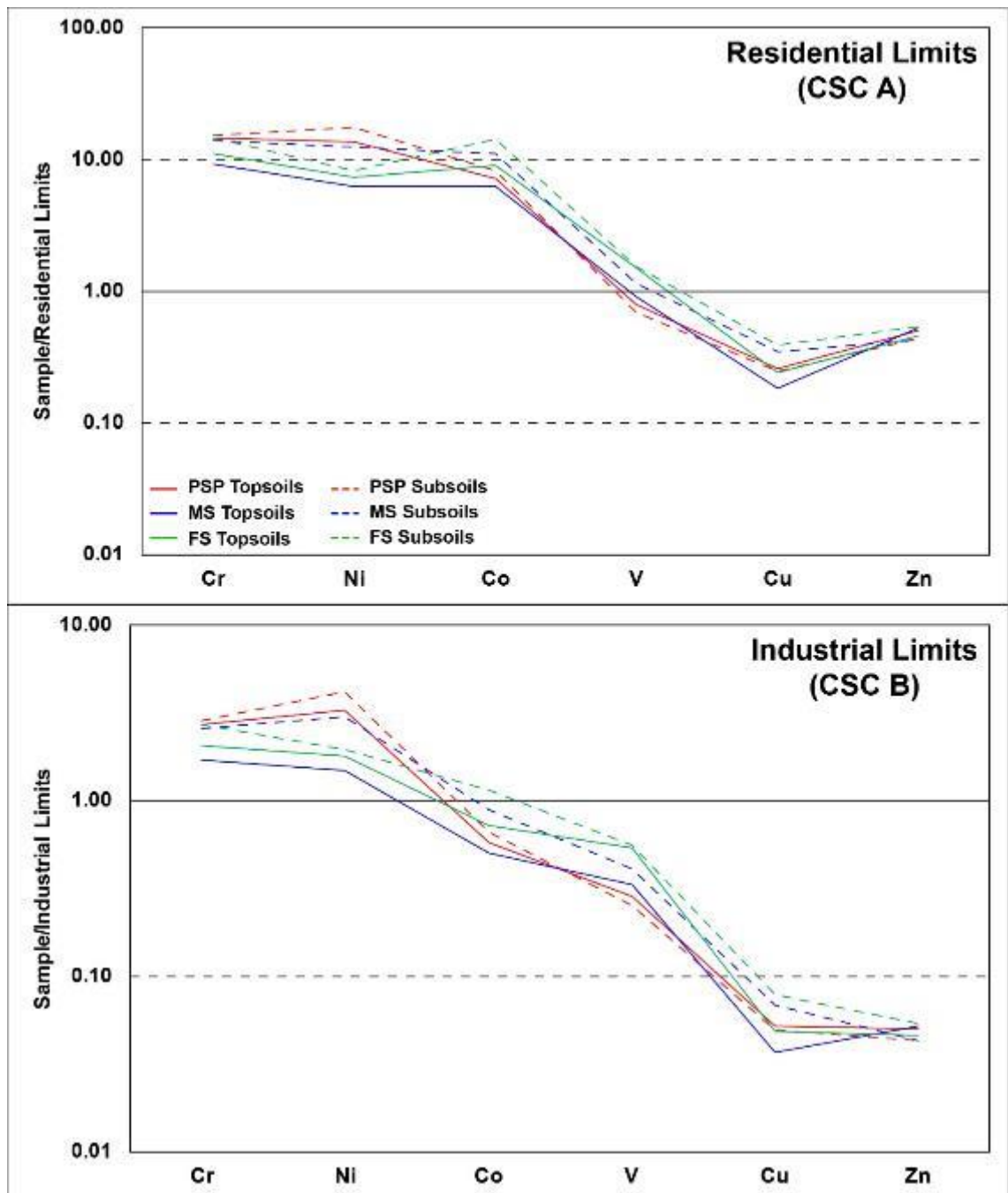


Fig. 6.15 PTEs concentration normalized to Italian threshold values for residential (A) and industrial (B) sites according to Italian law (D.M. 471/1999; D.Lgs 152/2006).

6.4. DISCUSSION

6.4.1. Major element variation and authigenic phases formation

Based on the combined chemical, mineralogical, crystallochemical, and granulometric data, all the investigated soils are very primitive soils characterized by weakly developed A and C horizons.

As expected in poor developed soils on ultramafic rocks (e.g., Alexander, 2007; Bonifacio et al., 2010; Kierczak et al., 2016), they preserve a clear mineralogical and chemical fingerprint of the original bedrocks.

The chemistry of the major elements shows a similar evolution for the three groups of investigated ultramafic soils.

Comparing to the bedrock chemistry, all the soils have a progressive and systematic decrease in Mg content and a progressive and systematic enrichment in Fe, and, subordinately in Si and Al (Fig. 6.11), in good agreement with the literature about the ultramafic soils in similar climatic condition (e.g., Cortesogno et al., 1979; Angelone et al., 1993; Venturelli et al., 1997; Bonifacio et al., 1997; D'Amico et al., 2008; Quantin et al., 2008; Caillaud et al., 2009; Kelepertizis et al., 2013; Bani et al., 2014; Baumeister et al., 2015; Kierczak et al., 2016). These variations are due to the low mobility of iron in contrast to the high mobility of Mg (Golightly, 2010) and in particular to the in situ reprecipitation of Fe-bearing authigenic minerals (mainly goethite). The relative enrichment of Al might be due either to the crystallization of Al-bearing clay minerals (i.e., illite and illite/smectite mixed layer clay) or to the enrichment in residual chlorite.

These general variations can be better explained considering the chemical and mineralogical variations observed along the soil profiles, from the bedrock toward topsoil.

In all the bedrock type Fe significantly increase toward the topsoil. This behavior is consistent with both the high weathering resistance of the spinel-group minerals (that tend to remain as residual minerals in the profile; Fig. 6.8 and Table 6.1) and the progressive precipitation of authigenic Fe-oxides, Fe-oxyhydroxides, Fe-rich amorphous phases and Fe-rich clay-oxide mixtures (i.e. iddingsitic mixtures), particularly in the subsoil and topsoil horizons (Hseu, 2006; Chardot et al., 2007; Hseu et al., 2007; Chon et al., 2008; Ho et al., 2013).

The most important Mg-bearing minerals in the bedrocks are olivine (PSP), pyroxenes (PSP and MS) and serpentine (PSP, MS, and FS). Olivine and pyroxenes have a much lower weathering resistance with respect to serpentines (Quantin et al., 2008; Kelepertizis et al., 2013; Bucher and Grapes, 2011; Bucher et al., 2015), the last representing the most common Mg-bearing residual phases in the soil skeleton clasts (Table 6.1). Nevertheless, also serpentine minerals evidence a progressive decrease from the saprolitic zone toward the topsoil (Fig.

6.8). The presence of serpentine minerals in the clay fraction (in particular in PSP soils; Fig 6.8) is mainly due to residual chrysotile fibers.

The significant enrichment of Al toward the topsoil is mainly due to the formation of the authigenic clay minerals (Angelone et al., 1993; Lee et al., 2003; Caillaud et al., 2004, 2009; Kierczak et al., 2007; Nguyen-Thanh et al., 2017) which are mainly represented by smectite, illite, illite/smectite mixed-layer clay, and, subordinately, vermiculite. Part of Al in MS and FS can be also present either in residual or new formed chlorites.

Moreover, the possibility of a minor presence of allochthonous materials in the superficial horizons cannot be excluded even though it was supposed that samples in the profile are not disturbed by external activities.

6.4.2. PTEs behavior along soil profiles

The presence and distribution of PTEs within the studied soils are typical of the ultramafic soils, which are commonly characterized by high concentrations of Cr, Ni, and Co, and subordinate but environmentally significant concentration of V, Cu, and Zn (e.g., Wells, 1960; Cortesogno et al., 1979; Bonifacio et al., 1997; Venturelli et al., 1997; Shallari et al., 1998; Burt et al., 2001; Oze et al., 2004a,b; Alexander et al., 2007; D'Amico et al., 2008; Caillaud et al., 2009; Cheng et al., 2009; Alloway, 2010; Marescotti et al., 2014; Tashakor et al., 2014).

The different behavior of PTEs along the studied soil profiles (see 6.3.6 and Fig. 6.14), is due both to the different weatherability of the primary minerals and to the relative mobility of the different metals involved in the pedogenetic processes. Moreover, the new forming authigenic phases can represent a permanent or transient trap for PTEs thus playing an important role in controlling their mobility (Sidhu et al., 1978, 1980; Chittleborough et al., 1984; Quantin et al., 2002).

Along the soil profile Ni concentrations significantly increase from the bedrock to the saprolitic horizons and then slightly decrease toward the surface. This trend is in agreement to what highlighted by Bonifacio et al. (2010) in a study on profiles of ultramafic soils of the lower Susa Valley (NW Italy).

This behavior is commonly observed in soil formed in similar pedological environments (Caillaud et al., 2009; Kelepertizis et al., 2013) but is also consistent with the tropical and subtropical environments where saprolitic "Ni-

deposits dominated by Ni-rich clay minerals" (e.g., Villanova-de-Benavent et al., 2013) forms in the lower part of the soil profile.

In the clay minerals (mainly smectites), Ni (up to 4 wt%) can be present both as an element absorbed in the interlayer and as a substitute for Fe²⁺ in octahedral sites (Villanova-de-Benavent et al., 2013). The Fe-oxide s.s. (and subordinate the Mn- and Al-oxides) tend to incorporate and/or adsorb non-negligible concentration of Ni (up to 12wt%) and subordinate Co (Gerth, 2005). In general, Goethite can incorporate much higher concentrations (up to 5 wt%) than hematite (Beukes et al., 2000; Elias, 2002).

Although the Co is present lower concentrations than Ni, it shows a similar behavior, being contained in the same mineralogical phases (as also highlighted by other authors Amir and Pineau, 2000; Cailloud et al., 2009; Tashakor et al. 2014).

Cr behavior along the soil profile is mostly correlated to the nature of the bedrocks. In PSP soil, Cr has a progressive enrichment from the bedrock to the topsoil because the most important Cr-bearing minerals are represented by spinel-group minerals (mainly magnetite and Cr-magnetite) and chlorite that are unaltered or slightly altered along the soil profile, even in the most superficial layers (Fig. 6.14).

In MS and FS soils Cr progressively decrease from the saprolite toward the topsoil. The most abundant Cr-rich mineral is magnetite (up to 35000 ppm ppm). In these soils. On the basis of the mineralogical results, this progressive depletion is mostly due to the significant alteration of magnetite in the lower part of the soil profile (saprolite and subsoils). Due to the low mobility of Cr in these conditions (Cheng et al., 2011; Kelepertizis et al., 2013) most of the new forming Cr-bearing minerals (goethite, hematite and clay minerals) appear to be concentrated in the saprolitic horizons and subordinately in the subsoils.

In summary, the critical PTEs concentrations and variation in the studied ultramafic soil profiles are linked both to the primary minerals, inherited by bedrocks, and to the stable authigenic products (Fe-oxides and oxyhydroxides and clay minerals). Considering the high stability of goethite, hematite and clay minerals in supergenic environment, it is evident that this mineral species are effective and often permanent traps for the most important PTEs of ultramafic soils and bedrocks, thus reducing its bioavailability.

6.4.3. Environmental concerns

The chemical dataset highlight that the concentration of Cr, Ni, and subordinately Co always exceed (up to one order of magnitude) the residential and industrial threshold values (CSC) according to Italian law (Fig. 6.15; D.M. 471/1999; D.Lgs 152/2006). Other detected elements of environmental concern (V, Cu, Zn, As, and Pb) even if present are generally below these limits.

In the ultramafic soils characterized by high concentrations in PTEs, it is not easy to discern whether these PTEs are completely related to geogenic sources or if they can be related to anthropogenic contamination.

In order to verify the potential contamination from anthropic sources, different environmental indexes have been proposed in literature (Kierczak et al., 2007; Lorito, 2010; Galan et al., 2014 and reference therein). In general, these indexes are based on a comparison between the element concentrations in the topsoil and in the subsoil. The PTEs concentrations determined in subsoil at about 50 cm of depth can considered as a "*geochemical background value*" since it has been demonstrated that may be considered unpolluted by supergenic anthropogenic sources (Huisman et al., 1997; Galan et al., 2014).

In this thesis, the Geoaccumulation Index (I_{geo}), Top Enrichment Factor (TEF), and the Geochemical Change (GC) have been used.

Geoaccumulation Index (I_{geo})

The Geoaccumulation index (I_{geo}) is obtained from the following formula (Müller, 1969; Förstner & Müller, 1981; Keshav Krishna et al., 2012; Galan et al., 2014):

$$I_{geo} = \log_2 C_n / (1.5 * B_n)$$

where:

C_n = element concentration in the topsoil

B_n = element concentration in the subsoil

1.5 = correction factor

Seven classes of contamination are distinguished on the basis of the different values assumed by the I_{geo} (Table 6.4).

I_{geo}	Soil Quality
<0	not contaminated
0-1	from not to moderate contaminated
1-2	moderate contaminated
2-3	from moderate to high contaminated
3-4	high contaminated
4-5	from high to extreme contaminated
>5	extreme contaminated

Table 6.4 Geoaccumulation Index (I_{geo}) classification.

All the investigated soils show I_{geo} close to 0 (Table 6.5), with the exception of As in MS soil (1.3) and PSP (0.6) and subordinately Pb. Considering that these elements are present in very low amounts in the studied bedrocks and subsoils, their superficial enrichment is presumably related to anthropic inputs.

I_{geo}	V	Cr	Co	Ni	Cu	Zn	As	Pb
FS	0.034	0.003	0.018	0.007	0.069	0.051	0.000	0.087
MS	0.041	0.003	0.021	0.004	0.072	0.066	1.333	0.145
PSP	0.065	0.003	0.029	0.003	0.111	0.064	0.600	0.292

Table 6.5 Geoaccumulation Index (I_{geo}) classification of the investigated soils

Top Enrichment Factor (TEF)

The Top Enrichment Factor (TEF) is defined by Colbourn and Thornton (1978) as:

$$TEF = C_t / C_s$$

where:

C_t = element concentration in the topsoil

C_s = element concentration in the subsoil

Three classes of contamination are distinguished on the basis of the different values assumed by the TEF (Table 6.6).

TEF	Soil Quality
≤ 1	subsoil enrichment (lithogenic element origin)
1-3	topsoil enrichment with possible anthropic contribution
>3	anthropogenic contamination

Table 6.6 Geoaccumulation Index (I_{geo}) classification.

All the investigated soils show the TEF minor or close to 1 for the majority of the PTEs (Fig. 6.16), with general higher value in PSP soils respect to serpentine soil s.s. (MS and FS). Also considering TEF the As and Pb possible anthropogenic contamination is confirmed.

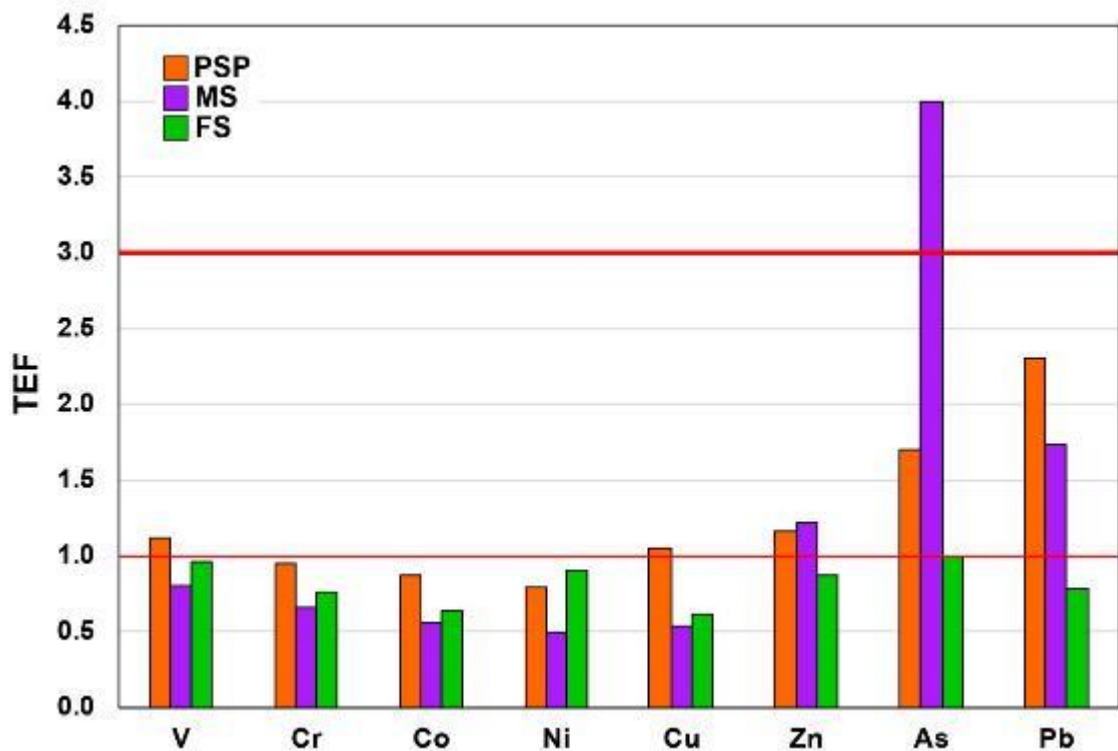


Fig. 6.16 Top enrichment factor (TEF) values of PTEs in the three ultramafic soil groups

Geochemical changes (GC)

Unlike the other two indices, the *geochemical changes (GC)* consider the variations of elements between the bedrock and the soil horizon. The GC of bulk soil and for each soil horizon relative to the rock was determinate as follows (Kierczak et al., 2007; Horen et al., 2014):

$$GC = [(S-R)*100]/R$$

where:

S = element concentration in the soil

R = element concentration in the rock

GC values higher than 0 indicate an enrichment of selected element in soil with respect to the bedrock, while GC values lower than 0 indicate its impoverishment. Also, in this case only Pb and As show GC value up to 1000 (Table 6.7 and Fig. 6.17)

Bedrock	GC	V	Cr	Co	Ni	Cu	Zn	As	Pb
PSP	Topsoil/Bedrock	86	70	76	-35	97	73	1515	2266
	Subsoil/Bedrock	66	79	101	-18	88	49	852	924
	Soil/Bedrock	76	74	88	-27	92	61	1184	1595
MS	Topsoil/Bedrock	148	-48	-37	-59	-23	93	307	2995
	Subsoil/Bedrock	117	-22	12	-18	44	57	-76	1686
	Soil/Bedrock	133	-35	-12	-38	10	75	115	2340
FS	Topsoil/Bedrock	302	-11	50	-34	-10	85	-58	4336
	Subsoil/Bedrock	317	17	137	-27	46	113	-58	5539
	Soil/Bedrock	310	3	93	-30	18	99	-58	4938

Table 6.7 Geochemical change value of the investigated soil.

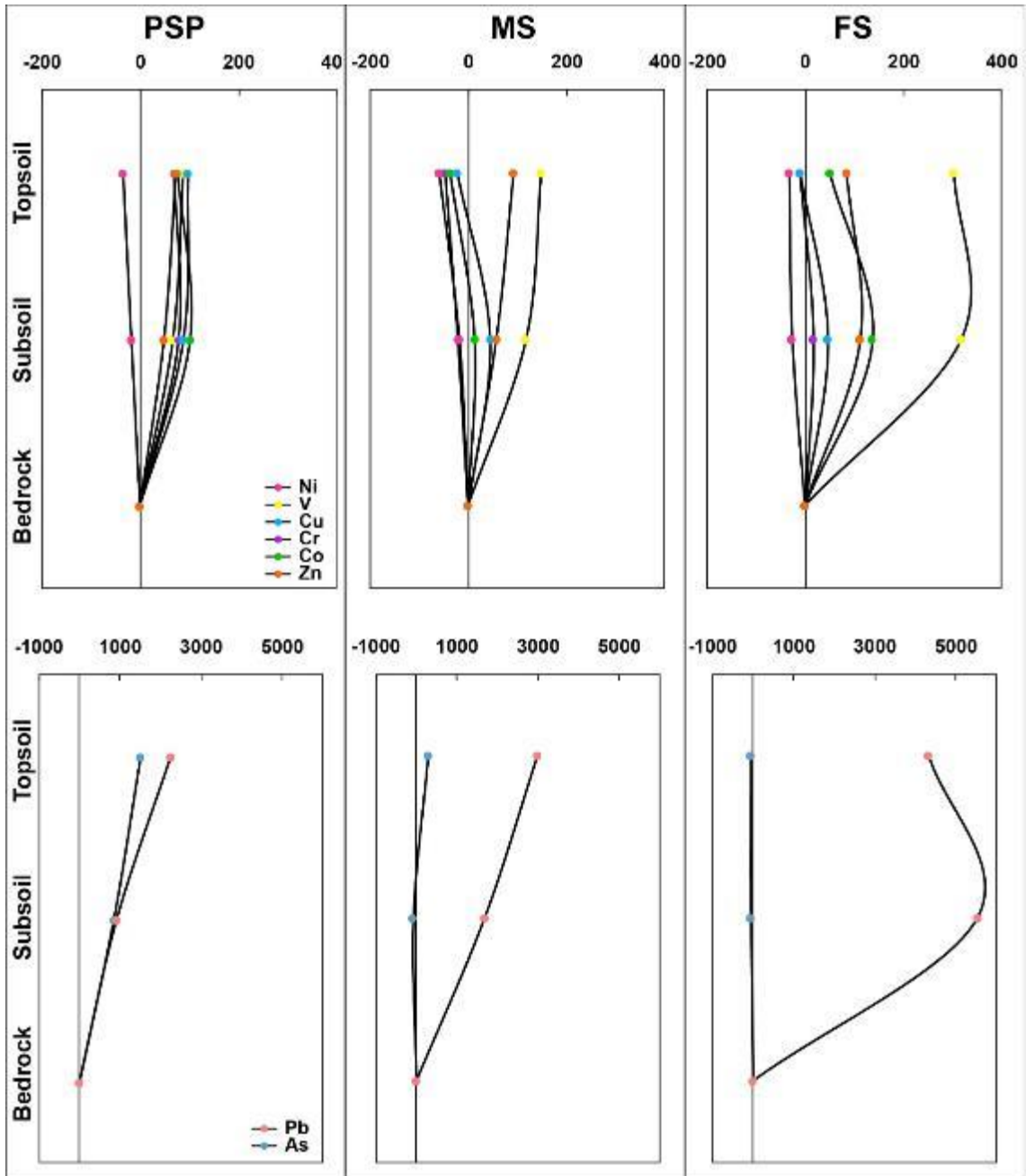


Fig. 6.17 GC value along the soil profile

In conclusion, even if most of the PTEs concentrations are higher than the law limits, the mineralogical, chemical, crystal-chemical framework, combined with the calculated environmental indices, shows that PTEs, with the exception of As and Pb, are related to geogenic inputs.

6.5. CONCLUSION

In this study, we have analyzed the behavior of Ni, Cr, Co, and other PTEs in ultramafic soil profiles deriving from a variety of bedrocks, from partially serpentinized lherzolites (PSP) through massive serpentinites (MS) to foliated serpentinites (FS).

All the investigated ultramafic soils soil profiles are weakly developed and vary in thickness from 35 to 80 cm. In particular all the soil profile is characterized, from the bedrock toward the topsoil, by a thick saprolitic zone (up to 50 cm) with a gradual transition to the C horizon. The C horizon grade progressively to the A horizon that is generally less developed. The O horizon, when present, is very thin (up to 5-10 cm; Fig. 6.3).

In general, in all the soils related to the three bedrock groups, the mineralogy of the skeleton (sandy and silty fractions) is closely related to bedrock mineralogy as expected for primitive A-C soils (in order of abundance: antigorite, chlorite, spinel-group minerals, pyroxenes, authigenic phases, quartz, olivine, and tremolite). A general trend observed in the three groups is the progressive increase of the clay fractions from the subsoils toward the topsoils. The clay fraction (that represents only the 5-10 % of the soil constituents) is mainly composed by amorphous or low-crystalline Fe-oxyhydroxides, serpentines, smectite and illite/smectite mixed-layer clay, and clinocllore.

The presence and distribution of PTEs within the studied soils are typical of the ultramafic soils with very high concentrations of Cr, Ni, and Co, and subordinate but environmentally significant concentration of V, Cu, and Zn.

The PTEs considered in this work are linked both to primary and authigenic minerals. In the primary minerals they are mainly present in serpentines, spinel-group minerals, pyroxenes, olivines, chlorites, tremolite, talc, ilmenite. Both the main authigenic minerals are able to scavenge significant amounts of Cr, Ni, and Co.

References

- Abollino, O., Giacomino, A., Malandrino, M., and Mentasti, E. (2008). Interaction of metal ions with montmorillonite and vermiculite. *Applied Clay Science*, 38(3-4), 227-236.
- Albanese, S., Sadeghi, M., Lima, A., Cicchella, D., Dinelli, E., Valera, P., Falconi, M., Demetriades, A., De Vivo, B., and the GEMAS Project Team (2015). GEMAS: cobalt, Cr, Cu and Ni distribution in agricultural and grazing land soil of Europe. *Journal of geochemical exploration*, 154, 81-93
- Alexander, E.B. (1988). Rates of soil formation: implications for soil-loss tolerance. *Soil Sci*, 145(1), 37-45.
- Alexander E.B. (2004). Serpentine soil redness, differences among peridotite and serpentinite materials, Klamath Mountains, California. *International Geology Review*, 46, 754–764.
- Alexander E.B. (2007). Serpentine geoecology of western North America: geology, soils, and vegetation. Oxford University Press, New York.
- Alexander, E.B. (2009). Serpentine geoecology of the eastern and southeastern margins of North America. *Northeastern Naturalist*, 16(sp5), 223-252.
- Alexander E.B. and DuShey J. (2011). Topographic and soil differences from peridotite to serpentinite. *Geomorphology* 135 (2011) 271–276.
- Alloway, B.J. (2010). Sources of heavy metals and metalloids in soils. In *Heavy metals in soils* (pp. 11-50). Springer, Dordrecht.
- Alves, S., Nabais, C., Gonçalves, M.D.L.S., and dos Santos, M.M.C. (2011). Nickel speciation in the xylem sap of the hyperaccumulator *Alyssum serpyllifolium* ssp. *lusitanicum* growing on serpentine soils of northeast Portugal. *Journal of plant physiology*, 168(15), 1715-1722.
- Amir, H., and Pineau, R. (2003). Release of Ni and Co by microbial activity in New Caledonian ultramafic soils. *Canadian Journal of microbiology*, 49(4), 288-293.
- Angelone, M., Vaselli, O., Bini, C., and Coradossi, N. (1993). Pedogeochemical evolution and trace elements availability to plants in ophiolitic soils. *Science of the total environment*, 129(3), 291-309.
- Antibachi, D., Kelepertzis, E., and Kelepertsis, A. (2012). Heavy metals in agricultural soils of the Mouriki-Thiva area (central Greece) and environmental impact implications. *Soil and Sediment Contamination: An International Journal*, 21(4), 434-450.
- Antić-Mladenović, S., Rinklebe, J., Frohne, T., Stärk, H.J., Wennrich, R., Tomić, Z., and Ličina, V. (2011). Impact of controlled redox conditions on nickel in a serpentine soil. *Journal of Soils and Sediments*, 11(3), 406-415.
- Baker, A.J.M., and Walker, P. (1989). Physiological responses of plants to heavy metals and the quantification of tolerance and toxicity. *Chemical Speciation and Bioavailability*, 1(1), 7-17.
- Bales, R.C., and Morgan, J.J. (1985). Dissolution kinetics of chrysotile at pH 7 to 10. *Geochimica et Cosmochimica Acta*, 49(11), 2281-2288.
- Bani, A., Echevarria, G., Zhang, X., Benizri, E., Laubie, B., Morel, J.L., and Simonnot, M.O. (2015). The effect of plant density in nickel-phytomining field experiments with *Alyssum murale* in Albania. *Australian Journal of Botany*, 63(2), 72-77.
- Baumeister, J.L., Hausrath, E.M, Olsen, A.A., Tschauner, O., Adcock, C.T. and Metcalf, R.V. (2015) Biogeochemical weathering of serpentinites: An examination of incipient dissolution affecting serpentine soil formation. *Applied Geochemistry* 54 (2015) 74–84.
- Beukes, J.P., Giesekke, E.W., and Elliott, W. (2000). Nickel retention by goethite and hematite. *Minerals Engineering*, 13(14-15), 1573-1579.
- Becquer, T., Quantin, C., Sicot, M., and Boudot, J.P. (2003). Chromium availability in ultramafic soils from New Caledonia. *Science of the Total Environment*, 301(1-3), 251-261.
- Becquer, T., Quantin, C., Rotte-Capet, S., Ghanbaja, J., Mustin, C., and Herbillion, A.J. (2006). Sources of trace metals in Ferralsols in New Caledonia. *European Journal of Soil Science*, 57(2), 200-213.

- Bergaya, F., and Lagaly, G. (2006). General introduction: clays, clay minerals, and clay science. *Developments in clay science*, 1, 1-18.
- Berre, A., Ducloux, J., and Dupuis, J. (1974). *Pédogénèse sur roches ultrabasiques en climat tempéré humide: les sols sur serpentinites du Limousin occidental*. *Science du sol. Bulletin de l'AFES*, 3, 135-146.
- Bogatyrev, K. P. (1958). Smolnitzi (smonitzi) of Albania. *Pochvovedenie*, 4, 14-22.
- Bonifacio, E., Zanini, E., Boero, V., and Franchini-Angela, M. (1997). Pedogenesis in a soil catena on serpentinite in north-western Italy. *Geoderma*, 75(1-2), 33-51.
- Bonifacio, E., Falsone, G., and Piazza, S. (2010). Linking Ni and Cr concentrations to soil mineralogy: does it help to assess metal contamination when the natural background is high? *Journal of Soils and Sediments*, 10(8), 1475-1486.
- Bucher, K., and Grapes, R. (2011). *Metamorphism of Ultramafic Rocks*. In *Petrogenesis of Metamorphic Rocks* (pp. 191-224). Springer, Berlin, Heidelberg.
- Bucher, K., Stober, I., and Müller-Sigmund, H. (2015). Weathering crusts on peridotite. *Contributions to Mineralogy and Petrology*, 169(5), 52.
- Bulmer, C.E., and Lavkulich, L.M. (1992). Pedogenic and geochemical processes of ultramafic soils along a climatic gradient in southwestern British Columbia. *Canadian Journal of Soil Science*, 74(2), 165-177.
- Burgess, J.L., Lev, S., Swan, C.M., and Szlavecz, K. (2009). Geologic and edaphic controls on a serpentine forest community. *Northeastern Naturalist*, 366-384.
- Burns, R.G., and Burns, V.M. (1977). *Mineralogy*. In *Elsevier Oceanography Series* (Vol. 15, pp. 185-248). Elsevier.
- Burt, R., Fillmore, M., Wilson, M.A., Gross, E.R., Langridge, R.W., and Lammers, D.A. (2001). Soil properties of selected pedons on ultramafic rocks in Klamath Mountains, Oregon. *Communications in Soil Science and Plant Analysis*, 32(13-14), 2145-2175.
- Butler, J.R. (1953). The geochemistry and mineralogy of rock weathering (1) The Lizard area, Cornwall. *Geochimica et Cosmochimica Acta*, 4(4), 157-178.
- Caillaud, J., Proust, D., Righi, D., and Martin, F. (2004). Fe-rich clays in a weathering profile developed from serpentinite. *Clays and Clay Minerals*, 52(6), 779-791.
- Caillaud J., Proust D., Righi D. (2006) weathering sequences of rock-forming minerals in a serpentinite: influence of microsystems on clay mineralogy. *Clays and Clay Minerals*, Vol. 54, No. 1, 87-100, 2006.
- Caillaud, J., Proust, D., Philippe, S., Fontaine, C., and Fialin, M. (2009). Trace metals distribution from a serpentinite weathering at the scales of the weathering profile and its related weathering microsystems and clay minerals. *Geoderma*, 149(3), 199-208.
- Chardot, V., Echevarria, G., Gury, M., Massoura, S., and Morel, J.L. (2007). Nickel bioavailability in an ultramafic toposequence in the Vosges Mountains (France). *Plant and Soil*, 293(1-2), 7-21.
- Cheng, C.H., Jien, S.H., Iizuka, Y., Tsai, H., Chang, Y.H., and Hseu, Z.Y. (2011). Pedogenic chromium and nickel partitioning in serpentine soils along a toposequence. *Soil Science Society of America Journal*, 75(2), 659-668.
- Cheng, C.H., Jien, S.H., Tsai, H., Chang, Y.H., Chen, Y.C., and Hseu, Z.Y. (2009). Geochemical element differentiation in serpentine soils from the ophiolite complexes, eastern Taiwan. *Soil Science*, 174(5), 283-291.
- Chittleborough, D.J., Oades, J.M., and Walker, P.H. (1984). Textural differentiation in chronosequences from eastern Australia, III. Evidence from elemental chemistry. *Geoderma*, 32(3), 227-248.
- Chon, C.M., Kim, J.G., Lee, G.H., and Kim, T.H. (2008). Influence of extractable soil manganese on oxidation capacity of different soils in Korea. *Environmental geology*, 55(4), 763-773.
- Colbourn, P., and Thornton, I. (1978). Lead pollution in agricultural soils. *Journal of Soil Science*, 29(4), 513-526.
- Cornell, R.M., and Schwertmann, U. (2003). *The iron oxides: structure, properties, reactions, occurrences and uses*. John Wiley & Sons.

- Cortesogno, L., Mazzucotelli, A., Vannucci, R. (1979) Alcuni esempi di pedogenesi su rocce ultrafemiche in clima mediterraneo. *Ofioliti* 4:295–312.
- D'Amico, M., Julitta, F., Previtali, F., and Cantelli, D. (2008). Podzolization over ophiolitic materials in the western Alps (Natural Park of Mont Avic, Aosta Valley, Italy). *Geoderma*, 146(1-2), 129-137.
- Darnley, A.G., Bjorklund, A., Bolviken, B., Gustavsson, N., Koval, P.V., Steenfelt, A., and Xuejing, X. (1995). A global geochemical database. Recommendations for international geochemical mapping. Final report of IGCP project, 259.
- Decreto Legislativo 3/04/2006 n° 152 "Norme in materia ambientale". G.U. 88. 14/04/2006.
- Decreto Ministeriale 25/10/1999 n° 471 "Regolamento recante criteri, procedure e modalità per la messa in sicurezza, la bonifica e il ripristino ambientale dei siti inquinati, ai sensi dell'articolo 17 del decreto legislativo 5 febbraio 1997, n. 22", e successive modificazioni e integrazioni. G.U. 293, 15/12/1999.
- Delvigne, J.E. (Eds. 1998). Atlas of micromorphology of mineral alteration and weathering (No. 549 A5).
- Dublet, G., Juillot, F., Morin, G., Fritsch, E., Fandeur, D., Ona-Nguema, G., and Brown Jr, G. E. (2012). Ni speciation in a New Caledonian lateritic regolith: A quantitative X-ray absorption spectroscopy investigation. *Geochimica et Cosmochimica Acta*, 95, 119-133.
- Ducloux, J., Meunier, A., and Velde, B. (1976). Smectite, chlorite and a regular interlayered chlorite-vermiculite in soils developed on a small serpentinite body, Massif Central, France. *Clay Minerals*, 11(2), 121-135.
- Echevarria, G. (2018). Genesis and behavior of ultramafic soils and consequences for nickel biogeochemistry. In *Agromining: Farming for Metals* (pp. 135-156). Springer, Cham.
- Elias, M. (2002). Nickel laterite deposits-geological overview, resources and exploitation. Giant ore deposits: Characteristics, genesis and exploration. CODES Special Publication, 4, 205-220.
- Estrade, N., Cloquet, C., Echevarria, G., Sterckeman, T., Deng, T., Tang, Y., and Morel, J.L. (2015). Weathering and vegetation controls on nickel isotope fractionation in surface ultramafic environments (Albania). *Earth and Planetary Science Letters*, 423, 24-35.
- Fandeur, D., Juillot, F., Morin, G., Olivi, L., Cognigni, A., Ambrosi, J.P., Guyot, F., and Fritsch, E. (2009). Synchrotron-based speciation of chromium in an Oxisol from New Caledonia: Importance of secondary Fe-oxyhydroxides. *American Mineralogist*, 94(5-6), 710-719.
- Folk, R.L. (1954). The distinction between grain size and mineral composition in sedimentary-rock nomenclature. *The Journal of Geology*, 62(4), 344-359.
- Förstner, U., and Müller, G. (1981). Concentrations of heavy metals and polycyclic aromatic hydrocarbons in river sediments: geochemical background, man's influence and environmental impact. *GeoJournal*, 5(5), 417.
- Francis, A.J., and Dodge, C.J. (1990). Anaerobic microbial remobilization of toxic metals coprecipitated with iron oxide. *Environmental Science & Technology*, 24(3), 373-378.
- Galán, E., González, I., Romero, A., and Aparicio, P. (2014). A methodological approach to estimate the geogenic contribution in soils potentially polluted by trace elements. Application to a case study. *Journal of soils and sediments*, 14(4), 810-818.
- Garnier, J., Quantin, C., Martins, E.S., and Becquer, T. (2006). Solid speciation and availability of chromium in ultramafic soils from Niquelândia, Brazil. *Journal of Geochemical Exploration*, 88(1-3), 206-209.
- Garnier J., Quantin C., Guimarães E., Garg V.K., Martins E.S., Becquer T. (2009) Understanding the genesis of ultramafic soils and catena dynamics in Niquelândia, Brazil. *Geoderma* 151 (2009) 204–214.
- Gasser, U.G., Juchler, S.J., Sticher, H., and Hobson, W.A. (1995). The fate of chromium and nickel in subalpine soils derived from serpentinite. *Canadian Journal of Soil Science*, 75(2), 187-195.
- Gerth, J. (2005). Effects of crystal modification on the binding of trace metals and arsenate by goethite (7 pp). *Journal of Soils and Sediments*, 5(1), 30-36.

- Golightly, J.P., and Arancibia, O.N. (1979). The chemical composition and infrared spectrum of nickel-and iron-substituted serpentine from a nickeliferous laterite profile, Soroako, Indonesia. *The Canadian Mineralogist*, 17(4), 719-728.
- Golightly, J.P. (2010). *Progress in understanding the evolution of nickel laterites: Society of Economic Geologists Special Publication 15*.
- Ho, C.P., Hseu, Z.Y., Iizuka, Y., and Jien, S.H. (2013). Chromium speciation associated with iron and manganese oxides in serpentine mine tailings. *Environmental Engineering Science*, 30(5), 241-247.
- Horen, H., Soubrand, M., Kierczak, J., Joussein, E., and Néel, C. (2014). Magnetic characterization of ferrichromite in soils developed on serpentinites under temperate climate. *Geoderma*, 235, 83-89.
- Holmes, E.P., Wilson, J., Schreier, H., and Lavkulich, L.M. (2012). Processes affecting surface and chemical properties of chrysotile: Implications for reclamation of asbestos in the natural environment. *Canadian Journal of Soil Science*, 92(1), 229-242.
- Hseu, Z.Y. (2006). Concentration and distribution of chromium and nickel fractions along a serpentinitic toposequence. *Soil Science*, 171(4), 341-353.
- Hseu, Z.Y., Tsai, H., Hsi, H.C., and Chen, Y.C. (2007). Weathering sequences of clay minerals in soils along a serpentinitic toposequence. *Clays and Clay Minerals*, 55(4), 389-401.
- Huisman, D.J., Vermeulen, F.J.H., Baker, J., Veldkamp, A., Kroonenberg, S.B., and Klaver, G.T. (1997). A geological interpretation of heavy metal concentrations in soils and sediments in the southern Netherlands. *Journal of Geochemical Exploration*, 59(3), 163-174.
- Istok, J.D., and Harward, M.E. (1982). Influence of Soil Moisture on Smectite Formation in Soils Derived from Serpentinite 1. *Soil Science Society of America Journal*, 46(5), 1106-1108.
- IUSS Working Group WRB. (2015). *World Reference Base for Soil Resources 2014, update 2015 International soil classification system for naming soils and creating legends for soil maps. World Soil Resources Reports No. 106*, 192.
- Kabata-Pendias, A. (2011). *Trace Elements in Soils and Plants*. CRC Press, Taylor and Francis Group.
- Kelepertzis, E., Galanos, E., and Mitsis, I. (2013). Origin, mineral speciation and geochemical baseline mapping of Ni and Cr in agricultural topsoils of Thiva valley (central Greece). *Journal of Geochemical Exploration*, 125, 56-68.
- Kierczak J., Neel C., Bril H., Puziewicz J. (2007) Effect of mineralogy and pedoclimatic variations on Ni and Cr distribution in serpentine soils under temperate climate. *Geoderma* 142 (2007) 165–177.
- Kierczak J., Neel C., Aleksander-Kwaterczak U., Helios-Rybicka E., Bril H., Puziewicz J. (2008) Solid speciation and mobility of potentially toxic elements from natural and contaminated soils: A combined approach. *Chemosphere* 73 (2008) 776–784.
- Kierczak J., Pędziwiatr A., Waroszewski J. and Modelska M. (2016) Mobility of Ni, Cr, and Co in serpentine soils derived on various ultrabasic bedrocks under temperate climate. *Geoderma* 268 (2016) 78–91.
- Kim, J.G., Dixon, J.B., Chusuei, C.C., and Deng, Y. (2002). Oxidation of chromium (III) to (VI) by manganese oxides. *Soil Science Society of America Journal*, 66(1), 306-315.
- Kimpe, C.D., and Zizka, J. (1973). Weathering and clay formation in a dunite deposit at Asbestos. *Canadian Journal of Earth Sciences*, 10(10), 1533-1540.
- Kirkman, J.H. (1975). Clay mineralogy of some tephra beds of Rotorua area, North Island, New Zealand. *Clay Minerals*, 10(6), 437-449.
- Krishna, A.K., Mohan, K.R., Murthy, N.N., Periasamy, V., Bipinkumar, G., Manohar, K., and Rao, S S. (2013). Assessment of heavy metal contamination in soils around chromite mining areas, Nuggihalli, Karnataka, India. *Environmental earth sciences*, 70(2), 699-708.
- Lee, B.D., Graham, R.C., Laurent, T.E., Amrhein, C., and Creasy, R.M. (2001). Spatial distributions of soil chemical conditions in a serpentinitic wetland and surrounding landscape. *Soil Science Society of America Journal*, 65(4), 1183-1196.

- Lee, B.D., Sears, S.K., Graham, R.C., Amrhein, C., and Vali, H. (2003). Secondary mineral genesis from chlorite and serpentine in an ultramafic soil toposequence. *Soil Science Society of America Journal*, 67(4), 1309-1317.
- Lee, B.D., Graham, R.C., Laurent, T.E., and Amrhein, C. (2004). Pedogenesis in a wetland meadow and surrounding serpentinitic landslide terrain, northern California, USA. *Geoderma*, 118(3-4), 303-320.
- Lessovaia, S., Polekhovskiy, Y., and Pogozhev, E. (2010). Soil formation from ultrabasic rocks in bioclimatic conditions of mountainous tundra (the Polar Urals, Russia): Mineralogical aspects. In *Proceedings of the 19th World Congress of Soil Science, Soil Solutions for a Changing World*, Aug (pp. 1-6).
- Lessovaia, S. N., Dultz, S., Plötze, M., Andreeva, N., Polekhovskiy, Y., Filimonov, A., and Momotova, O. (2016b). Soil development on basic and ultrabasic rocks in cold environments of Russia traced by mineralogical composition and pore space characteristics. *Catena*, 137, 596-604.
- Lessovaia, S.N., Goryachkin, S., Polekhovskiy, Y., Ershova, V., and Filimonov, A. (2016a). Abiotic and Biotic Processes of Mineral Weathering in Tundra Soils on Ultramafic and Mafic Rocks of the Polar Urals, Russia. In *Biogenic—Abiogenic Interactions in Natural and Anthropogenic Systems* (pp. 223-236). Springer, Cham.
- Lorito, S. (2010). Il monitoraggio suolo-pianta per la valutazione dell'inquinamento da metalli pesanti nell'ambiente urbano. Dottorato di ricerca in: *Culture erbacee. Genetica agraria, Sistemi Agroterritoriali Ciclo XXII*. Alma Mater Studiorum—Università di Bologna.
- Manceau, A., Schlegel, M.L., Musso, M., Sole, V.A., Gauthier, C., Petit, P.E., and Trolard, F. (2000). Crystal chemistry of trace elements in natural and synthetic goethite. *Geochimica et Cosmochimica Acta*, 64(21), 3643-3661.
- Marescotti P., Solimano M., Beccaris G., Scotti E., Crispini L., Poggi E., Brancucci M., Fornasaro S. (2014). La presenza naturale di metalli nei suoli: criticità operative e possibili soluzioni. *ECO*, vol. 29, p. 60-63
- Marsili, S., Roccotiello, E., Rellini, I., Giordani, P., Barberis, G., and Mariotti, M.G. (2009). Ecological studies on the serpentine endemic plant *Cerastium utriense* Barberis. *Northeastern Naturalist*, 405-421.
- Massoura, S.T., Echevarria, G., Becquer, T., Ghanbaja, J., Leclerc-Cessac, E., and Morel, J.L. (2006). Control of nickel availability by nickel-bearing minerals in natural and anthropogenic soils. *Geoderma*, 136(1-2), 28-37.
- McKenzie, R.M. (1977) *Manganese oxides and hydroxides. Minerals in Soil Environments*. Soil Science Society of America, Inc.; 181-93 51.
- Morrison J.M., Goldhaber M.B., Lee L, Holloway J.M., Wanty R.B., Wolf R.E. and Ranville J.F. (2009) A regional-scale study of chromium and nickel in soils of northern California, USA. *Appl Geochem* 24:1500–1511. doi: 10.1016/j.apgeochem.2009.04.027.
- Munsell, S.C.C. (2000). *Munsell color*. Grand Rapids, Michigan.
- Muller, G. (1969). Index of geoaccumulation in sediments of the Rhine River. *Geojournal*, 2, 108-118.
- Nguyen-Thanh, L., Hoang-Minh, T., Herbert, H.J., Kasbohm, J., Lai, L.T., Nguyen, M.N., and Mählmann, R.F. (2017). Development of Fe-rich clay minerals in a weathering profile derived from serpentinitized ultramafic rock in Nui Nua massif, Vietnam. *Geoderma*, 308, 159-170.
- Nyamangara, J., and Mzezewa, J. (1999). The effect of long-term sewage sludge application on Zn, Cu, Ni and Pb levels in a clay loam soil under pasture grass in Zimbabwe. *Agriculture, ecosystems and environment*, 73(3), 199-204.
- Oze C., Fendorf S., Bird D.K., Coleman R.G. (2004a) Chromium geochemistry in serpentinitized ultramafic rocks and serpentine soils from the Franciscan complex of California. *Am J Sci* 304:67–101.
- Oze C., Fendorf S., Bird D.K., Coleman R.G. (2004b) Chromium Geochemistry of Serpentine Soils. *Int Geol Rev* 46:97–126. doi: 10.2747/0020-6814.46.2.97.

- Oze, C., Bird, D.K., and Fendorf, S. (2007). Genesis of hexavalent chromium from natural sources in soil and groundwater. *Proceedings of the National Academy of Sciences*, 104(16), 6544-6549.
- Pędziwiatr, A., Kierczak, J., Waroszewski, J., Ratié, G., Quantin, C., and Ponzevera, E. (2018). Rock-type control of Ni, Cr, and Co phytoavailability in ultramafic soils. *Plant and Soil*, 423(1-2), 339-362.
- Quantin, C., Becquer, T., and Berthelin, J. (2002). Mn-oxide: a major source of easily mobilisable Co and Ni under reducing conditions in New Caledonia Ferralsols. *Comptes Rendus Geoscience*, 334(4), 273-278.
- Quantin C., Ettler V., Garnier J., Sebek O. (2008) Sources and extractibility of chromium and nickel in soil profiles developed on Czech serpentinites. *C. R. Geoscience* 340 (2008) 872–882.
- Rabenhorst, M.C., Fanning, D.S., and Foss, J.E. (1982). Regularly interstratified chlorite/vermiculite in soils over meta-igneous mafic rocks in Maryland. *Clays and Clay Minerals*, 30(2), 156-158.
- Rajapaksha, A.U., Vithanage, M., Ok, Y.S., and Oze, C. (2013). Cr (VI) formation related to Cr (III)-muscovite and birnessite interactions in ultramafic environments. *Environmental science and technology*, 47(17), 9722-9729.
- Raous, S., Echevarria, G., Sterckeman, T., Hanna, K., Thomas, F., Martins, E.S., and Becquer, T. (2013). Potentially toxic metals in ultramafic mining materials: identification of the main bearing and reactive phases. *Geoderma*, 192, 111-119.
- Ratié, G., Jouvin, D., Garnier, J., Rouxel, O., Miska, S., Guimarães, E., Cruz Vieira, L., Sivry, Y., Zelano, I., Monterges-Palletier, E., Thil, F., and Quantin, C. (2015). Nickel isotope fractionation during tropical weathering of ultramafic rocks. *Chemical Geology*, 402, 68-76.
- Roberts, B.A., and Proctor, J. (Eds.). (1991). *The ecology of areas with serpentinized rocks: a world view* (Vol. 17). Springer Science and Business Media.
- Salminen, R., Tarvainen, T., Demetriades A., Duris M., Fordyce F.M., Gregorauskiene V., Kahelin H., Kivisilla J., Klaver G., Klein H., Larson J.O., Lis J., Locutura J., Marsina K., Mjartanova H., Mouvet C., O'Connor P., Odor L., Ottonello G., Paukola T., Plant J.A., Reimann C., Schermann O., Siewers U., Steenfelt A., Van der Sluys J., de Vivo B. & Williams L. (1998). FOREGS geochemical mapping field manual.
- Schreier, H. (1989). *Asbestos in the natural environment* (Vol. 37). Elsevier.
- Schreier, H., Omuetti, J.A., and Lavkulich, L.M. (1987). Weathering Processes of Asbestos-rich Serpentinic Sediments 1. *Soil Science Society of America Journal*, 51(4), 993-999.
- Schwertmann, U.T.R.M., and Taylor, R.M. (1989). Iron oxides. *Minerals in soil environments, (minerals in soil)*, 379-438.
- Shallari, S., Schwartz, C., Hasko, A., and Morel, J.L. (1998). Heavy metals in soils and plants of serpentine and industrial sites of Albania. *Science of the Total Environment*, 209(2-3), 133-142.
- Shirvani, M., Kalbasi, M., Shariatmadari, H., Nourbakhsh, F., and Najafi, B. (2006). Sorption–desorption of cadmium in aqueous palygorskite, sepiolite, and calcite suspensions: isotherm hysteresis. *Chemosphere*, 65(11), 2178-2184.
- Sidhu, P.S., Gilkes, R.J., and Posner, A.M. (1978). The synthesis and some properties of Co, Ni, Zn, Cu, Mn and Cd substituted magnetites. *Journal of Inorganic and Nuclear Chemistry*, 40(3), 429-435.
- Sidhu, P.S., Gilkes, R.J., and Posner, A.M. (1980). The Behavior of Co, Ni, Zn, Cu, Mn, and Cr in Magnetite during Alteration to Maghemite and Hematite 1. *Soil Science Society of America Journal*, 44(1), 135-138.
- Singh, B., and Gilkes, R.J. (1992). Properties and distribution of iron oxides and their association with minor elements in the soils of south-western Australia. *Journal of soil Science*, 43(1), 77-98.
- Shtiza, A., Swennen, R., and Tashko, A. (2005). Chromium and nickel distribution in soils, active river, overbank sediments and dust around the Burrel chromium smelter (Albania). *Journal of Geochemical Exploration*, 87(3), 92-108.
- Swindale, L.D. (1966). *A mineralogical study of soils derived from basic and ultrabasic rocks in New Zealand* (Vol. 435).

- Stoops, G., Marcelino, V., and Mees, F. (Eds.). (2010). *Interpretation of micromorphological features of soils and regoliths*. Elsevier.
- Tashakor, M., Yaacob, W.Z.W., Mohamad, H., and Ghani, A.A. (2014). Geochemical characteristics of serpentinite soils from Malaysia. *Malaysian Journal of Soil Science*, 18, 35-49.
- Tashakor, M., Hochwimmer, B., and Imanifard, S. (2015). Control of grain-size distribution of serpentinite soils on mineralogy and heavy metal concentration. *Asian Journal of Earth Sciences*, 8(2), 45.
- Ulven, O.I., Beinlich, A., Hövelmann, J., Austrheim, H., and Jamtveit, B. (2017). Subarctic physicochemical weathering of serpentinitized peridotite. *Earth and Planetary Science Letters*, 468, 11-26. USA. *Geoderma*, 118(3-4), 303-320.
- van der Ent, A., Cardace, D., Tibbett, M., and Echevarria, G. (2018). Ecological implications of pedogenesis and geochemistry of ultramafic soils in Kinabalu Park (Malaysia). *Catena*, 160, 154-169.
- Velde, B. (Ed.). (1995). *Origin and mineralogy of clays: clays and the environment*. Springer Science and Business Media.
- Veniale, F., and Van der Marel, H.W. (1963). An interstratified saponite-swelling chlorite mineral as a weathering product of lizardite rock from St. Margherita Staffora (Pavia Province), Italy.
- Venturelli, G., Contini, S., Bonazzi, A., and Mangia, A. (1997). Weathering of ultramafic rocks and element mobility at Mt. Prinzera, Northern Apennines, Italy. *Mineralogical Magazine*, 61(6), 765-778.
- Vepraskas, M.J., and Guertal, W.R. (1992). Morphological indicators of soil wetness. *International Soil Correlation Meeting (ICOM)(USA)*.
- Vepraskas, M.J., Teets, S.J., Richardson, J.L., and Tandarich, J.P. (1995). *Development of redoximorphic features in constructed wetland soils*. Chicago, IL: Wetlands Research Inc.
- Villanova-de-Benavent, C., Proenza, J.A., Galí, S., García-Casco, A., Tauler, E., Lewis, J.F., and Longo, F. (2014). Garnierites and garnierites: Textures, mineralogy and geochemistry of garnierites in the Falcondo Ni-laterite deposit, Dominican Republic. *Ore Geology Reviews*, 58, 91-109.
- Vithanage M., Rajapaksha A.U., Oze C, Rajakaruna N. and Dissanayake C.B. (2014) Metal release from serpentine soils in Sri Lanka. *Environ Monit Assess* 186:3415–3429. doi: 0.1007/s10661-014-3626-8.
- Wells, M.A., Ramanaidou, E.R., Verrall, M., and Tessarolo, C. (2009). Mineralogy and crystal chemistry of "garnierites" in the Goro lateritic nickel deposit, New Caledonia. *European Journal of Mineralogy*, 21(2), 467-483.
- Wells, N. (1960). Total elements in topsoils from igneous rocks: an extension of geochemistry 1. *Journal of Soil Science*, 11(2), 409-424.
- Whitney, D. L., & Evans, B. W. (2010). Abbreviations for names of rock-forming minerals. *American mineralogist*, 95(1), 185-187.
- Wildman, W.E., Jackson, M.L., and Whittig, L.D. (1968). Iron-Rich Montmorillonite Formation in Soils Derived from Serpentinite 1. *Soil Science Society of America Journal*, 32(6), 787-794.

GENERAL REMARKS

Conclusions

The main objective of this PhD thesis was to determinate the mineralogy and the chemistry of PTEs of ultramafic soil profiles from the Voltri Massif and to evaluate how lithological, textural, and structural properties of the ultramafic bedrock with various degree of serpentinization and deformation may affect the re-distribution and the fate of PTEs in the soils during pedogenesis, as well as to assess their environmental implications in the ecosystem.

The multidisciplinary and multiscale approach, used in this PhD thesis, has allowed to highlight a series of considerations that led to the following conclusions:

Rock

- 1) The studied rocks, that represent the bedrocks of the investigated soil profiles, were divided in three groups according to the degree of serpentinization and the style of deformation (partially serpentinized lherzolites, massive serpentinites, and foliated serpentinites).
- 2) In the studied rocks, Cr, Ni, and, subordinately, Co are invariably the PTEs with the highest concentrations; in addition, V, Cu, and Zn are generally found in high concentrations. The main factors controlling the PTEs distribution within the studied ultramafic rocks appeared to be the serpentinization degree and the deformation style and intensity which, in turn, strictly control the mineral assemblages and the mineral chemistry.
- 3) In the studied rocks, spinel-group minerals are the main source of the PTEs. Moreover, PTEs-bearing phases are also represented by the other rock-forming minerals (such as serpentines, olivines, pyroxenes, and chlorites) and some accessory phases (e.g., ilmenite and other oxides, sulfides).
- 4) The chemical composition of the spinel-group minerals in the studied rocks was investigated in relation to different textures, microstructures and various degree of serpentinization and deformation. At a general scale,

the PTEs variability is primarily related to the petrologic and tectonic evolution but, at a local scale, also the mineralogical, lithological, structural, and textural features correlated to the degree of serpentinization and/or deformation significantly influence PTEs distribution and concentration.

- 5) In the rocks, the spinel-group minerals occur with particular textural and microstructural features that can be grouped into three classes: i) spinel-group mineral porphyroclasts with various degree of recrystallization, scattered within partially serpentinized lherzolites and massive serpentinite; ii) spinel-group minerals within pseudomorphic and non-pseudomorphic textures; iii) spinel-group minerals re-oriented along the foliation.

Soil profiles

- 1) The studied ultramafic soil profiles vary in thickness from 35 to 80 cm and are characterized by weakly developed A and C horizons and a very thin O horizon (up to 5-10 cm).
- 2) In general, in all the soils related to the three bedrock groups, the mineralogy of the skeleton (sandy and silty fractions) is closely related to bedrock mineralogy as expected for primitive A-C soils (in order of abundance: antigorite, chlorite, spinel-group minerals, pyroxenes, authigenic phases, quartz, olivine, and tremolite). A general trend observed in the three groups is the progressive increase of the clay fractions from the subsoils toward the topsoils. The clay fraction is mainly composed by amorphous or low-crystalline Fe-oxyhydroxides, serpentines, smectite and illite/smectite mixed-layer clay, and clinochlore.
- 3) In the soils, more than 90% of the PTEs is represented by: Cr, Ni, Co, Cu, Zn, and V. Cr and Ni values have very variable concentrations over a wide range. Cr and Ni decrease according to serpentinization degree of bedrock. Co, Zn, and Cu do not show a clear correlation with bedrock serpentinization. V increase with the serpentinization of the bedrock.
- 4) The PTEs concentrations in the studied ultramafic soil profiles are linked both to the primary minerals, inherited by bedrocks (e.g., serpentines,

spinel-group minerals, pyroxenes, chlorites), and to their stable authigenic products (Fe-oxyhydroxides and clay minerals). The PTEs leached from the primary minerals is mainly scavenged by goethite, and subordinate by clay.

Environmental concerns

The results evidence that Cr, Ni, and, Co systematically exceed (up to one order of magnitude) the residential and industrial threshold values (CSC) according to Italian law (D.M. 471/1999; D.Lgs 152/2006) both in rocks and soils. Among the other elements, only V evidence concentration of environmental concern, since they are above the residential CSC in soils.

However, combining the mineralogical, chemical, crystal-chemical framework, combined with the calculated environmental indices, I have demonstrated that the critical PTEs concentrations in the studied ultramafic soil profiles have a geogenic origin and are linked both to the primary minerals, inherited by bedrocks, and to their stable authigenic products (Fe-oxyhydroxides and clay minerals). Considering the high stability of goethite, hematite and clay minerals in supergenic environment, it is evident that this mineral species are effective and often permanent traps for the most important PTEs of ultramafic soils and bedrocks, thus reducing its bioavailability.

The results of this study cast doubt on the only use of threshold limits for the environmental management and land use planning if not coupled with site-specific mineralogical and geological investigations in areas with a high natural geochemical background variation.

A study of this kind that combine the bulk chemistry of outcropping rocks and the relative soil profiles with their geological, structural, mineralogical, and crystallochemical data, can be also a useful tool in environmental concerns to determine the PTEs distribution, to evaluate their potential mobility and bioavailability as well as to discriminate the natural geochemical background from possible source of contamination.

This approach could be possibly extended to other soil types characterized by high metal loads as well as to anthropogenic contaminated soils.

Possible future developments

The research that has been undertaken for this thesis has highlighted a number of topics on which further research would be beneficial:

- 1) *Synchrotron XRF microanalysis or TEM-EDS analysis of the authigenic minerals*. This analysis can give a substantial contribution for a better identification and characterization of clay minerals and oxyhydroxides of environmental concern, because it is possible to obtain the mineral identification and perform accurate structural and crystallochemical characterization of submicron-sized minerals, even when they occur in complex assemblages.
- 2) *Physico-chemical soil parameters (pH, Eh, CEC, Organic content, electrical conductivity, color with spectrophotometer)*. The fate of PTEs can be also controlled by some other physicochemical and chemical soil properties such as pH, Eh, and organic matter content.
- 3) *Geostatistical analysis* can be a useful tool for the identification of the main factors controlling PTEs variability in the soils. Moreover, geostatistics (e.g., Principal Component Analysis, Cluster Analysis) will be used to construct regional distribution maps, which will be compared to the geographical, geological, and land use regional database using Geographical Information System (GIS) software.
- 4) Quantitative mineralogical data will be further used to perform *mass balance calculations* as well as to interpret and model the results of batch leaching experiments that will be conducted on the different soil fractions.
- 5) *Chemical analysis* on the three different granulometric fraction can better determine the control of particle size (that influenced the drainage condition) on concentration of PTEs in the soils.

APPENDIX A
Site Description

A1. BRIC GIPPONE (BG)

SITE DESCRIPTION


	Coordinate: 44°29.201N; 8°30.814E
	Province: Savona
	Town: Sassello
	Altitude: 575 m.a.s.l.
	Slope: 25°
	Slope orientation: S
	Land use: Road cut (SP 49)
Extension: 600 m ²	
Vegetation: chestnut, oak coppice wood	

Fig. 1 Satellite image of study area (in red box BG site)

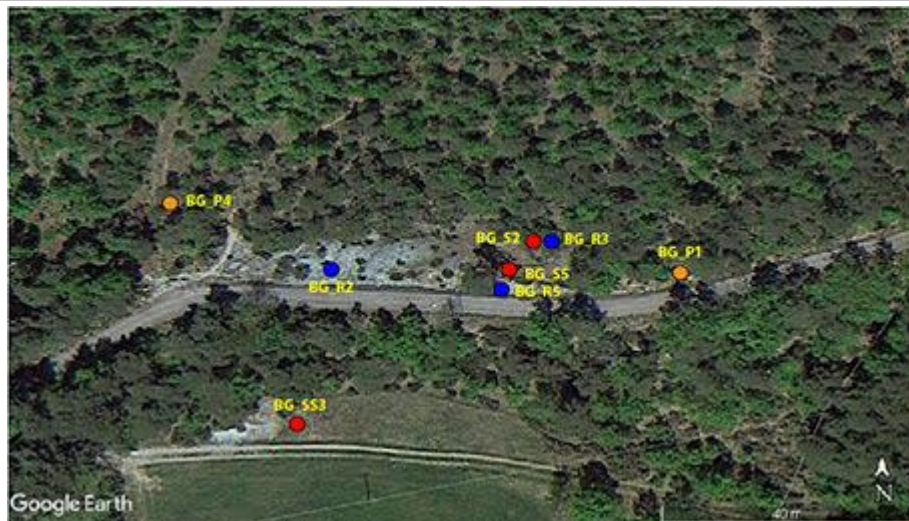


Fig. 2 Location of sampled profiles (orange), rocks (blue), and soils (red) in BG site (Google Earth ®)

Location

BG site is located in Bric Gippone locality, near Sassello village (SV – Italy), along the route SP 49, at 2.7 km from the towncentre. The outcrop covers a total area of about 600 m², extends in length, parallel to the road. The site is located near a landslide, recognizable for a trench under the road.



Fig. 3 Overview of Bric Gippone site

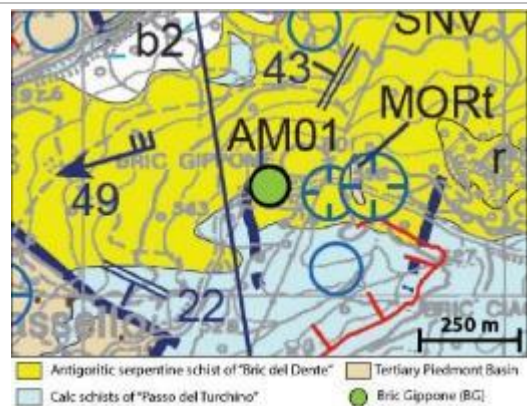


Fig. 4 Geological map of BG

Field evidences

Bric Gippone site is formed by serpentinites, which different degree of deformation (from massive to foliated, to serpentine schists). Massive serpentines are from centimetric to decametric fractured bodies with amygdale shape, surrounded by cataclastic to mylonitic serpentinites.

The rock, to outcrop scale, has no relevant physical or chemical alteration evidence, there is only not uniform yellow-reddish surface on massive serpentinites, due to oxidation of iron oxides. The soil deposit is planar shape; the front inclination is from sub-vertical to slightly tilted. Soil has a homogeneous structure and are not visible erosion evidence; in the detection period the soil it appeared moist.

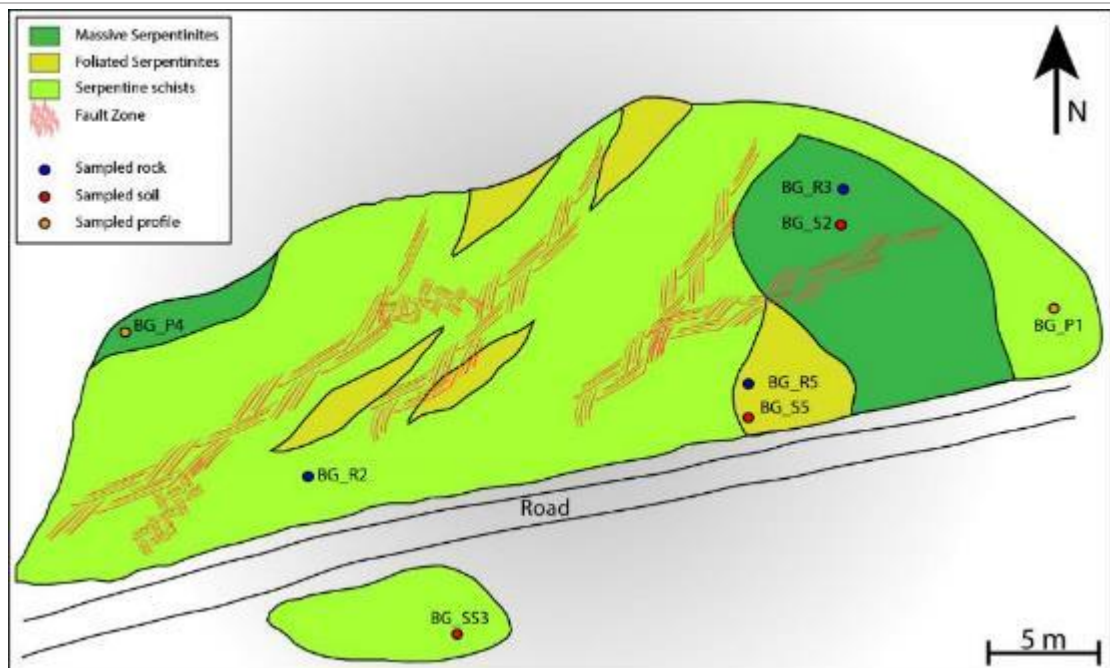


Fig. 5 Geological sketch of BG site with sample location.



Fig. 6 Outcrop of massive serpentinites



Fig. 7 Outcrop of foliated serpentinites

PROFILE & SAMPLING OF BRIC GIPPONE

PROFILE BG_P1

BG_P1 (0-100 cm) poorly developed profile with a reduced thickness of about 100 cm, homogeneous soil structure, grey-brown color with reddish oxidation patina.



Fig. 8 Overview of BG_P1 soil profile

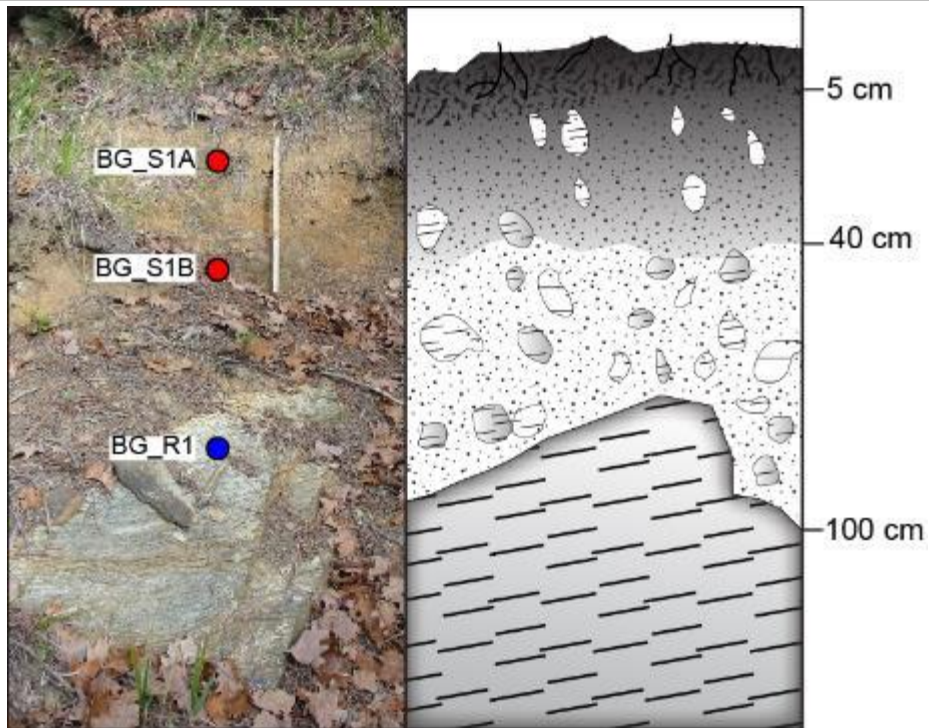


Fig. 9 BG_P1 soil profile and relative sketch

BG_S1A (5-40 cm): topsoil, dark yellowish brown (10YR 4/6), gravelly mud, damp, high organic fraction, with fine to medium roots and leaves. Granular soil structure, with rounded aggregates.

Depth: 5-40 cm

Thickness: 35 cm

Grain-shape: angular to rounded

Color: 10YR 4/6

Water: damp


Granulometry: gravelly mud





Fig. 10 Topsoil sample BG_S1A



Fig. 10a Thin section of soil skeleton

<p>BG_S1B (40-100 cm): subsoil, strong brown, gravelly mud, damp, minor organic fraction (millimetric roots). Abundant angular medium and coarse gravel (strongly weathered serpentinites, directly originated from the bedrock weathering). Clear smooth boundary with bedrock.</p>	<p>Depth: 40-100 cm</p>
	<p>Thickness: 60 cm</p>
	<p>Grain-shape: angular to rounded</p>
	<p>Color: 7.5YR 4/6</p>
	<p>Water: damp</p>
	<p>Granulometry: gravelly mud</p>
 <p><i>Fig. 11 Subsoil BG_S1B</i></p>	 <p><i>Fig. 11a Thin section of soil skeleton</i></p>

<p>BG_R1 (>100cm): foliated serpentinite, fine grained, dark green to brownish green. The main foliation is marked by from elongated to pseudo-fiber serpentine minerals, chlorites and micrograined magnetite. Sample surface is covered by reddish brown oxidation patina.</p>	
 <p><i>Fig. 12 Rock sample BG_R1</i></p>	<p>Rock: foliated serpentinite</p>
	<p>Texture: foliated</p>
	<p>Grain size: fine</p>
	<p>Minerals: serpentine, magnetite, chlorite</p>
	<p>Color: dark green</p>
	<p>Weathering: superficial oxidation patina</p>

<p style="text-align: center;">PROFILE BG_P4</p>	
<p>BG_P4 (0-60 cm): profile is poorly developed with a reduced thickness about 60 cm, homogeneous soil structure, gray-brown color with reddish oxidation patina. The topsoil is darker and reddish (10YR 4/3) than the subsoil (7.5YR 5/4). The BG_P4 soil has a greater gravel fraction than BG_P1. The trend in the increase of redness moving from the bottom to the top of the profile.</p>	 <p><i>Fig. 13 Overview of BG_P4 soil profile</i></p>

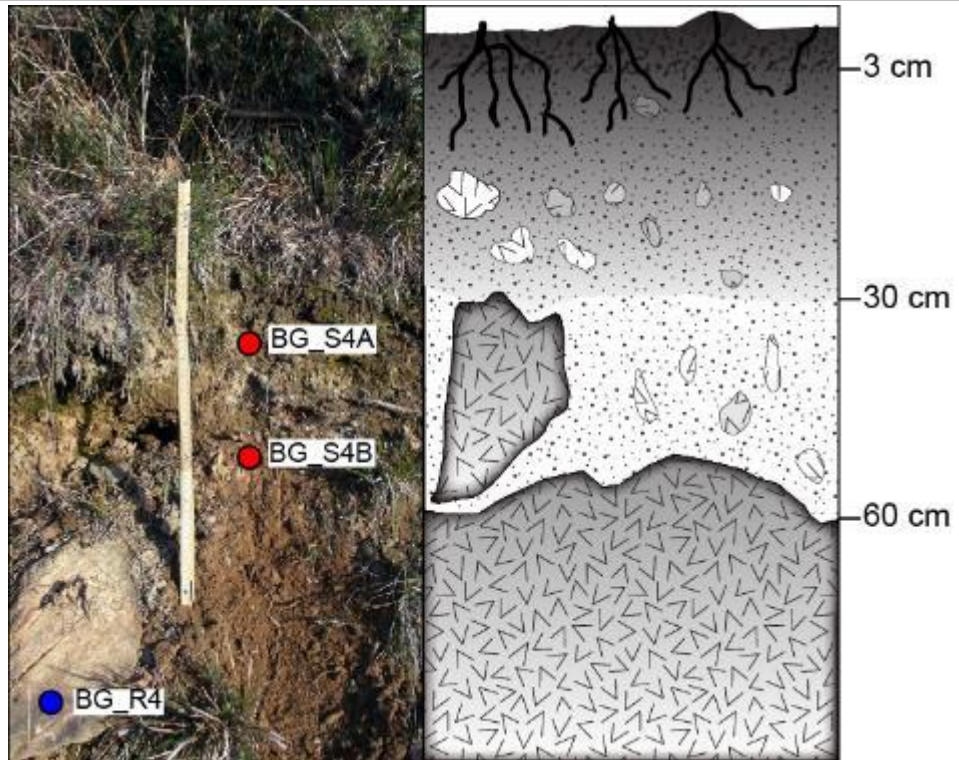


Fig. 14 BG_P4 soil profile and relative sketch

BG_S4A (3-30 cm): topsoil, brown (10YR 4/3), muddy gravel, wet, high organic fraction, with fine roots and leaves. Granular soil structure, with rounded aggregates.

Depth: 3-30 cm

Thickness: 27 cm

Grain-shape: angular

Color: 10YR 4/3

Water: wet

Granulometry: muddy gravel



Fig. 15 Topsoil sample BG_S4A



Fig. 15a Thin section of soil skeleton

BG_S4B (30-60 cm): subsoil, brown, muddy gravel, wet, minor organic fraction (mm roots). Abundant angular medium and coarse gravel (strongly weathered serpentinites, originated from the bedrock weathering). Clear smooth boundary with bedrock.

Depth: 30-60 cm

Thickness: 30 cm

Grain-shape: rounded

Color: 7.5YR 5/4

Water: wet

Granulometry: muddy gravel



Fig. 16 Subsoil sample BG_S4B



Fig. 16a Thin section of soil skeleton

BG_R4 (>60 cm): massive antigorite-serpentinite with weak foliation. Light greenish-gray, with reddish-brown oxidation patina.



Fig. 17 Rock sample BG_R4

Rock: massive serpentinites
Texture: weak foliation
Grain size: fine
Minerals: serpentine minerals, chlorite
Color: greenish-gray
Weathering: reddish-brown patina

PROFILE BG_P2

BG_P2 (0-70 cm) poorly developed profile with a reduced thickness of about 70 cm, homogeneous soil structure, orange-brown color with reddish oxidation patina.



Fig. 18 Overview of BG_P2 soil profile

BG_SS3 (10-70 cm): composite sample, light gray to dark brown, gravelly mud, damp, organic fraction is 30 wt% (roots and leaves). Abundant angular to rounded medium and coarse gravel (strongly weathered serpentinites, directly originated from the weathering of bedrock). Bedrock contact is not visible.



Fig. 19 Soil sample BG_SS3

Depth: 10-70 cm
Thickness: 60 cm
Grain-shape: rounded to elongated
Color: 2.5YR5/2 moist, 5YR7/2 dry
Water: damp
Granulometry: gravelly mud

BG_R2 (>10 cm): high foliated serpentinite (pencil cleavage), fine grained, with millimetric sub-rounded dark-brown oxide (presumably magnetite). No superficial alteration evidences. Green-gray to gray-blue. Fracturing subparallel to foliation, with millimetric opening and filled by whitish "soft" mineral (presumably talc).

	Rock: foliated serpentinite
	Texture: high foliated
	Grain size: fine
	Minerals: serpentine, magnetite, talc (?)
	Color: green-gray to gray-blue
	Weathering: absent

Fig. 20 Rock sample BG_R2


<p>PROFILE BG_P5</p> <p>BG_P5 (0-20 cm) poorly developed profile with a reduced thickness of about 20 cm, homogeneous soil structure, brown color with reddish oxidation patina.</p>	
--	--

Fig. 21 Overview of BG_P5

BG_S5 (10-20 cm): composite sample, light yellowish brown to strong brown, muddy gravel, damp, organic fraction 28 wt% (roots and leaves). Subrounded and elonged coarse gravel (strongly weathered serpentinites, directly originated from the weathed bedrock). Clear smooth boundary with bedrock.


	Depth: 10-20 cm
	Thickness: 10 cm
	Grain-shape: subraounded to elonged
	Color: 7.5YR 4/4 (moist), 10YR 6/4 (dry)
	Water: moist
	Granulometry: muddy gravel

Fig. 22 Soil sample BG_S5

BG_R5 (>20 cm): foliated serpentinite, fine grained, foliation is marked by elonged and prismatic antigorite grain. Gray-brown to gray-green, with rare brown oxidation patina on surface. Not frequent fractures with soft white mineral (talc?).

	Rock: foliated serpentinite
	Texture: foliated
	Grain size: fine to medium
	Minerals: serpentine minerals
	Color: gray-green to brown
	Weathering: moderate

Fig. 23 Rock sample RG_R5



Fig. 24 Location of sampling point of soil sample BG_S2

PROFILE BG_P6

BG_P2 (0-70 cm) poorly developed profile with a reduced thickness of about 70 cm, homogeneous soil structure, orange-brown color with reddish oxidation patina. Bedrock contact is not visible (sampling by hand auger).

BG_S2 (10-50 cm): composite sample, yellowish brown (10YR 5/4, dry color) to strong brown (10YR 5/6, moist color), gravelly mud, damp, organic fraction 38 wt% (roots and leaves). Subrounded and elongated coarse gravel (strongly weathered serpentinites, directly originated from the bedrock weathering).



Fig. 25 Soil sample BG_S2

Depth: 10-50 cm
Thickness: 40 cm
Grain-shape: subrounded
Color: 10YR5/4 dry, 10YR5/6 moist
Water: damp
Granulometry: gravelly mud

BG_R3 (>50 cm): massive serpentinite, medium-size grained. Gray-green to gray-white, with millimetric yellowish gray altered edge. Alteration is also along fractures. Millimetric light green rounded aggregates are visible.

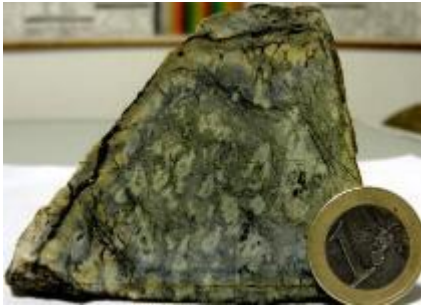
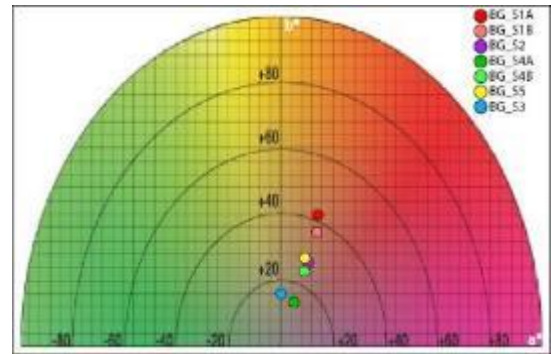
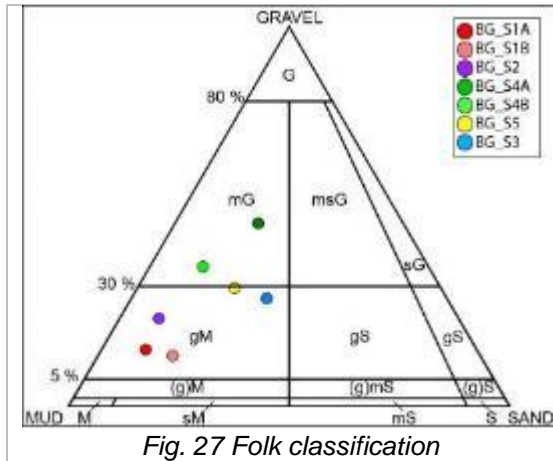


Fig. 26 Rock sample BG_R3

Rock: massive serpentinites
Texture: massive
Grain size: medium
Minerals: magnetite, serpentine
Color: gray-green to gray-white
Weathering: millimetric yellowish edge

SOIL CLASSIFICATION



A2. BADIA TIGLIETO (BT)

SITE DESCRIPTION

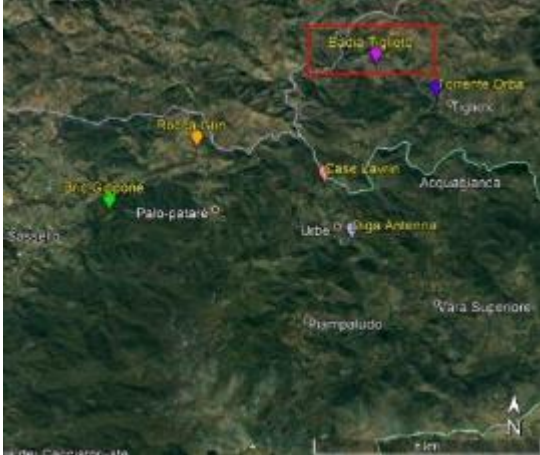
	Coordinate: 44°31'30"N; 8°36'07"E
	Province: Genova
	Town: Tiglieto
	Altitude: 380 m a.s.l.
	Slope: subvertical
	Slope orientation: SW-NE
	Land use: Abandoned quarry
Extension: 400 m ²	
	Vegetation: chestnut, oak coppice wood

Fig. 1 Satellite image of study area (in red box BT site)

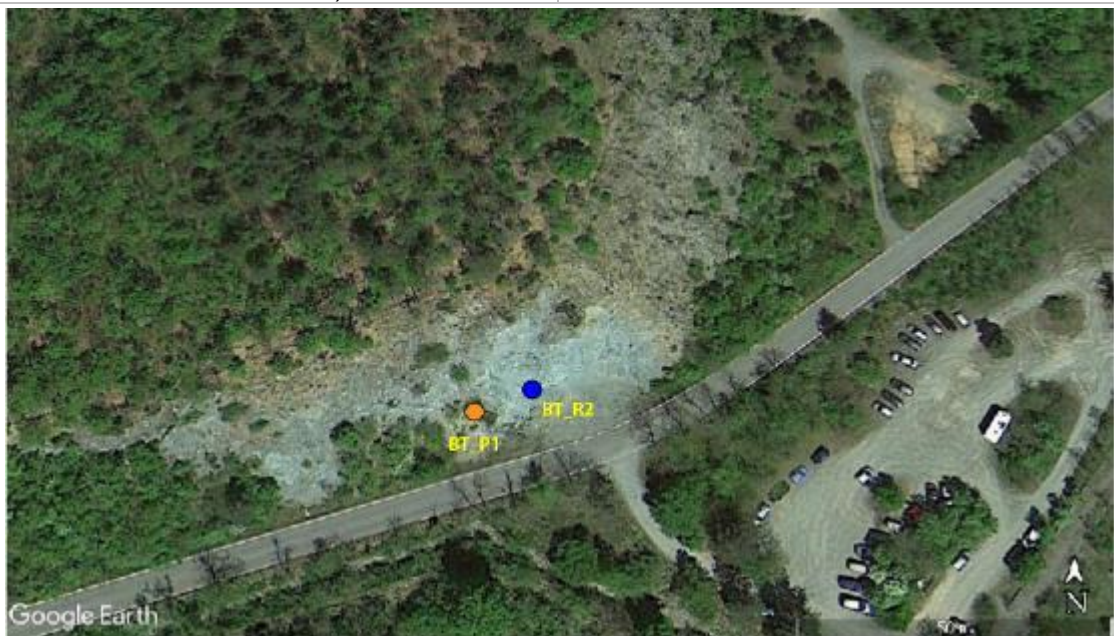


Fig. 2 Location of sampled profiles (orange), rocks (blue) in Badia Tiglieto site (Google Earth)

Location

BT site is located near Abbazia di Santa Maria della Croce, along the route SP 76, at 2 km from Tiglieto town-center. The site is an abandoned quarry of railway ballast. Unique quarry face (oriented SW-NE), without benching evidence.

Field evidences

There are many shear zone (fracture system) with associated cataclastic zone, that divided the rock mass in metric and decametric blocks. On fracture surface there is a white patina, with slip fiber. Presence of TC lens.



Fig. 3 Overview of Badia Tiglieto site.

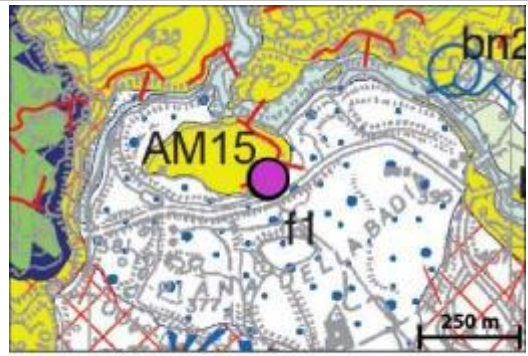


Fig. 4 Geological map of BT

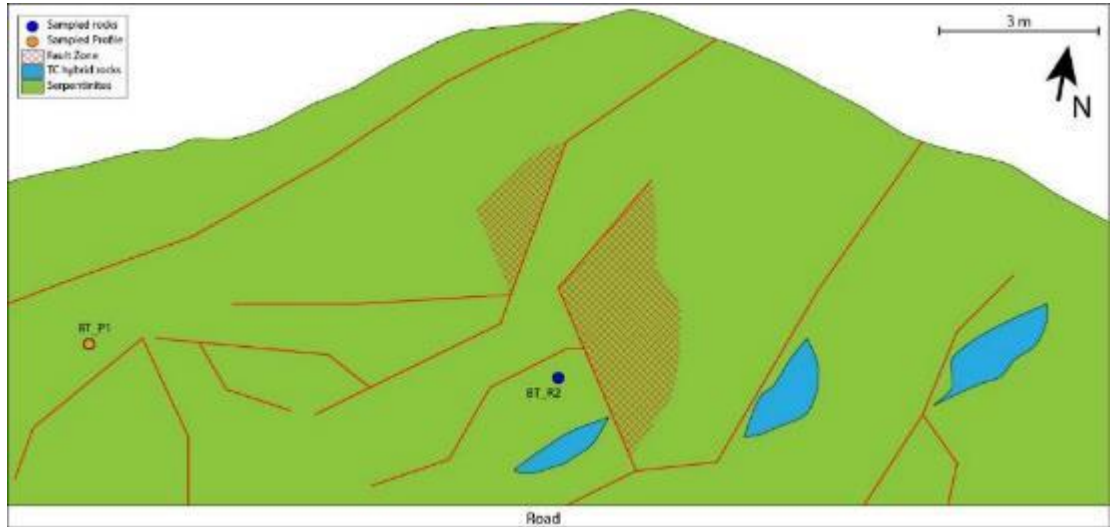


Fig. 5 Geological sketch of BT site with sample location



Fig. 6 Outcrop of foliated serpentinites



Fig. 7 Outcrop of TC

PROFILE & SAMPLING OF BADIA TIGLIETO

PROFILE BT_P1

(5-50 cm) poorly developed profile with a reduced thickness of about 100 cm, homogeneous soil structure, grey-brown color with reddish oxidation patina.

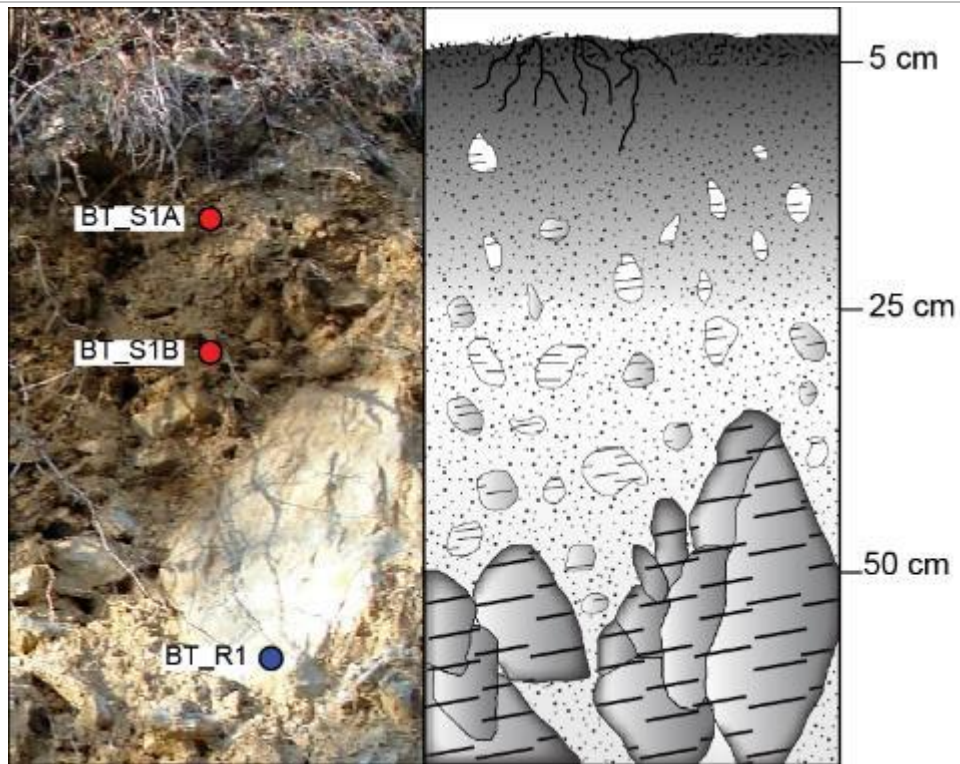


Fig. 8 BT_P1 soil profile and relative sketch

BT_S1A (10-25 cm): topsoil, light yellowish brown, muddy sandy gravel, very wet, high organic fraction, with bioturbation and medium roots. Coarse fraction represents ~50 wt.%. Soil structure is poliedric with low developed aggregates.

Depth: 10-25 cm

Thickness: 15 cm

Grain-shape: angular and elongated

Color: 2.5Y 6/3 (dry)

Water: very wet

Granulometry: muddy sandy gravel



Fig. 9 Soil sample BT_S1A



Fig. 9a Thin section of soil skeleton

BT_S1B (25-50 cm): subsoil, light yellowish brown, muddy sandy gravel, very wet. Low organic matter content. High coarse fraction directly originated from the weathering of bedrock). Clear smooth boundary with bedrock.



Fig. 10 Soil sample BT_S1B

Depth: 25-50 cm

Thickness: 25 cm

Grain-shape: angular and elongated

Color: 2.5Y 6/4 (dry)

Water: very wet

Granulometry: muddy sandy gravel

BT_R1 (>50 cm): foliated antigorite-serpentinite, fine grained, dark green. The main foliation is marked by from elongated to pseudo-fiber serpentine minerals, chlorites and micrograined magnetite. Low weathering evidence on sample surface.



Fig. 11 Rock sample BT_R1

Rock: Foliated serpentinites

Texture: foliated

Grain size: fine

Minerals: magnetite, serpentine minerals

Color: dark green

Weathering: very low

BT_R2 (from 20m to soil profile): foliated serpentinite, fine grained, dark green. The main foliation is marked by from elongated to pseudo-fiber serpentines, chl and micrograined magnetite, with little white interlayers. Low weathering evidence on sample surface, white patina with slip fiber.



Fig. 12 Rock sample BT_R2

Rock: Foliated serpentinite + TC

Texture: foliated

Grain size: fine

Minerals: serpentine minerals, talc (?)

Color: dark green, lighter layer

Weathering: very low, slip fibers

SOIL CLASSIFICATION

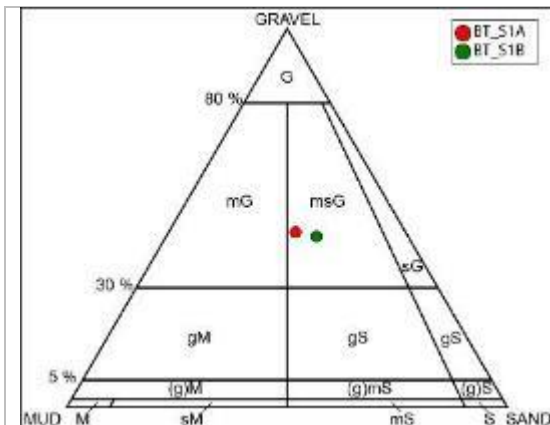


Fig. 13 Folk classification

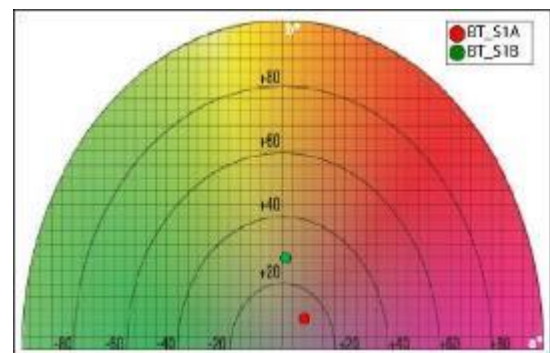


Fig. 14 Color CIE-L*a*b* classification

A3. CASE LAVRIN (CL)

SITE DESCRIPTION


	Coordinate: 44°29.741 N, 8°35.155 E
	Province: Savona
	Town: Urbe
	Altitude: 650 m.a.s.l.
	Slope: 30°
	Slope orientation: SE
	Land use: stone dump (quarry tailings)
Extension: 500 m ²	
Vegetation: grass	

Fig. 1 Satellite image of study area (in red box CL site)

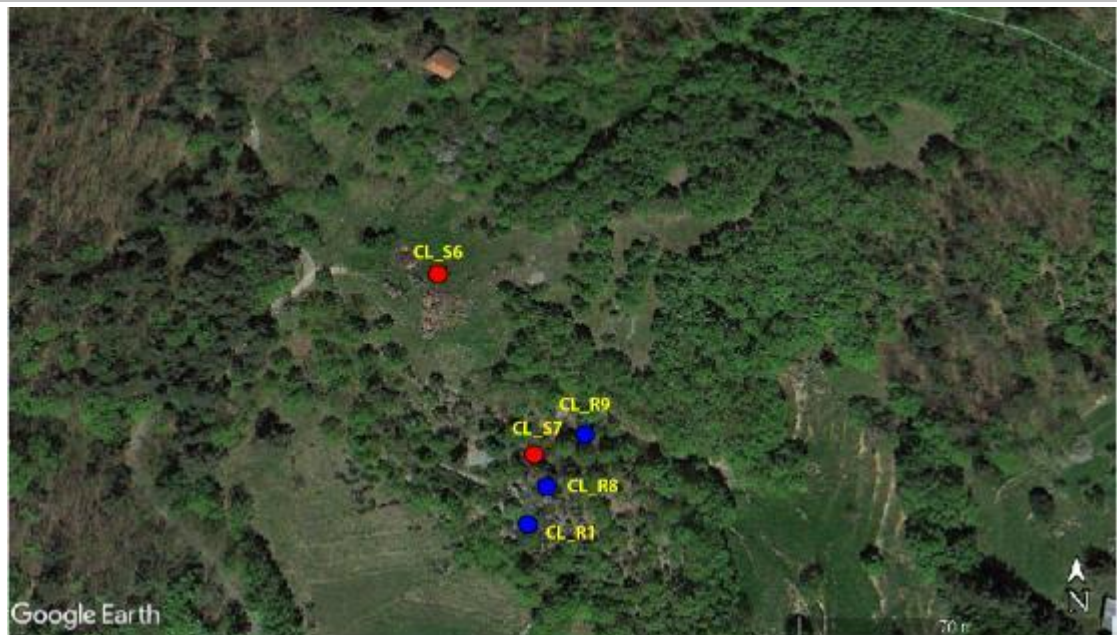


Fig. 2 Location of sampled rocks (blue), and soils (red) in Case Lavrin site (Google Earth®)

Location

This site is “homemade” former quarry from which materials for rural building were extracted. It left behind a large amount of waste material scattered over the studied site, as well as tailing areas. The outcrop is located on a rocky spur, with a slope up to 30°.

Field evidences

Rocks outcrop with discontinuity in vertical body with height from 1 to 2.5 m, and a width from 4 to 10 m. There are decametric to centimetric chevron fold. The main structure is represented by different set veins. Set veins with fibrous filling are: i) syntectonic fibers vein; ii) cross fibers vein; iii) slip fibers vein.



Fig. 3 Overview of Case Lavrin site.

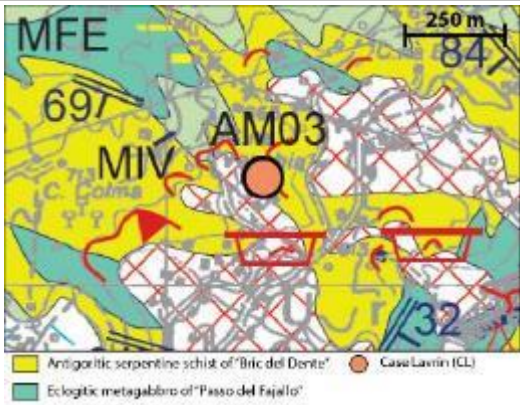


Fig. 4 Geological map of CL



Fig. 5 Outcrop of foliated serpentinites



Fig. 6 Stone waste

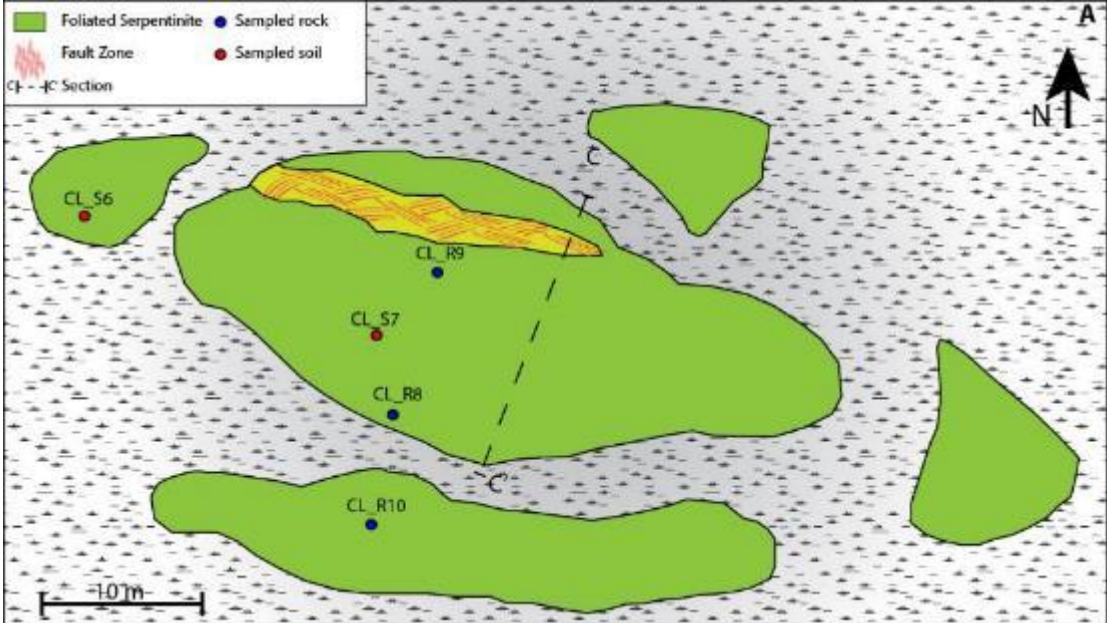
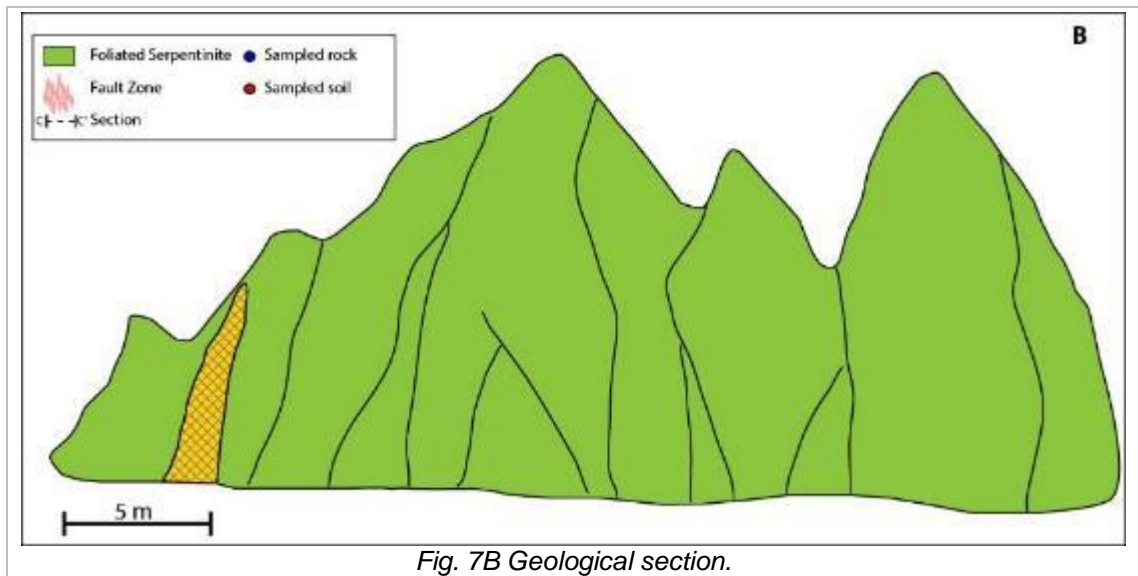


Fig. 7A Geological sketch of CL site with sample location



SOIL SAMPLE


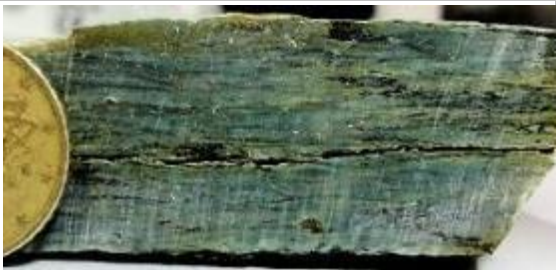
<p>CL_S6 (10-50 cm) composite soil, from 10-15m rock, at the top of slope deposit. Brown-green to brown gray-green, gravelly mud, organic fraction 16 wt%. Abundant angular to rounded medium and coarse gravel (directly originated from the bedrock). Bedrock contact is not visible.</p>	Depth: 10-50 cm	
	Thickness: 40 cm	
	Grain-shape: angular to rounded	
	Color: Gley1 4/5G wet, Gley1 8/10Y dry	
	Water: wet	
<p>CL_S7 (10-25 cm): composite soil, sampled near outcropping rocks. Soil is poor developed, with thickness <50cm (rhizosphere <15cm). Brown green-blue to gray-blue, muddy gravel, very wet. Abundant angular to rounded medium and coarse gravel (strongly weathered serpentinites, directly originated from the bedrock desegregation). Organic fraction is 24wt% (mainly leaves).</p>	Granulometry: gravelly mud	
		Depth: 10-25 cm
		Thickness: 15 cm
		Grain-shape: angular to rounded
		Color: Gley1 5/5GY (dry)
Water: very wet		
Granulometry: muddy gravel		


Fig. 8 Soil sample CL_S7

ROCK SAMPLE

<p>CL_R8: high foliated serpentinite (pencil cleavage), fine grained, with millimetric (2-5mm) subrounded dark-brown oxide (mag?). Fracturing subparallel to foliation, with mm opening and filled by whitish "soft" mineral (tal?). Foliation marked by elongated atg and rounded mag trails. Color is not homogeneous, vary from green-gray to blue-gray on fresh surfaced; exposed surface is yellow-gray to yellow-brown</p>	Rock: foliated serpentinite
	Texture: foliated

 <p><i>Fig. 9 Rock sample CL_R8</i></p>	Grain size: fine
	Minerals: serpentine mineral, magnetite
	Color: gray-green to yellow-green
	Weathering: surface yellow patina

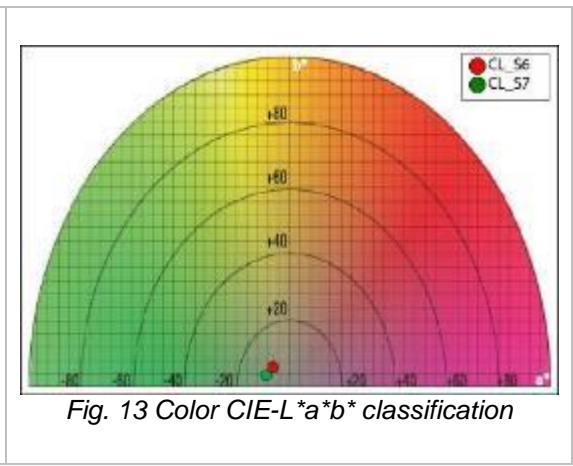
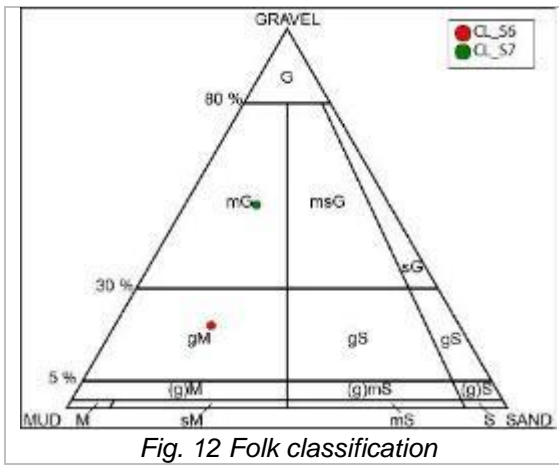
CL_R9: high foliated serpentinite (pencil cleavage), fine grained, with millimetric (2-8 mm) sub-rounded dark-brown oxide (mag?). Fracturing subparallel to foliation, with mm opening and filled by whitish “soft” mineral (talc?). Foliation marked by elongated atg and rounded magn trails. Color vary from green-gray to blue-gray; exposed surface is yellow-gray to yellow-brown

 <p><i>Fig. 10 Rock sample CL_R9</i></p>	Rock: foliated serpentinite
	Texture: high foliated
	Grain size: fine
	Minerals: serpentine minerals, magnetite
	Color: green-gray to blue-gray
	Weathering: surface yellow patina

CL_R10: high foliated serpentinite (pencil cleavage), fine grained, with millimetric (2-8 mm) sub-rounded dark-brown oxide (presumably mag). Fracturing subparallel to foliation, with millimetric opening and filled by whitish “soft” mineral (tlc?). Color is green-black; exposed surfaces are yellow-brown and characterized by presence of slip fibers.

 <p><i>Fig. 11 Rock sample CL_R10</i></p>	Rock: foliated serpentinite
	Texture: high foliated
	Grain size: fine
	Minerals: n.d.
	Color: green-black
	Weathering: yellow patina with slip fibers

SOIL CLASSIFICATION



A4. DIGA ANTENNA (DA)

SITE DESCRIPTION

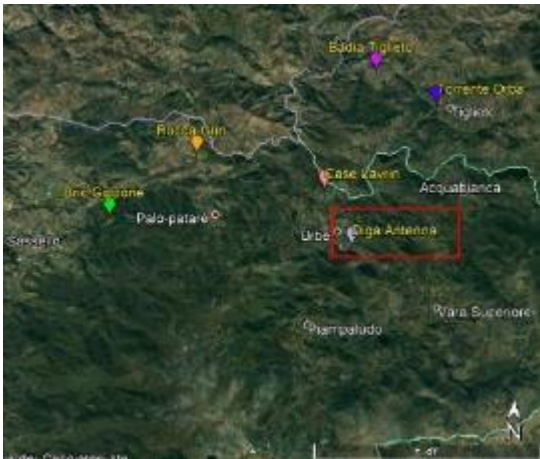
	Coordinate: 44°28.942 N, 8°35.744 E
	Province: Savona
	Town: Urbe (S. Pietro d'Orba)
	Altitude: 560 m.a.s.l.
	Slope: subvertical
	Slope orientation: SW
	Land use: road cut (SP 40)
Extension: 3mx3m (90% rock exposition)	
Vegetation: chestnut, oak coppice woods	

Fig. 1 Satellite image of study area (in red box DA site)



Fig. 2 Location of sampled rocks (blue) and soils (red) in Diga Antenna site (Google Earth ©)

Location

Diga Antenna site is located near Diga Antenna dam, near S. Pietro d'Orba village, along the route SP 40, bordering the artificial lake of Antenna. The outcrop is a wall rock of 3 m in height and 30 m in lengths, rock outcrops for 90% of total area.

Field evidences

Site is formed by from massive to foliated serpentinites, with interlayer of TC schist, near contact with eclogitic metagabbros. At W part of outcrop, there are metric to decametric massive serpentinites block; central part of outcrop is made of interlayering of FS and TC; E part is represented by eclogitic metagabbros (not sampled). There are many shear zones with mylonitic and cataclastic zone; it notes in these damage zones water is abundant. Soil is poor develop (thickness 30-50 cm), discontinuous and irregular. It follows the slop morphology. Soil structure is homogeneous without significant evidence of erosion, soil color is brow to green. At sampling time, it was wet.



Fig. 3 Overview of Diga Antenna site

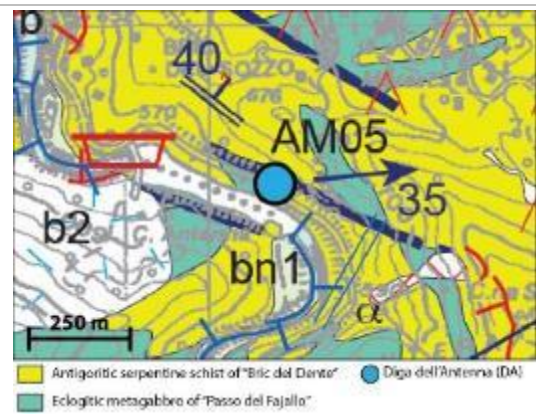


Fig. 4 Geological map of DA

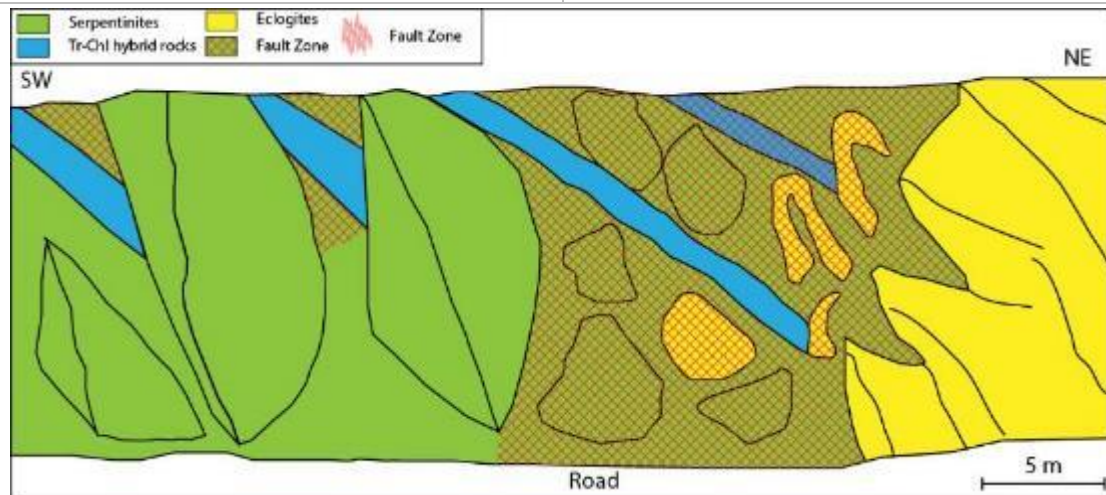


Fig. 5 Geological sketch of DA

SOIL SAMPLE

DA_S4 (10-30cm): composite sample, olive yellow to yellowish brown, muddy gravel, dump, organic fraction is 35wt% (roots and leaves). Abundant angular to rounded medium and coarse gravel (strongly weathered serpentinites or TC, directly originated from the rock disaggregation). Bedrock contact is not visible.



Fig. 6 Soil sample DA_S4

Depth: 10-30 cm

Thickness: 20 cm

Grain-shape: angular to rounded

Color: 10YR 4/2 (wet); 2.5Y 6/4 (dry)

Water: dump

Granulometry: muddy gravel

DA_S5 (10-30 cm): composite sample, light brownish gray (dry color) to gray brown (wet color), muddy gravel, dump, organic fraction is 38wt% (roots and leaves). Abundant angular to elongated-rounded medium and coarse gravel (strongly weathered serpentinites or TC schist, directly originated from the alteration of bedrock). Bedrock contact is not visible.

Depth: 10-30 cm

Thickness: 20 cm


	Grain-shape: angular to rounded
	Color: 10YR 3/2 (wet); 2.5Y 6/2 (dry)
	Water: dump
	Granulometry: muddy gravel

Fig. 7 Soil sample DA_S5

ROCK SAMPLE

DA_R6: slightly foliated serpentinite with TC, fine to medium grained, dark green to black-purple. The foliation is marked by opaque minerals (mainly mag)



Fig. 8 Rock sample DA_R6

Rock: massive serp. + TC
Texture: massive/slightly foliated
Grain size: fine to medium
Minerals: serpentine, oxide
Color: dark green, dark gray, black purple
Weathering: absent

DA_R7: foliated serpentinite, fine grained, grey-dark green. Presence of fiber minerals on the sample surface. Not weathering evidence.



Fig. 9 Rock sample DA_R7

Rock: foliated serpentinites
Texture: foliated
Grain size: fine to medium
Minerals: serpentine, oxide
Color: grey-dark green
Weathering: absent

SOIL CLASSIFICATION

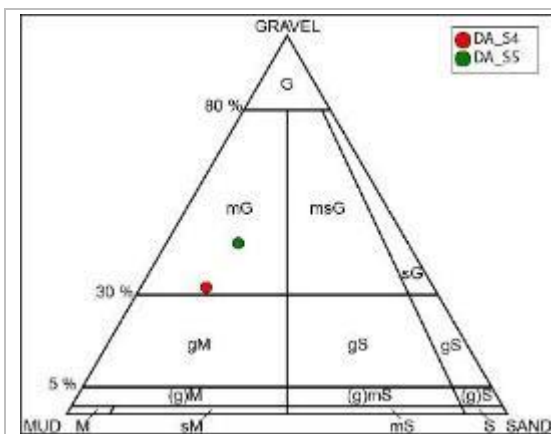
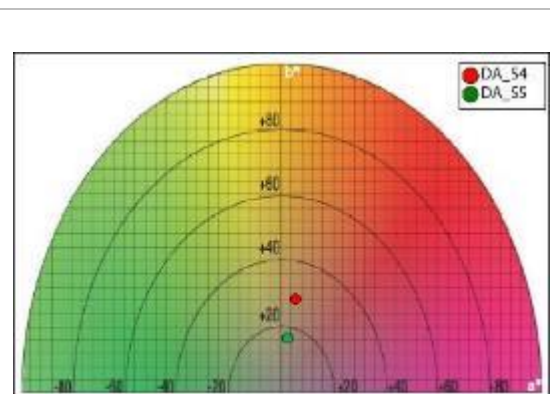


Fig. 10 Folk classification



*Fig. 11 Color CIE-L*a*b* classification*

A5. STRADA GIUSVALLA (GIU)

SITE DESCRIPTION

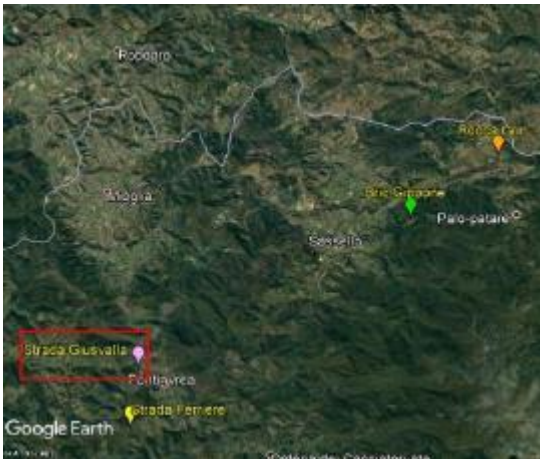
	Coordinate: 44°26'53"N 8°25'32"E
	Province: Savona
	Town: Pontinvrea
	Altitude: 433 m.a.s.l.
	Slope: subvertical
	Slope orientation: S
	Land use: Road cut
Extension: 30 m x 4 m	
	Vegetation: chestnut, oak coppice woods

Fig. 1 Satellite image of study area (in red box GIU site)



Fig. 2 Location of sampled profiles (orange) in Strada Giusvalla site (Google Earth ®)

Location

GIU site is located along the SP (n°43), near Pontinvrea village (SV – Italy). The outcrop is a road cut and covers an area of 120 m², extends in length, parallel to the road.

Field evidences

GIU site is formed by antigorite serpentinites, with different rheologic behavior (from massive to cataclastic/mylonitic serpentinite). Present of vein of chrysotile and fibrous amphiboles.



Fig. 3 Overview of Strada Giusvalla site

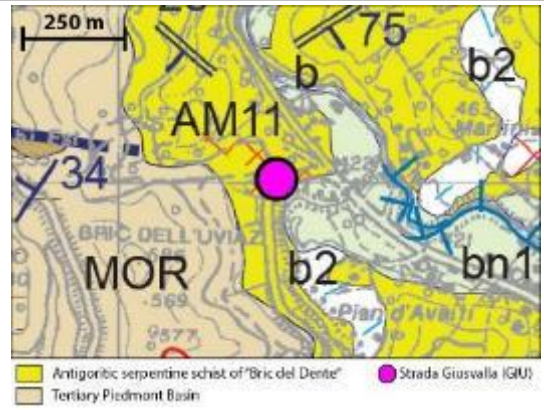


Fig. 4 Geological map of GIU

PROFILE & SAMPLING of STRADA GIUSVALLA

PROFILE GIU_P1

(0-80 cm) poorly developed profile with a reduced thickness of about 80 cm, homogeneous soil structure, grey-brown.

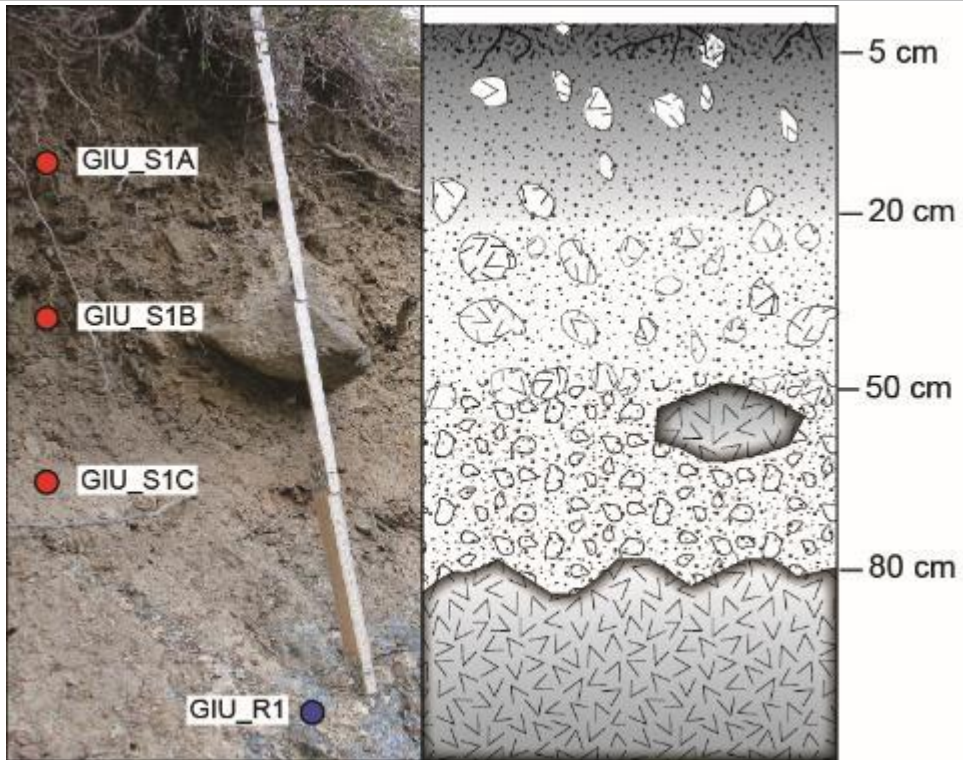


Fig. 5 GIU_P1 soil profile and relative sketch

GIU_S1A (5-20 cm): topsoil, yellowish brown, muddy gravel, dump, high organic fraction (bioturbation, leaves, and roots). Polyandric soil structure, rare centimetric rounded clasts or aggregate.

Depth: 5-20 cm

Thickness: 15 cm

Grain-shape: angular rounded

Color: 10 YR 5/4 (dry)

Water: dump

Granulometry: muddy gravel



Fig. 6 Topsoil sample GIU_S1A



Fig. 6a Thin section of soil skeleton

GIU_S1B (20-50 cm): intersoil, yellowish brown, muddy gravel (increase of coarse fraction), dump. Abundant angular medium and coarse gravel (strongly weathered serpentinites, directly originated from the weathering of bedrock).

Depth: 20-50 cm
Thickness: 30 cm
Grain-shape: angular to rounded
Color: 10 YR 5/4 (dry)
Water: dump
Granulometry: muddy gravel



Fig. 7 Intersoil sample GIU_S1B



Fig. 7a Thin section of soil skeleton

GIU_S1C (50-80 cm): subsoil (probably C horizon), dark yellowish brown, muddy sandy gravel, wet. Abundant angular medium and coarse gravel (strongly weathered serpentinites, directly originated from the weathering of bedrock).

Depth: 50-80 cm
Thickness: 30 cm
Grain-shape: angular
Color: 10 YR 3/4 (dry)
Water: wet
Granulometry: muddy sandy gravel



Fig. 8 Subsoil sample GIU_S1C

Fig. 8a Thin section of soil skeleton

GIU_R1 (>80 cm): massive serpentinite, medium to coarse grained, dark green to olive green (relics?). Micrometric (opening 0.5 mm) sets vein filling by oxides or fibrous serpentine. Not evidence of superficial alteration.

Rock: massive serpentinite
Texture: massive
Grain size: medium to coarse



Fig. 9 Rock sample GIU_R1

Minerals: srp, magmatic relics (ol? px?)

Color: black to olive dark green

Weathering: not evidence

SOIL CLASSIFICATION

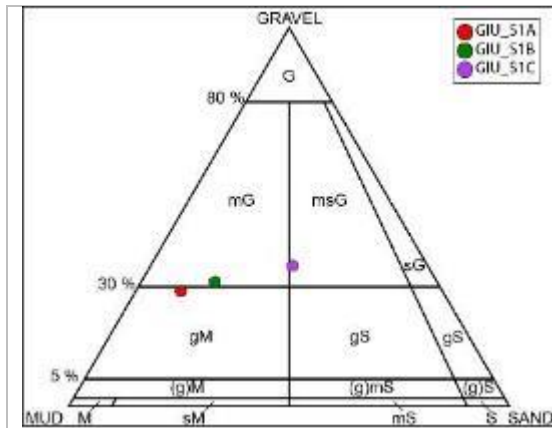


Fig. 10 Folk classification

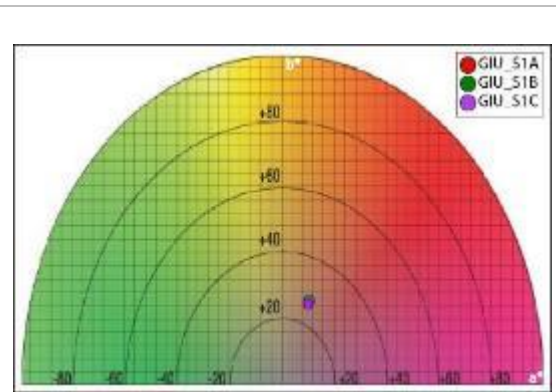


Fig. 11 Color CIE-L*a*b* classification

A6. ROCCA GRIN (RG)

SITE DESCRIPTION

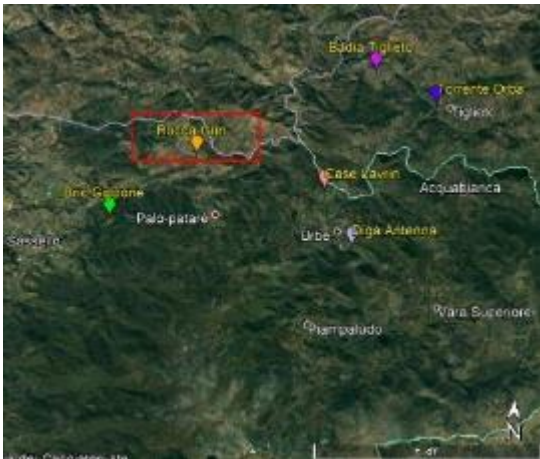
	Coordinate: 44°30.161N 8°32.542E
	Province: Savona
	Town: Sassello
	Altitude: 630 m a.s.l.
	Slope: subvertical
	Slope orientation: SW
	Land use: abandoned quarry
Extension: 70x30 m	
Vegetation: chestnut, oak coppice wood	

Fig. 1 Satellite image of study area (in red box RG site)

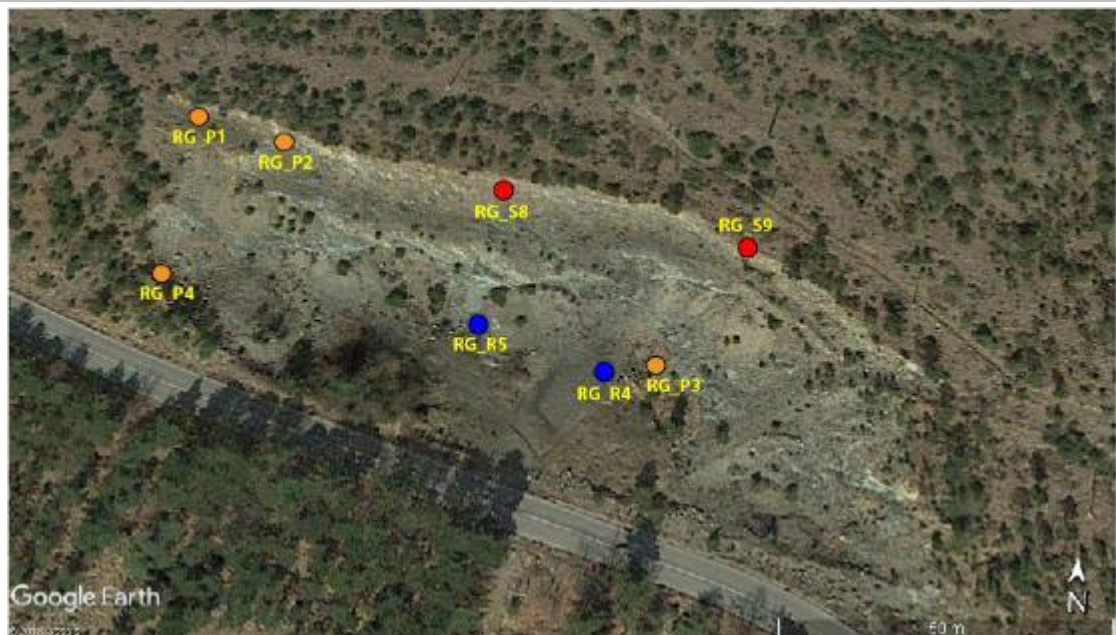


Fig. 2 Location of sampled profiles (orange), rocks (blue), and soils (red) in RG site (Google Earth ©)

Location

Abandoned railway ballast quarry, with a quarry face of 8 m high and 75 m wide, partially recognizable branch cultivation, with a height of about 3 m of elevation. The quarry has an area of about 70x30 m.

Field evidences

In Rocca Grin site rocks are peridotite with varying degrees of serpentinization. At mesoscale, the rock has no relevant physical or chemical alteration evidence, except for yellow-reddish surface patine, due to oxidation of iron oxides, in particular on less serpentinized peridotite.

Evident correlation between rock deformation, structural domain and set veins presence. Presence of three different set vein: a) extensional set vein with cross fiber chrysotile, chlorite, Fe-oxides, talc; b) syn-tectonic set vein with chrysotile, antigorite, chlorite, Fe-oxides; c) shear vein with slip fiber.

Soil has a thickness ranging to 80-90 cm, is homogeneous without stratification evidence from bedrock to rhizosphere.



Fig. 3 Overview of Rocca Grin site

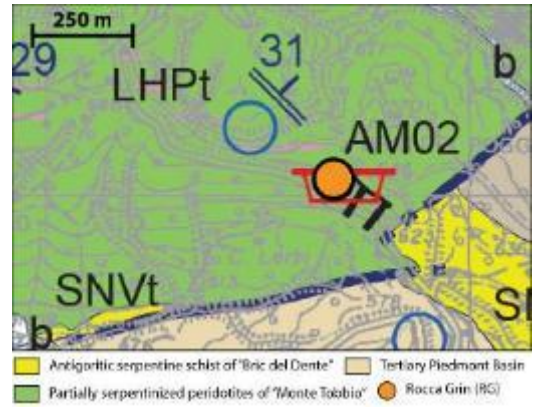


Fig. 4 Geological map of RG

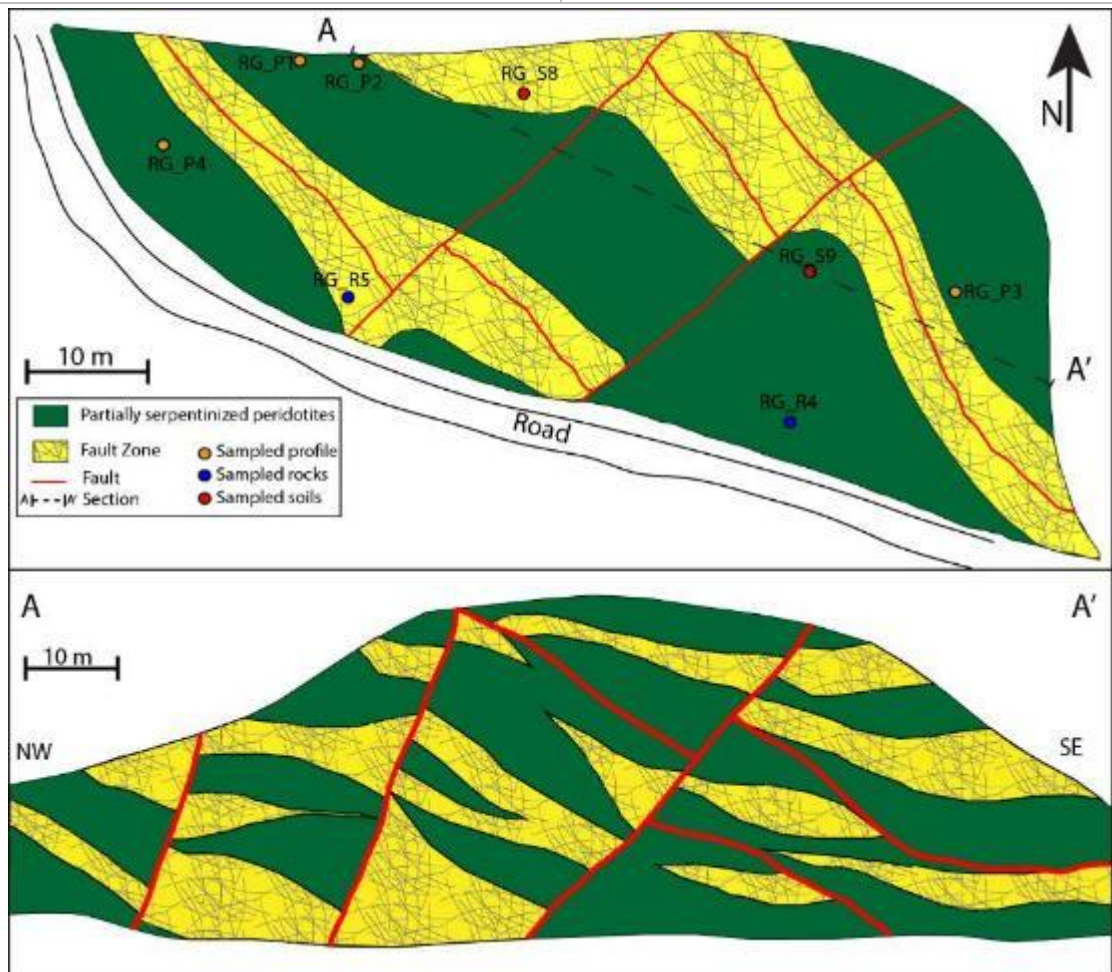


Fig. 5 Geological sketch and geological section of RG site with sample location

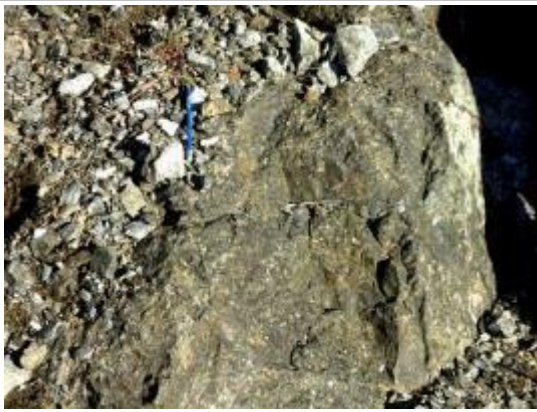


Fig. 6 Partially serpentinized peridotite



Fig. 7 Fault zone

PROFILE & SAMPLING OF ROCCA GRIN

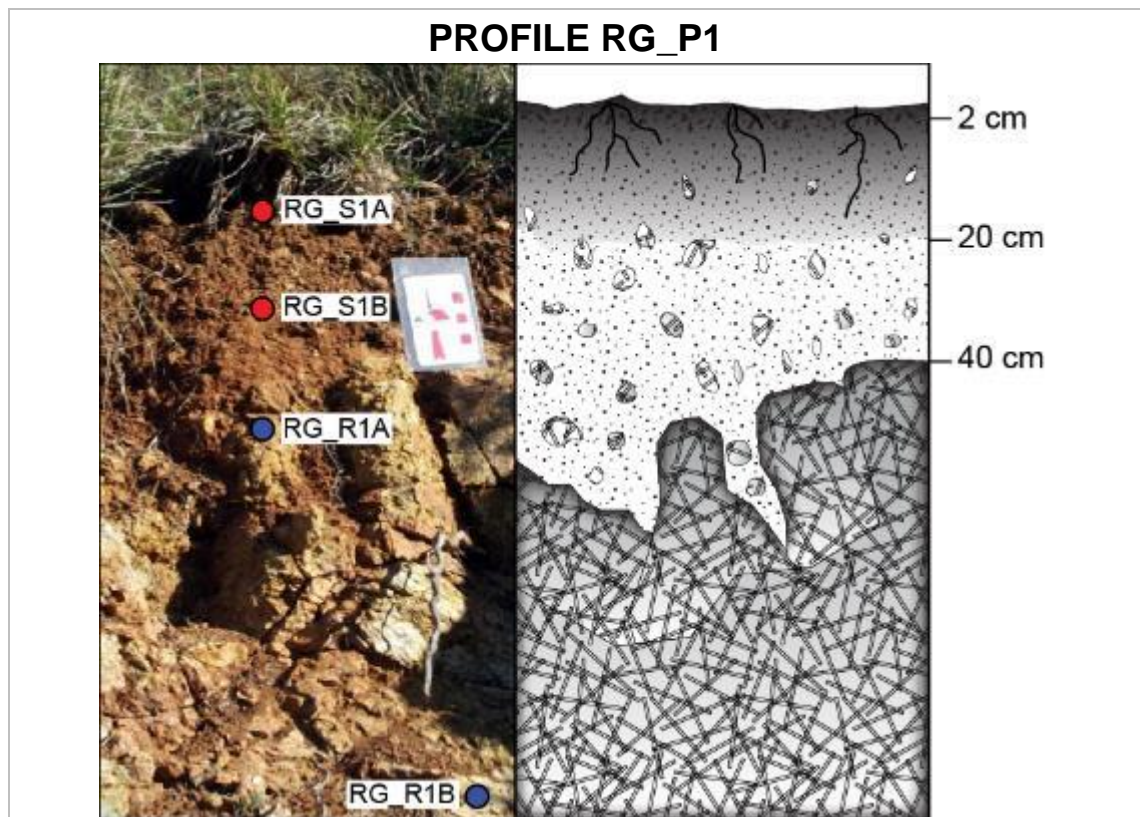


Fig. 8 RG_P1 soil profile and relative sketch



Fig. 9 Topsoil sample RG_S1A

Depth: 0-20 cm

Thickness: 20 cm

Grain-shape: rounded




Color: 5YR 4/8

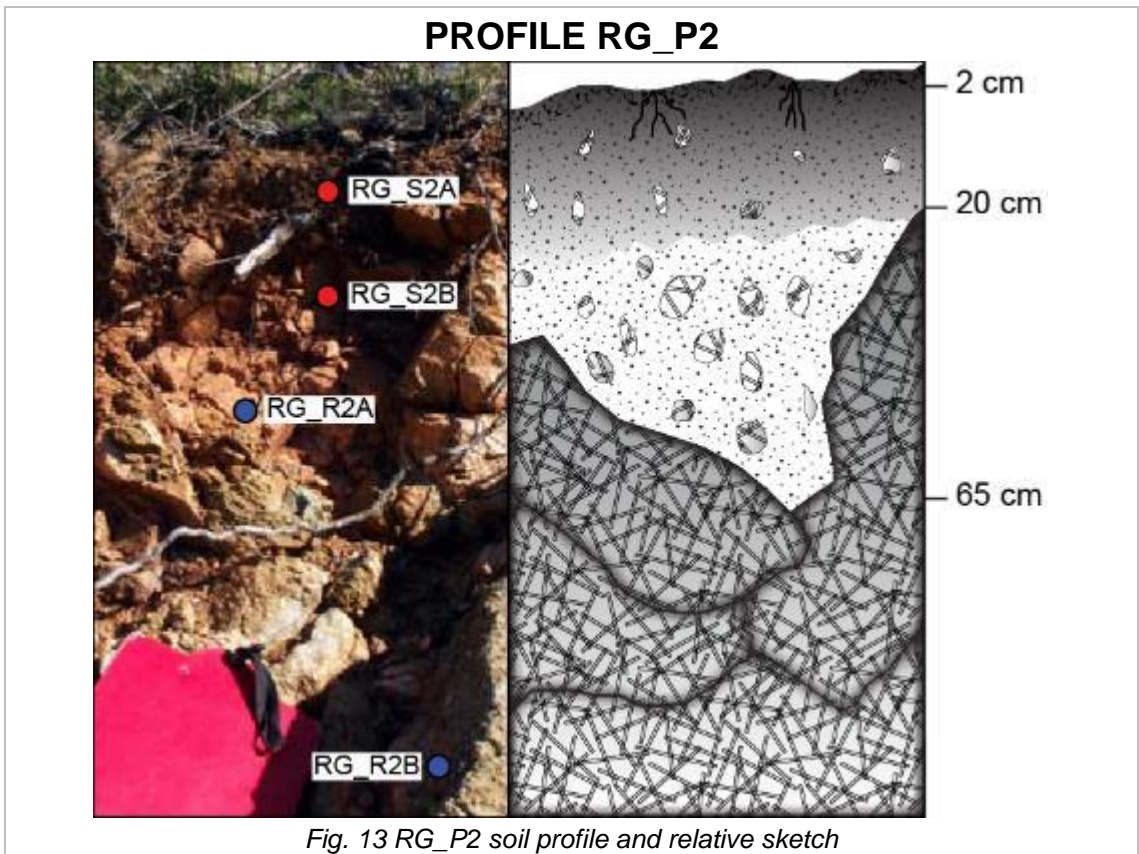
Water: dump




Granulometry: muddy gravel/gravelly mud

Depth: 20-40 cm

Thickness: 20 cm

 <p><i>Fig. 10 Subsoil sample RG_S1B</i></p>	Grain-shape: subrounded
	Color: 2.5YR 3/6
	Water: dump
	Granulometry: gravelly mud
 <p><i>Fig. 11 Weathered rock sample RG_R1A</i></p>	Rock: partially serpentinized peridotite
	Serp. Degree: 75-80 %
	Texture: massive
	Grain size: medium
	Minerals: serpentine minerals, pyroxene
	Color: green to black
	Weathering: superficial red patine
 <p><i>Fig. 12 Unweathered rock sample RG_R1B</i></p>	Rock: partially serpentinized peridotite
	Serp. Degree: 75-80 %
	Texture: massive to slightly foliated
	Grain size: medium
	Minerals: serpentine minerals, pyroxene
	Color: green to black
	Weathering: less superficial red patine



	<p>Depth: 2-20 cm</p> <p>Thickness: 18 cm</p> <p>Grain-shape: rounded to subangular</p> <p>Color: 2.5 Y 2.5/4 (dry)</p> <p>Water: dump</p> <p>Granulometry: gravelly mud</p>
	<p>Depth: 20-65 cm</p> <p>Thickness: 45 cm</p> <p>Grain-shape: angular</p> <p>Color: 2.5 Y 3/4</p> <p>Water: wet</p> <p>Granulometry: muddy sandy gravel</p>
	<p>Rock: partially serpentinized peridotite</p> <p>Serp. Degree: 80-90 %</p> <p>Texture: foliated</p> <p>Grain size: medium</p> <p>Minerals: rare relict, fiber minerals</p> <p>Color: dark to brown</p> <p>Weathering: network vein</p>
	<p>Rock: partially serpentinized peridotite</p> <p>Serp. Degree: 80-85 %</p> <p>Texture: massive to slightly deformed</p> <p>Grain size: medium</p> <p>Minerals: serpentine minerals, pyroxene</p> <p>Color: green to black</p> <p>Weathering: oxidation patine</p>

PROFILE RG_P3

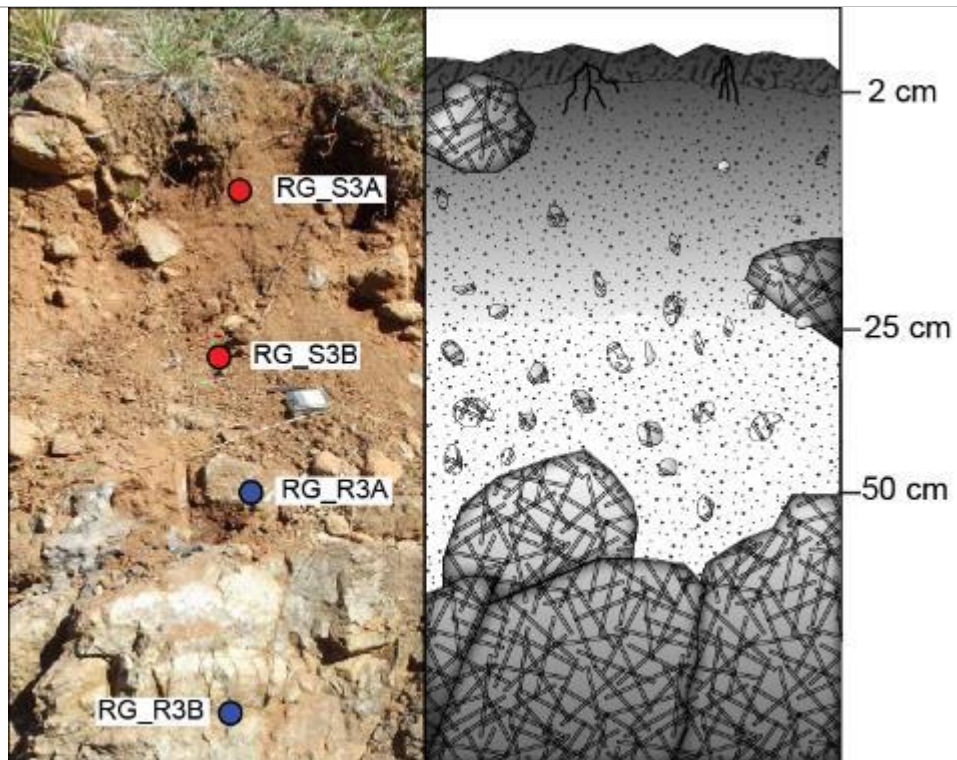


Fig. 18 RG_P3 soil profile and relative sketch



Fig. 19 Topsoil sample RG_S3A

Depth: 2-25 cm
Thickness: 23 cm
Grain-shape: subrounded
Color: 2.5 Y 2.5/4
Water: wet
Granulometry: muddy sandy gravel



Fig. 20 Subsoil sample RG_S3B

Depth: 25-50 cm
Thickness: 25 cm
Grain-shape: rounded
Color: 5YR 3/6
Water: dump
Granulometry: gravelly mud



Fig. 21 Weathered rock sample RG_R3A

Rock: partially serpentinized peridotite
Serp. Degree: 80-85 %
Texture: foliated
Grain size: medium
Minerals: serpentine minerals, pyroxene
Color: green to black
Weathering: rare oxidation patine
Rock: partially serpentinized peridotite



Fig. 22 Unweathered rock sample RG_R3B

Serp. Degree: 75-80 %
Texture: massive
Grain size: medium
Minerals: serpentine minerals, pyroxene
Color: green to black
Weathering: rare oxidation patine

PROFILE RG_P4

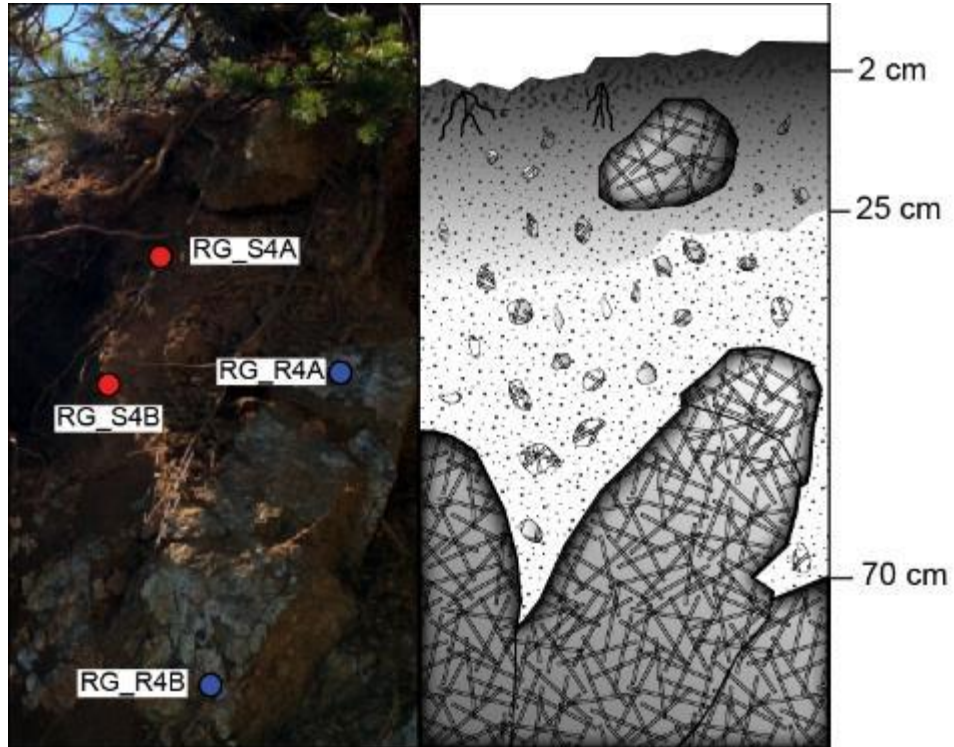


Fig. 23 RG_P4 soil profile and relative sketch





Fig. 24 Topsoil sample RG_S4A

Depth: 2-25 cm
Thickness: 23 cm
Grain-shape: rounded to subangular
Color: 7.5YR 5/6
Water: dump
Granulometry: gravelly mud



Fig. 25 Subsoil sample RG_S4B

Depth: 25-70 cm
Thickness: 45 cm
Grain-shape: subrounded
Color: 2.5Y 5/10
Water: dump
Granulometry: gravelly mud

	Rock: partially serpentinized peridotite
	Serp. Degree: 80-90 %
	Texture: massive to foliated
	Grain size: medium
	Minerals: magmatic relics, fiber minerals
<i>Fig. 26 Weathered rock sample RG_R4A</i>	
	Rock: partially serpentinized peridotite
	Serp. Degree: 75-80 %
	Texture: massive
	Grain size: medium
	Minerals: olivine relics
<i>Fig. 27 Unweathered rock sample RG_R4B</i>	
	Color: brown
	Weathering: oxide patine

OTHER SAMPLES




	Depth: 10-35 cm
	Thickness: 25 cm
	Grain-shape: subangular to rounded
	Color: 2.5 YR 3/6 (wet), 7.5 YR 4/6 (dry)
	Water: dump
<i>Fig. 28 Soil sample RG_S8</i>	
	Depth: 10-40 cm
	Thickness: 30 cm
	Grain-shape: subangular to rounded
	Color: 2.5 YR 3/4 (wet), 7.5 YR 4/6 (dry)
	Water: dump
<i>Fig. 29 Soil sample RG_S9</i>	
	Rock: partially serpentinized peridotite
	Serp. Degree: 75-80 %
	Texture: massive to foliated
	Grain size: medium to coarse
	Minerals: serpentine, px, (talc vein?)
<i>Fig. 30 Rock sample RG_R4</i>	
	Color: black-brown to dark green
	Weathering: white patine



Fig. 31 Rock sample RG_R5

Rock: partially serpentinized peridotite
Serp. Degree: 75-80 %
Texture: foliated
Grain size: medium to coarse
Minerals: serpentine, px, (talc vein?)
Color: black-brown to dark green
Weathering: white patine

SOIL CLASSIFICATION

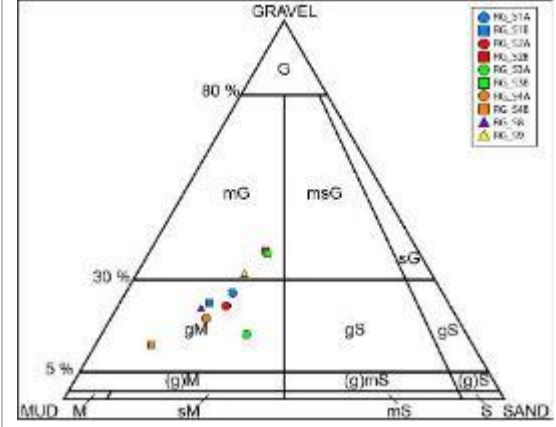


Fig. 32 Folk classification

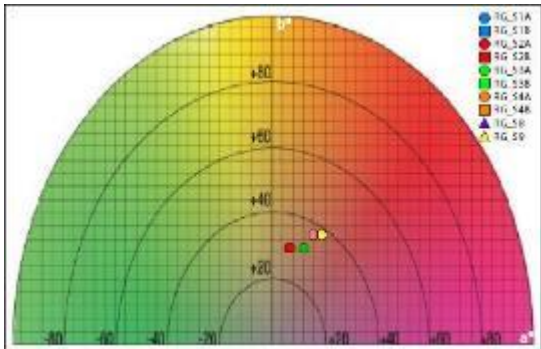


Fig. 33 Color CIE-L*a*b* classification

A7. STRADA FERRIERA

SITE DESCRIPTION

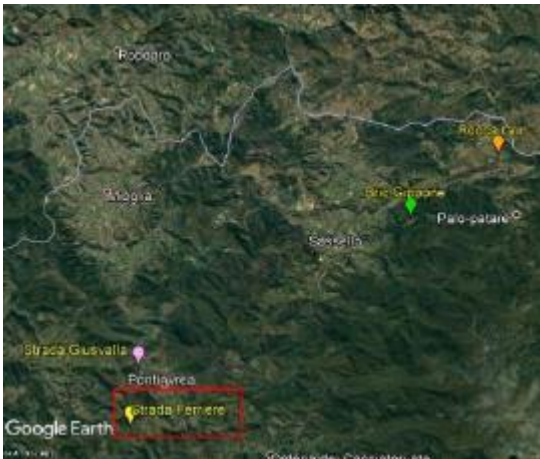
	Coordinate: 44°26'2"N; 8°25'27"E
	Province: Savona
	Town: Pontinvrea
	Altitude: 578 m.a.s.l.
	Slope: subvertical
	Slope orientation: SE
	Land use: Road cut (SP 41)
Extension: 10 m x 5 m	
Vegetation: chestnut, oak coppice woods	

Fig. 1 Satellite image of study area (in red box SF site)

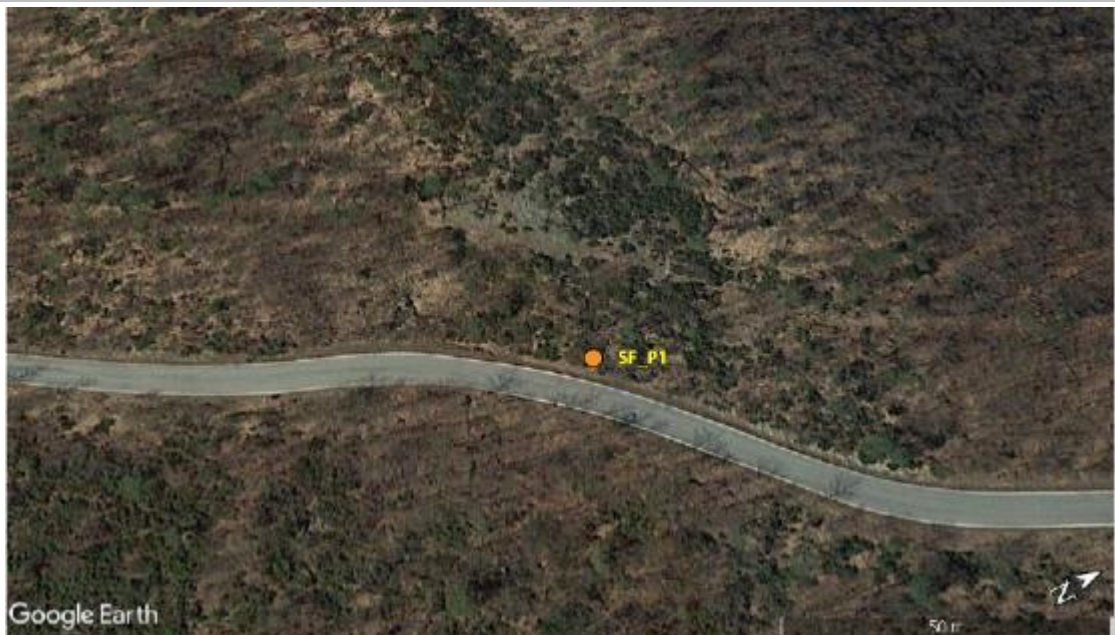


Fig. 2 Location of sampled profiles (orange) in Strada Ferriera site (Google Earth ®)



Fig. 3 Overview of Strada Ferriera site

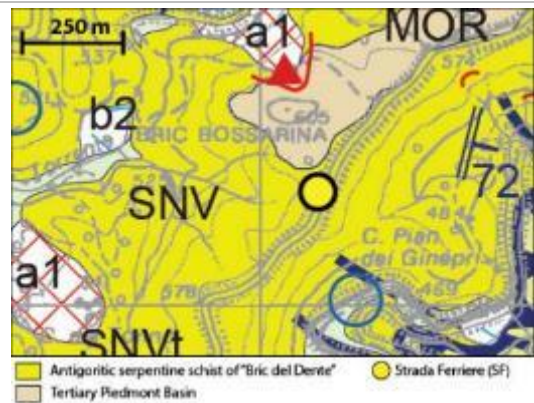


Fig. 4 Geological map of SF

Location

SF site is located along the SP 41, at Km of Ferriera Village. The outcrop is a road cut and covers an area of 50 m², extends in length, parallel to the road. SF site is formed by massive serpentinites with superficial red patine of oxidation.

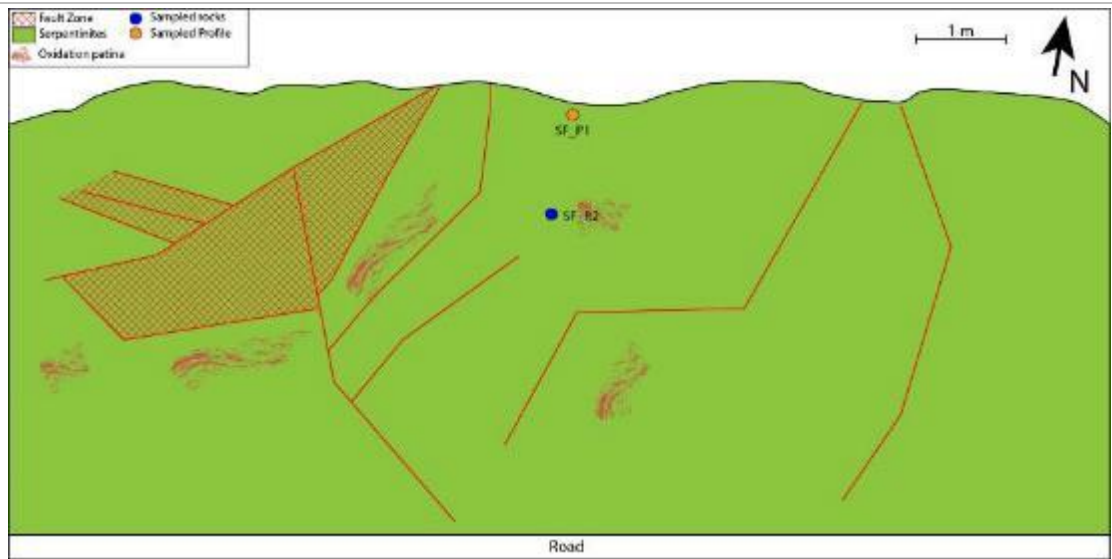


Fig. 5 Geological sketch of SF site with sample location.

PROFILE & SAMPLING OF STRADA FERRIERA

PROFILE SF_P1

(0-80 cm) poorly developed profile with a reduced thickness of about 80 cm, homogeneous soil structure, grey-brown to yellowish grey.

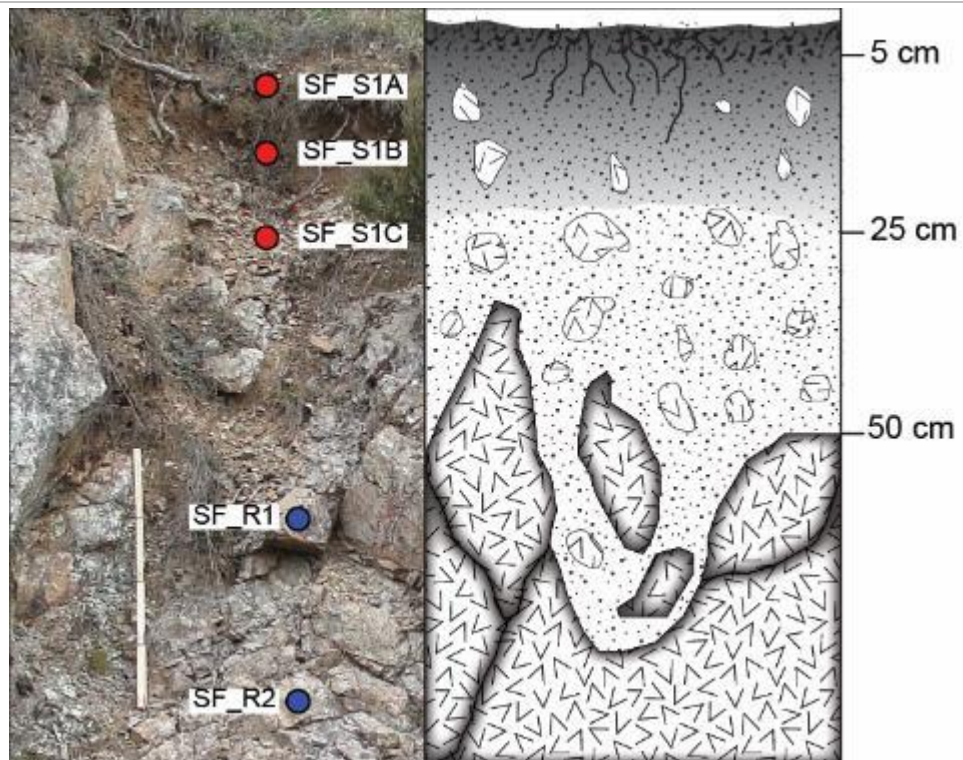


Fig. 6 SF_P1 soil profile and relative sketch

SF_S1A (5-25 cm): topsoil, dark yellowish brown (10 YR 4/4), gravelly mud, dump,

Depth: 5-25 cm

Thickness: 20 cm

Grain-shape: subangular to subrounded





<p>soil aggregates are rare. High organic fraction (bioturbation and roots).</p>	<p>Color: 10 YR 4/4 (dry) Water: dump Granulometry: gravelly mud</p>
 <p><i>Fig. 7 Topsoil sample SF_S1A</i></p>	 <p><i>Fig. 7a Thin section of soil skeleton</i></p>
<p>SF_S1B (25-50 cm): intersoil, brown, gravelly mud. Abundant angular medium and coarse gravel (strongly weathered serpentinites). Erosion evidence (superficial water erosion).</p>	<p>Depth: 25-50 cm Thickness: 25 cm Grain-shape: angular Color: 10 YR 4/3 (dry) Water: dump Granulometry: gravelly mud</p>
 <p><i>Fig. 8 Soil sample SF_S1B</i></p>	 <p><i>Fig. 8a Thin section of soil skeleton</i></p>
<p>SF_S1C (50-80 cm): subsoil (C horizon), dark brown, dump, gravelly mud. Abundant angular medium and coarse gravel (strongly weathered serpentinites, directly originated from the weathering of bedrock). Clear smooth boundary with bedrock.</p>	<p>Depth: 50-80 cm Thickness: 30 cm Grain-shape: angular Color: 10 YR 3/3 (dry) Water: dump Granulometry: gravelly mud</p>
 <p><i>Fig. 9 Soil sample SF_S1C</i></p>	 <p><i>Fig. 9a Thin section of soil skeleton</i></p>
<p>SF_R1 (>80 cm): weathered bedrock, massive serpentinite with red oxidation patine.</p>	<p>Rock: massive serpentinite Texture: massive Grain size: medium to coarse</p>



Fig. 10 Rock sample SF_R1

Minerals: magmatic relic (?), serpentine, oxides, hydroxides

Color: dark green, dark red, brown

Weathering: superficial and internal red patine (hematite?), weathered rock

SF_R2 (>100 cm): unweathered bedrock, massive serpentinite with red oxidation patine.



Fig. 11 Rock sample SF_R2

Rock: massive serpentinite

Texture: massive

Grain size: medium to coarse

Minerals: magmatic relic (?), serpentine, oxides, hydroxides

Color: dark green, dark red, brown

Weathering: superficial and internal red patine (hematite?)

SOIL CLASSIFICATION

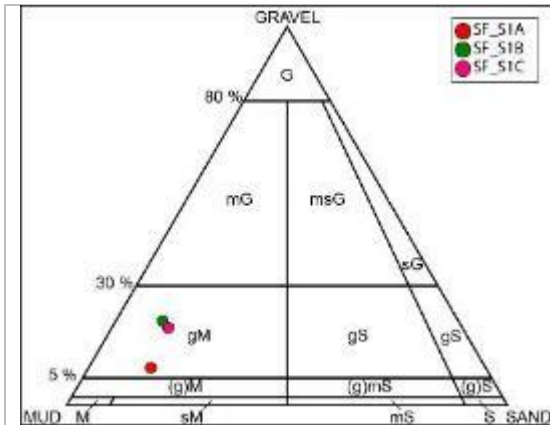


Fig. 12 Folk classification

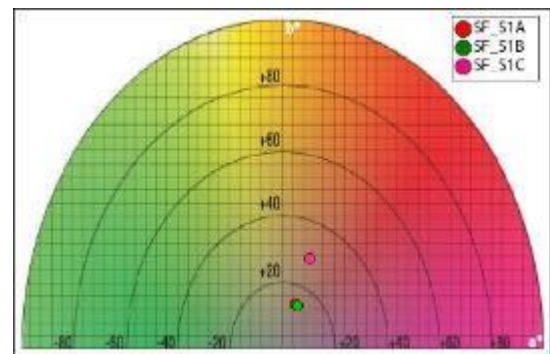


Fig. 13 Color CIE-L*a*b* classification

A8. Torrente ORBA (TO)

SITE DESCRIPTION

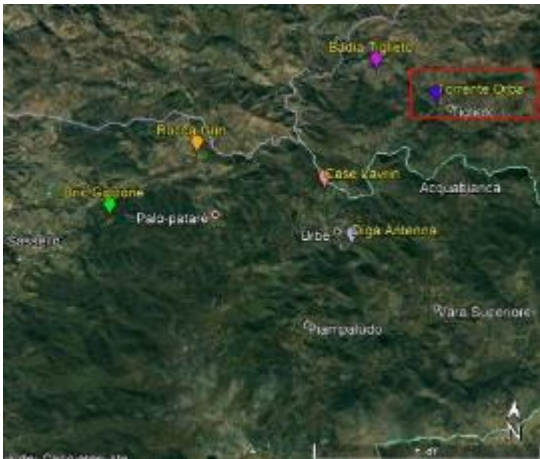
	Coordinate: 44°31'3"N, 8°37'22"E
	Province: Genova
	Town: Tiglieto
	Altitude: 418 m a.s.l.
	Slope: subvertical
	Slope orientation: W
	Land use: Abandoned quarry, stream bank
Extension: 200 m ²	
	Vegetation: chestnut, oak coppice woods

Fig. 1 Satellite image of study area (in red box TO site)



Fig. 2 Location of sampled profiles (orange) and rocks (blue) in TO site (Google Earth®)

Location

TO site is an abandoned quarry on the stream bank of the Orba creek and the Provincial Road No. 64, between Tiglieto and Acquabianca village. The quarry has been cultivated with a single front and the signs left by the wedges for the extraction of the blocks are still visible, probably abandoned due to the rheological variability of the material given the presence of more massive portions and others with very pervasive low angle cleavage.

Field evidences

- Vein with pluri-centimetric serpentine fibers (antigorite).
- Presence of low-angle cleavage.



Fig. 3 Overview of Torrente Orba site



Fig. 4 Geological map of TO



Fig. 5 Foliated serpentinites



Fig. 6 Serpentinites with Tr-Chl hybrid rocks

PROFILE & SAMPLING OF TORRENTE ORBA

PROFILE TO_P1

(5-50 cm) poorly developed profile with a reduced thickness of about 45 cm, homogeneous soil structure, green-gray. Bedrock contact is not clear visible.

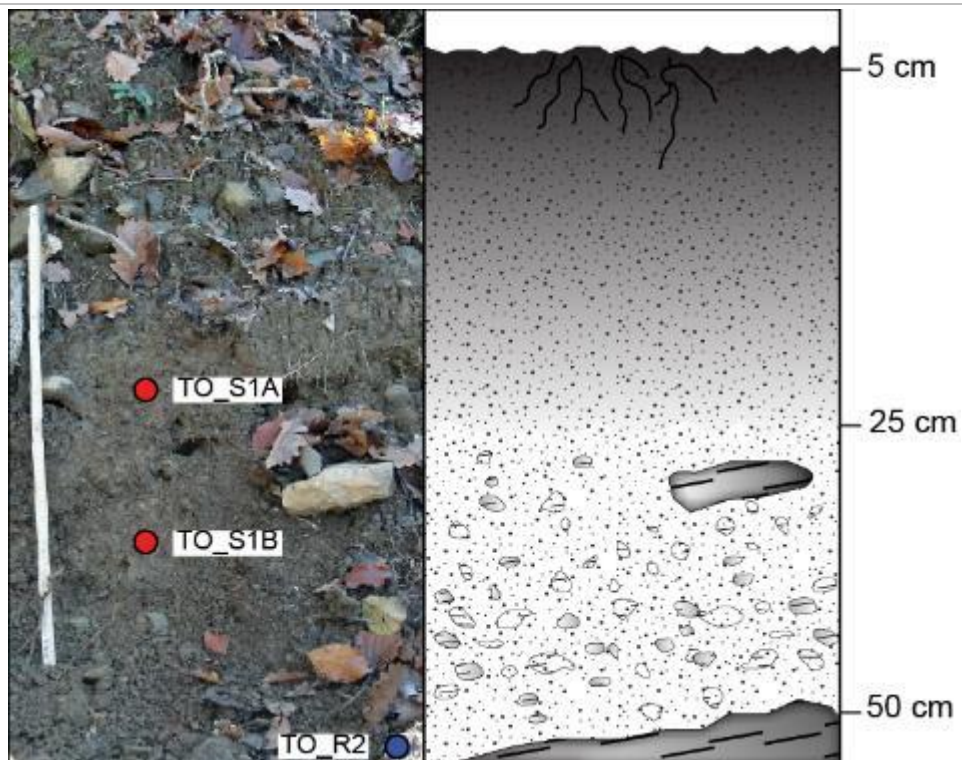
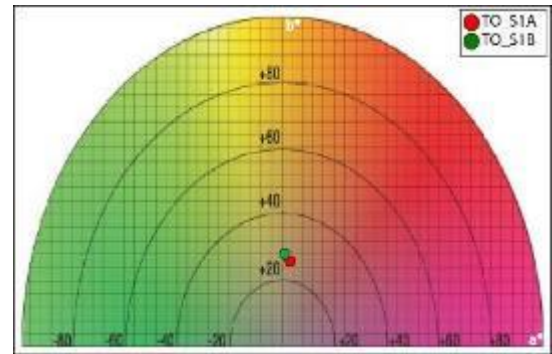
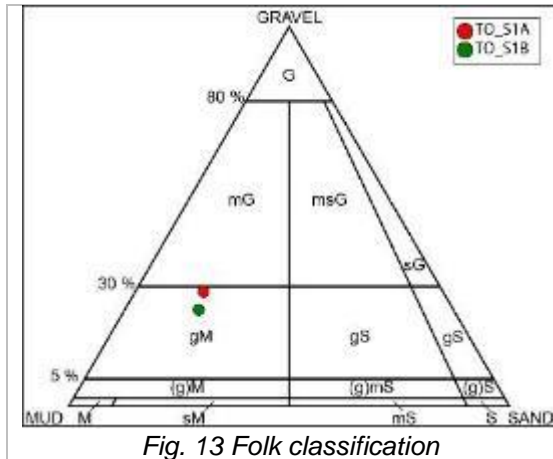


Fig. 8 TO_P1 soil profile and relative sketch

Depth: 5-25 cm

<p>TO_S1A (5-25 cm): topsoil, pale yellow (2.5 Y 3/4), dump. High organic fraction, with fine roots, leaves, and bioturbation. Granular soil structure, with rounded aggregates.</p>	<p>Thickness: 20 cm</p> <p>Grain-shape: subangular to subrounded</p> <p>Color: 2.5 Y 3/4 (dry)</p> <p>Water: dump</p> <p>Granulometry: muddy gravel/gravelly mud</p>
 <p><i>Fig. 9 Topsoil sample TO_S1A</i></p>	 <p><i>Fig. 9a Thin section of soil skeleton</i></p>
<p>TO_S1B (25-50 cm): subsoil (C horizon), reddish brown (2.5 Y 7/4), dump. Very low organic fraction. Abundant angular medium and coarse gravel (strongly weathered serpentinites, directly originated from the weathering of bedrock). Bedrock contact is not clear visible.</p>	<p>Depth: 25-50 cm</p> <p>Thickness: 25 cm</p> <p>Grain-shape: angular to rounded</p> <p>Color: 2.5 Y 7/4 (dry)</p> <p>Water: dump</p> <p>Granulometry: gravelly mud</p>
 <p><i>Fig. 10 Topsoil sample TO_S1B</i></p>	 <p><i>Fig. 10a Thin section of soil skeleton</i></p>
 <p><i>Fig. 11 Rock sample TO_R2</i></p>	<p>Rock: foliated serpentinites</p> <p>Texture: high foliated</p> <p>Grain size: very fine grained</p> <p>Minerals: n.d.</p> <p>Color: black to dark green</p> <p>Weathering: superficial patine</p>
 <p><i>Fig. 12 Rock sample TO_R5</i></p>	<p>Rock: tremolite-chlorite schist</p> <p>Texture: high foliated</p> <p>Grain size: fine</p> <p>Minerals: fiber mineral</p> <p>Color: black to dark blue</p> <p>Weathering: white and orange patine</p>

SOIL CLASSIFICATION



APPENDIX B

Supplementary Database

Available only on electronic support

B1. Major and trace element analysis (EMPA-WDS) of the PTEs-minerals in the rocks and calculated formula (*Original data*).

B2. Major and trace element analysis (EMPA-WDS) of the PTEs-minerals in the soils and calculated formula (*Original data*).

B3. Trace and ultra-trace analysis (LA-ICP-MS) of the PTEs-minerals in rocks and soils (*Original data*).

B4. Major and trace elements compositions for compiled ultramafic rocks worldwide.

B5. Major and trace elements compositions for compiled ultramafic soils worldwide.

B6. Major and trace elements compositions for compiled silicate minerals of ultramafic rocks worldwide.

B7. Major and trace elements compositions for compiled spinel-group minerals of ultramafic rocks worldwide.

B8. Major and trace elements compositions for minerals of ultramafic soils worldwide.

B9. XR-Powder Diffraction data with Rietveld refinement (*Original data*).